A STUDY OF CLOUD-TO-GROUND LIGHTNING PROCESSES WITH EMPHASIS ON DATA ANALYSIS AND MODELING OF THE RETURN STROKE

By

RAJEEV THOTTAPPILLIL

A DISSERTATION PRESENTED TO THE GRADUATE SCHOOL OF THE UNIVERSITY OF FLORIDA IN PARTIAL FULFILLMENT OF THE REQUIREMENTS FOR THE DEGREE OF DOCTOR OF PHILOSOPHY

UNIVERSITY OF FLORIDA

1992

UNIVERSITY OF FLORIDA LIBRARIES

ACKNOWLEDGEMENTS

Writing the acknowledgements is one of the most difficult tasks in a dissertation because in a period of a few years one intellectually interacts with colleagues and other researchers under various circumstances, and it is often difficult to recollect which person or which conversation has helped in formulating an idea reported in the dissertation. My case is no different from this general rule, and my apologies are extended to anyone whose contribution might have gone unacknowledged in this dissertation. I am certain that it was the inspiring leadership of Dr. Martin A. Uman and the constant companionship of Dr. Vladimir A. Rakov and Dr. Marcos Rubinstein that enabled me to complete the research successfully. I am indebted to Dr. Uman for giving proper direction to the research and setting it on course whenever I tended to go wayward. The dedication, scholarship, and thoroughness of Dr. Rakov was an example to me. I consider the hilarious, at the same time intellectually stimulating, Friday lunches at Sonny's with Dr. Douglas M. Jordan as an integral part of my research work. Dr. Ewen M. Thomson's critical comments have helped me in improving this dissertation. It was Dr. Gerhard Diendorfer who introduced me to return stroke modeling. I think it was Dr. Rakov who first suggested to me the idea of comparing return stroke models using simultaneously measured current and electric field data. I thank Dr. D. K. McLain for the help he has given in generalizing the Diendorfer-Uman model and Mr. Jamie Stone for enhancing my computer literacy. I am grateful to Dr. J. C. Willett for providing the simultaneous triggered lightning return stroke current, field, and speed data used in Chapters 5, 6, and 7, and to Mr. R. J. Fisher and Mr. G. H. Schnetzer

of Sandia National Laboratories and Mr. William Jafferis of the NASA Kennedy Space Center for providing the triggered lightning data used in Chapter 4. My wife Ranjana and son Rohith have shown great understanding and patience during the preparation of this manuscript, and I am very thankful to them.

TABLE OF CONTENTS

page

ACKNOWLEDGEMENTS ii

LIST OF FIGURES vi

LIST OF TABLES xv

ABSTRACT xvi

1 INTRODUCTION 1

2 CRITICAL REVIEW OF LITERATURE 4

2.1 Natural Lightning 4

2.1.1 Current Measurements 7
2.1.2 Electric and Magnetic Field Measurements 9
2.1.3 Photographic Measurements 14

2.2 Triggered Lightning 16

2.2.1 Current Measurements 16
2.2.2 Field Measurements 18
2.2.3 Photographic Measurements 18

2.3 Comparison of Triggered and Natural Lightning 19
2.4 Return Stroke Models 21
2.5 Modeling of Continuing Currents and M Components 31

3 EXPERIMENTAL DATA USED 35

3.1 Natural Lightning Data 35
3.2 Triggered Lightning Data from the Sandia National Laboratories 37
3.3 Triggered Lightning Data of Willett et al. (1988, 1989) from the NASA Kennedy Space Center 39

4 ANALYSIS OF EXPERIMENTAL DATA 45

4.1 Natural Lightning 45

4.1.1 Subsequent-Stroke Peak Greater than the First-Stroke Peak 46
4.1.2 Spatial Separation of the Flash Ground Terminations 54
4.1.3 Discussion 56

4.2 Triggered Lightning 59

4.2.1 Return Stroke Current Parameters 59
4.2.2 Interstroke Intervals, Continuing Currents, and M Components . . 60
4.2.3 Discussion 62

5 COMPARISON OF PREVIOUS RETURN-STROKE CURRENT MODELS 80

5.1 Comparison of Models Reviewed in Section 2.4 82
5.2 Discussion 92

6 GENERALIZATION OF THE DIENDORFER-UMAN MODEL 136

6.1 Mathematical Analysis for Single Channel Discharge Time Constant 137
6.2 Application 142
6.3 Comparison With Other Models for Triggered Lightning 145
6.4 Summary and Discussion 148

7 A NEW CHANNEL DISCHARGE MODEL WITH HEIGHT-VARIABLE TIME CONSTANT 164

7.1 Mathematical Analysis 165
7.2 Application 170

8 MODELING OF CONTINUING CURRENTS AND M COMPONENTS 178

8.1 Theory 178
8.2 Application 181
8.3 Discussion 185

9 SUMMARY AND CONCLUSIONS 200

APPENDICES 205

A LIST OF JOURNAL AND CONFERENCE PAPERS DEVELOPED AS PART OF THIS Ph.D. DISSERTATION WORK 206
B COMPUTER PROGRAM LISTINGS 207

REFERENCES 229

BIOGRAPHICAL SKETCH 237

LIST OF FIGURES

Figure 2-1. Geometry used in deriving the field equations given in equations (2-1) and (2-2). 34

Figure 4-1. Histogram of subsequent-stroke initial electric field peak for 46 natural lightning flashes recorded near Tampa, Florida. 49

Figure 4-2. Histogram of the ratio of subsequent-stroke field peak to the first stroke field peak. 50

Figure 4-3. Histogram of the interstroke interval duration. 51

Figure 4-4. Histogram of subsequent leader duration. 52

Figure 4-5. Histogram of the distance between the multiple terminations of 22 individual ground flashes recorded near Tampa, Florida. 55

Figure 4-6. Example of a triggered lightning return stroke current waveshape with relatively fast rise time recorded at Ft. McClellan, Alabama. a) Waveform on a longer time scale; b) The front portion on an expanded time scale. . . 65

Figure 4-7. Example of a triggered lightning return stroke current waveshape with relatively slow rate-of-rise at the beginning and a fast rate-of-rise near the peak recorded at Ft. McClellan, Alabama. a) Waveform on a longer time scale; b) The front portion on an expanded time scale. 66

Figure 4-8. Example of a triggered lightning return stroke current waveshape with a slowly rising ramp at the beginning recorded at Ft. McClellan, Alabama. a) Waveform on a longer time scale; b) The front portion on an expanded time scale. 67

Figure 4-9. Histogram of return-stroke peak current for triggered lightning. 68

Figure 4-10. Histogram of return-stroke current rise time for triggered lightning. 69

Figure 4-11. Scatter plot of return-stroke peak current vs. rise time for triggered lightning. 70

Figure 4-12. Example of the current record of a 10 stroke flash. 71

Figure 4-13. Portion of the flash between the arrows shown in Figure 4-12. 72

Figure 4-14. Example of an M-current pulse waveshape. 73

Figure 4-15. Histogram of interstroke interval for triggered lightning. 74

Figure 4-16. Histogram of stroke duration including continuing current for triggered lightning. 75

Figure 4-17. Histogram of the portion of interstroke interval at which current flow is not detected. 76

Figure 4-18. Histogram of M-current rise time. 77

Figure 4-19. Histogram of M-current duration. 78

Figure 4-20. Histogram of M-current interval. 79

Figure 5-1. Geometrical parameters used in the models. 98

Figure 5-2. Current waveform for return stroke 8705_1 from triggered lightning at KSC, 1987. a) Total available waveform; b) The wavefront on an expanded scale. 99

Figure 5-3. Current waveform for return stroke 8705_3. a) Total available waveform; b) The wavefront on an expanded scale. 99

Figure 5-4. Current waveform for return stroke 8705_5. a) Total available waveform; b) The wavefront on an expanded scale. 100

Figure 5-5. Current waveform for return stroke 8705_6. a) Total available waveform; b) The wavefront on an expanded scale. 100

Figure 5-6. Current waveform for return stroke 8715_2. a) Total available waveform; b) The wavefront on an expanded scale. 101

Figure 5-7. Current waveform for return stroke 8715_3. a) Total available waveform; b) The wavefront on an expanded scale. 101

Figure 5-8. Current waveform for return stroke 8715_4. a) Total available waveform; b) The wavefront on an expanded scale. 102

Figure 5-9. Current waveform for return stroke 8715_6. a) Total available waveform; b) The wavefront on an expanded scale. 102

Figure 5-10. Current waveform for return stroke 8715_7. a) Total available waveform; b) The wavefront on an expanded scale. 103

Figure 5-11. Current waveform for return stroke 8715_8. a) Total available waveform; b) The wavefront on an expanded scale. 103

Figure 5-12. Current waveform for return stroke 8715_9. a) Total available waveform; b) The wavefront on an expanded scale. 104

Figure 5-13. Current waveform for return stroke 8715_10. a) Total available waveform; b) The wavefront on an expanded scale. 104

Figure 5-14. Current waveform for return stroke 8717_3. a) Total available waveform; b) The wavefront on an expanded scale. 105

Figure 5-15. Current waveform for return stroke 8717_5. a) Total available waveform; b) The wavefront on an expanded scale. 105

Figure 5-16. Current waveform for return stroke 8725_1. a) Total available waveform; b) The wavefront on an expanded scale. 106

Figure 5-17. Current waveform for return stroke 8725_2. a) Total available waveform; b) The wavefront on an expanded scale. 106

Figure 5-18. Current waveform for return stroke 8725_3. a) Total available waveform; b) The wavefront on an expanded scale. 107

Figure 5-19. Current waveform for return stroke 8725_4. a) Total available waveform; b) The wavefront on an expanded scale. 107

Figure 5-20. Current waveform for return stroke 8725_5. a) Total available waveform; b) The wavefront on an expanded scale. 108

Figure 5-21. Current waveform for return stroke 8725_4. a) Total available waveform; b) The wavefront on an expanded scale. 108

Figure 5-22. Current waveform for return stroke 8726_2. a) Total available waveform; b) The wavefront on an expanded scale. 109

Figure 5-23. Current waveform for return stroke 8726_3. a) Total available waveform; b) The wavefront on an expanded scale. 109

Figure 5-24. Current waveform for return stroke 8726_4. a) Total available waveform; b) The wavefront on an expanded scale. 110

Figure 5-25. Current waveform for return stroke 8726_5. a) Total available waveform; b) The wavefront on an expanded scale. 110

Figure 5-26. Current waveform for return stroke 8728_10. a) Total available waveform; b) The wavefront on an expanded scale. 111

Figure 5-27. Current waveform for return stroke 8728_11. a) Total available waveform; b) The wavefront on an expanded scale. 111

Figure 5-28. Current waveform for return stroke 8732_1. a) Total available waveform; b) The wavefront on an expanded scale. 112

Figure 5-29. Current waveform for return stroke 8732_2. a) Total available waveform; b) The wavefront on an expanded scale. 112

Figure 5-30. An example of comparison of electronically integrated and numerically integrated return stroke electric field waveforms. a) Overall waveform; b) The front portion on an expanded scale. 113

Figure 5-31. Comparison of calculated fields from the various models with the measured field at 5.16 km for the return stroke 8705_1. The measured current at the channel base and the measured return stroke speed are given in Figure 5-2. a) TL model; b) MTL model; c) TCS model; d) DU model. 114

Figure 5-32. Comparison of calculated fields from the various models with the measured field at 5.16 km for the return stroke 8705_3. The measured current at the channel base and the measured return stroke speed are given in Figure 5-3. a) TL model; b) MTL model; c) TCS model; d) DU model. 115

Figure 5-33. Comparison of calculated fields from the various models with the measured field at 5.16 km for the return stroke 8705_5. The measured current at the channel base and the measured return stroke speed are given in Figure 5-4. a) TL model; b) MTL model; c) TCS model; d) DU model. 116

Figure 5-34. Comparison of calculated fields from the various models with the measured field at 5.16 km for the return stroke 8705_6. The measured current at the channel base and the measured return stroke speed are given in Figure 5-5. a) TL model; b) MTL model; c) TCS model; d) DU model. 117

Figure 5-35. Comparison of calculated fields from the various models with the measured field at 5.16 km for the return stroke 8715_9. The measured current at the channel base and the measured return stroke speed are given in Figure 5-12. a) TL model; b) MTL model; c) TCS model; d) DU model. 118

Figure 5-36. Comparison of calculated fields from the various models with the measured field at 5.16 km for the return stroke 8715_10. The measured current at the channel base and the measured return stroke speed are given in Figure 5-13. a) TL model; b) MTL model; c) TCS model; d) DU model. 119

Figure 5-37. Comparison of calculated fields from the various models with the measured field at 5.16 km for the return stroke 8725_1. The measured current at the channel base and the measured return stroke speed are given in Figure 5-16. a) TL model; b) MTL model; c) TCS model; d) DU model. 120

Figure 5-38. Comparison of calculated fields from the various models with the measured field at 5.16 km for the return stroke 8725_2. The measured current at the channel base and the measured return stroke speed are given in Figure 5-17. a) TL model; b) MTL model; c) TCS model; d) DU model. 121

Figure 5-39. Comparison of calculated fields from the various models with the measured field at 5.16 km for the return stroke 8725_3. The measured current at the channel base and the measured return stroke speed are given in Figure 5-18. a) TL model; b) MTL model; c) TCS model; d) DU model. 122

Figure 5-40. Comparison of calculated fields from the various models with the measured field at 5.16 km for the return stroke 8725_5. The measured current at the channel base and the measured return stroke speed are given in Figure 5-20. a) TL model; b) MTL model; c) TCS model; d) DU model. 123

Figure 5-41. Comparison of calculated fields from the various models with the measured field at 5.16 km for the return stroke 8726_1. The measured current at the channel base and the measured return stroke speed are given in Figure 5-21. a) TL model; b) MTL model; c) TCS model; d) DU model. 124

Figure 5-42. Comparison of calculated fields from the various models with the measured field at 5.16 km for the return stroke 8726_2. The measured current at the channel base and the measured return stroke speed are given in Figure 5-22. a) TL model; b) MTL model; c) TCS model; d) DU model. 125

Figure 5-43. Comparison of calculated fields from the various models with the measured field at 5.16 km for the return stroke 8726_3. The measured current at the channel base and the measured return stroke speed are given in Figure 5-23. a) TL model; b) MTL model; c) TCS model; d) DU model. 126

Figure 5-44. Comparison of calculated fields from the various models with the measured field at 5.16 km for the return stroke 8726_4. The measured current at the channel base and the measured return stroke speed are given in Figure 5-24. a) TL model; b) MTL model; c) TCS model; d) DU model. 127

Figure 5-45. Comparison of calculated fields from the various models with the measured field at 5.16 km for the return stroke 8728_10. The measured current at the channel base and the measured return stroke speed are given in Figure 5-26. a) TL model; b) MTL model; c) TCS model; d) DU model. 128

Figure 5-46. Comparison of calculated fields from the various models with the measured field at 5.16 km for the return stroke 8728_11. The measured current at the channel base and the measured return stroke speed are given in Figure 5-27. a) TL model; b) MTL model; c) TCS model; d) DU model. 129

Figure 5-47. Comparison of calculated fields from the various models with the measured field at 5.16 km for the return stroke 8732_1. The measured current at

the channel base and the measured return stroke speed are given in Figure 5-28. a) TL model; b) MTL model; c) TCS model; d) DU model. 130

Figure 5-48. Comparison of calculated fields from the various models with the measured field at 5.16 km for the return stroke 8732_2. The measured current at the channel base and the measured return stroke speed are given in Figure 5-29. a) TL model; b) MTL model; c) TCS model; d) DU model. 131

Figure 5-49. Example of the range of calculated electric field amplitudes possible due to 25% absolute error in return-stroke speed measurement for the return stroke 8725_2. a) TL model; b) MTL model; c) TCS model; d) DU model. 132

Figure 5-50. Scatter plot illustrating the tendency in which the measured return-stroke currents having a maximum di/dt occurring near the peak current is associated with remotely measured electric field having a very narrow spike at the field peak. 133

Figure 5-51. Return stroke channel-base current waveshape of a stroke which produced upward discharges as observed in video records. a) Overall current waveform; b) The front portion expanded showing the position of maximum rate-of-rise of current near the peak. 134

Figure 5-52. Comparison of channel current distribution at 0.2 μs, 0.5 μs, and 0.8 μs for TL and DU models. a) For return stroke 8715_10; b) For return stroke 8726_2. 135

Figure 6-1. Channel base current and its division into two components assumed for the calculation of the fields in Diendorfer and Uman (1990) and in Figures 6-2 to 6-7. 151

Figure 6-2. Comparison of the channel charge distribution for an initial return stroke speed of 1.3×10^8 m/s exponentially decaying with height with decay constant $\lambda = 2000$ m and the charge distribution for a constant return stroke speed of 1.3×10^8 m/s, both cases producing the same total channel base current, shown in Figure 6-1. a) Up to a height of 250 m; b) Up to a height of 2500 m. 152

Figure 6-3. Comparison of the current distribution along the channel as a function of time for an initial return stroke speed of 1.3×10^8 m/s exponentially decaying with height with a decay constant $\lambda = 2000$ and the current distribution for a constant return stroke speed of 1.3×10^8 m/s, both cases producing the same total channel base current, shown in Figure 6-1. . . 153

Figure 6-4. Comparison of the early part of the far electric fields for an initial return stroke speed of 1.3×10^8 m/s with exponential decay constant $\lambda = 1000$ m, 2000 m, 3000 m and infinity. a) Comparison of initial field peaks; b) Comparison of initial field derivatives. 154

Figure 6-5. Comparison of the zero crossing and other features of the far fields for an initial return stroke speed of 1.3 x 10^8 m/s with exponential decay factors λ = 1000 m, 2000 m, 3000 m, and infinity. 155

Figure 6-6. Comparison of the near electric fields for an initial return stroke speed of 1.3 x 10^8 m/s with exponential decay factors λ = 1000 m, 2000 m, 3000 m, and infinity. a) Fields for the first 25 μs; b) Fields for 100 μs. 156

Figure 6-7. Comparison of the near magnetic fields for an initial return stroke speed of 1.3 x 10^8 m/s with exponential decay factors λ = 1000 m, 2000 m, 3000 m, and infinity. a) Fields for the first 25 μs; b) Fields for 100 μs. 157

Figure 6-8. Comparison of calculated field from the MDU model with the measured field at 5.16 km. a) Return stroke 8705_1; b) Return stroke 8705_3; c) Return stroke 8705_5; d) Return stroke 8705_6. 158

Figure 6-9. Comparison of calculated field from the MDU model with the measured field at 5.16 km. a) Return stroke 8715_9; b) Return stroke 8715_10; c) Return stroke 8725_1; d) Return stroke 8725_2. 159

Figure 6-10. Comparison of calculated field from the MDU model with the measured field at 5.16 km. a) Return stroke 8725_3; b) Return stroke 8725_5; c) Return stroke 8726_1; d) Return stroke 8726_2. 160

Figure 6-11. Comparison of calculated field from the MDU model with the measured field at 5.16 km. a) Return stroke 8726_3; b) Return stroke 8726_4; c) Return stroke 8728_10; d) Return stroke 8728_11. 161

Figure 6-12. Comparison of calculated field from the MDU model with the measured field at 5.16 km. a) Return stroke 8732_1; b) Return stroke 8732_2. . . . 162

Figure 6-13. Comparison of calculated field from the MDU model with the measured field at 5.16 km for return stroke 8726_2. The return stroke is assumed to start from ground with a speed v_0 and increase the speed exponentially to reach the measured speed v_b at a height z_b, and thereafter decrease the speed exponentially with a decay factor λ. 163

Figure 7-1. Channel discharge time constant as a function of height for the VCTC model for the charge distribution given in Figure 6-2 (curve 2) and channel base current given in Figure 6-1 (curve 3). a) For a height of 250 m; b) For a height of 2500 m. 174

Figure 7-2. Charge distribution along the channel for the DU model (Figure 8 of Diendorfer and Uman, 1990) for two time constants 0.1 μs and 5 μs, and the associated channel-base currents shown in Figure 6-1. a) The bottom 250 m; b) The bottom 2500 m. 175

Figure 7-3. Comparison of current distribution along the channel as a function of time for the assumed return stroke speed of 1.3×10^8 m/s for the DU and VCTC models. 176

Figure 7-4. Comparison of calculated field from the VCTC model at 5.16 km for return stroke 8715_10. The measured current at the channel base and the measured return stroke speed are given in Figure 5-13. The discharge time constant is assumed to be 0.1 μs at ground and increases linearly with height with a slope 1 μs/km. The return stroke speed is assumed to decrease exponentially with a decay factor of 2000 m. 177

Figure 8-1. Geometry used to calculate the electric fields from the continuing current and M components. 187

Figure 8-2. Measured continuing current waveshape from triggered lightning used for calculating the electric fields given in Figure 6-3 to 6-11. 188

Figure 8-3. Calculated electric fields at 1000 m from the channel with the current waveshape in Figure 8-2 propagating down the vertical channel with a speed of 1x107 m/s. Current source is assumed at a height of 7500 m. . 189

Figure 8-4. Calculated electric fields at 5000 m from the channel with current waveshape in Figure 8-2 propagating down the vertical channel with a speed of 1×10^8 m/s. Current source is assumed at a height of 7500 m. . . 190

Figure 8-5. A case identical to that described in Figure 8-3. But only the static component of the field is calculated. The contribution to the field due to the charges on the channel and the due to charge depletion at the top of the channel in the cloud are shown separately. 191

Figure 8-6. Calculated electrostatic fields at 1000 m from the channel with the current waveshape in Figure 8-2 propagating down the vertical channel with a speed of 1×10^6 m/s. Current source is assumed at a height of 7500 m. . . 192

Figure 8-7. Calculated electrostatic fields at 1000 m from the channel with the current waveshape in Figure 8-2 propagating down the vertical channel with a speed of 1×10^8 m/s. Current source is assumed at a height of 7500 m. . . 193

Figure 8-8. Calculated electrostatic fields at 5000 m from the channel with the current waveshape in Figure 8-2 propagating down the vertical channel with a speed of 1×10^7 m/s. Current source is assumed at a height of 7500 m. . . 194

Figure 8-9. Calculated electrostatic fields at 5000 m from the channel with the current waveshape in Figure 8-2 propagating down the vertical channel with a speed of 1×10^6 m/s. Current source is assumed at a height of 7500 m. . . 195

Figure 8-10. Calculated electrostatic fields at 1000 m with the current waveshape in Figure 8-2 propagating towards the ground with a speed of $1x10^7$ m/s. The geometry of the problem is shown on the figure. 196

Figure 8-11. Calculated electrostatic fields at 10000 m with the current waveshape in Figure 8-2 propagating towards the ground with a speed of $1x10^7$ m/s. The geometry of the problem is shown on the figure. 197

Figure 8-12. Calculated electrostatic fields at 1000 m from the channel with the current waveshape in Figure 8-2 propagating up the vertical channel from ground with a speed of $1x10^7$ m/s. Current source is assumed at a height of 7500 m. Note that the direction of the M-component field change relative to the continuing current field change is opposite to what is observed in natural lightning flashes. 198

Figure 8-13. Calculated field waveshapes at 1000 m from a M-component current pulse propagating down a vertical channel at various speeds. Current source is assumed at a height of 7500 m. a) Measured M-current pulse waveshape assumed at the top of the channel; b) Increase in the amplitude and duration of the electric field waveshapes with decreasing downward propagation speeds. 199

LIST OF TABLES

Table 2-1. Lightning current parameters for negative flashes from Berger et al. (1975). 8

Table 2-2. Summary of current front shape parameters (Adapted from Anderson and Eriksson, 1980). 9

Table 2-3. Statistics on return stroke electric field waveforms of negative cloud-to-ground lightning. 11

Table 3-1. Data from 1987 triggered lightning return strokes adapted from Willett et al. (1989). 44

Table 4-1. Geometric mean values for distributions shown in Figure 4-1 to 4-4. 53

Table 5-1. Comparison of peak amplitudes of the model fields with the measured peak field amplitudes. 86

Table 5-2. Summary of statistics on the error of the model peak fields given in Table 5-1. 87

Table 5-3. Position of maximum rate of change of current on the return stroke wavefront. 97

Table 6-1. Comparison of calculated field peak amplitudes from the MDU model with the measured field peak amplitudes. 147

Table 6-2. Summary of statistics on the error of the modal peak fields given in Table 6-1. 147

Abstract of the Dissertation Presented to the Graduate School of the
University of Florida in Partial Fulfillment of the Requirements for the
Degree of Doctor of Philosophy

A STUDY OF CLOUD-TO-GROUND LIGHTNING PROCESSES WITH EMPHASIS ON DATA ANALYSIS AND MODELING OF THE RETURN STROKE

By

Rajeev Thottappillil

August 1992

Chairman: Martin A. Uman
Major Department: Electrical Engineering

Properties of cloud-to-ground lightning are determined from electric field and optical records of natural lightning flashes and from electric field, current, and optical records of triggered-lightning flashes. Some of these results are used to compare existing return-stroke models, develop two new return-stroke models, and model continuing currents and M components.

Analysis of electric field records of natural lightning in conjunction with multiple station TV images of the lightning channel has yielded new properties of natural lightning which impact lightning protection standards.

Lightning return stroke current parameters and other flash current parameters have been determined from the currents recorded at the base of the channel during triggered-lightning experiments. Current pulses during continuing current have been correlated with the corresponding optical events in streak-camera records showing that these current pulses, named

M-current pulses, are associated with optical M-components. Properties of M-current pulses are given.

Existing return-stroke current models are compared by using simultaneous measurements of channel base currents, return stroke speeds, and remote electric fields from triggered lightning. The influence of the waveshape of the channel-base current on the model predictions are discussed. Measured return-stroke currents having a maximum rate-of-rise occurring near the peak current tend to be associated with remotely measured electric field having a very narrow spike at the field peak, while a maximum current rate-of-rise occurring earlier does not produce a remote field with such a spike.

The Diendorfer-Uman model is generalized to include a varying upward return-stroke speed with height and a varying downward discharge current speed with height. A new return-stroke model is proposed which allows the calculation of spatial and temporal distribution of current along the channel for a specified current at the channel base and for any specified upward return-stroke speed, downward discharge current speed, and discharge time constant, each as a different and arbitrary function of height.

A model for continuing currents and M components is developed. From the model it is inferred that the M component wavefront travels from cloud to ground and not from ground to cloud.

CHAPTER 1
INTRODUCTION

The research work reported in this dissertation deals with two aspects of lightning research: (1) determination of the properties of cloud-to-ground lightning processes from electric field, current, and optical records and (2) modeling of the lightning return stroke, continuing current, and M component. A review of literature relevant to this research is given in chapter 2.

Chapter 3 describes the natural and triggered lightning data used in this dissertation. The analysis of those data is presented in chapter 4. The correlated natural lightning data from electric field records and a network of TV camera images, recorded near Tampa, Florida, in 1979, are used to investigate the subsequent strokes in a flash which have larger field peaks than the first stroke and to find the distance between the ground terminations within a flash. The triggered lightning data obtained by the Sandia National Laboratories at Kennedy Space Center (KSC), Florida, in 1990 and at Ft. McClellan, Alabama, in 1991 are used to investigate the parameters of return strokes and other flash current parameters. Some of the larger current pulses occurring between the return strokes are identified in streak-camera records as due to the optical M components. Statistics on the return stroke and flash current characteristics such as return-stroke peak current, 10-90% current rise time, interstroke interval, stroke current duration, and zero-current interval preceding the return stroke are presented. Statistics on the properties of the M current pulses such as interval, duration, and 10-90% rise time are also presented.

In chapter 5, the existing return-stroke current models for cloud-to-ground lightning that allow the use of measured channel-base current and return-stroke speed as inputs are compared and evaluated using simultaneously measured triggered lightning channel-base current, return-stroke speed, and electric field at about 5 km recorded at KSC, Florida in 1987 and reported in Willett et al. (1989). The models compared are the Transmission Line (TL) model, the Modified Transmission Line (MTL) model, the Travelling Current Source (TCS) model, and the Diendorfer-Uman (DU) model. The fields calculated from the models are found to be sensitive to the channel-base current waveshape. It is found that return strokes producing very narrow spikes (about 0.1 μs wide) in the measured electric fields at 5 km have a maximum rate-of-rise of channel-base current closer to the peak of the measured channel-base current than do return strokes not exhibiting narrow field spikes. For one of the return strokes recorded at KSC in 1990, with current waveform having maximum rate-of-rise of current near the peak, the correlated video images of the bottom portion of the channel recorded upward discharges.

In chapter 6, the DU model is generalized to include a variable upward return-stroke speed and a variable downward discharge-current speed. This Modified Diendorfer-Uman (MDU) model is compared with the other models and evaluated using the same set of simultaneous measurements.

A new return stroke model is proposed in chapter 7 which is similar to the MDU model but allows the variation of channel-charge discharge time constant with height. The new model eliminates the division of the channel into an inner core or breakdown region and an outer corona region, along with the division of channel base current into two associated current components, as is necessary in the DU and MDU models. The new model is used to calculate the discharge time constant profile as a function of height along the channel in place of the two current components and the associated two time constants of the DU model.

A model, similar to the Transmission Line model for the return stroke, is developed for continuing currents and M components. The characteristics of the calculated electric fields from the model are compared with the measured continuing current and M component electric field waveforms found in literature. Based on the model-predicted fields, it is inferred that the M current pulse responsible for the M hook-shaped field change travels from cloud to ground rather than from ground to cloud. The influence of different downward speeds of the M current pulse on the duration and amplitude of the hook-shaped field change is investigated. It is found that slower downward M speeds produce larger amplitude hooks of longer duration than do faster speeds.

CHAPTER 2
CRITICAL REVIEW OF LITERATURE

In this chapter, literature pertinent to this dissertation is reviewed. The properties of both natural and triggered cloud-to-ground lightning are described. The relationship between return-stroke peak current and peak field is examined. Presently available models for return strokes, continuing currents, and M components are reviewed.

2.1 Natural Lightning

Lightning is a transient electric discharge which lasts, on average, a half a second and exhibits a path length of some kilometers. The most common source of lightning is the cumulonimbus cloud in which the majority of charges are assumed to be separated into upper positive and lower negative regions, although the charge structure is more complex than a simple vertical dipole. Lightning between the cloud and earth is called ground lightning. All other discharges which do not involve the ground (e.g., air discharges, intracloud discharges, intercloud discharges) are called cloud lightning or cloud discharges. In ground lightning the lightning initiation can occur from cloud-to-ground (downward lightning), as is normally the case, or from ground-to-cloud (upward lightning), usually from tall objects. Lightning which lowers net negative charge to ground is known as negative lightning, and lightning which lowers net positive charge to ground is called positive lightning. In this dissertation only negative cloud-to-

ground lightning is studied. A downward lightning event can be subdivided into several different processes starting from its inception in the thundercloud. These are briefly described below.

The thundercloud is generally considered to have a tri-polar structure: a positively charged region at the top, a negatively charged region below it, and a small positive charge region below the main negative charge region. The major positive and negative charges separated and stored in a single thunderstorm cell can be tens or more of Coulombs. Uman (1987) gives a drawing illustrating some of the various processes comprising a negative cloud-to-ground lightning flash. The measured electric fields in the thunderclouds are typically $1\text{-}2\text{x}10^5$ V/m (Uman 1987, page 64) which is much lower than the electrical breakdown value of $3\text{x}10^6$ V/m between parallel plates in dry air at sea level although the break-down fields at elevated altitudes in clouds containing particulates can be expected to be lower than the value at sea level. Under certain conditions, not well understood, the electric field in some regions can exceed the breakdown value and local breakdown occurs, possibly between the negative charge region and the small positive charge region at the lower part of the cloud. This stage is known as the preliminary breakdown and culminates in the initiation of a downward-moving stepped leader which is negatively charged. The potential at the tip of the stepped leader when it nears the ground is thought to be of the order of 10 million Volts. As the stepped leader approaches ground the electric field around sharp objects and irregularities on ground exceeds the break-down value of air and positive streamers propagate upward, one of which will meet the stepped leader a few tens of meters above ground, a sequence called the attachment process, bringing the bottom of the stepped leader to ground potential. Thereafter a ground potential wave called the return stroke propagates upward at about one third the speed of light, discharging the leader channel. The first return stroke typically produces a peak current near the ground of 30 kA which falls to half value in about 50 μs. The return stroke heats the channel to about 30,000 K,

so that it emits light, and the high pressure channel expands producing shock waves which become thunder. The return stroke current generally ceases to flow within a few milliseconds. If no other stroke follows, the discharge is called a single-stroke flash. If sufficient charge is made available to the top of the channel in the cloud, a subsequent leader will follow the decaying first stroke channel causing another return stroke. The sequence of leader and return-stroke may occur a number of times. The mean number of strokes in a flash is about 5 (e.g., Rakov and Uman, 1990a) and the mean time interval between strokes in the same channel is 56 ms (Rakov et al., 1992). The total duration of the flash is typically about 0.5 s. Usually, the subsequent return-stroke current peaks are smaller than the first stroke current peaks, but have faster rise time to peak. Often a current of the order of 100 A continues to flow for many milliseconds to tens of milliseconds after the return stroke. This current flow is called a continuing current. Continuing current produces a slow, more or less linear, large, field change in close electric field records and a continuing luminosity of the channel in optical records. Sometimes during continuing current the channel brightens for a millisecond or so, a process called an M component. Between the end of the return stroke and the beginning of the subsequent leader, J-processes occur in the cloud which produce a slow variation of electric field at the ground. Step-like field changes, called K changes, indicative of charge motion within the cloud, occur with a duration of about a millisecond during the J-changes.

Some of the properties of naturally occurring cloud-to-ground lightning flashes, as obtained from current, field, and photographic records are reviewed in the following sections with emphasis on the return stroke, continuing current, and M process.

2.1.1 Current Measurements

Berger and his coworkers measured natural lightning currents that struck the two instrumented towers on the summit of Mt. San Salvatore near Lake Lugano in southern Switzerland. The currents were measured using resistive shunts, were displayed on oscilloscopes, and were photographed from the oscilloscopic faces. Berger et al. (1975) review the results of about two decades of measurements. The current parameters obtained in Switzerland for negative cloud-to-ground lightning flashes are summarized (Berger et al., 1975) in Table 2.1. Garbagnati and co-workers have measured lightning currents striking TV towers on two mountains in northern Italy (Garbagnati et al., 1975, Garbagnati and Lo Piparo, 1982) not far from Mt. San Salvatore. Results from both Switzerland and Italy are similar. Some of the parameters listed in Table 2-1 involving short time intervals such as return-stroke front duration and maximum rate-of-rise of current may be influenced by inadequate measurement techniques including frequency limitations in instrumentation.

Anderson and Eriksson (1980) summarize the lightning parameters important for engineering applications based on the Berger et al. (1975) data, but analyzed using a computer processing technique. They considered several return-stroke current shape parameters such as the peak current, time duration between 10% and 90% amplitude intercepts on the front (T-10), time duration between 30% and 90% amplitude intercepts on the front (T-30), rate of rise of current at 10% amplitude (TAN-10), maximum rate of rise of current on the front (TAN-G), the average current steepness between 10% and 90% amplitude intercepts (S-10), and the average current steepness between the 30% and 90% amplitude intercepts (S-30). The results obtained by Anderson and Eriksson (1980) for negative return strokes are summarized in Table 2-2.

Some subsequent return strokes have current peaks larger than the corresponding first return-stroke peak within the same flash, contrary to the common belief (e.g., Anderson, 1982; Military Standard, 1983). Five (15%) of the 33 negative downward multiple-stroke flashes striking instrumented towers in Switzerland (Atlas of Lightning Currents, Berger, 1967), contained one or two subsequent strokes with initial return stroke peak currents greater than their respective first-stroke peak currents.

Table 2-1. Lightning current parameters for negative flashes from Berger et al. (1975).

No.	Parameters	Unit	95%	50%	5%
	Peak current (minimum 2 kA)				
101	First strokes	kA	14	30	80
135	Subsequent strokes	kA	4.6	12	30
	Charge				
93	First strokes	C	1.1	5.2	24
122	Subsequent strokes	C	0.2	1.4	11
94	Complete flash	C	1.3	7.5	40
	Impulse charge				
90	First strokes	C	1.1	4.5	20
117	Subsequent strokes	C	.22	0.95	4
	Front duration (2 kA to peak)				
89	First strokes	μs	1.8	5.5	18
118	Subsequent strokes	μs	.22	1.1	4.5
	Maximum di/dt				
92	First strokes	kA/μs	5.5	12	32
122	Subsequent strokes		12	40	120
	Stroke duration (2 kA to half value)				
90	First strokes	μs	30	75	200
115	Subsequent strokes	μs	6.5	32	140
	Integral (i^2dt)				
91	First strokes	A^2s	6.0×10^3	5.5×10^4	5.5×10^5
88	Subsequent strokes	A^2s	5.5×10^2	6.0×10^3	5.2×10^4
	Time interval				
133	Between negative stroke	ms	7	33	150

Table 2-2. Summary of current front shape parameters (Adapted from Anderson and Eriksson, 1980).

Parameter	Sample size	Units	Geometric mean
First stroke			
T-10	80	μs	4.5
T-30	80	μs	2.3
TAN-10	75	kA/μs	2.6
S-10	75	kA/μs	5.0
S-30	73	kA/μs	7.2
TAN-G	75	kA/μs	24.3
PEAK	75	kA	27.7
Subsequent strokes			
T-10	114	μs	0.6
T-30	114	μs	0.4
TAN-10	108	kA/μs	18.9
S-10	114	kA/μs	15.4
S-30	114	kA/μs	20.1
TAN-G	113	kA/μs	39.9
PEAK	114	kA	11.8

2.1.2 Electric and Magnetic Field Measurements

The overall electric field variations from cloud-to-ground lightning flashes have been published by many investigators (e.g., Brook et al., 1962; Kitagawa et al., 1962; Krehbiel et al., 1979; Thomson, 1980; Rakov and Uman, 1990a,b,c). Electric field waveforms on a millisecond scale have been used to find the charge lowered and the magnitude of continuing current (e.g., Krehbiel et al., 1979, and Brook et al., 1962). Simultaneous measurements of lightning electric field change at 8 different stations enabled Krehbiel et al. (1979) to prove that the charges involved in successive strokes are displaced horizontally at a more or less constant elevation,

rather than displaced vertically at increasing elevation, a widely-held erroneous view up to that time (e.g., Malan and Schonland, 1951).

Return-stroke electric field waveforms on a microsecond-scale have been presented, for example, by Weidman and Krider (1978), Lin et al. (1979), Lin and Uman (1973), Cooray and Lundquist (1982,1985), Master et al. (1984), and Rakov and Uman (1990a). The characteristics of return stroke electric field waveforms are summarized in Table 2-3.

Lin et al. (1979) present typical return stroke waveforms for vertical electric field intensity and horizontal magnetic flux density at ground level on a microsecond scale for various distances from the channel and identify the salient characteristics of the waveforms. Rakov and Uman (1990a) found that about 50% of their 76 flashes recorded near Tampa, Florida in 1979 had multiple ground terminations, that is, spatially separate ground strike points within the flashes. Rakov and Uman (1990a) found a geometric mean (GM) value of initial electric field peak normalized to a distance of 100 km of 6.2 V/m for 63 first strokes in multiple-stroke flashes, 4.7 V/m for 13 strokes in single-stroke flashes, and 4.1 V/m for 38 subsequent strokes creating a ground termination different from that of the first stroke in the flash (see Table 2-3). The GM field peak of 232 subsequent strokes that followed a previously formed channel was 2.7 V/m.

Even though the typical subsequent-stroke field peak is less than half the typical first-stroke field peak in multiple stroke flashes, some of the subsequent stroke peak within a multiple stroke flash can be larger than the first-stroke peak, similar to the case of current peaks discussed in section 2.1.1. Namasivayam et al. (1990) recorded lightning flashes, the majority of them at distances from 50 km to 300 km, in Sweden using a triggered transient waveform recorder. They found that about one-third of 1205 subsequent strokes had electric field peaks that were greater

Table 2-3. Statistics on return stroke electric field waveforms of negative cloud-to-ground lightning.

	First strokes			Subsequent strokes		
	No.	Mean	SD	No.	Mean	SD
Initial peak (V/m) (normalized to 100 km)						
Rakov and Uman (1990a)						
[All cases]	76	5.9(GM)		270	2.9(GM)	
[Multiple-stroke flashes]	63	6.2(GM)				
[Single-stroke flashes]	13	4.7(GM)				
[Strokes creating new termination]				38	4.1(GM)	
[Strokes following previous channel]				232	2.7(GM)	
Cooray and Lundquist (1982)	553	5.3	2.7			
Lin et al. (1979)						
[KSC]	51	6.7	3.8	83	5.0	2.2
[Ocala]	29	5.8	2.5	59	4.3	1.5
Zero-crossing time (μs)						
Cooray and Lundquist (1985)						
[Sweden]	102	49	12	94	39	8
[Sri Lanka]	91	89	30	143	42	14
Lin and Uman (1973)	46	54	18	77	36	17
Zero-to-peak rise time (μs)						
Master et al. (1984)	105	4.4	1.8	220	2.8	1.5
Cooray and Lundquist (1982)	140	7.0	2.0			
Lin et al. (1979)						
[KSC]	51	2.4	1.2	83	1.5	0.8
[Ocala]	29	2.7	1.3	59	1.9	0.7
10-90% rise time (μs)						
Master et al. (1984)	105	2.6	1.2	220	1.5	0.9

Note: The numbers with GM in parenthesis are the Geometric Mean values.

than the first-stroke peak. The geometric mean value of the ratio of the subsequent return stroke peak to the first-stroke peak reported by Namasivayam et al. (1990) is 0.86.

Kitagawa et al. (1962) and Brook et al. (1962) have correlated photographic and electric field records of cloud to ground lightning flashes and have shown that the large slow electric field changes of the same sign as the return stroke initial field change and following it are accompanied by continuing luminosity on photographic records, which is indicative of continuing current flow in the channel. Forty-six percent of the flashes in New Mexico that they have analyzed contained long-continuing currents, which they defined as continuing current with a duration greater than 40 ms. Shindo and Uman (1989) found that the return stroke electric field peaks of the strokes initiating the long continuing-currents and the inter-stroke intervals immediately preceding them are smaller, on the average, than those of the other strokes and inter-stroke intervals. Rakov and Uman (1990a) analyzed 76 flashes from Florida summer thunderstorms and found that 49% of the multiple stroke flashes contained long continuing-currents, while only 6% of the single stroke flashes contained long continuing-currents. They also found a tendency for the stroke immediately preceding the relatively small stroke initiating the long continuing-current to be relatively large.

The temporary increases in the luminosity of the faintly luminous channel (due to a continuing current) observed after some ground return strokes were first described by Malan and Collens (1937) and are known as M components. The term "M change" is used (e.g., Kitagawa et al. 1962; Uman, 1987) to denote electric field changes accompanying M components. From correlated electric field and photographic observations in South Africa, Malan and Schonland (1947) reported that M field changes recorded at close range (mostly 6 km or less) with measurement system having decay time constants of 1 to 21 ms exhibited a characteristic hook-like shape. They estimated the duration of the hook-shaped M changes to be typically from 200 to 800 μs, although values up to 1.6 ms were observed. The most recent studies of the characteristics of M changes are given by Thottappillil et al. (1990) and Rakov et al. (1992).

Thottappillil et al. (1990) found, in Florida ground flashes, a geometric mean M-change duration of 0.9 ms and a geometric mean time interval between M changes of 2.1 ms. Rakov et al. (1992) show that the majority of the M changes has microsecond-scale pulses at the very beginning of the hook-shaped field change with an initial polarity, in most cases, the same as the initial field change of the hook. Malan and Schonland (1947, p. 498) claimed that the M process is, in fact, a leader without a discernible return stroke which lowers negative charge to ground but "the charge is usually not large enough, and the other conditions are not always such as, to give rise to a return stroke from the ground." However, later Schonland (1956, p. 596) described M components as manifestations of processes of unknown nature, probably due to branching hidden inside the cloud. Ogawa and Brook (1964) hypothesized that the K process (which produce the K change in electric field records described in Section 2.1.1) in both ground and cloud flashes is a negative "recoil streamer" that occurs when a positive J-type streamer propagating within the cloud encounters a region of concentrated negative charge. Kitagawa et al. (1962) suggested that M components are due to K processes that occur at the time when there is a relatively low level continuing current flowing in the channel to ground. This hypothesis was based on their observations in New Mexico that K and M field waveforms appeared similar in their "fast antenna" records (undoubtedly distorted by the fast instrumentation decay) and that the histograms of the time intervals between successive K changes and the respective histogram for M changes were similar. Thottappillil et al. (1990) presented statistics on the K-change and M-change intervals in Florida which do not support the latter observation. They argued that there was no real evidence to claim the similarity between K and M processes. Rakov et al. (1992) found that the K and M changes are different in terms of the microsecond-scale field changes. Kitagawa et al. (1962) describe the M component as "a momentary current increase without involving the leader process" which is produced "by the development of new streamers within

the cloud, these streamers making contact with the already existing main channel". This view is somewhat different both from the interpretation of M components given by Malan and Schonland (1947) and from the recoil-streamer concept of K processes (e.g., Ogawa and Brook, 1964) which were claimed by Kitagawa et al. (1962) to be responsible for producing M components.

2.1.3 Photographic Measurements

In the early days of lightning research, the 1930s, time-resolved photographic measurements of lightning played a decisive role in identifying the stepped and dart leaders that propagate downward and the return stroke that propagates upward. Still photographic measurements of return-stroke channel radii by Schonland (1937) gave values in the range of 5.5 to 11.5 cm. Orville et al. (1974), using more sophisticated photographic techniques, determined the radius to be in the 2 to 4 cm range. From high-speed spectroscopic studies of lightning, Orville (1968a-c) found that the peak temperature of the return-stroke channel within the first 10 μs of the return stroke initiation was of the order of 30,000 K.

Schonland et al. (1935) found that 4 of 33 multiple-stroke flashes had one or more subsequent strokes that had more intense luminosity than the respective first-stroke luminosity, similar to the behavior of some of the subsequent return stroke current and field peaks (see Section 2.1.2 and 2.1.3). They also found that these large (in terms of luminosity) subsequent strokes were preceded by longer interstroke intervals and had slower leaders.

Jordan and Uman (1983) investigated the light waveshapes of subsequent return-strokes as a function of height using a streak camera. For nine strokes in 3 flashes they found that the peak luminosity of the return stroke decreases, approximately, as an exponential function with

height decay constant of 0.6 to 0.8 km. The rise time of the light intensity waveshape was a few microseconds at ground level and increased by a factor of two between 1 and 2 km. The logarithm of the initial peak light intensity near ground was linearly related to the initial peak electric field intensity. Ganesh et al. (1984) used a photoelectric system and found that the light and electric field from the return-stroke channel are correlated, although they were unable to determine the analytical relationship. Mach and Rust (1989) measured return-stroke speed using a photoelectric technique. The rise time of their optical waveform increased with height and the peak relative light intensity decreased with height, supporting the observations of Jordan and Uman (1983).

Orville et al. (1978) measured return stroke speeds ranging from 1.2×10^8 to 1.4×10^8 m/s from daytime streak-camera photography. Idone and Orville (1982) present return-stroke speed data in which the speed measured within about 1.3 km of ground decreased with height.

Jordan et al. (1992) reported, for both natural and triggered lightning, a positive correlation between subsequent-leader propagation speed and the ensuing return-stroke initial electric field peak.

Malan and Collens (1937) observed that out of 9 M components that they studied, 7 progressed downward from the cloud while 2 developed upward from ground. For four of the M components travelling downward, they measured a speed in the range 2.0 - 4.7×10^7 m/s.

Jordan (1990) did not find any optical M components in the streak-camera records for three M changes after a return stroke in the electric field records, even though he could observe the subsequent leader of that stroke in the streak camera record and the M change in the field record was comparable with the leader field change. For two M components following a return stroke in another flash, Jordan (1990) inferred that the M components propagated downward with a speed of 6.7×10^7 m/s if the return-stroke speed was 2.0×10^8 m/s, and with a speed of 1×10^8 m/s

if the return stroke speed was 1.0×10^8 m/s. The relative peak light intensity and the risetime of the light waveform did not change measurably with height for these M components, whereas the relative peak light intensity decreased and the risetime of the light waveform increased with height for the return stroke.

2.2 Triggered Lightning

The technique of artificially initiating lightning from thunderclouds by firing small rockets with trailing ground wire was developed in the late 1960's (Newman et al., 1967) and is described in Fieux et al. (1975) and Hubert et al. (1984). A rocket is fired upward with a speed of the order of 200 m/s when the electric field at ground is sufficiently high, generally a few kV/m. An upward positive leader starts from the tip of the rocket when the rocket is about 200-300 m high, typically initiating a continuous current flow that vaporizes the wire. After the cessation of this continuous current, the downward-leader upward return-stroke sequences occurring (if any) are believed to be very similar to the subsequent strokes of natural cloud-to-ground lightning. A brief review of lightning properties as determined from triggered lightning experiments is given in the following sections.

2.2.1 Current Measurements

Hubert et al. (1984) report the results of the triggered lightning experiment performed at Langmuir Laboratory, near Soccoro, New Mexico. The triggering site was at 3230 m above sea level. The currents at the base of the channel were measured using a coaxial shunt and recorded on magnetic tape recorders. The rise time of the current pulse measuring system was

0.3 μs. The highest current pulse peak recorded was 40 kA and there were, on average, 15 pulses per flash above 2 kA. The presentation of results in Hubert et al. (1984) is rather confusing because often they do not separate the return-stroke current pulses from other kind of pulses (e.g., pulses during continuing current after a return stroke). Also it is not clear whether they reserve the term 'continuous current' only for the initial continuous current which vaporizes the wire or also for the continuing current after a return stroke, similar to that observed in natural lightning, as well. Hubert et al. (1984) observed that during the continuous current the current pulses (above the system noise level of 0.3 kA) have a slow rise-time, 50% of them having a rise time greater than about 20 μs. The median value of the largest current peak in a flash was 18 kA and the 10 to 90% rise time was 0.5 μs. They remark that 'when a continuous current is present, the dart leader return stroke mechanism seldom exists, and when it exists, the return stroke velocity is smaller than usual.'

Leteinturier et al. (1990), and Leteinturier et al. (1991) present measured triggered lightning current (I) and current derivative (dI/dt) in Florida and France. The currents were measured using milliohm coaxial shunts with a 10 to 90% rise time of 20 ns for a step input. An 8 bit digitizer operating at 100 Mega-samples/s was used to acquire the data. The current derivative signals were measured using a wide-band inductive sensor of toroidal shape with a rise time of approximately 1 ns. The peak currents ranged from 5 to 76 kA and the peak dI/dt amplitude ranged from 13 to 411 kA/μs. The median value of the current was 15 kA and the median value of the current derivative was 110 kA/μs. The dI/dt peak is positively correlated with the I peak with a linear correlation coefficient between 0.7 to 0.8. The median value of the 10 to 90% rise time of the return-stroke current was 0.34 μs.

2.2.2 Field Measurements

Based on simultaneous measurements of return-stroke current and electric field from 28 triggered lightning return strokes, Willett et al. (1989) proposed an empirical formula for the estimation of lightning return stroke peak current, I in A, from measured peak electric field, E in V/m, at a range D in m, which is $I = -3.9 \times 10^{-2} DxE - 2.7 \times 10^{3}$. In the equation, I is assumed to be positive, and E is assumed to be negative. The formula of Willett et al. (1989) is obtained from the regression of E on I, instead of I on E, and hence is not the least squares fit and for that reason not the best expression for predicting the peak current from the measured peak electric field. But the formula can be used in estimating the peak electric field at ground at a distance D from the measured peak current. Based on the Willett et al. (1989) data and the regression of I on E, Rakov et al. (1992) give the correct formula for estimating the peak current from peak electric field in triggered lightning, which is $I = 1.5 - 0.037xDxE$, where I is in kA and taken as negative, E is positive and in V/m, and D is in km. When used to estimate the peak current, the Willett et al. (1989) formula results in an error that varies from -15 percent to +2.6 percent over the range of peak field values of 1.9 to 11 V/m (normalized to 100 km) used to derive the two relations.

Jordan et al. (1992) used the Willett et al. (1989) formula to convert peak currents to peak fields for triggered lightning strokes in Florida and in New Mexico.

2.2.3 Photographic Measurements

Idone et al. (1984) reported a return stroke speed range of 6.7×10^{7} to 1.7×10^{8} m/s in triggered lightning from streak-camera measurements (three-dimensional speed).

Mach and Rust (1989) found a return stroke speed range of $6x10^7$ to $1.6x10^8$ m/s from photoelectric measurements in the lowest channel section longer than 500 m ("long-channel" two-dimensional speed). Accompanying photoelectric measurements in channel sections less than 500 m ("short-channel" two-dimensional speed) resulted in a somewhat wider range of speeds of $6x10^7$ to $2x10^8$ m/s.

Willett et al. (1989) obtained two-dimensional return stroke speeds in the range of $1.2x10^8$ to $1.9x10^8$ m/s from streak-camera measurements, values which are at the higher end of the return-stroke speed ranges measured previously. Jordan et al. (1992) found that the dart-leader speed and the following return-stroke field peak or current peak in New Mexico and Florida triggered lightning and in Florida natural lightning are positively correlated.

Idone (1990) has observed upward connecting discharges in triggered lightning subsequent strokes recorded at NASA Kennedy Space Center (KSC), Florida in 1989 using high spatial and temporal resolution (0.3 m and 0.5 μs) streak-camera records. The triggering technique was the same as that reported by Willett et al. (1989) for the triggered lightning experiment at KSC in 1987. For nine subsequent strokes the mean length of the estimated upward connecting discharges was 12, 13 or 19 m, depending on the method of estimation. The unconnected upward discharges had a length from 0.2 to 1.6 m. In natural lightning, Orville and Idone (1982) report one case of a stroke initiated by a dart-stepped leader that apparently produced a connecting discharge of about 20 m in length.

2.3 Comparison of Triggered and Natural Lightning

The technique of initiating lightning by firing small rockets with trailing grounded wires to study the properties of lightning has become very popular in recent years (e.g., Hubert et al.,

1984; Idone et al., 1984; Kito et al., 1985; Idone and Orville, 1985, 1988; Willett et al., 1988, 1989; Leteinturier et al., 1990; Jordan et al., 1992; Fisher et al., 1992). These measurements were done, in large part, because of the belief that except for the initial process, which is an upward leader followed by continuous current in triggered lightning and a downward stepped leader followed by an upward-propagating first return stroke in natural lightning, triggered and natural lightning flashes are similar and hence triggered lightning could be a convenient way of investigating the properties of natural lightning. In this section the information available in the literature comparing natural lightning and triggered lightning is reviewed briefly.

Le Vine et al. (1989) report that the return-stroke electric field waveshapes in Florida triggered lightning are fairly similar to subsequent strokes in Florida natural lightning. But Idone et al. (1984) reported that triggered flashes in New Mexico had a smaller magnitude of the return-stroke peak current, a larger number of strokes per flash, a higher dart-leader propagation speed, and a shorter interstroke interval duration than natural lightning.

Jordan et al. (1992) found that the relation between leader speed and return-stroke field or current peak is similar for natural and triggered lightning in Florida, possibly indicating a similarity between some features of dart leaders and return strokes in natural and triggered lightning at the same geographical location. However, leader speed as a function of return-stroke field or current peak in New Mexico triggered lightning (3.2 km above sea level) appears distinctly different from that in Florida natural and triggered lightning (at sea level). The average leader speeds in New Mexico triggered lightning are approximately twice as large as in Florida natural and triggered lightning. Orville and Idone (1982) observed similar dart-leader speeds (mean value 11×10^6 m/s) in natural lightning of Florida (at sea level) and in New Mexico (presumably at 2 km above sea level).

In triggered lightning, a rocket with a trailing wire initiates the lightning before the conditions are ripe for natural initiation. The stepped leader and the following first stroke are missing in triggered lightning and the channel may be contaminated by metal vapor from the vaporized wire. Often some of the experimental objectives necessitated complicated triggering structure (e.g., Hubert et al.,1984; Willett et al., 1988) which may influence the measurements in unknown ways. On the other hand, natural lightning may be strike trees, towers, or other complex structures. The foregoing review on the comparison of triggered and natural lightning reveals that, even though many of the parameters of triggered and natural lightning are similar, the equivalency of triggered and natural lightning is not well established.

2.4 Return Stroke Models

Of the many events making up a cloud-to-ground lightning flash, the return stroke has attracted the most attention. The return stroke is, to a first approximation, a ground potential step-function that travels from ground to cloud along a previously charged, ionized, high potential channel formed by a leader travelling from cloud to ground. Currents of a few kiloamperes to hundreds of kiloamperes flow in the return stroke channel producing heat, light, and strong electromagnetic radiation over a wide band from d.c to radio frequencies and above. Many models have been proposed in the past for the return stroke from different perspectives giving emphasis to one or more aspects of the return stroke. Some of the models invoke the breakdown physics and the channel-section physics, examples of which are Papet-LeVine (1961), Hill (1971,1975), Plooster (1971), Klingbeil et al. (1972), Straw (1979), Fowler (1976, 1982), and Cooray (1989). There are electrostatic models (e. g., Krehbiel et al., 1979), acoustic models (e. g., Few, 1969 and 1981; Hill, 1971; Dessler, 1973), optical models (Paxton et al., 1986 and

1987), R-L-C circuit models (e. g., Price and Pierce, 1977; Little, 1978 and 1979; Gorin 1985), and channel-base current models (e. g., Bruce and Golde, 1941; Wagner, 1960; Uman and Mclain, 1969; Lin et al., 1980; Rakov and Dulzon, 1980 and 1987; Heidler, 1985; Nucci et al., 1988; Diendorfer and Uman, 1990). Measurement of lightning channel parameters like temperature, pressure, and electron and ion concentrations are relatively difficult to make. On the other hand, the measurement of remote electromagnetic fields due to lightning return strokes is comparatively easy (e.g., Weidman and Krider, 1978; Lin et al., 1979). Measurement of current at the base of the channel for natural lightning strikes to towers (e.g., Berger et al., 1975; Eriksson, 1978) and for artificially triggered lightning (e. g., Willett et al., 1988, 1989; Leteinturier et al., 1990) have been frequently made. Many optical measurements of the lightning return stroke speed also exist (e. g., Idone and Orville, 1982; Mach and Rust, 1989). Therefore models which use current and speed (e. g., channel-base current models) are easier to verify and more popular for calculating the electromagnetic fields. Moreover, there is a strong interest in the power, telecommunication, and defense arenas in developing a realistic model based on measured and well-documented lightning characteristics that is capable of predicting the electromagnetic fields from lightning. A review of return-stroke current models is given below.

The important return stroke current models in historical order are the Bruce-Golde (BG) model, the Transmission Line model (TL), the Master-Uman-Lin-Standler model (MULS), the Modified Transmission Line model (MTL), the Travelling Current Source model (TCS), and the Diendorfer-Uman model (DU). A detailed review and comparison of the BG, TL, MULS, MTL and TCS models can be found in Nucci et al. (1990). The models give the temporal and spatial distribution of the current along the return stroke channel for a given current at the base of the channel and a given return stroke speed. All models assume a straight vertical channel above a perfectly conducting ground plane. The return stroke is assumed to begin at ground level. Uman

et al. (1975) derive the expressions for fields at a point in space from a vertically-oriented current dipole in the absence of a ground plane

$$\begin{aligned}\overline{dE}(\overline{R},t) = \frac{dz'}{4\pi\epsilon_0}\Bigg[&\cos\theta\left(\frac{2}{R^3}\int_0^t i\left(z',\tau-\frac{R}{c}\right)d\tau\right.\\&\left.+\frac{2}{cR^2}i\left(z',t-\frac{R}{c}\right)\right)\overline{a_R}\\&+\sin\theta\left(\frac{1}{R^3}\int_0^t i\left(z',\tau-\frac{R}{c}\right)d\tau\right.\\&\left.+\frac{1}{cR^2}i\left(z',t-\frac{R}{c}\right)+\frac{1}{c^2R}\frac{\partial i\left(z',t-\frac{R}{c}\right)}{\partial t}\right)\overline{a_\theta}\Bigg]\end{aligned} \tag{2-1}$$

$$\begin{aligned}\overline{dB}(\overline{R},t) = \frac{\mu_0 dz'}{4\pi}\sin\theta\Bigg[&\frac{1}{R^2}i\left(z',t-\frac{R}{c}\right)\\&+\frac{1}{cR}\frac{\partial i\left(z',t-\frac{R}{c}\right)}{\partial t}\Bigg]\overline{a_\phi}\end{aligned} \tag{2-2}$$

The geometry used in deriving the Equations (2-1) and (2-2) is given in Figure 2-1. For a given distribution of the current along the channel, Equations (2-1) and (2-2) can be used to calculate the fields from the lightning channel by integrating over the entire length of the channel and by using image theory to take into account the reflected waves from the ground plane. In the special case of the calculation of fields at ground level, the horizontal electric field at ground is zero (neglecting the effect of finite ground conductivity). The vertical electric field $E_z(D,\phi,z,t)$ and the horizontal magnetic field $B_\phi(D,\phi,z,t)$ at ground level, $z = 0$, and at a distance D from the base of the channel can be found using equation (2-3) and equation (2-4) respectively (e.g.,

Uman, 1985). The first, second, and the third terms in (2-3) are called the static, induction, and radiation terms, respectively. The first and second terms in equation (2-4) are called magnetostatic and radiation terms, respectively.

$$E_z(d,\phi,0,t)=\frac{1}{2\pi\epsilon_0}\int_0^h\left[\frac{2z'^2-d^2}{R^5}\int_0^t i\left(z',\tau-\frac{R}{c}\right)d\tau\right.$$

$$+\frac{2z'^2-d^2}{cR^4}i\left(z',t-\frac{R}{c}\right) \qquad \textbf{(2-3)}$$

$$\left.-\frac{d^2}{c^2R^3}\frac{\partial i\left(z',t-\frac{R}{c}\right)}{\partial t}\right]dz'$$

$$B_\phi(d,\phi,0,t)=\frac{\mu_0}{2\pi}\int_0^h\left[\frac{d}{R^3}i\left(z',t-\frac{R}{c}\right)\right. \qquad \textbf{(2-4)}$$

$$\left.+\frac{d}{cR^2}\frac{\partial i\left(z',t-\frac{R}{c}\right)}{\partial t}\right]dz'$$

If required, the fields can be corrected for the finite conductivity of the propagation path (e. g., Cooray and Lunquist, 1983) or calculated directly taking account of the ground conductivity (e.g., Sommerfeld, 1909). Uman et al. (1976) experimentally found that the rise times of the electric fields were increased, on the average, about 1 μs in propagating about 200 km over the land in Florida where the conductivity of the soil was probably between 0.001 and 0.003 S/m.

In the model for the return stroke proposed by Bruce and Golde (1941), the current at any point on the channel below the return-stroke wave front is assumed to be the same as the current at the base of the channel. Above the wave front the current is zero.

$$\begin{aligned} i(z',t) &= i(0,t) \qquad z' \le vt \\ i(z',t) &= 0 \qquad\quad z' > vt \end{aligned} \tag{2-5}$$

In the BG model there is a discontinuity in the channel current at the wavefront. The charge is deposited or neutralized only at the wavefront. From continuity equation relating the charge and the current, Nucci et al. (1990) give an expression for charge per unit length removed by the return stroke from the leader channel as

$$\rho_L(z',t) = \frac{i(0,\frac{z'}{v})}{v} \tag{2-6}$$

In the TL model (Uman and McLain, 1969), the current at the base of the channel is assumed to propagate upward with the speed of the return stroke as if the channel were a lossless transmission line (Uman and McLain, 1969). For a constant return stroke speed v, the current at any height z′ on the channel is given by

$$\begin{aligned} i(z',t) &= i(0,t-\frac{z'}{v}) \qquad z' \le vt \\ i(z',t) &= 0 \qquad\qquad\quad z' > vt \end{aligned} \tag{2-7}$$

The current at a given height is equal to the current at ground at a time z′/v earlier.

For the TL model, neglecting the propagation effects, Uman et al. (1975) derive a simple expression relating the current with the electric and magnetic radiation fields far from the channel

$$i(0,t) = -\frac{2\pi\varepsilon_0 c^2 d}{v} E_{far}(d,t+\frac{d}{c}) \tag{2-8}$$

Leteinturier et al. (1988) present an expression relating the derivative of the current and the derivative of the far field

$$\frac{di(0,t)}{dt} = -\frac{2\pi\varepsilon_0 c^2 d}{v}\frac{dE_{far}(d,t+\frac{d}{c})}{dt} \tag{2-9}$$

Equation (2-9) is the same as that obtained by taking the derivative of both sides of equation (2-8). Both the equations (2-8) and (2-9), are obtained from equation (2-3) or (2-4) by neglecting static and induction terms, since they are only a small fraction of the radiation term far from the channel, and making the approximation that D=R. The return stroke speed is assumed to be a constant. The charge discharged by the TL model along the channel is zero since the channel simply acts as a lossless transmission line for the upward propagating current wave.

Lin et al. (1980), after reviewing the simultaneous two-station measurements of return-stroke electric fields (Lin et al., 1979), proposed a return stroke model. Based on the observed characteristics of the measured fields and some reasoning, they assumed that the return stroke current at channel base is composed of three separate components: (1) an upward propagating pulse of short duration associated with the wavefront and travelling as if along a transmission line, (2) a uniform leader current which is assumed to flow even during the return-stroke phase, and (3) a corona current which result from the removal of charge stored by the leader. Lin et al. (1980) modeled the corona current as current sources distributed along the channel which propagate down the channel at the speed of light after being released by the return stroke wavefront. A double exponential waveform whose amplitude decreases exponentially with height was assumed for the corona currents. The corona current source is expressed as

$$\begin{aligned} di_c(z'',t) &= 0 \quad t < \frac{z''}{v}+t_{on} \\ di_c(z'',t) &= I_0 e^{-\frac{z''}{\lambda_c}}\left(e^{-\alpha(t-t')} - e^{-\beta(t-t')}\right)dz'' \quad t \geq \frac{z''}{v}+t_{on} \end{aligned} \tag{2-10}$$

where $1/\alpha$ and $1/\beta$ are the time constants of the double exponential function of the single corona source, I_0 is approximately the peak injected current per unit length, λ_c is the height decay

constant, and t_{on} is the zero to peak time of the breakdown pulse current. Master et al. (1981) proposed an exponential decay with height for the breakdown pulse, given by

$$i_p(z',t) = e^{-\frac{z'}{\lambda_p}} i_p(0,t-\frac{z'}{v}) \qquad \textbf{(2-11)}$$

The other two components of the currents in the Master-Uman-Lin-Standler (MULS) model are the same as those originally proposed by Lin et al. (1980). The explicit assumption of a double exponential current waveform in the MULS model allowed Rachidi and Nucci (1990) to show analytically that the corona current which discharges and travels to ground at the speed of light can be alternatively expressed as a transmission line current travelling upward with the speed of the return stroke.

In the Modified Transmission Line (MTL) model it is assumed that the return stroke current specified at ground propagates up the channel as if it were a special kind of lossy transmission line. The amplitude of the current decreases with height. In the model proposed by Dulzon and Rakov (1980), and Rakov and Dulzon (1987) the decrease of the current amplitude is assumed to be a linear function of height and in the model proposed by Nucci et al. (1988) it is assumed to be exponential. Rakov and Dulzon (1987) describe the current at a height, z′ by the expression

$$i(z',t) = (1-\frac{z'}{H})i(0,t-\frac{z'}{v}) \qquad \textbf{(2-12)}$$

where H is the assumed height of the cloud charge center. Nucci et al. (1988) describe the current at a height, z′ by the expression

$$i(z',t) = e^{-\frac{z'}{\lambda_I}} i(0,t-\frac{z'}{v}) \qquad \textbf{(2-13)}$$

where λ_I is an assumed constant. Nucci et al. (1988) assumed the return stroke speed to be constant, while Rakov and Dulzon (1987) considered both constant and exponentially decaying speed. A comparison of the modified transmission line models with various different current-attenuation factors is presented by Rakov and Dulzon (1991).

In the Travelling Current Source (TCS) model proposed by Heidler (1985), the charge on the channel is assumed to be instantaneously removed by the return stroke wave front propagating upward with a constant speed and the discharged current is assumed to propagate to ground with the speed of light.

$$\begin{aligned} i(z',t) &= i(0,t+z'/c) \qquad z' \le vt \\ i(z',t) &= 0 \qquad\qquad\quad z' > vt \end{aligned} \qquad \textbf{(2-14)}$$

The current at a given height, given by equation (2-14), is equal to the current at ground a time z'/c later.

Nucci et al. (1990) compare the fields produced, the spatial and temporal distribution of the current along the channel, and the charge removed by the BG, TL, MULS, TCS, and MTL models for an assumed channel base current. They found that the TL model is unrealistic for field calculations longer than 5 or 10 μs, and that the other four models produced overall fields which are reasonable approximations of measured natural lightning fields. However, BG and TCS models did not produce the observed distant-field zero crossing and the MTL and MULS models did not produce the magnetic hump observed after the initial peak at close range. None of the models produced the fine structure observed in the measured fields. They found that the BG model is an excellent approximation to the TCS model. The BG and the TCS models

produce larger and narrower initial field peaks than the TL, MTL, and the MULS models. Also, the ratio of the peak field derivative to the peak current derivative is nearly equal to the ratio of peak field to peak current for MTL and MULS models and equal for the TL model, while the ratio of peak field derivative to peak current derivative is about twice the ratio of peak field to peak current for the BG and TCS models. For their calculations Nucci et al. (1990) used only a single current waveshape at ground which approximates the subsequent stroke current.

Diendorfer and Uman (1990) proposed a return stroke model to avoid the physical inconsistencies of the earlier models and to give a better match between the measured and calculated fields. In the DU model the return stroke wavefront initiates an exponential discharge of the charge on the channel and the currents propagate to the ground at the speed of light. Diendorfer and Uman (1990) obtain an analytical expression relating the component current at the ground and the current at any height

$$i(z',t) = i(0,t+\frac{z'}{c}) - i(0,\frac{z'}{v}+\frac{z'}{c})e^{-(t-\frac{z'}{v})/\tau_D}, \qquad t \geq \frac{z'}{v} \tag{2-15}$$

where τ_D is the discharge time constant. The speed of the return stroke front is assumed to be a constant. Further, Diendorfer and Uman (1990) considered the channel currents to be the sum of two components, one due to a fast discharge (small discharge time constant) of stored leader charge and the other due to a slower discharge (larger discharge time constant). The DU model gives an increasing rise time for the currents with height, which is consistent with the observation of increasing risetime with height for the light intensity profile (assuming a positive correlation between these characteristics of the light intensity profile and the current profile) by Jordan and Uman (1983), whereas in other models discussed above the risetime of the current do not change with height along the channel. Diendorfer and Uman (1990) also modeled the influence of the

height of the structure on which the lightning strikes and found that the increased height of the structure increases the initial field peak.

The applicability of the Transmission Line equations (TL equations) (2-8) and (2-9) for relating the radiation peak field and peak current was investigated by Willett et al. (1988) and Willett et al. (1989) using simultaneous measurement of currents, fields, and return stroke speeds from triggered lightning at KSC in 1985 and 1987 respectively. They found that the peak fields and peak currents are linearly correlated. The majority of the electric field waveforms measured at about 5 km by Willett et al. (1988) from the triggered lightning experiment of 1985 at Kennedy Space Center (KSC) had a narrow initial spike less than 0.2 us wide superimposed on the return stroke peak field. The waveforms of natural lightning measured about 20 km away by Willett et al. (1988) with a similar measuring system had initial spikes about 0.5 us wide. Both the 5 km and 20 km propagation paths were over salt water. Any instrumentation problem was ruled out as responsible for the spikes, and it was hypothesized that the spikes were due to simultaneous upward and downward propagating current waves from the return stroke that begins at some height above the striking object, whose tip was about 20 m high above the ground. For the triggered lightning experiment done at KSC in 1987 (Willett et al., 1989), where the triggering structure was above salt water and the striking object was 5 m high, less than half of the return stroke fields had observed narrow spikes at 5 km. Willett et al. (1989) also show that the measured current and the fields are correlated for only the first 1 or 2 us after the initiation of the return strokes and hence the TL model is valid only for that time, if at all. Leteinturier et al. (1990) made simultaneous measurements of channel base current derivative and electric field derivative at 50 m for return strokes from triggered lightning at KSC in 1985 and found a linear correlation between the peak current derivative and the peak electric field derivative. Out of these, for 7 return strokes Willett et al. (1988) had simultaneous measurements of channel base

current and the electric field at 5 km. Leteinturier et al. (1990) show that there is a significant discrepancy in the average return stroke speed of 1.91×10^8 m/s calculated from equation (2-8) using the current and the electric field at 5 km and between the return stroke speed of 2.8×10^8 m/s calculated from equation (2-9) using the current derivative and the electric field derivative at 50 m. Willett et al. (1989) report a discrepancy in calculated return stroke speeds at 5.16 km, where the mean return stroke speed from current and field peak measurements (equation 2-8) is 1.62×10^8 m/s and the mean speed from current and field derivative peak measurements (equation 2-9) is 2.02×10^8 m/s. Cooray (1989) performs calculations showing the influence of near field components and propagation effects in the return stroke current parameters derived from the derivative of the field using the TL model. Cooray and Orville (1990) discuss the effect of variations in the parameters of the current profile along the channel on the electromagnetic fields.

2.5 Modeling of Continuing Currents and M Components

As mentioned earlier, after some return strokes there is a low-level current flow in the channel for many tens of milliseconds (e.g., Atlas of lightning currents, Berger, 1967). According to Malan (1954) the continuing current occurs when the cloud charge density along the path of the interstroke junction process exceeds a critical value. Brook et al. (1962) calculated the charge brought down by the continuing currents using an electrostatic model. They assumed a vertical development of the flash, successive strokes discharging charge centers at increasing height. The charge volumes were modelled as point charges. The continuing current was assumed to discharge a charge between the preceding and succeeding return-stroke charge volumes. The height of the return-stroke charge volume was determined from the photographically determined leader duration t_p below the cloud base at height h, and the total

leader duration t_e from the electric field records using the relation, $H_R = ht_e/t_p$. The charge lowered by the continuing current was obtained from the measured electric field change recorded at a distance d using the relation

$$\Delta E = \frac{1}{2\pi\epsilon_0} \frac{2Q_c H_c}{(d^2+H_c^2)^{3/2}} \qquad \textbf{(2-16)}$$

where H_c is the mid-point of the preceding and succeeding return-stroke charge volume heights. From the average continuing current charge of 12 C and the average continuing current duration of 150 ms, Brook et al. (1962) estimate the average magnitude of the continuing current as 80 A. Brook et al. (1962) hypothesize that a photographically dark current of the order of 10 A should be flowing in the channel to maintain the ionization even during the interstroke periods without detectable continuing currents. Uman and Vorshall (1968), via theoretical considerations, showed that such a dark current between strokes is not necessary to maintain the conductivity of the channel during the interstroke interval. Kitagawa et al. (1962) considered M components as due to the development of new streamers within the cloud making contact with the already existing main channel to ground.

Krehbiel et al. (1979) used a point charge (monopole) model to calculate the charge lowered by consecutive portions of a single continuing current, from fields measured simultaneously at eight stations. In this way they found that the continuing current charge volumes are more extended in space horizontally than are discrete stroke charge volumes. Krehbiel et al. (1979) found that the monopole model for continuing currents gave the best fit to the data only if the preceding interstroke field change is assumed to be existing throughout the continuing current field change, thus indicating that the continuing current process is decoupled from the interstroke process. Krehbiel et al. (1979) found that the interstroke activity often

persisted in the vicinity of earlier stroke volumes while the successive strokes and continuing currents discharged more horizontally distant regions of the cloud.

To date there is no published literature on the mathematical modeling of M component currents or charges, only the view noted above by Kitagawa et al. (1962) and the characteristics of current pulses given by Hubert et al. (1984), some of which are likely associated with M components.

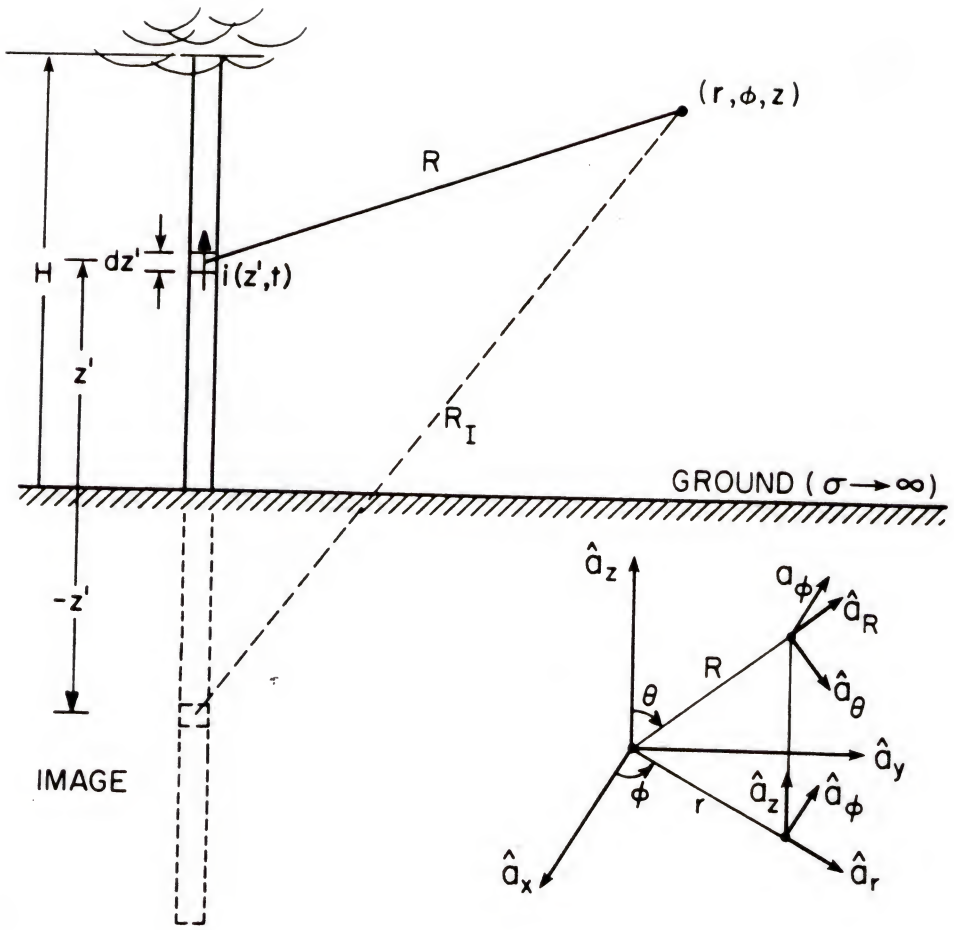

Figure 2-1. Geometry used in deriving the field equations given in equations (2-1) and (2-2).

CHAPTER 3
EXPERIMENTAL DATA USED

In this chapter the experimental data used in this dissertation are described. The natural lightning data used in the investigation of the distance between the channels within a flash and the largest return stroke within a flash are described in section 3.1. Section 3.2 presents the triggered lightning data obtained by the Sandia National Laboratories (Sandia) in the years 1990 and 1991, which are used in the investigation of the current parameters of triggered lightning. Simultaneous records of return stroke current, electric field, and return stroke speed for triggered lightning return strokes from Willett et al. (1988) and Willett et al. (1989) are presented and discussed in section 3.3. Only the data of Willett et al. (1989) are used for evaluating return stroke models, but the data and results of Willett et al. (1988) are necessary to understand fully the former.

3.1 Natural Lightning Data

The natural lightning data, primarily, electric field and TV measurements, are from negative ground flashes which occurred during 3 convective thunderstorms in July of 1979 near Tampa, Florida. A description of the measuring systems can be found in Beasley et al. (1982), Master et al. (1984), Thomson et al. (1984), and Shindo and Uman (1989). Three flat plate antennas were used to sense the derivative of the electric fields and the output of these antennas were electronically integrated to obtain the fields and then were recorded on 7 channels of an

Ampex FR-1900 instrumentation tape recorder. The electric field signals provided by two of the antennas (0.5 m^2 and 0.2 m^2 in area) had a frequency band from 0.03 Hz to 1 MHz and were recorded on four of the channels of the tape recorder in the FM mode at different gains with a resultant 6-dB bandwidth from near d.c. to 500 kHz. The third antenna (0.2 m^2 in area) provided electric field signals with a 3 dB bandwidth from 160 Hz to 2 MHz which was digitized using a Biomation 805 Digital Waveform Recorder and displayed on Textronix 555 oscilloscopes at two different gains. The digitizer was triggered by the initial portion of the return stroke waveform and the pre-trigger delay ensured that the complete waveform was obtained. The oscilloscopic traces were photographed using a camera with moving film to obtain spatially separated record of the waveforms of the return stroke electric fields. The effective 3-dB bandwidth of these records was from 160 Hz to 2 MHz. Signals from the third antenna were also recorded continuously in the direct mode on one of the channels of the tape recorder with a 3-dB bandwidth from 400 Hz to 1.5 MHz. Statistics on the return stroke electric field peaks from the above described records were published by Master et al. (1984). Since the original magnetic tapes were deteriorating, the signals were re-recorded in 1988 on new magnetic tapes using a Honeywell 101 tape recorder. The re-recorded data were used by Rakov and Uman (1990a,b,c), Rakov et al. (1990), and Thottappillil et al. (1990) to investigate the various properties of cloud-to-ground lightning flashes.

In the 1979 experiment, a network of 5 TV cameras was used to record continuously lightning flashes on video tape. The field-of-view of each TV had a resolution of about a degree, and they were placed some kilometers apart. It was possible to locate the ground strike point of the lightning by triangulation if the event were recorded by more than one TV camera. A dynamic microphone sensed thunder and recorded the signal on one channel of a strip chart recorder, which was also recording electric field signals on other channels. The distance to the

lightning channel was estimated from the time delay of thunder signals relative to the electric field signals using an average speed of sound in air of 333 m/s.

The data used in chapter 4 include simultaneous single-station wideband electric field and multiple-station TV records of 76 negative flashes (63 of them multiple-stroke flashes) analyzed previously by Rakov and Uman (1990a, b, c) and Thottappillil et al. (1990). Rakov and Uman (1990b) have presented statistics on the initial electric field peaks of return strokes for these 76 cloud-to-ground lightning flashes. They found a geometric mean (GM) value normalized to a distance of 100 km of 6.2 V/m for 63 first strokes in multiple-stroke flashes, 4.7 V/m for 13 strokes in single-stroke flashes, and 4.1 V/m for 38 subsequent strokes creating a ground termination different from that of the first stroke in the flash. The GM field peak of 232 subsequent strokes that followed a previously formed channel was 2.7 V/m. Rakov and Uman (1990b) also found that about 50 percent of their 76 flashes had multiple ground terminations, that is, spatially separate ground strike points within the flash.

3.2 Triggered Lightning Data from the Sandia National Laboratories

In the summer of 1990, personnel from the Sandia National Laboratories (Sandia) in Albuquerque, New Mexico conducted an experiment at the NASA Kennedy Space Center (KSC) to evaluate the effect of triggered lightning strikes on various metallic samples. The following summer, in 1991, Sandia conducted another experiment at Ft. McClellan, Alabama in which the response of an instrumented munitions bunker was tested by triggering lightning to it. For both years Sandia obtained excellent quality records of currents at the base of the lightning channel for most of the duration of the flashes (70 strokes in 17 flashes).

The 1990 experiment was described by Schnetzer and Fisher (1991) and Fisher and Schnetzer (1991). The lightning current was sensed by a 0.5 milliohm Current Viewing Resistor (CVR) which had a rise time of 0.16 μs (about 2.1 MHz bandwidth) inserted between the lightning strike rod and the earthing system. Signals representing the currents were sent to the recording devices through fiber-optic links. Return stroke currents were directly digitized by a LeCroy 9400A oscilloscope with a sampling interval of 80 ns to form record lengths of 200 μs. The trigger level of the return stroke recording channel was set to 1 kA with a pre-trigger delay of about 10 μs. The sensitivity of the digitizer was adjusted to record up to 100 kA without saturation. Another digitizer sampled current for the whole flash with a sampling interval of 40 μs and an upper amplitude limit of about 1 kA. These low level currents, below 1 kA, were additionally recorded at two different gains on the FM channels of a tape recorder with overall bandwidth of D.C. to 500 kHz. The minimum detectable signal in the high gain channel is about 4 A because of inherent noise. Return stroke records with a sampling interval of 50 ns, provided by KSC, were also available for all the flashes for which Sandia had low level current records. The KSC channel current measuring system employed a shunt to sense the current and was placed below the CVR employed by Sandia on the same lightning strike rod. The trigger level of the KSC system was at about 5 kA. The mean difference between the peak return-stroke currents measured by Sandia and KSC was less than 10% of the peak value.

For the triggered lightning at Ft. McClellan, Alabama in 1991, the lightning current was sensed by a low impedance CVR with an insertion resistance of 1 milliohm and a rise time of just under 60 ns. The sensed current signal was transmitted to the digitizers and tape recorders via fiber optic links. A 6-MHz low pass filter was used at the output of each of the fiber optic receivers to reduce the noise. The return stroke currents were directly digitized with a sampling interval of 20 ns, and the sensitivity of the LeCroy 9400A digitizing oscilloscope was adjusted

to record a maximum current of 48 kA without saturation. The trigger level was set at 2 kA. Low level currents below 2 kA were recorded at two different gains on the FM channels of a tape recorder with overall bandwidth of D.C. to 500 kHz. The minimum detectable signal amplitude in the high gain channel was about 4 A because of the noise.

A video recording system and 16-mm filming system were employed both at KSC and at Ft. McClellan. At KSC the video recording system was employed to monitor one meter above and one meter below the lightning strike point. At Ft. McClellan at least four video records from various angles were made of each triggered event. Time resolution was limited to successive video frames, which was about 35 ms for both sites. The 16-mm filming system employed at KSC covered about 20 m of the lower portion of the channel and had a shutter speed of 1/1000 s and framing rate of 200 fps giving a time resolution of about 5 ms. At Ft. McClellan the 16-mm filming system had a better time resolution of about 3 ms.

For four of the flashes from KSC for which there were current records, streak camera images of the channel were obtained by the University of Florida, in cooperation with Chubu University, Japan. The streak camera images had a time resolution of about 10 μs and were taken from a distance of about 2.2 km.

3.3 Triggered Lightning Data of Willett et al. (1988, 1989) from the NASA Kennedy Space Center

Simultaneous records of currents, electric fields, and return stroke speeds were obtained from the triggered lightning experiment at KSC in 1985 and are described by Willett et al. (1988). A major objective of the experiment was to verify the Transmission Line (TL) model of the lightning return stroke (described in section 2.4). The currents near the channel base were measured using coaxial shunts with rise times less than 20 ns and recorded with digitizers

sampling every 0.01 μs or 0.1 μs. Oscilloscope photographs yielding an overall bandwidth of 1 MHz and FM analog tape recorder with a 500-kHz bandwidth were also used to record the currents. The vertical electric field, E, at 5.15 km was recorded using flat plate antennas, one of whose outputs was connected through an analog integrator with a 160-ns rise time and a 1-ms decay time to a digitizer sampling every 0.1 μs. Another output fed a digitizer sampling at every 0.01 μs through a wideband amplifier to record the time derivative of the field, dE/dt, with a bandwidth of better than 30 MHz. The requirements of other experiments in the 1985 triggered lightning campaign necessitated a complex triggering structure. The vertical metallic rod directing current to the current sensors was mounted on an elevated grounded platform above a Faraday cage at a height of about 5 m from ground. Above the rod was suspended a 12 m long metal cylinder, electrically isolated from ground but capable of being grounded by shorting out the 30 cm spark gap between the cylinder and the rod either by hard-wiring prior to the lightning or sparkover during a lightning discharge. The top of the lightning strike object was about 20 m above ground.

Willett et al. (1988) observed a narrow initial spike less than 0.2 μs wide in the electric field waveforms, but did not find a similar narrow spike in the current waveforms. The existence of these narrow spikes, without corresponding narrow spikes in the current waveform can not be modelled by a single upward-moving current pulse (TL model), even if the current waveform and speed are allowed to vary with time in a reasonable manner. Therefore, to resolve this discrepancy, according to the TL model, between the electric field and current waveforms, Willett et al. (1988) invoked the explanation proposed by Weidman et al. (1986) by which the return stroke may begin at a junction point between the downward propagating leader and the upward connecting discharge a few tens of meters above ground and propagate in both directions. This bi-directional development of the return stroke last only for a fraction of a microsecond and

enhances the initial electric field, producing the narrow spike. On the strength of this argument, Willett et al. (1988) removed the initial narrow spikes from his electric field waveform before testing the TL model. In Table 2 of Willett et al. (1988), sixteen out of seventeen electric field peaks are so modified. The correlation between the field peak and the current peak improved slightly but not statistically significantly when modified field peaks were used instead of the unmodified field peaks (Table 3 of Willett et al., 1988), presumably lending credence to the process of removing the spikes if the TL model is valid.

In 1987 at the Kennedy Space Center (KSC) simultaneous records of current (I), time derivative of current (dI/dt), electric field (E), and time derivative of electric field (dE/dt) were obtained by Willett et al. (1989) for 28 return strokes from 7 triggered flashes. Eighteen of the return strokes had return stroke speed (v) measurements. The triggering was done by shooting a rocket with a trailing wire from a floating platform in shallow brackish water about 30 m offshore in Mosquito Lagoon. The tip of the lightning strike rod was about 5 m high above the water level. A complete description of the experimental setup and data can be found in Willett et al. (1989).

The currents from the return strokes that attach to the lightning rod were measured with a coaxial shunt and the current derivatives were measured with a toroidal inductive sensor. Both the I and dI/dt were digitized directly and recorded with 10-ns time resolution and absolute amplitude error of $\pm 10\%$ as described by Leteinturier et al. (1990). Return stroke speeds averaged over 2-D channel lengths of 457-625 m were measured with a high speed streak camera from a distance of 2.2 km with errors ranging from ± 15 to $\pm 25\%$, as described by Idone and Orville (1982). Electric fields and field derivatives were recorded at a distance of 5.16 km from the triggering site, where the propagation path was almost entirely over brackish water, as

described by Willett et al. (1988). The time resolution of the digital records of E and dE/dt were 100 ns and 10 ns respectively, with errors in amplitude of $\pm 5\%$.

In the 1987 data presented by Willett et al. (1989), 11 of the 28 return stroke electric field waveforms obtained by integrating the electric field derivative records had narrow initial spikes of about 0.1 μs in width, somewhat similar to those observed by Willett et al. (1988). These were hypothesized by Willett et al. (1989), following Willett et al. (1988), to be evidence of an upward-connecting discharge rising to meet the downward propagating dart leader with return stroke starting at the junction point and propagating in both directions. The electric field waveforms obtained by electronic integration did not show these spikes presumably due to undersampling (0.1 μs sampling interval) and insufficient bandwidth (approximately 5 MHz). The data used in chapters 5,6, and 7 are the simultaneous records from Willett et al. (1989) of current and numerically integrated electric field derivative for 18 return strokes for which speed measurements are available and the current records for the remaining 10 return strokes for which there were no speed measurements. Eleven of the 28 return stroke electric fields had the very narrow peaks, and the average amplitude of these spikes deduced from Table 1 of Willett et al. (1989) were about 5 V/m (standard deviation = 7 V/m) or on the average about 5% of the peak value. The measured return stroke speeds were taken from Table 1 of Willett et al. (1989). Relevant data for this dissertation are presented in Table 3-1, which is adapted from Table 1 of Willett et al. (1989). The first column of Table 3-1 gives the stroke identification, the first 4 digits indicating the flash and the last digit the stroke number. The peak values of the return stroke currents are given in column 2, followed by the measured peak derivative values of the return stroke currents in column 3. The fourth column gives the measured electric field peak (numerically integrated dE/dt), E_p, at 5.16 km before removing the narrow spikes as described before, while the fifth column gives the values of the modified electric field peaks after removing

the narrow spikes, if present. The peak values of the measured electric field derivatives at 5.16 km are given in sixth column. The measured 2-D speeds of the return strokes are given in the seventh column. The estimated error in the speed determinations and the channel heights over which the speeds were determined are given in column eight and nine respectively.

Table 3-1. Data from 1987 triggered lightning return strokes adapted from Willett et al. (1989).

Flash_Stroke 1	i_p, kA 2	$(di/dt)_p$, kA/μs 3	E_p at 5.16 km, V/m 4	E_p' V/m 5	$(dE/dt)_p$ at 5.16 km, V/m/μs 6	v 10^8 m/s 7	Error in v, % 8	H, m 9
July 30								
8705_1	8.2	97.	76.	61.	840.	1.8	25	558
8705_3	7.7	108.	64.	46.	930.	1.6	25	558
8705_5	10.3	141.	80.	71.	940.	1.7	25	558
8705_6	11.6	157.	84.	76.	990.	1.9	25	558
July 31								
8715_2	7.4	76.	46.	46.	580.	-	-	-
8715_3	11.2	114.	70.	70.	1040.	-	-	-
8715_4	10.1	103.	63.	63.	900.	-	-	-
8715_6	12.4	119.	72.	72.	950.	-	-	-
8715_7	19.9	216.	137.	137.	1730.	-	-	-
8715_8	9.0	70.	52.	52.	640.	-	-	-
8715_9	33.	260.	206.	206.	1720.	1.4	20	625
8715_10	15.6	108.	88.	88.	820.	1.4	20	625
8717_3	7.0	119.	53.	40.	1050.	-	-	-
8717_5	9.1	162.	75.	57.	1270.	-	-	-
August 19								
8725_1	20.3	87.	109.	108.	690.	1.6	25	609
8725_2	16.7	110.	84.	84.	840.	1.5	25	609
8725_3	43.0	254.	196.	196.	1680.	1.7	20	609
8725_4	7.6	67.	38.	36.	570.	-	-	-
8725_5	11.7	107.	60.	60.	910.	1.4	25	609
8726_1	$\geq$38.*	187.	188.	188.	1180.	1.5	15	595
8726_2	26.9	123.	174.	157.	1060.	1.2	15	595
8726_3	16.4	140.	95.	95.	1160.	1.4	15	595
8726_4	22.4	123.	143.	134.	850.	1.4	20	595
8726_5	24.8	153.	140.	140.	1190.	-	-	-
8728_10	26.9	140.	144.	144.	1010.	1.4	25	486
8728_11	16.1	97.	88.	88.	740.	1.4	25	486
8732_1	18.0	140.	126.	108.	980.	1.5	20	457
8732_2	16.8	113.	97.	97.	1000.	1.6	20	457

CHAPTER 4
ANALYSIS OF EXPERIMENTAL DATA

In this chapter the properties of cloud-to-ground lightning flashes derived from the data described in section 3.1 and section 3.2 are presented.

4.1 Natural Lightning

In chapter 2 it was noted that normally the first return stroke in natural cloud-to-ground lightning is the largest in terms of the luminosity, initial return stroke peak current, and initial electric field peak. But as also noted in chapter 2, there are instances in which it is one of the subsequent return stroke that is the largest in a flash. Further, some of the subsequent strokes take a spatially separate channel from the first stroke, as further noted in chapter 2. In this section we present detailed data on subsequent strokes whose electric field peaks are greater than the first-stroke peak in the same flash. To compare with the electric field measurements, data on downward lightning currents directly measured by Berger (Atlas of Lightning Currents, Berger, 1967) in Switzerland are analyzed and the properties of subsequent-stroke current peaks whose values exceed those of the first stroke in the flash are presented. The results are of particular interest in that they both illustrate an aspect of lightning flash physics not previously explored and are inconsistent with the implication of present lightning protection standards that the first stroke is always the greatest within a flash. Additionally, statistics on the distance

between the spatially separate channels in both single-stroke and multiple-stroke flashes having multiple terminations on ground are given.

The data used in this study, a description of the measuring system, and the processing of the tape-recorded data are described in section 3.1. A new stroke channel is defined as a channel having a ground contact point spatially separate from the ground contact point of the previously-formed stroke channel within the flash, and no attempt is made to distinguish between "new channel" and "new termination on ground" as they were defined by Rakov and Uman (1990a, p. 5459). Following Rakov and Uman (1990a), a sequence of strokes is considered to arise from a single flash if each stroke occurs within 500 ms of the previous one. The initial electric field peak, the duration of the previous interstroke interval, and the leader duration were measured in the manner described by Rakov and Uman (1990a-c).

4.1.1 Subsequent-Stroke Peak Greater than the First-Stroke Peak

For the analysis of subsequent strokes whose peak fields exceeding those of the first strokes in the flash, we studied 46 multiple-stroke flashes from the Tampa data base, for which a location of each ground termination for all the strokes was available via multiple-station TV records and thunder ranging. Often there was redundant information regarding each channel location. The distance from the electric field antenna to the flashes varied from 3.7 km to 11 km. To exclude the distance dependence the measured electric field peaks are normalized, via the inverse-distance dependence, to an arbitrary distance, chosen as 100 km.

Of the 46 multiple-stroke flashes referred to above, 15 flashes (33 percent) had one to five subsequent strokes with electric field peaks greater than the first stroke peak of the flash. These larger-field-peak subsequent strokes were further examined as to whether they occurred along the

first-stroke channel or a different channel to ground. Nine of the 15 flashes had subsequent strokes with field peak greater than that of the first stroke, that followed the same channel as the first stroke only, 5 flashes had greater subsequent strokes that followed a different channel to ground, and one flash had subsequent strokes with greater peaks that were associated with both the first-stroke channel and a different channel. The breakdown of stroke count is as follows: 13 strokes (in 10 flashes) followed the same channel as the first stroke and 12 strokes (in 6 flashes, one of which appeared also in the previous category) followed a channel different from the first-stroke channel. For this last group of 12 strokes along channels other than the first-stroke channel, 6 strokes created new channels to ground and the remaining 6 strokes followed a previously-formed channel.

Figures 4-1 to 4.4 give histograms of subsequent stroke properties. In all the histograms, the three categories of subsequent strokes with field peaks greater than the first stroke field peak of the flash are shown with different shading. The unshaded data represent the remainder of the subsequent strokes from the 46 multiple-stroke flashes. Figure 4-1 gives the histogram of the initial electric field peak, Figure 4-2 the histogram of the ratio of subsequent stroke field peak to the first stroke peak, Figure 4-3 the histogram of the interstroke interval durations, and Figure 4-4 the histogram of subsequent leader durations. None of the subsequent strokes with field peak exceeding the first-stroke peak in any category had a preceding interstroke interval shorter than 35 ms. All the distributions in Figures 4-1 to 4-4 appear approximately log-normal with geometric mean values being given in Table 4-1. Thirteen subsequent strokes with greater peaks in the first group (row 1 of Table 4-1) have a GM field peak of 7.7 V/m which is 1.2 times greater than the GM of 6.3 V/m for the first-stroke field peaks. The GM interstroke interval immediately prior to the subsequent strokes with greater peaks is 98 ms. Three of the interstroke intervals contained long continuing currents. For 8 subsequent strokes for which the leader

durations could be measured, the GM leader duration was 0.55 ms. Row 2 of Table 4-1 gives the information on 6 subsequent strokes with greater peaks that created a new termination on ground. The GM peak value of 5.9 V/m for these strokes was 1.7 times the first stroke peak GM of 3.5 V/m. The preceding interstroke intervals had a GM of 130 ms and the durations of 5 leaders had a GM of 15 ms. The third row gives the information on 6 subsequent strokes with greater peaks following a previously formed channel with ground termination different from that of the first stroke. The GM peak value of 3.9 V/m is 1.6 times the first-stroke GM peak value of 2.5 V/m. The GM of the preceding interstroke interval was 86 ms and the GM duration of 4 leaders was 2.4 ms. In the fourth row all the subsequent strokes with greater peaks (Rows 1, 2, and 3) are grouped together. The fifth row of Table 4-1 gives the values for all the subsequent strokes from the 46 multiple-stroke flashes while the sixth row gives values for only those subsequent strokes that follow a previously-formed channel.

Subsequent-stroke current peak greater than the first-stroke current peak: Five (15 percent) of the 33 negative downward multiple-stroke flashes striking instrumented towers in Switzerland (Atlas of lightning currents, Berger, 1967), contained one or two subsequent strokes with initial return stroke peak currents greater than their respective first-stroke peak currents. There were 8 subsequent strokes with greater current peaks than the first stroke peak (7 percent of all 115 subsequent strokes in the 33 flashes mentioned above), all of them necessarily following the same channel to the instrumented tower as the first stroke. The subsequent current peaks greater than the first had a GM of 26 kA, which is about 1.2 times the GM of the first stroke current peaks of those flashes and about 2.2 times the GM for all the 115 subsequent stroke current peaks. The GM of the immediately preceding interstroke interval for the subsequent strokes with greater peaks was 69 ms, about 1.6 times the 43 ms GM for all the interstroke intervals.

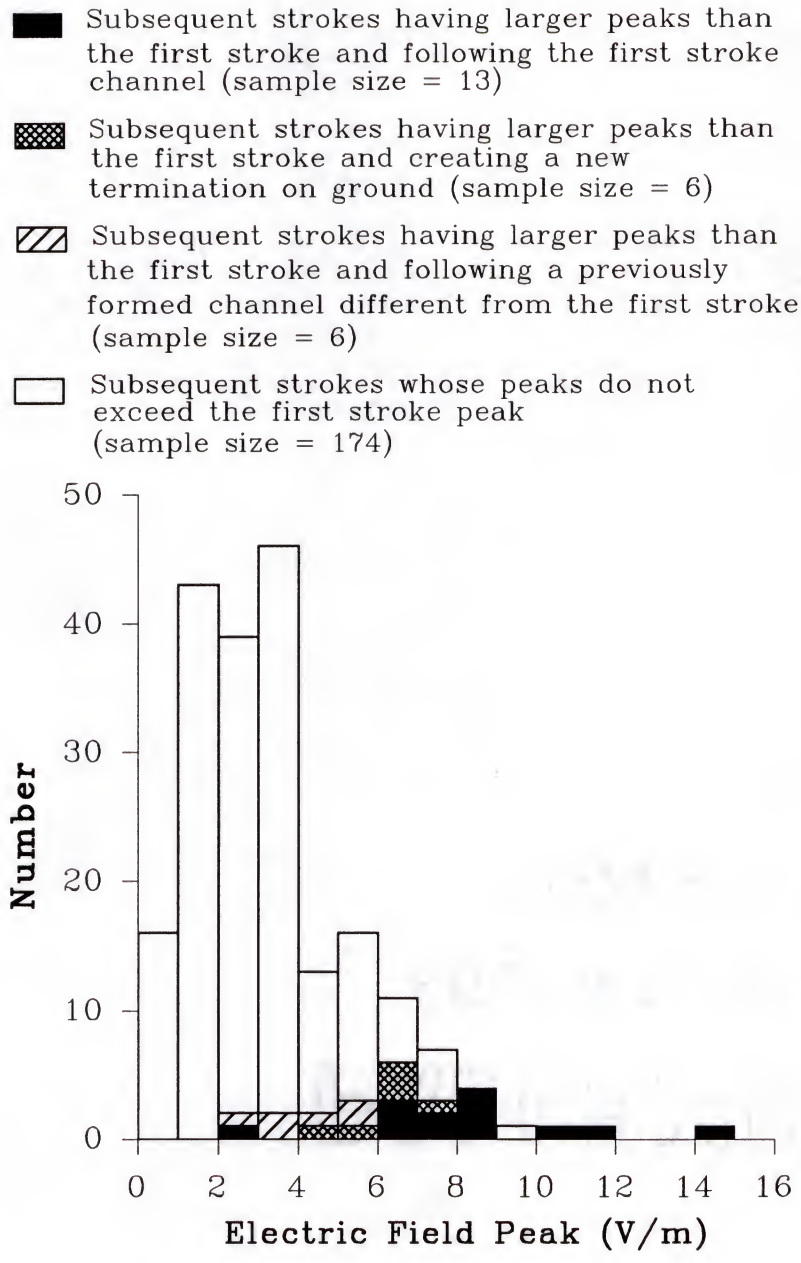
Subsequent strokes having larger peaks than the first stroke and following the first stroke channel (sample size = 13)
Subsequent strokes having larger peaks than the first stroke and creating a new termination on ground (sample size = 6)
Subsequent strokes having larger peaks than the first stroke and following a previously formed channel different from the first stroke (sample size = 6)
Subsequent strokes whose peaks do not exceed the first stroke peak (sample size = 174)
Number
50
40
30
20
10
0
0
2
4
6
8
10
12
14
16
Electric Field Peak (V/m)

Figure 4-1. Histogram of subsequent-stroke initial electric field peak for 46 natural lightning flashes recorded near Tampa, Florida.

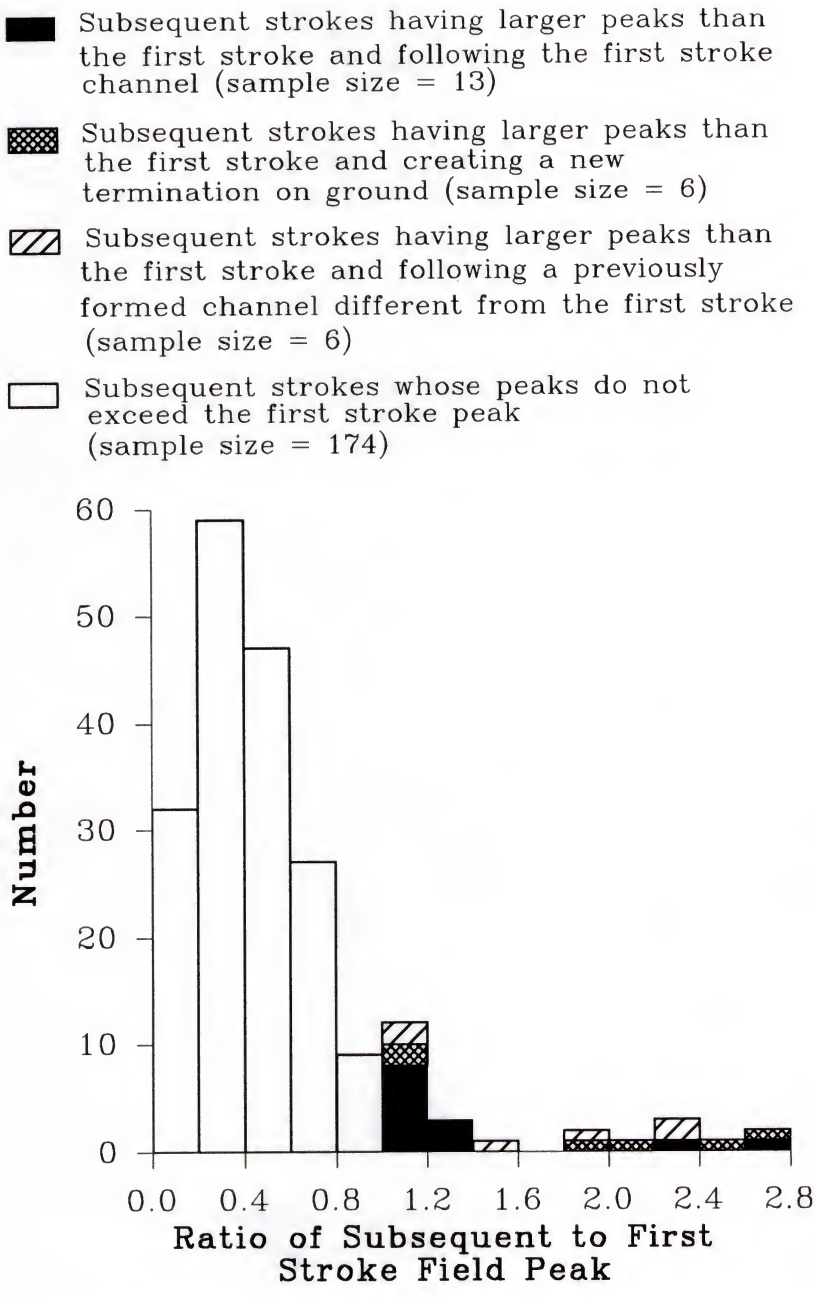
Subsequent strokes having larger peaks than the first stroke and following the first stroke channel (sample size = 13)
Subsequent strokes having larger peaks than the first stroke and creating a new termination on ground (sample size = 6)
Subsequent strokes having larger peaks than the first stroke and following a previously formed channel different from the first stroke (sample size = 6)
Subsequent strokes whose peaks do not exceed the first stroke peak (sample size = 174)
Number
60
50
40
30
20
10
0
0.0
0.4
0.8
1.2
1.6
2.0
2.4
2.8
Ratio of Subsequent to First Stroke Field Peak

Figure 4-2. Histogram of the ratio of subsequent-stroke field peak to the first stroke field peak.

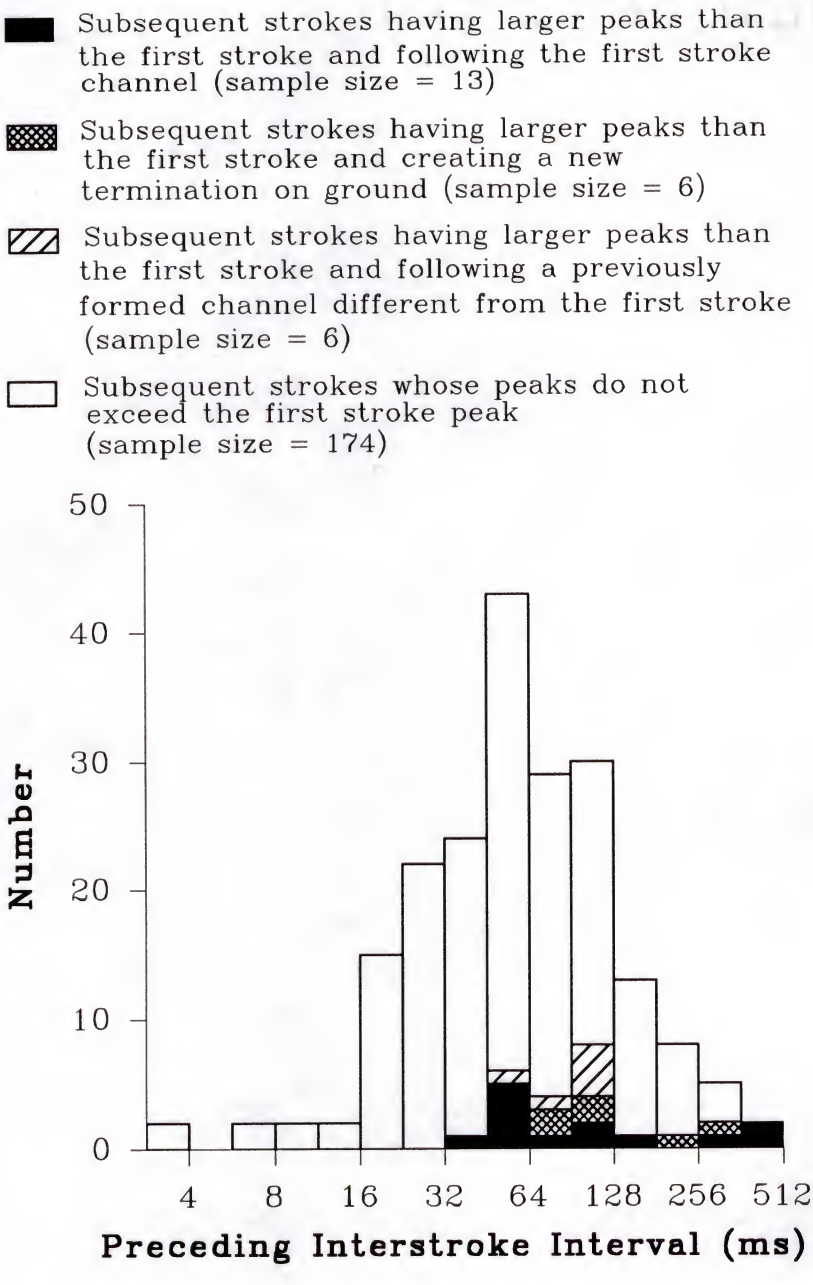
Subsequent strokes having larger peaks than the first stroke and following the first stroke channel (sample size = 13)
Subsequent strokes having larger peaks than the first stroke and creating a new termination on ground (sample size = 6)
Subsequent strokes having larger peaks than the first stroke and following a previously formed channel different from the first stroke (sample size = 6)
Subsequent strokes whose peaks do not exceed the first stroke peak (sample size = 174)
Number
50
40
30
20
10
0
4
8
16
32
64
128
256
512
Preceding Interstroke Interval (ms)

Figure 4-3. Histogram of the interstroke interval duration.

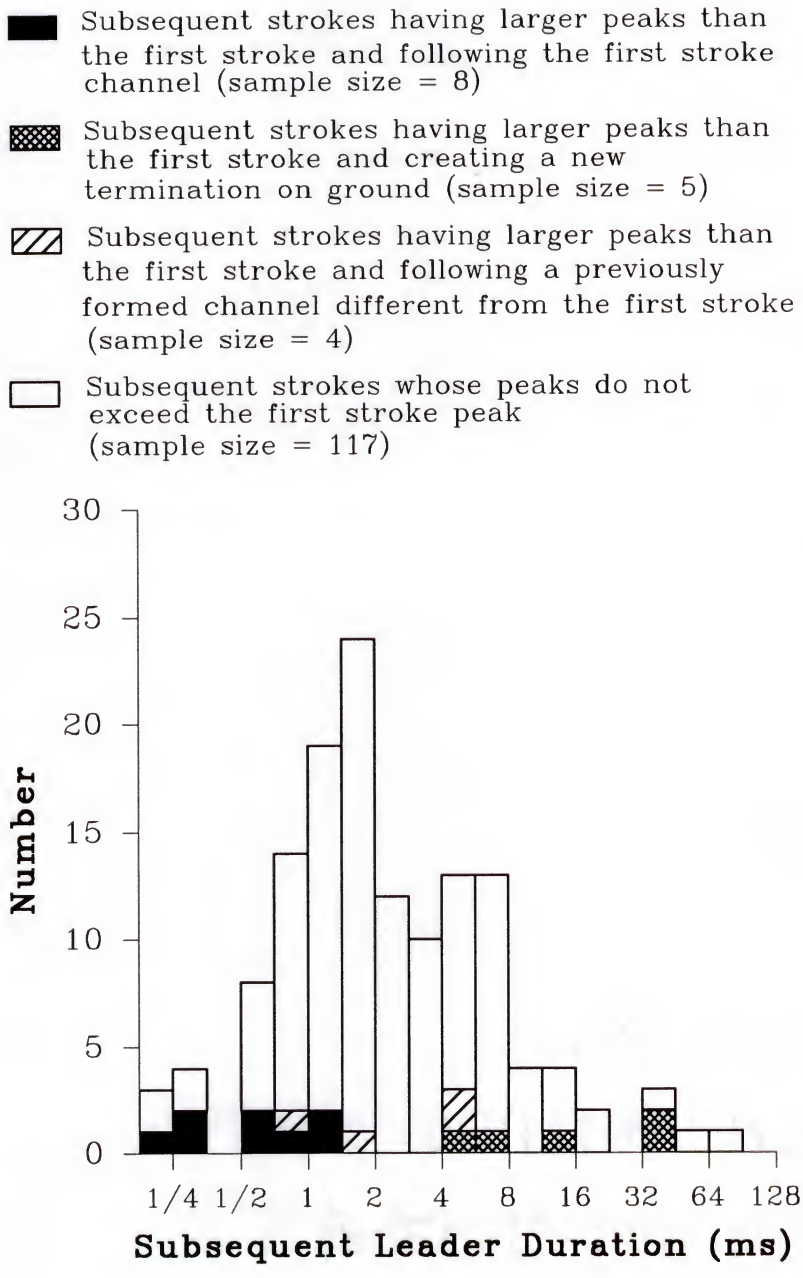
Subsequent strokes having larger peaks than the first stroke and following the first stroke channel (sample size = 8)
Subsequent strokes having larger peaks than the first stroke and creating a new termination on ground (sample size = 5)
Subsequent strokes having larger peaks than the first stroke and following a previously formed channel different from the first stroke (sample size = 4)
Subsequent strokes whose peaks do not exceed the first stroke peak (sample size = 117)
Number
30
25
20
15
10
5
0
1/4
1/2
1
2
4
8
16
32
64
128
Subsequent Leader Duration (ms)

Figure 4-4. Histogram of subsequent leader duration.

Table 4-1. Geometric mean values for distributions shown in Figure 4-1 to 4-4.

Row	Chararacterization of subsequent strokes having peak fields greater than the first	Subsequent stroke field peak, V/m	Ratio of subseq. to first stroke field peak	Preceding interstroke interval, ms	Leader duration, ms
1	Strokes in the same channel as the first stroke	7.7 (13)	1.2	98 (13)	0.55 (8)
2	Strokes creating a new termination on ground	5.9 (6)	1.7	130 (6)	15 (5)
3	Strokes following a previously-formed channel but different from the first-stroke channel	3.9 (6)	1.6	86 (6)	2.4 (4)
4	Total strokes: Rows 1, 2, and 3	6.1 (25)	1.5	101 (25)	2.0 (17)
	Characterization of all subsequent strokes regardless of their peak fields				
5	All strokes in 46 flashes without selection	2.7 (199)	0.42	57 (199)	2.3 (135)
6	All strokes following a previously formed channel	2.6 (176)	0.39	53 (176)	1.8 (117)

Notes: The numbers given in the parentheses are the sample sizes.

4.1.2 Spatial Separation of the Flash Ground Terminations

The distance between the multiple channels of a flash has been measured in 22 single-stroke and multiple-stroke ground flashes, and the results are presented in Figure 4-5. One single-stroke flash had two channels to ground (apparently due to a multi-grounded stepped leader), and four multiple-stroke flashes with no subsequent strokes creating a new channel had first strokes with two channels to ground (each apparently produced by a multi-grounded leader). Seventeen other multiple-stroke flashes had multiple channel terminations on ground associated with different strokes, that is the channels created by different leaders. Two of these 17 flashes also had double channels to ground, apparently associated with a multi-grounded stepped leader and a multi-grounded dart-stepped leader. Thus, there were 7 strokes with double channels produced by individual multi-grounded leaders in 7 flashes. Data for those are shown shaded in the histogram of Figure 4-5. Up to 4 different channels were observed in one flash. The distance between all possible pairs of channels within a flash were measured. For example, in a flash with three channels the distances between the first and second channel, second and third channel, and the first and third channel were measured. The distribution of the distance between the channels shown in Figure 4-5 appears approximately log-normal. The GM distance between the channels was 1.7 km for 33 distance measurements. The GM distance between the different channels associated with the same stroke (data shown shaded in Figure 4-5) was also 1.7 km. The minimum and the maximum distances measured between the channels in a flash were 0.3 km and 7.3 km, respectively.

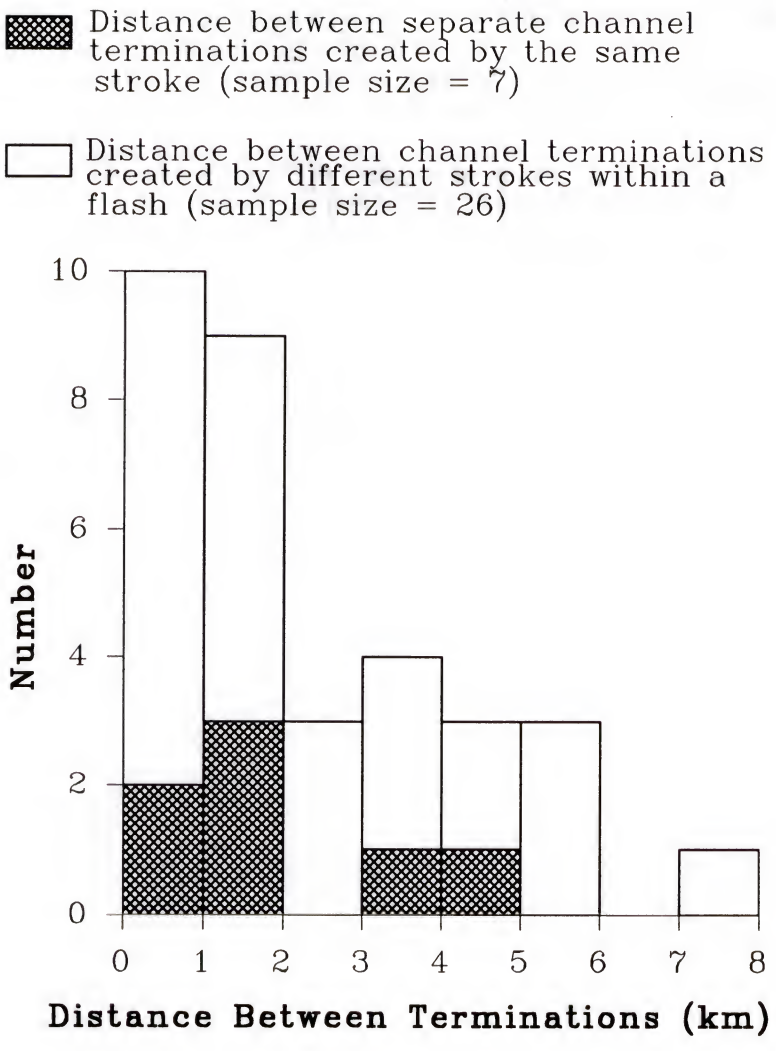
Distance between separate channel terminations created by the same stroke (sample size = 7)
Distance between channel terminations created by different strokes within a flash (sample size = 26)
Number
10
8
6
4
2
0
0 1 2 3 4 5 6 7 8
Distance Between Terminations (km)

Figure 4-5. Histogram of the distance between the multiple terminations of 22 individual ground flashes recorded near Tampa, Florida.

4.1.3 Discussion

The first-stroke GM field peak value of 6.3 V/m for the flashes which have subsequent-stroke peaks higher than the first-stroke peaks following the same channel to ground is near the GM peak value of 6.4 V/m for the first strokes in the 46 multiple-stroke flashes (6.2 V/m for the first strokes in 63 multiple-stroke flashes in Rakov and Uman, (1990a), implying that the first strokes are more or less typical. The subsequent stroke peaks greater than the first in the first-stroke channel have a GM value of 7.7 V/m, about 1.2 times greater than the first-stroke GM value of multiple-stroke flashes and about 3 times greater than the 2.6 V/m GM peak value of all the subsequent strokes following a previously- formed channel from the 46 flashes (2.7 V/m for 63 flashes in (Rakov and Uman, 1990a). This result is similar to that from the Swiss current data in which the GM of the subsequent-stroke current peaks greater than the first is 1.2 times greater than the GM of the first-stroke peaks of those 5 flashes and 2.2 times the GM of all the 115 subsequent-stroke current peaks. In our data, the interstroke interval immediately prior to larger subsequent strokes in the first-stroke channel have a GM value of 98 ms which is about 1.7 times greater than the GM value of 57 ms for all the 199 interstroke intervals. Similarly, in the Swiss current data the GM of the interstroke interval of 69 ms, preceding the larger subsequent strokes, is 1.6 times the GM (43 ms) for the interstroke intervals of all the subsequent strokes, although the interstroke interval values in the current data are appreciably smaller than the interstroke interval values in our data set. The shorter leader durations (GM of 0.55 ms) for the larger subsequent strokes following the same channel as the first stroke, compared to the leader durations (GM of 1.8 ms) for all 117 subsequent strokes in a previously formed channel probably implies a significantly faster leader for those larger subsequent strokes.

For larger subsequent strokes initiating a separate channel to ground, the first-stroke GM field peak of 3.5 V/m is only about half of the GM (6.2 V/m) for first strokes in multiple-stroke flashes, and about 75 percent of the GM (4.7 V/m) for first strokes in single-stroke flashes (Rakov and Uman, 1990a), implying that these first strokes are unusual and that their smallness may in some way be related to the fact that a large subsequent stroke (GM 5.9 V/m), not too dissimilar from a typical first stroke, will follow along a separate channel.

The first stroke GM field peak value of 2.5 V/m of the three flashes with larger subsequent strokes following a previously-formed channel different from the first-stroke channel is smaller than that for the first strokes of flashes in any of the three categories. In two of these flashes the second stroke forms a new channel whose field peak is larger than the first-stroke peak. These two flashes have also been included in category 2 of Table 1 and are discussed in the previous paragraph. In one flash the larger third stroke went along the second-stroke channel, in the other, larger strokes of order four, five and six went along the third-stroke channel, different from the second-stroke channel. For the third flash, whose first-stroke peak was 2.7 V/m, there is also a second stroke following a separate channel, but it is smaller than the first stroke. The third stroke is larger than the first and propagates along the second-stroke channel.

The results of the analysis presented above can be summarized as follows.

1. Of the 46 multiple-stroke flashes, 15 flashes (33 percent) had at least one subsequent stroke, whose initial electric field peak was greater than that of the first return stroke. This relatively large percentage of flashes containing larger subsequent strokes does not allow us to consider them as rare or exceptional.

2. Subsequent strokes with larger field peaks were observed both in the first-stroke channel (13 strokes) and in a different channel (12 strokes). For the last group of 12 strokes, 6

strokes created new channels to ground and the remaining 6 strokes followed a previously-formed channel.

3. Subsequent strokes with larger field peaks which followed the same channel as the first stroke were initiated by relatively fast leaders as inferred from the leader durations, the latter being more than 3 times shorter than for all our leaders traversing previously-formed channels. The larger subsequent strokes, both in the first-stroke channel and in a different channel, were preceded by relatively long interstroke intervals, never shorter than 35 ms.

4. Many features of larger subsequent strokes observed in Florida electric field records are similar to those found in current records from Switzerland.

5. TV-located multiple channel terminations on ground within the flash were separated by 0.3 to 7.3 km with a geometric mean separation distance of 1.7 km. In view of our observation in Florida that about a half of ground flashes have multiple channels, this may bear a great impact to the lightning protection concept.

The return-stroke current models reviewed in section 2.4 are generally applicable to the subsequent strokes and not to the first strokes. In the preceding analysis of natural lightning return strokes it was found that 33% of the flashes had a subsequent stroke that had the largest electric field peak, and hence possibly the largest current peak, in the flash. These larger-than-first subsequent strokes are larger than the first strokes of multiple stroke flashes by about 20%. Hence modeling of the subsequent return strokes is important in the context of lightning protection studies which are concerned mostly with the largest stroke in a flash. Chapters 5, 6, and 7 deal with the various aspects of the return stroke modeling applicable to the subsequent return strokes.

4.2 Triggered Lightning

The triggered lightning data obtained by the Sandia National Laboratories and made available to the University of Florida for analysis are described in section 3.2. The analysis of the data and the results pertinent to the later discussion of return stroke modeling in chapters 5, 6, and 7 and to the modeling of M components and continuing current in chapter 8 are presented in the following sections.

4.2.1 Return Stroke Current Parameters

Directly digitized current records described in section 3.2 are used in determining the return stroke current parameters. Two types of digital records, with 50 ns sampling interval at KSC and with 20 ns sampling interval at Ft. McClellan, are used. Thirty-four return strokes from the KSC experiment and 37 return strokes from the Ft. McClellan experiment were used in the analysis of current waveform parameters. Examples of return stroke current waveforms are shown in Figures 4-6 to 4-8. Figures 4-6a, 4-7a, and 4-8a show the waveforms on a 50-μs scale and Figures 4-6b, 4-7b, and 4-8b show the front portion of the waveforms on an expanded scale. The return stroke shown in Figure 4-6 (9107_3) has a faster rate-of-rise of current at the beginning than the rate-of-rise near the peak. The return stroke in Figure 4-7 (9107_1) has a slow rate-of-rise of current at the beginning and a fast rate-of-rise of current near the peak. In Figure 4-8, the return stroke (9113_4) has a slowly-rising current ramp of about 0.2 μs duration at the beginning and thereafter a rapid rise to peak.

Distributions of the peak value of the return stroke current and the time duration between the 10% and the 90% of the peak amplitude intercepts (10-90% rise time) on the return stroke

wavefront are presented in the form of histograms in Figures 4-9 and 4-10, respectively. In both figures, data from KSC are shown shaded and data from Ft. McClellan are shown unshaded. The distributions are approximately log-normal. The sample size and the geometric mean (GM) for both KSC and Ft. McClellan data are shown separately and together on Figures 4-9 and 4-10. The overall GM of the peak currents is 11 kA, and the overall GM for the 10-90% rise time is 0.37 μs.

Figure 4-11 is a scatter plot of the return-stroke peak current against the 10 to 90% rise time of the return strokes. The dark circles represent the data from KSC and the hollow circles represent the data from Ft. McClellan. In the figure, an overall tendency for the larger return-stroke rise times (10 to 90%) to be associated with smaller return-stroke peaks, can be seen. Most of the larger rise-times and smaller peaks are from KSC.

4.2.2 Interstroke Intervals, Continuing Currents, and M Components

The overall current record of a 10 stroke flash (following the so-called wire-burn stage) from KSC is shown in Figure 4-12. The return strokes are numbered and the saturation level of about 1 kA is shown. The current pulses occurring between the return strokes and superimposed on the continuing currents are referred to as M-current pulses. For this flash, all of the return strokes and six largest M-current pulses were correlated with the corresponding optical images in the streak camera records, confirming that the current pulses during continuing currents we identified as due to optical M-components were indeed so. In Figure 4-12, before each return stroke there is a small time interval when the current measured at the channel base is zero (within the amplitude resolution of about 4 A). The portion of the flash between the vertical arrows in Figure 4-12 is shown in Figure 4-13 on an expanded scale, which shows the

eighth return stroke followed by a continuing current of about 30 A and two M-current pulses. M-current pulse M_2, which saturates at about 1 kA in the current record, is identifiable as an M-component in the streak camera records. The return stroke current in Figure 4-13 (peak = 5.8 kA) has a 10-90% rise time of 1.4 μs which is about two orders of magnitude less than the 10-90% rise time of the succeeding M-currents shown in the Figure. An example of an M-current waveform, which has an amplitude of about 800 A above the continuing current level of about 1 kA and a 10-90% rise time of about 0.5 ms is given in Figure 4-14, from a flash recorded at Ft. McClellan.

The distributions of the time interval between return strokes (interstroke interval), the time from the start of the return stroke to the time when current becomes zero (stroke duration including the continuing current), the interstroke interval just preceding a return stroke where there is no detectable current flow (zero-current interval), the M-current pulse rise time (10 to 90%), the M-current pulse duration, and the time interval between M-current pulses are given in the form of histograms in Figure 4-15, 4-16, 4-17, 4-18, 4-19, and 4-20, respectively. In all the figures the shaded area represents the data from the KSC, and the unshaded area represents the data from the Ft. McClellan. Only the unsaturated M-current pulses (the saturation level was about 1 kA in the KSC data and about 2 kA in the Ft. McClellan data) are included in the distributions for the M current pulses shown in Figures 4-18, 4-19, and 4-20, perhaps introducing some bias towards the smaller M-current pulses. None of the current pulses during the wire-burn stage at the beginning of the flash are included in the distributions. The time interval between the beginning and end of the M-current pulse is treated as the M-current pulse duration and is similar to the criteria used by Thottappillil et al. (1990) (see Figure 8 for example of measurement) for M changes in electric field records. Very often it is difficult to determine the starting point and end point of a M current pulse with certainty and errors up to 25% may be

expected in the M-current time duration measurements. The time interval between the M-current pulses are measured between the peaks of the successive M-current pulses, as done in Thottappillil et al. (1990) for M changes in electric field records. All the distributions appear to be approximately log-normal, and hence geometric means (GM) are computed. The overall GM of the interstroke interval, stroke duration, and the zero-current interval are 47 ms, 11 ms, and 29 ms, respectively. The overall GM of the M-current pulse rise time (10 to 90%), the M-current duration, and the interval between M-current pulses are 0.44 ms, 2.0 ms, and 4.5 ms, respectively. The GM of the parameters for the data from KSC and Ft. McClellan are also given separately in the histograms. Note that the 10-90% rise times of the M-current pulses (GM = 0.44 ms) is three orders magnitude higher than the 10-90% rise time of the return stroke current pulses (GM = 0.37 μs) from the same data set.

4.2.3 Discussion

We did not find any current pulses having rise time of a few microseconds or shorter, that is characteristic of subsequent return strokes, while there was a detectable continuing current flow at the base of the channel. In triggered lightning flashes in New Mexico, Hubert et al. (1984) reported that they observed, although rarely, leader-return stroke sequences during the continuing current stage. Since the New Mexico triggered flashes often had upward-branched channels with common lower portions, it is possible that continuing current flowed in one branch while a leader and return stroke propagated along another branch producing the superposition of the continuing luminosity and leader-return stroke images in the common lower portion in time-resolved optical images and the superposition of currents measured at ground. Brook et al. (1962) postulated that in natural lightning flashes there exists a small steady photographically dark

current for an average duration of 50 ms to maintain some minimum ionization between the return strokes. They believed that without such a small continuing current of the order of 10 A multiple strokes in identical channel would be rare. Later, Uman and Voshall (1968) presented calculations to show that, in the absence of additional input energy, the lightning channel temperature decays slowly enough to maintain the channel temperature an order of magnitude higher than the ambient temperature at the end of a typical interstroke period of 50 ms. Uman and Voshall (1968) argued that no small dark currents are required to keep the channel in a state such that a dart leader can be initiated along the same channel after an interstroke period of tens of milliseconds. The failure to observe any small currents (above the minimum detectable signal level of 4 A) throughout the interstroke interval in the triggered lightning data analyzed in this section appears to negate the hypothesis of Brook et al. (1962). However, it should be pointed out that the lightning currents are measured at the bottom of the channel and if the channel is cut off above the bottom and small currents are flowing in the channel above it, such currents would not be detected by the current measuring system.

The tendency of the larger rise times to be associated with smaller return strokes in our data is opposite to the observation of Berger et al. (1975) for natural negative lightning strikes to towers. They found a positive correlation between the return stroke current rise times and the return stroke peaks. Perhaps the disparity is due to the fact that we measured the rise times from the 10% to 90% of the peak amplitude, whereas Berger et al. (1975) measured the rise time between the 2 kA point on the pulse front and the peak. The 2 kA to peak rise-time will be always larger than the 10-90% rise time for return strokes having peak currents larger than 20 kA and may be smaller for return strokes having peak currents less than 20 kA.

In our data, the rise times of the M-current pulses (GM = 0.44 ms) are 2 to 3 orders of magnitudes larger than the rise times of the return stroke pulses (GM = 0.37 μs). The duration

of the M-component pulses in the current records (GM = 2.0 ms) presented in this chapter for triggered lightning is more than 2 times larger than the duration of M-component pulses in electric field records (GM = 0.9 ms) presented in Thottappillil et al. (1990) for natural lightning. In chapter 8 the continuing currents and M components are modeled yielding one possible explanation for the difference in the durations of M components measured in current and field records. The interval between M-component pulses in the triggered lightning current records (GM = 4.5 ms) is more than two times larger than the interval between M-component pulses in the electric field records (GM = 2.1 ms) in natural lightning (Thottappillil et al., 1990).

On the whole the triggered lightning statistics in Florida and Alabama are similar. Further the interstroke intervals in the negative triggered lightning of Florida (GM = 51 ms) is similar to the interstroke intervals preceding strokes in previously-formed channel in negative natural lightning of Florida (GM = 56 ms), measured from the electric field records (Rakov et al. 1992).

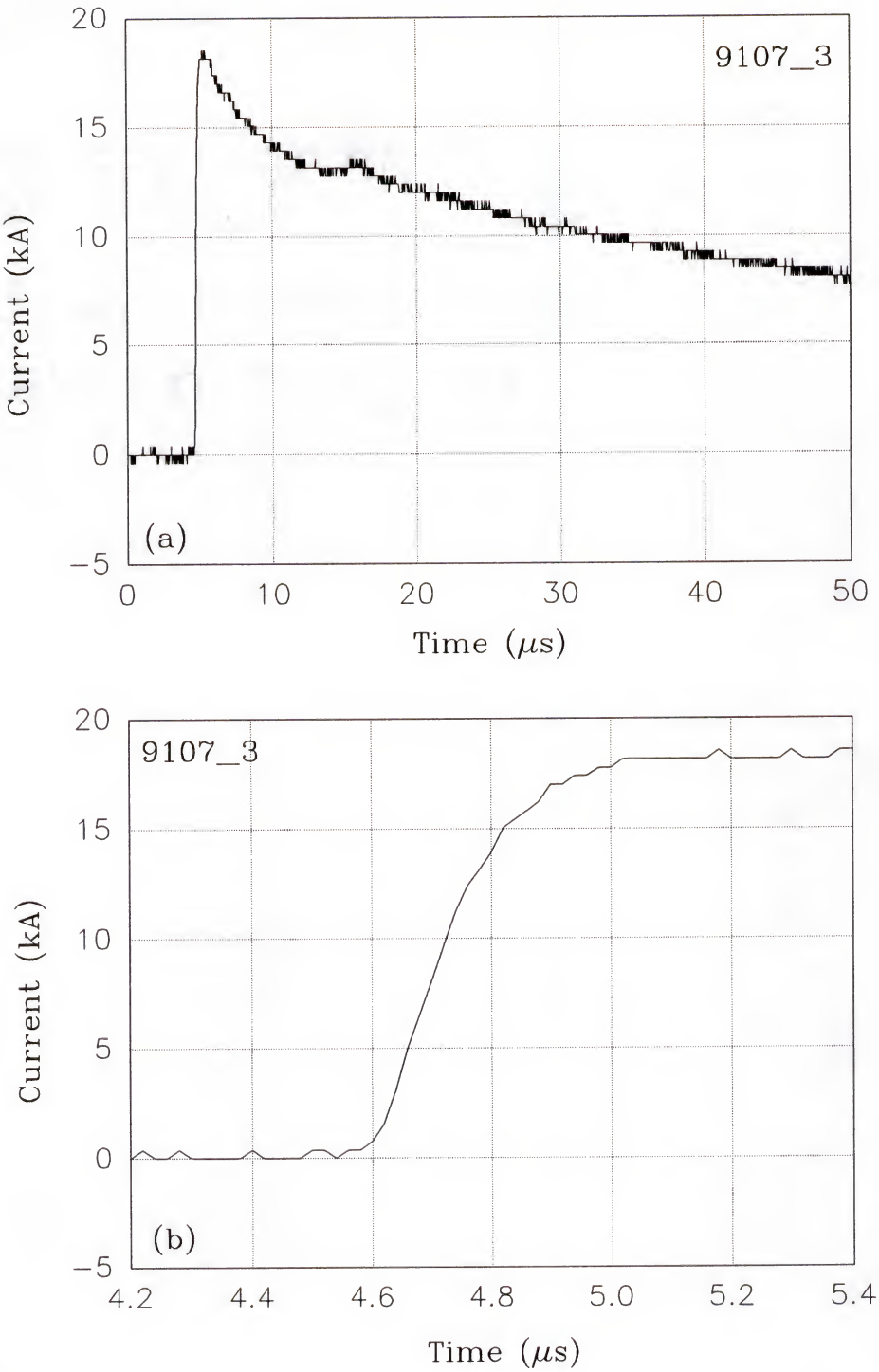

Figure 4-6. Example of a triggered lightning return stroke current waveshape with relatively fast rise time recorded at Ft. McClellan, Alabama. a) Waveform on a longer time scale; b) The front portion on an expanded time scale.

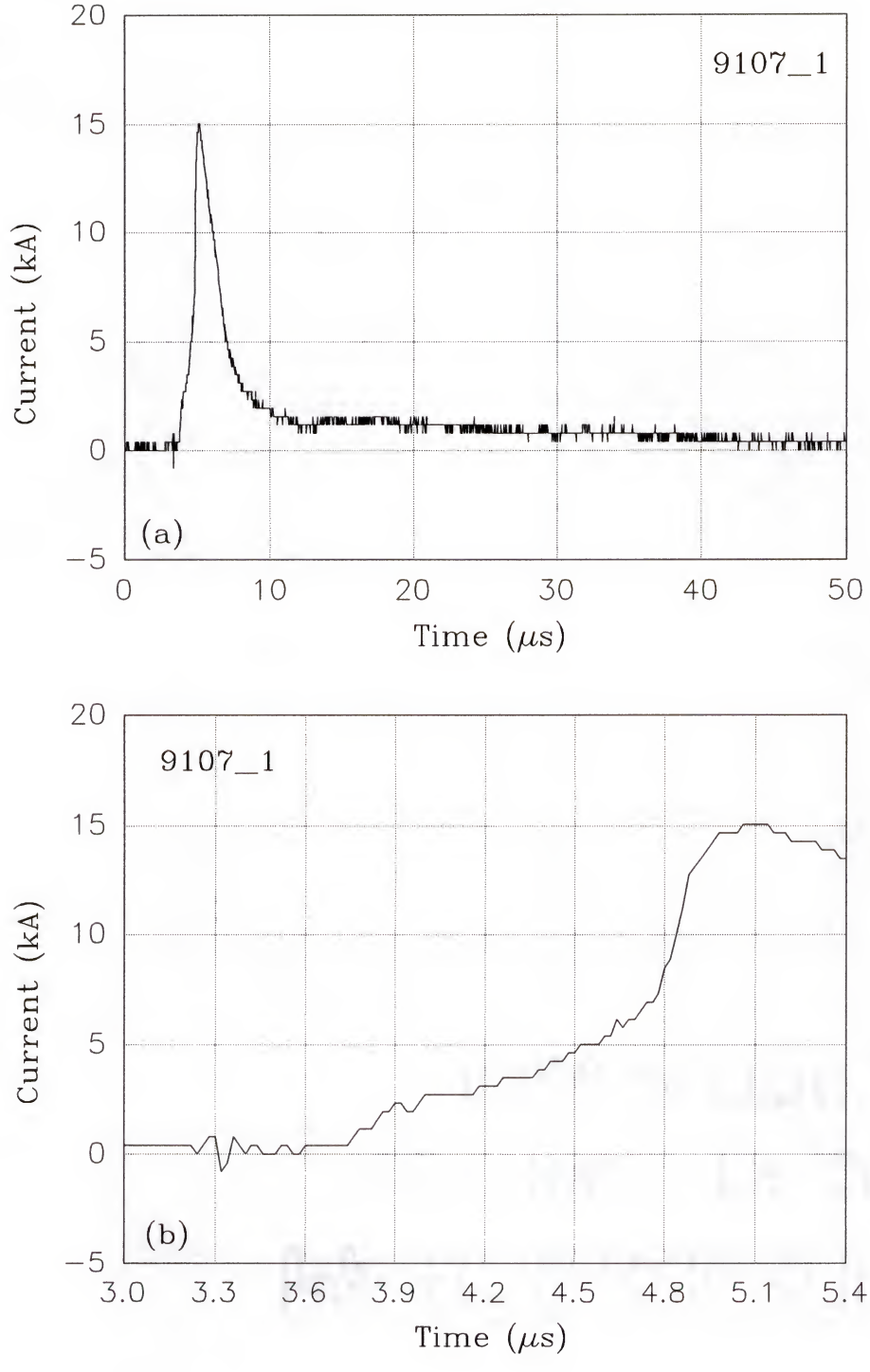

Figure 4-7. Example of a triggered lightning return stroke current waveshape with relatively slow rate-of-rise at the beginning and a fast rate-of-rise near the peak recorded at Ft. McClellan, Alabama. a) Waveform on a longer time scale; b) The front portion on an expanded time scale.

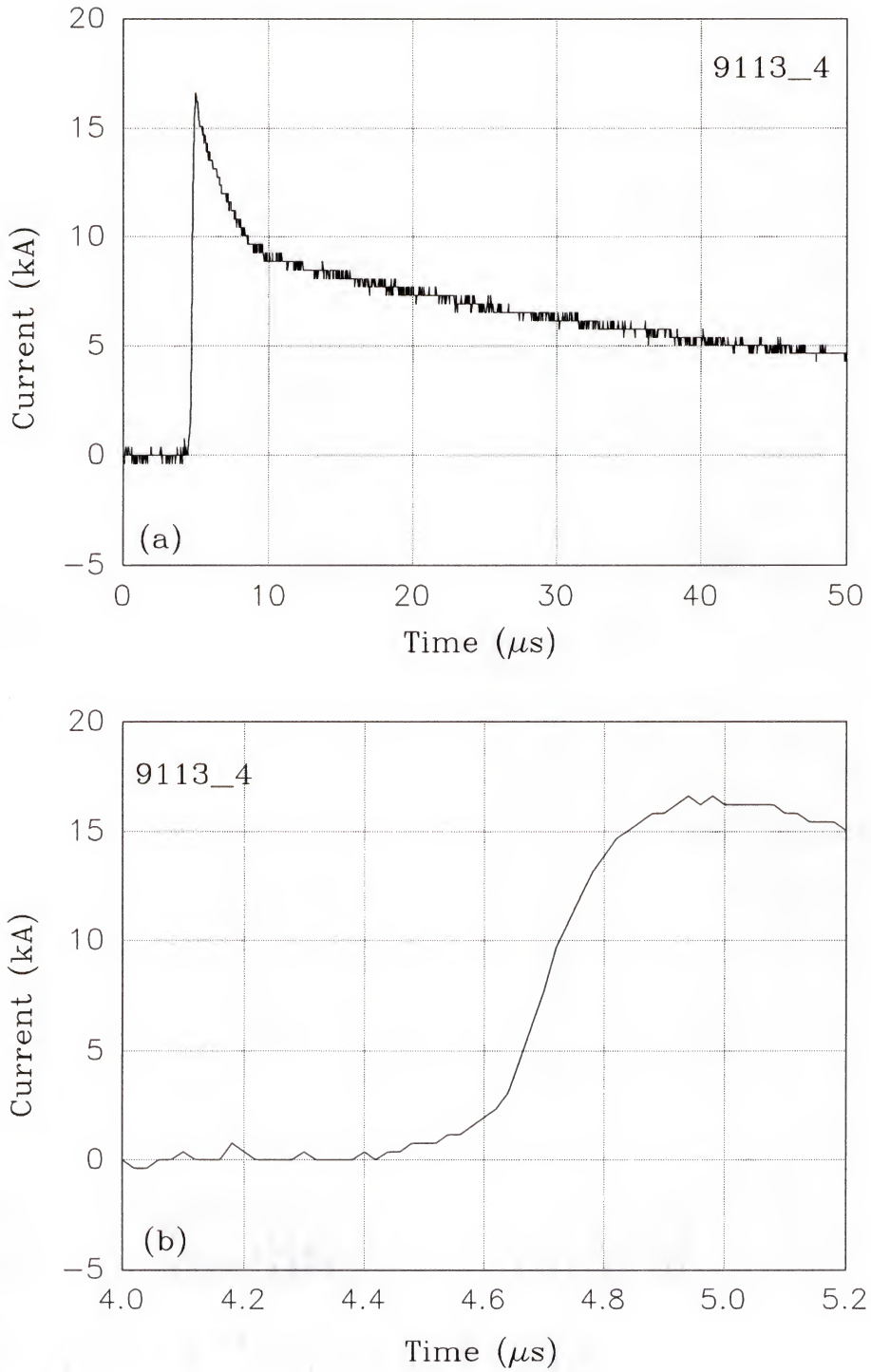

Figure 4-8. Example of a triggered lightning return stroke current waveshape with a slowly rising ramp at the beginning recorded at Ft. McClellan, Alabama. a) Waveform on a longer time scale; b) The front portion on an expanded time scale.

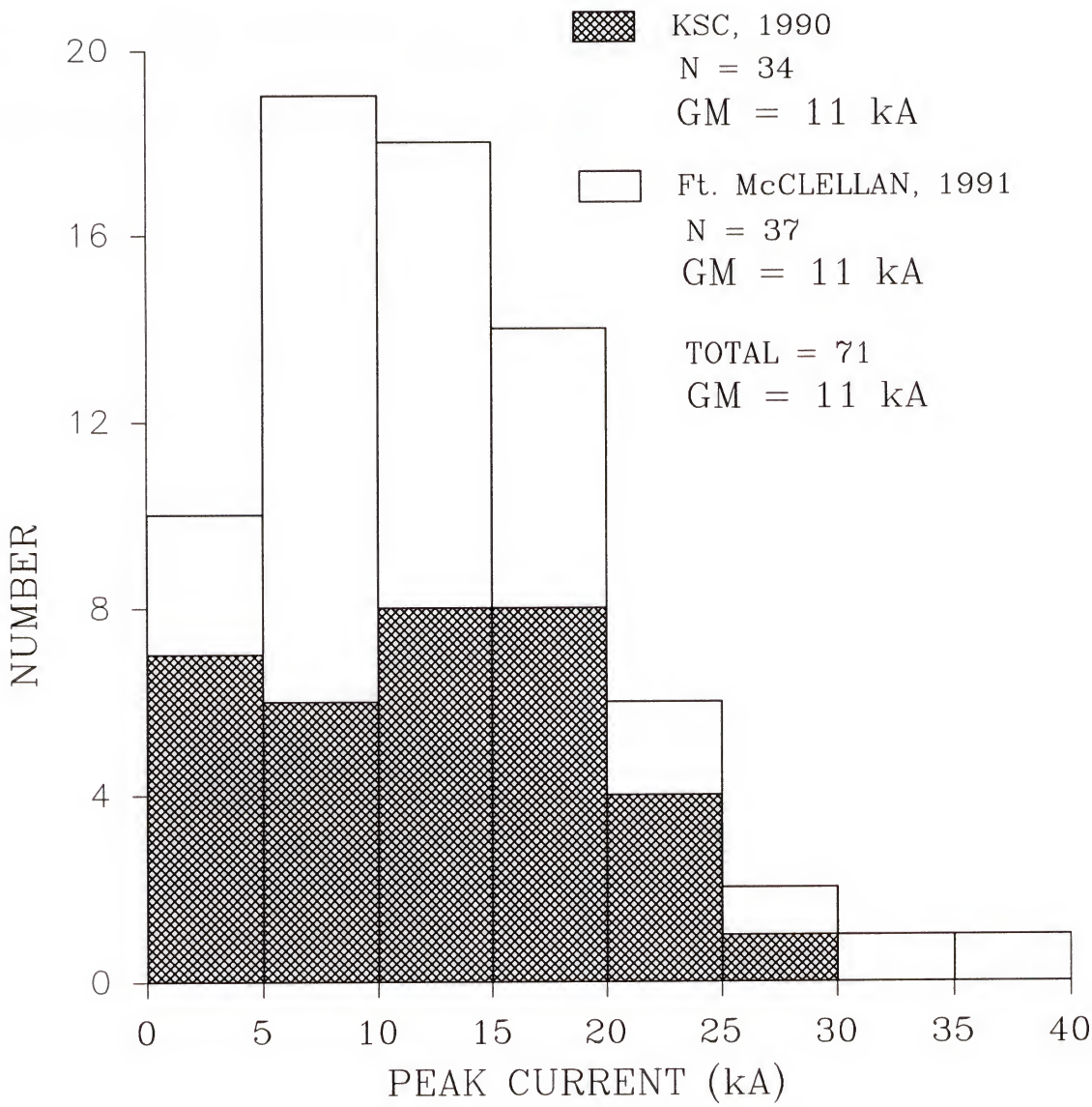

Figure 4-9. Histogram of return-stroke peak current for triggered lightning.

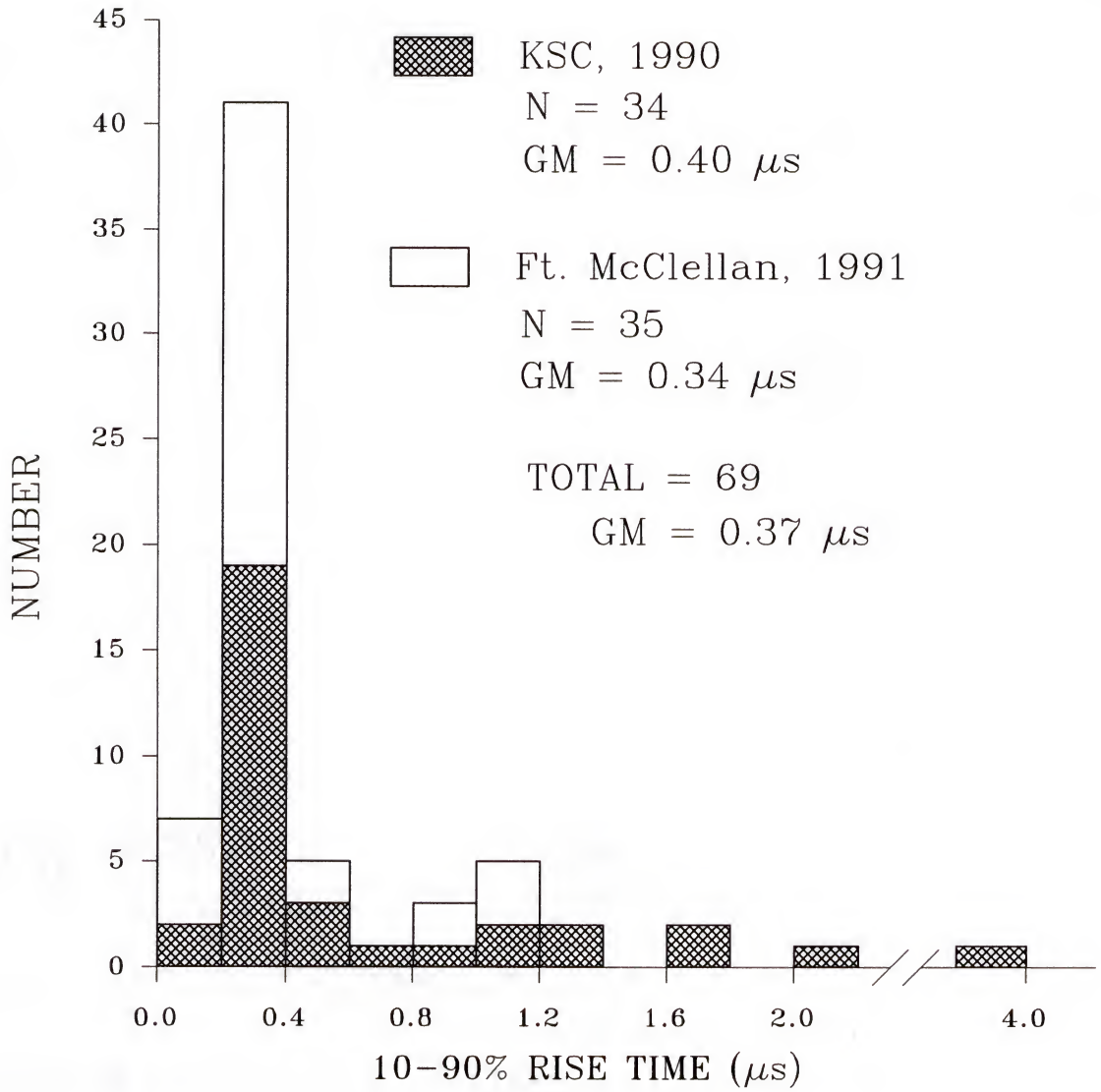

Figure 4-10. Histogram of return-stroke current rise time for triggered lightning.

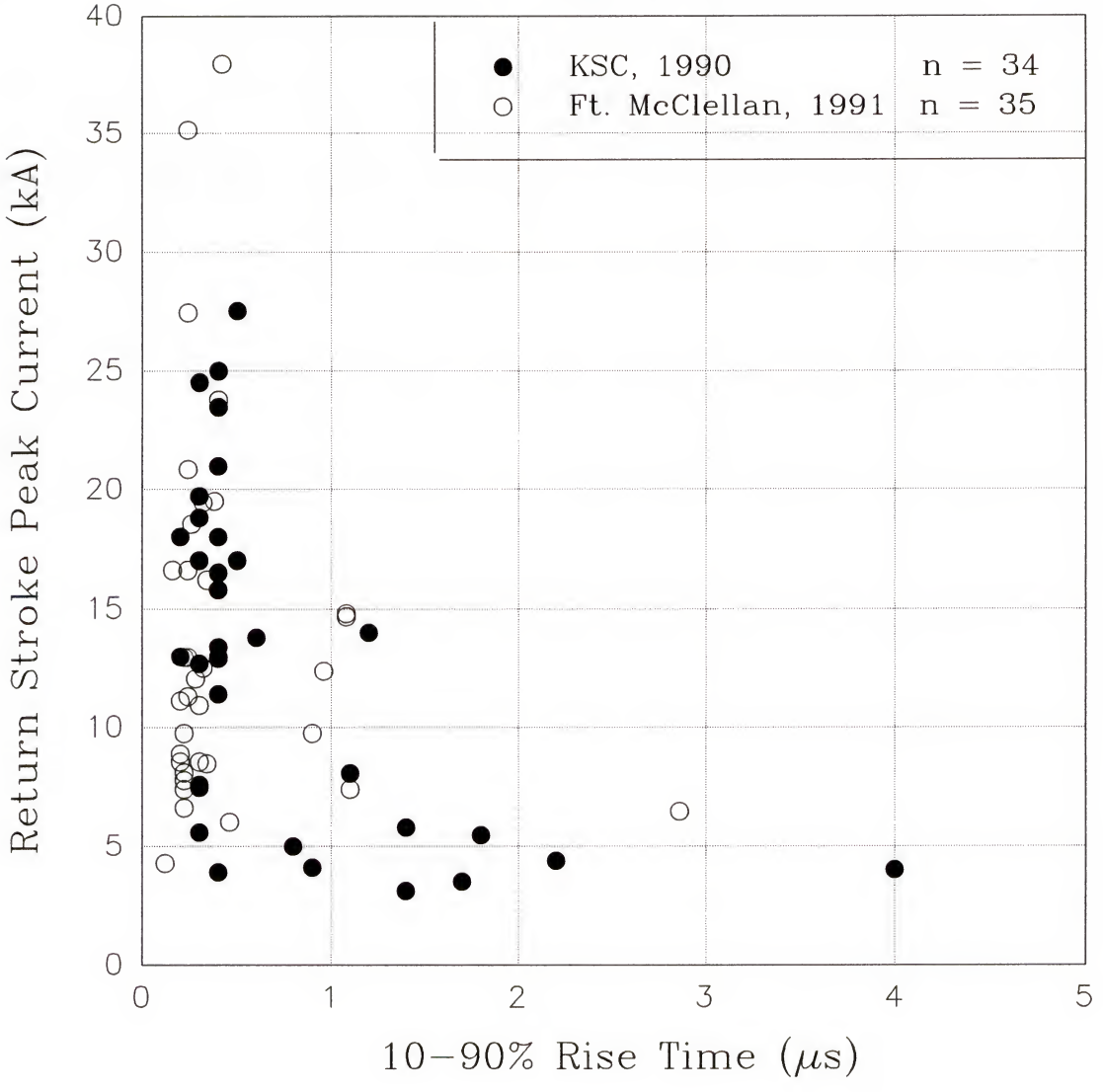

Figure 4-11. Scatter plot of return-stroke peak current vs. rise time for triggered lightning.

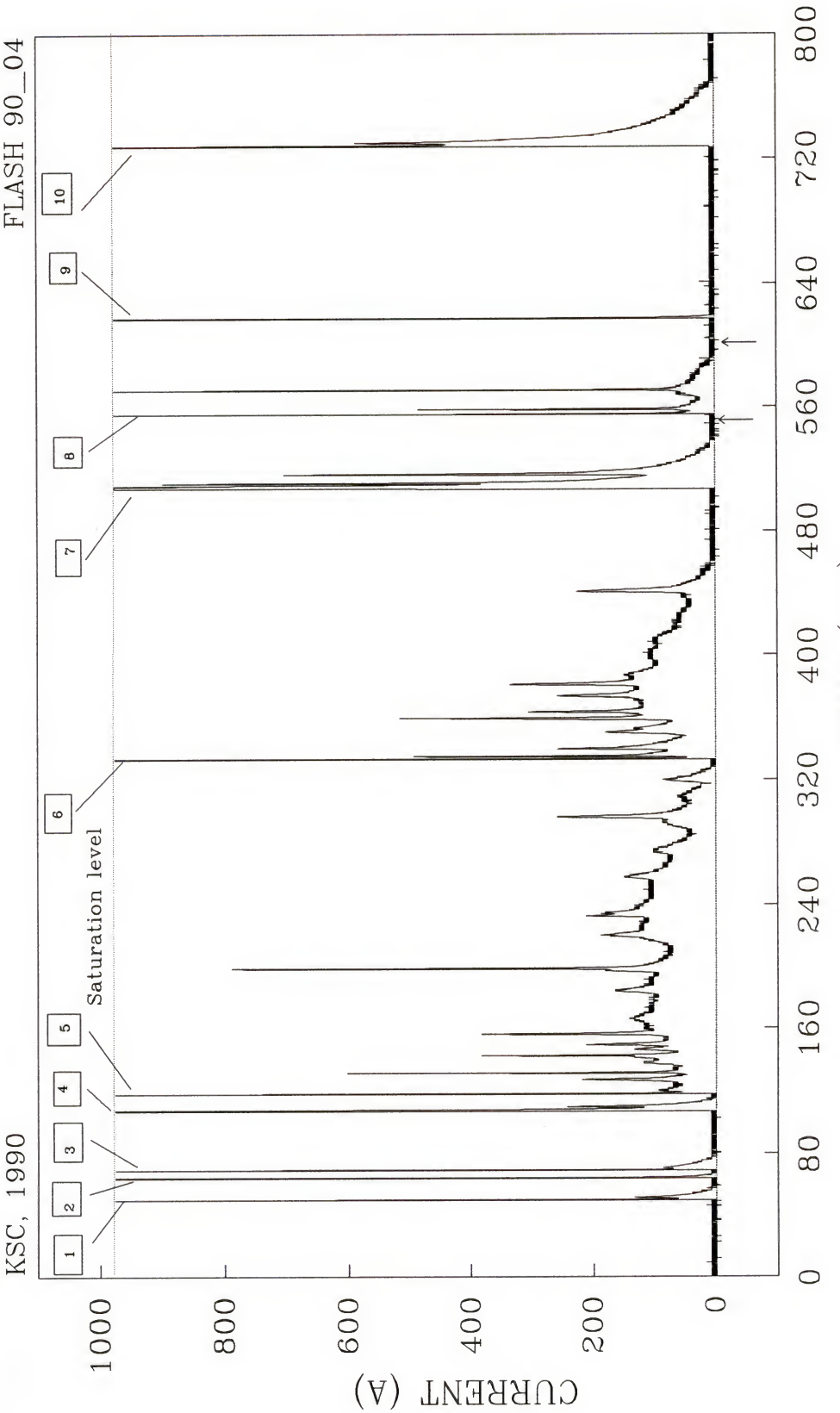

Figure 4-12. Example of the current record of a 10 stroke flash.

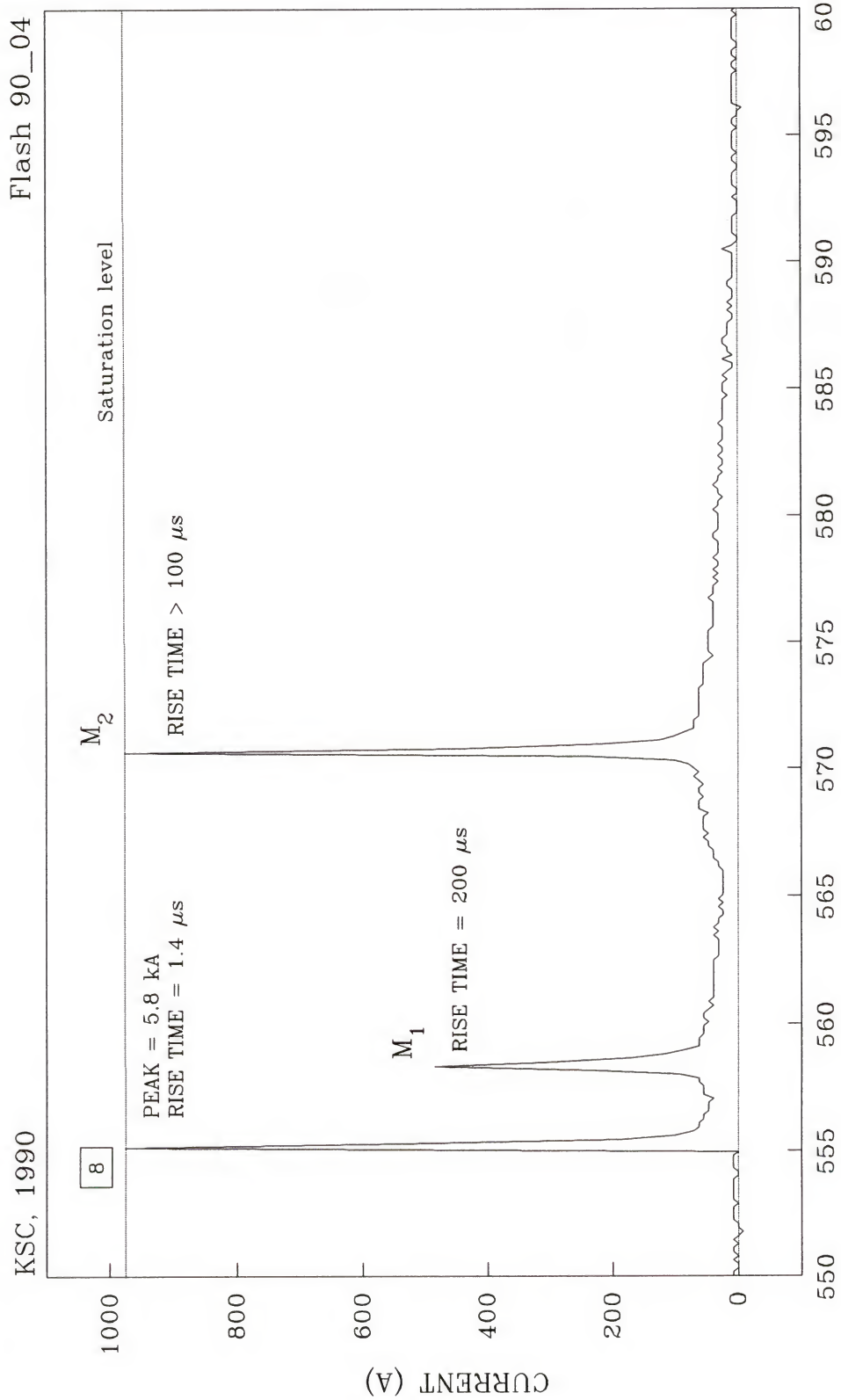

Figure 4-13. Portion of the flash between the arrows shown in Figure 4-12.

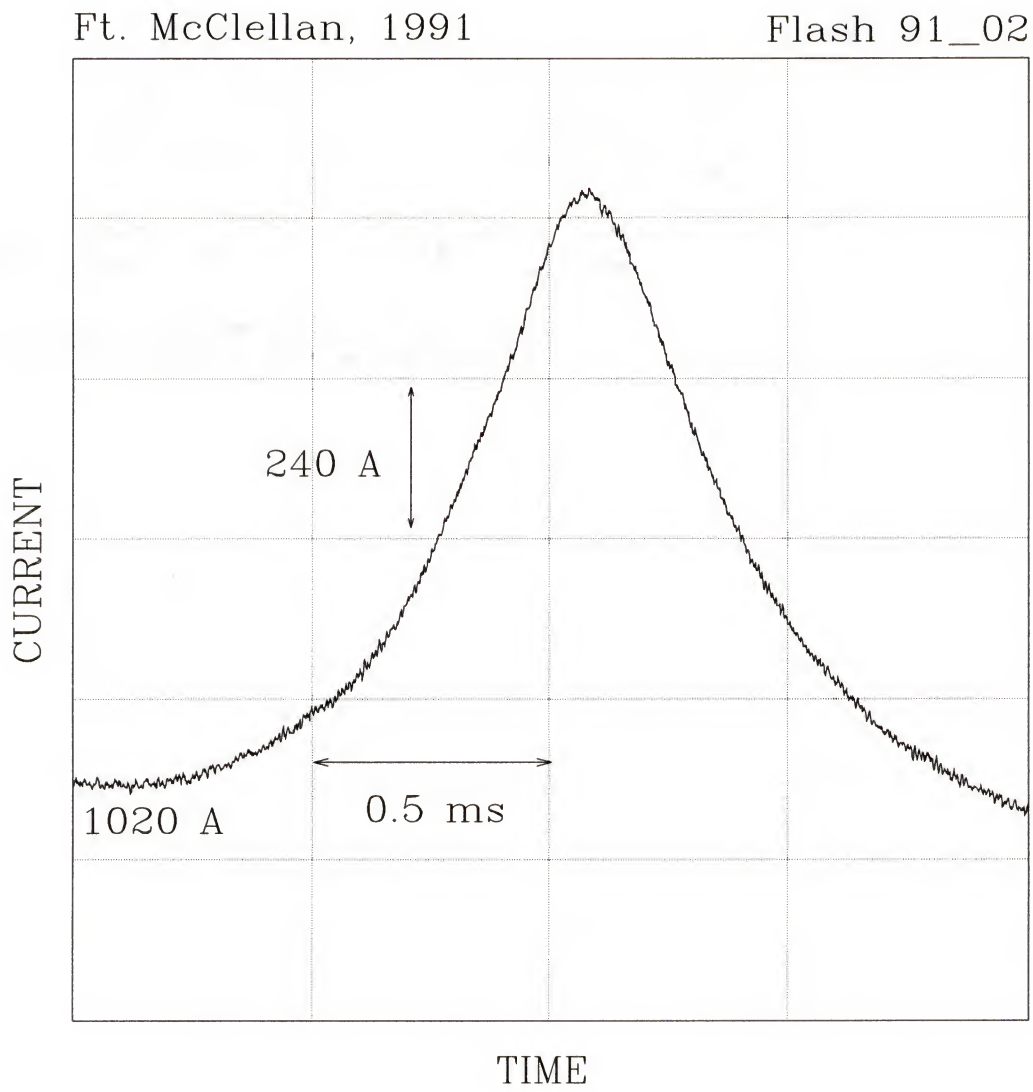

Figure 4-14. Example of an M-current pulse waveshape.

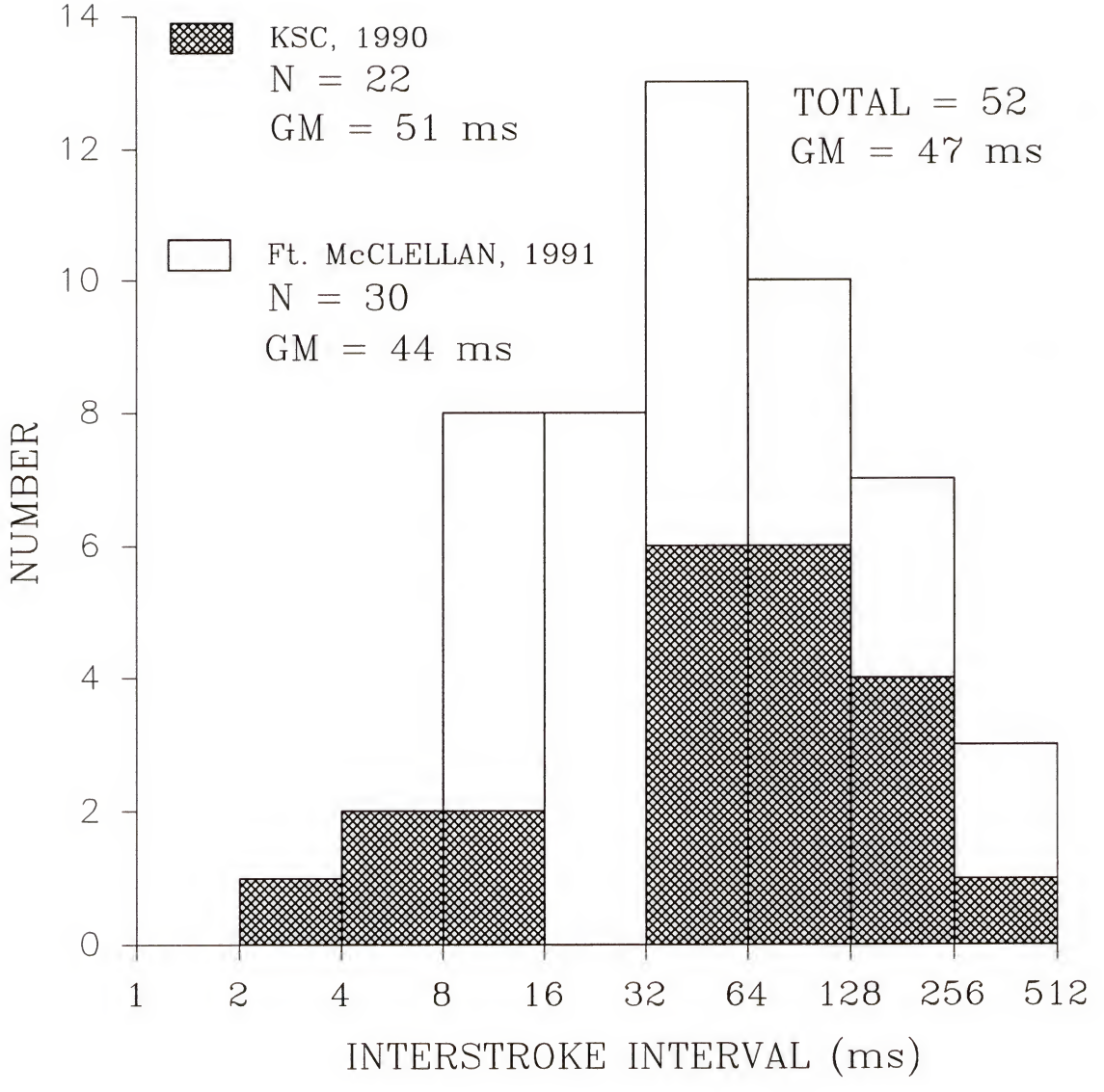

Figure 4-15. Histogram of interstroke interval for triggered lightning.

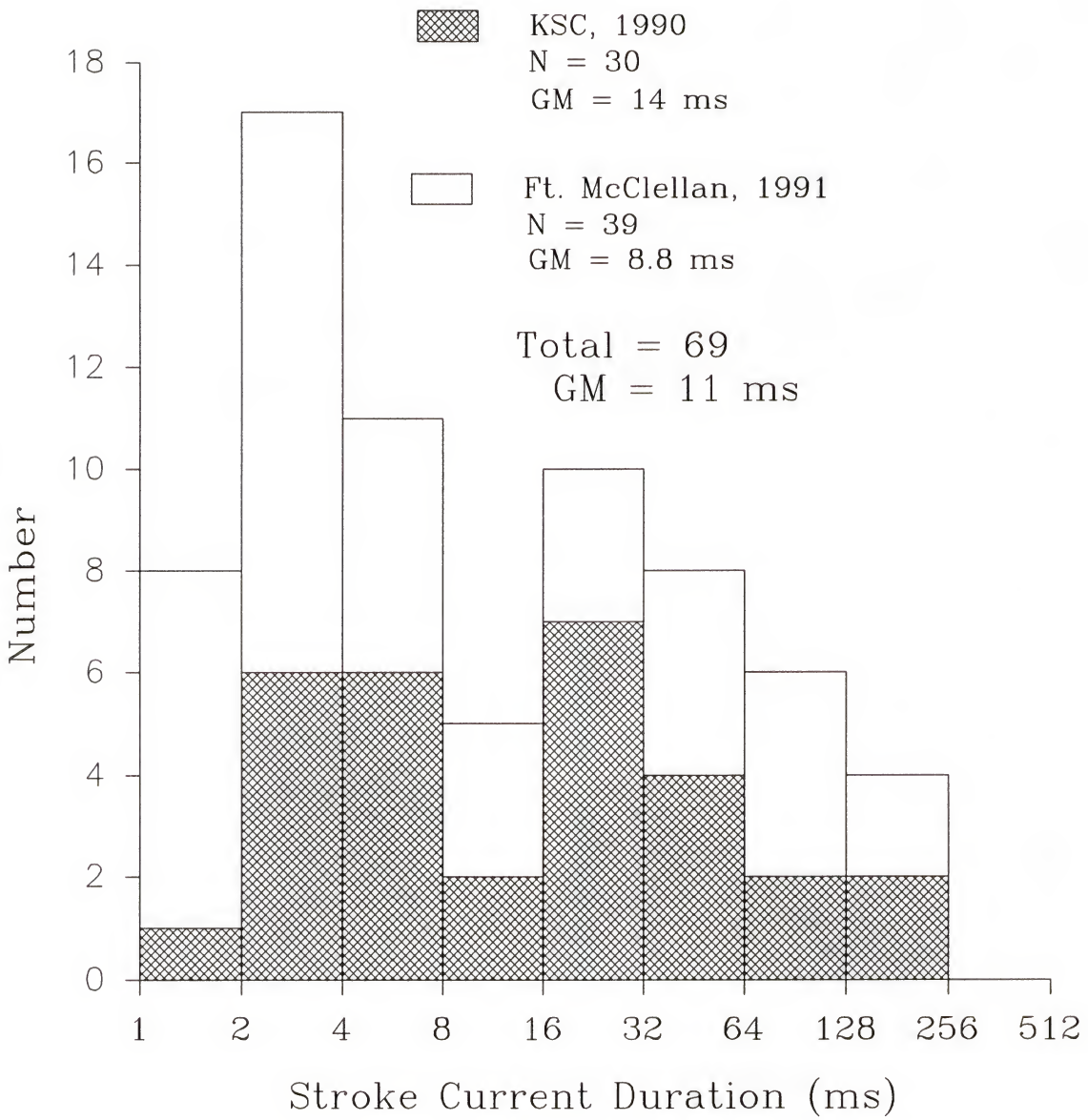

Figure 4-16. Histogram of stroke duration including continuing current for triggered lightning.

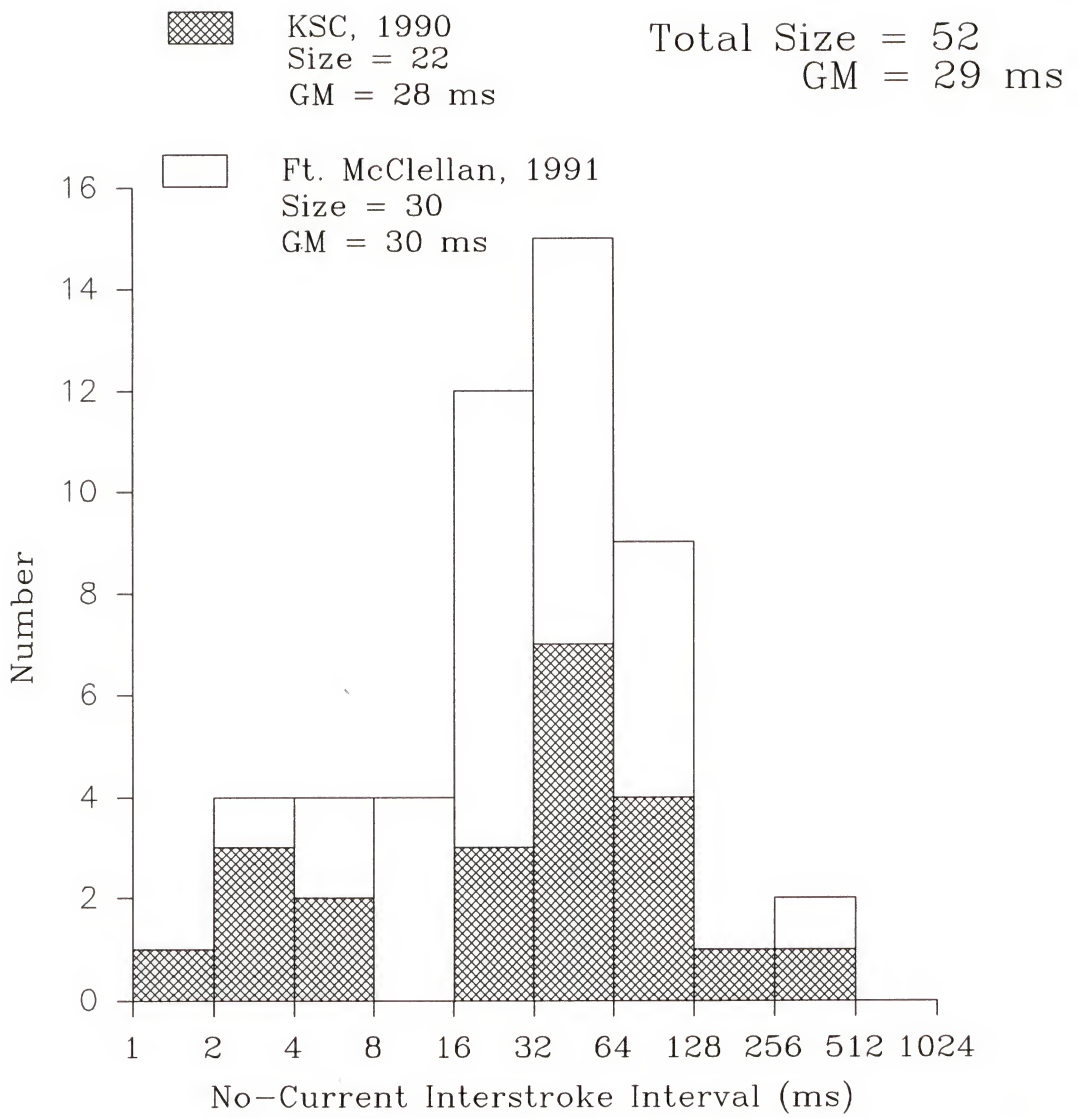

Figure 4-17. Histogram of the portion of interstroke interval at which current flow is not detected.

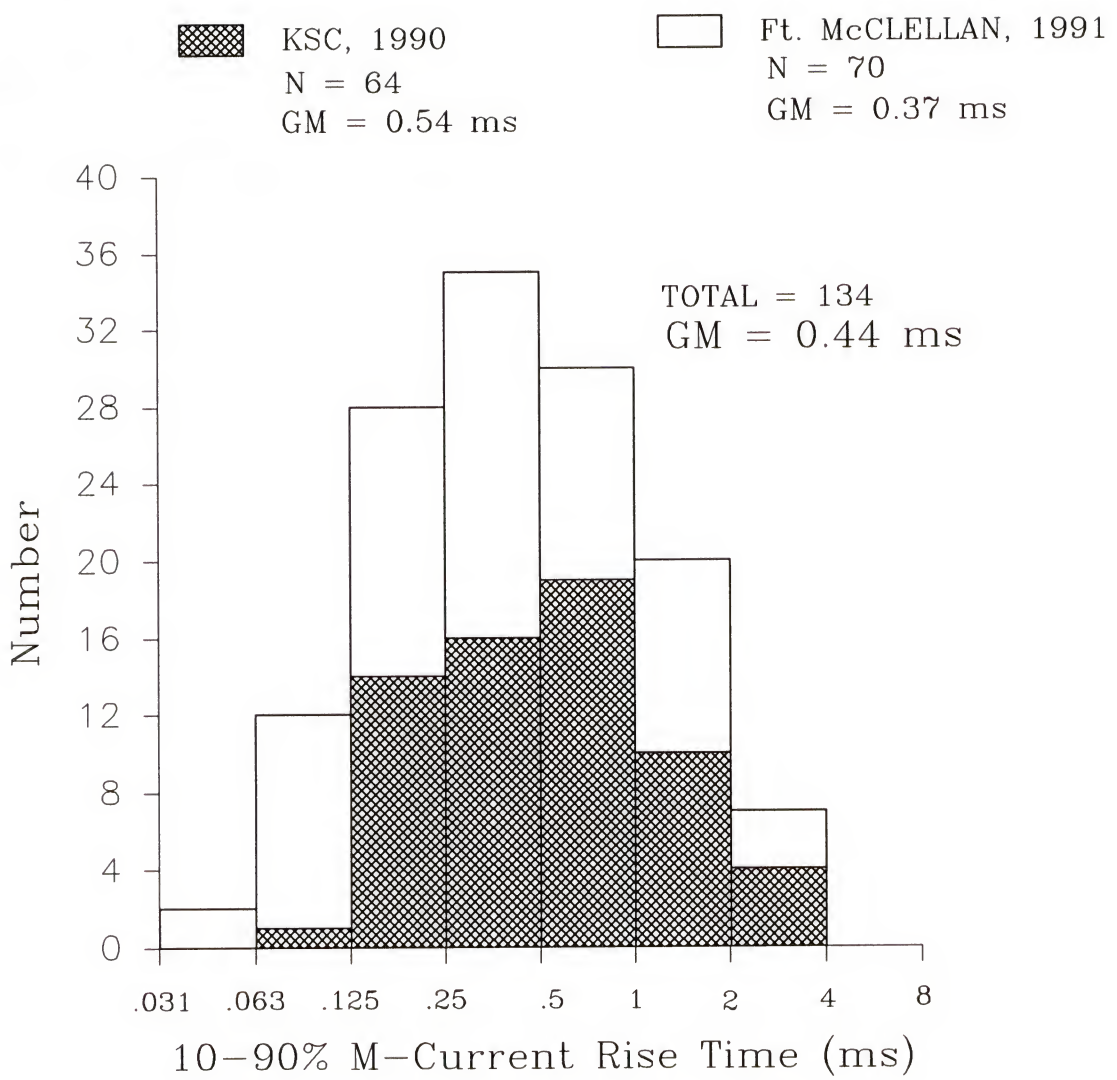

Figure 4-18. Histogram of M-current rise time.

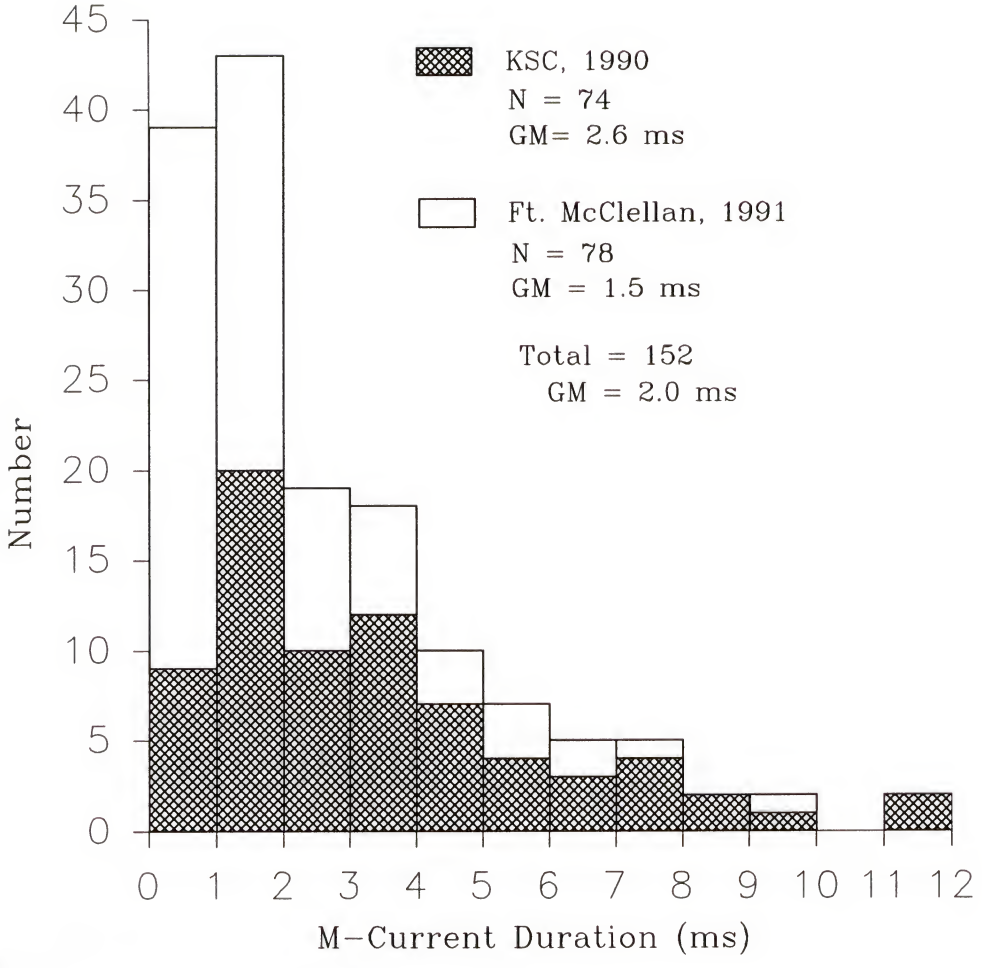

Figure 4-19. Histogram of M-current duration.

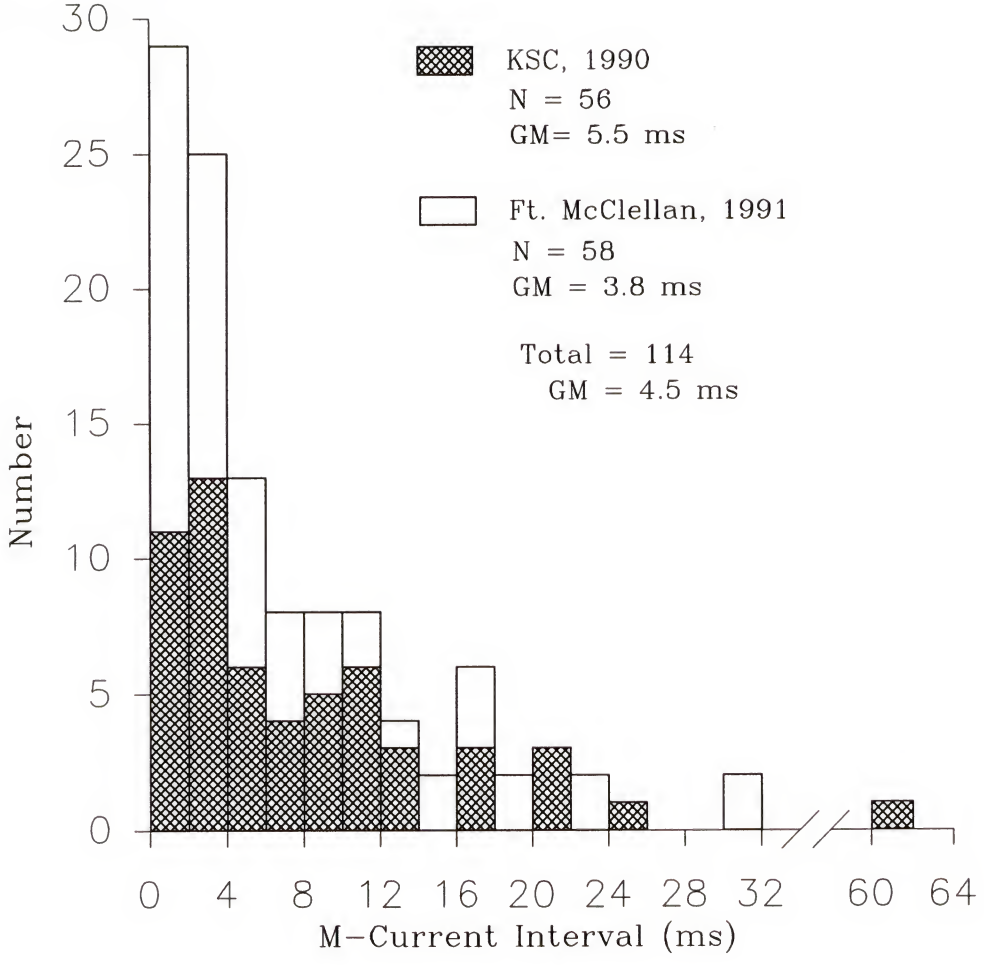

Figure 4-20. Histogram of M-current interval.

CHAPTER 5
COMPARISON OF PREVIOUS RETURN-STROKE CURRENT MODELS

In section 2.4 return-stroke current models available prior to the research involved in this dissertation were reviewed. In all these models, the temporal and spatial distribution of the current along the channel is given as a function of the current at the channel base, in addition to being dependent on the return-stroke speed and the parameters specific to the models. It follows that the current distribution along the channel changes, as do the fields resulting from that current distribution, when the waveform of the channel-base current is varied. From an inspection of the defining equations of the various models considered (Equations 2-5, 2-7, 2-10, 2-11, 2-12, 2-13, 2-14, and 2-15) it is evident that the variations in the assumed channel-base current waveshape affect the predictions of the different models in different ways. To illustrate with a simple example, consider the TL and TCS models described by equations (2-7) and (2-14), respectively. If the current at the ground is assumed to increase linearly with time (a rough approximation to the return stroke wavefront), the current at all heights below the return-stroke front, for any given return stroke speed, will be higher for the TCS model than for the TL model. The opposite result is obtained if the current at ground is assumed to decrease linearly with time (a rough approximation to the return stroke waveshape after the initial peak). For any realistic return-stroke current, the situation is more complex. Adequate attention has not been paid by previous investigators to the sensitivity of the model predictions to the channel-base current waveshape. Nucci et al. (1990) used only one channel-base current waveshape to compare the different models. However they did mention that, even though the fields at 100 km

for the BG and TCS models do not cross zero for the current assumed at ground, the fields can cross zero for a channel-base current whose tail falls off faster than was assumed.

Thottappillil et al. (1991) (see Appendix A) compared the fields calculated from the TCS, MTL, and DU models using the channel-base current assumed in Nucci et al. (1990) with the fields calculated for these three models using the channel-base current assumed in Diendorfer and Uman (1990). Thottappillil et al. (1991) show that even though both channel-base currents are reasonable approximations to typical subsequent return-stroke currents, the behavior of the calculated far fields, notably its zero-crossing, and the behavior of the near magnetic fields, notably the "hump" after the peak, are different for a given model for each of the two currents. It is conceivable that the differences that Nucci et al. (1990) found between the BG and TCS models on one hand and the TL, MTL, and MULS models on the other hand in terms of the initial field peak, the field-peak to current-peak ratio, and the field-derivative peak to current-derivative peak ratio depend, to some extent, on the particular choice of current at the channel base.

From the foregoing discussion it is clear that the comparison and evaluation of the models is surely more definitive if the model fields are calculated using the current waveshapes actually measured at the lightning channel base and if these model fields are compared with simultaneously measured fields. As described in chapter 3, Willett et al. (1988) and Willett et al. (1989) have tested the Transmission Line (TL) model for triggered lightning using simultaneous measurement of current, electric field, and return stroke speed and assuming the radiation field approximation of the TL model (equations 2-8 and 2-9). The investigations reported in this dissertation are the first to evaluate the different return stroke models using simultaneous measurements of current, electric field, and return stroke speed.

5.1 Comparison of Models Reviewed in Section 2.4

In this section simultaneously-measured currents and return stroke speeds from Willett et al. (1989), described in Chapter 3, are used as input to the TL, TCS, MTL, and DU models, and the calculated electric fields from the models are compared with the simultaneously measured electric fields at 5.16 km given by Willett et al. (1989). A description of the data was given in section 3.3. Eighteen return-stroke currents for which there are simultaneously measured return-stroke speeds and fields are used in calculating the fields from the models. We do not calculate the fields from the BG model (Bruce and Golde, 1941) because its uniform current distribution along the channel at a given time does not allow the calculation of fields from measured currents without excessive numerical noise. The MULS model (Master et. al. 1981) is not discussed because it requires an arbitrary division of the channel base current into three separate parts, with a resultant lack of uniqueness in deriving the channel currents from the measured channel base current. The complete DU model also requires an arbitrary division of current into a breakdown part and a corona part. That was not done in this analysis. Rather, only one component for the current and the associated single time constant are used in calculating the fields from the DU model, the justification being that for the first few microseconds the fields are dominated by the breakdown component of the current (Diendorfer and Uman, 1990). For the MTL model the current is assumed to be exponentially attenuated with height (Equation 2-13).

A listing of the computer program in FORTRAN used for calculating the fields from the models is given in Appendix B. The geometry of the problem is shown in Figure 5-1. The observer or the point where the field is calculated is located on a perfectly conducting ground at a distance, d, from the straight vertical channel. The return stroke is assumed to start from ground level at time $t=0$. For each time step the program first calculates the height of the

wavefront as seen from the field measuring point. This "effective" height, h, is obtained from the solution of the equation

$$t = \frac{h}{v} + \frac{\sqrt{d^2+h^2}}{c} \qquad \textbf{(5-1)}$$

The effective channel height, h, is divided into very small segments and the current in each segment is found for the model. The vertical component of the electric field from the channel at a given time is obtained by adding the vertical field from each channel segment, knowing the distance of each segment from the field point and using equation (2-3).

All 28 measured return stroke currents discussed in Willett et al. (1989) and in section 3.3 are shown in Figures 5-2 to 5-29. As an example, consider Figure 5-2 which shows stroke 8705_1 on a longer time scale in Figure 5-2a and the current front portion on an expanded scale in Figure 5-2b. The current waveshapes shown in Figures 5-2 to 5-29 are in general agreement with the current waveshapes measured by Sandia National Laboratories (Sandia) at KSC in 1990, and at Ft. McClellan in 1991, three examples of which are given in Figures 4-6, 4-7 and 4-8. The Geometric Mean (GM) peak value of the currents shown in Figures 5-2 to 5-29 is 14.9 kA, which is about 35% higher than the GM peak current of 11 kA obtained by Sandia. The Geometric Mean (GM) value of the 10-90% rise time of the currents shown in Figures 5-2 to 5-29 is 0.27 μs, which is about 37% lower than the GM peak value of 0.37 μs of 10-90% rise time of the currents measured by Sandia. Fields are calculated for 18 return strokes which had speed measurements, as given in Table 3-1. Current waveforms for these 18 return strokes are shown in Figures 5-2 to 5-5, 5-12 to 5-13, 5-16 to 5-18, 5-20 to 5-24, and Figures 5-26 to 5-29. The time zero at which the return strokes are assumed to start propagating upwards from ground level is indicated by vertical arrows in all the Figures of current waveforms. The current axes give the absolute value of the measured current in kA. Of the 18 return stroke current records used in

field calculations, 2 were available for about 14 μs in time from the start of the return stroke, 4 were available for about 9 μs, and the remaining 12 for about 4 μs. The raw current data exhibited spurious high-frequency noise with an amplitude of the order of ± 1 kA (see Willett et al., 1989, page 13276). To minimize this noise a three-point moving average (spanning 20 ns of time) was applied to all the current data used to calculate the fields, but the current waveforms in the Figures of this chapter are shown without any averaging. It has been verified that such averaged data do not affect the results and conclusions obtained from the comparison of the model fields presented here, but only reduce the noise in the model fields.

As discussed in section 3.3, the experimental electric fields with which the calculated fields are compared are obtained by numerically integrating the measured electric field derivatives to get better time resolution (10 ns) and to restore the narrow initial peaks of about 0.1 μs wide lost in the directly measured (electronically integrated) electric fields due to insufficient time resolution (100 ns). The numerically integrated dE/dt waveforms have been compared with the corresponding measured electronically integrated electric field waveforms to ensure that the offset present in the measured dE/dt waveform is removed correctly so that there is no distortion in the numerically integrated fields. In Figure 5-30, as an example, the numerically integrated dE/dt waveform (dashed line) is compared with the electronically integrated waveform (solid line) for return stroke 8705_1. Both waveforms are very similar, as can be seen from Figure 5-30a, except for the absence of narrow initial peak in the electronically integrated waveform. Figure 5-30b shows the front portion of the waveforms in Figure 5-30a on an expanded scale. The circles denote the actual data points (0.1 μs sampling interval) on the electronically integrated waveform. The narrow peak (about 0.1 μs wide) does not appear on the electronically integrated waveforms, probably because of insufficient bandwidth (about 5 MHz) and under-sampling.

Figures 5-31 to 5-48 compare the calculated electric fields (dotted line) from the TL, MTL, TCS, and DU models with the measured electric fields (solid line) for the 18 return strokes using the measured channel base currents shown in Figures 5-2 to 5-5, 5-12 to 5-13, 5-16 to 5-18, 5-20 to 5-24, and Figures 5-26 to 5-29. The measured return stroke speeds used in the calculations are given in Table 3-1 and are assumed to be constant. In the MTL model an exponential attenuation of current with height (equation 2-13) was assumed with an attenuation factor λ_I = 2000 m as adopted by Nucci et al. (1990). For the DU model the breakdown discharge time constant was assumed to be 0.1 μs, a value used by Diendorfer and Uman (1990) to model triggered lightning return strokes. The calculated and measured fields were displayed on a computer screen and the beginning of the fast rising portion of the measured and calculated fields were visually aligned. In Figures 5-31 to 5-48 the zero on the time axes denote the starting point of the return stroke for the calculated field waveforms and corresponds to the starting time of the return stroke current waveforms designated by the vertical arrows in the corresponding figures for the currents. Zero on the field axes coincides with the zero of the calculated return stroke field change, but may not indicate the start of the return stroke in the measured field waveform because of the preceding leader field change.

We now compare the measured fields with the calculated fields of the models. The peak values of the TL and MTL model fields are almost equal because the attenuation of the current on the channel in the case of the MTL model is small at the time the peak value is attained. After the peak, the model field from the MTL model is less than that of the TL model field and the difference increases with increasing time. The peak values of the TCS model fields are always greater than the peak values of the TL, MTL, and DU model fields. After the peak, the DU and TCS model fields are almost equal. In Table 5-1 the calculated return stroke field peak amplitudes are compared with the measured field peak amplitudes. The final amplitude of the

preceding leader field change appearing in the measured field is subtracted from the peak field, and hence, the peak field amplitudes, E_m, of the measured waveforms listed in column 2 of

Table 5-1. Comparison of peak amplitudes of the model fields with the measured peak field amplitudes.

1	2	3				4			
Stroke	Measured Peak Field, E_m V/m	Calculated Peak fields, E_c V/m				Ratio, $(E_c-E_m)/E_m$			
		TL	MTL	TCS	DU	TL	MTL	TCS	DU
8705_1	72	57	54	93	80	-0.21	-0.25	+0.29	+0.11
8705_3	64	47	47	95	68	-0.27	-0.27	+0.48	+0.06
8705_5	78	69	67	95	63	-0.12	-0.14	+0.22	-0.19
8705_6	78	84	84	130	84	+0.08	+0.08	+0.67	+0.08
8715_9	157	181	176	214	195	+0.15	+0.12	+0.36	+0.24
8715_10	88	86	84	100	88	-0.02	-0.05	+0.14	0.00
8725_1	98	130	120	150	145	+0.33	+0.22	+0.53	+0.48
8725_2	82	98	90	104	98	+0.20	+0.10	+0.27	+0.20
8725_3	190	286	275	350	310	+0.51	+0.45	+0.84	+0.63
8725_5	58	64	62	80	55	+0.10	+0.07	+0.38	-0.05
8726_1	165	200	195	260	245	+0.21	+0.18	+0.58	+0.48
8726_2	160	125	120	275	245	-0.22	-0.25	+0.72	+0.53
8726_3	88	88	88	105	85	0.00	0.00	+0.19	-0.03
8726_4	140	123	120	245	200	-0.12	-0.14	+0.75	+0.43
8728_10	125	150	142	155	150	+0.20	+0.14	+0.24	+0.20
8728_11	88	88	85	105	85	0.00	-0.03	+0.19	-0.03
8732_1	122	107	100	180	132	-0.12	-0.18	+0.48	+0.08
8732_2	82	105	98	110	108	+0.28	+0.20	+0.34	+0.32

Table 5-1 are less than the peak field amplitudes, E_p, listed in column 4 of Table 3-1 by up to 15%, except for stroke 8715_9 where the difference is about 40%. The calculated peak field values of the return strokes, E_c, from the TL, MTL, TCS, and DU models are given in column 3 of Table 5-1. Column 4 gives the error in the calculated field peaks. The summary of statistics on the error in the model peak fields is given in Table 5-2.

Table 5-2. Summary of statistics on the error of the model peak fields given in Table 5-1.

	Error				Absolute error			
	TL	MTL	TCS	DU	TL	MTL	TCS	DU
Mean	+0.05	+0.01	+0.43	+0.20	0.17	0.16	0.43	0.23
Standard deviation	0.21	0.20	0.22	0.23	0.12	0.11	0.22	0.20
Minimum	-0.27	-0.27	+0.14	-0.19	0.00	0.00	0.14	0.00
Maximum	+0.51	+0.45	+0.84	+0.63	0.51	0.45	0.84	0.63

From Table 5-2 it is seen that the TL, MTL, and the DU models, on the average, predict the electric field peaks within an absolute error of about 0.2. The TCS model field peak has the greatest error, about 0.4. In all the 18 return strokes the TCS model predicted field peaks were higher than the measured field peaks. For the TL and MTL models the calculated field peaks are more or less symmetrically distributed around the measured field peaks. It has to be noted that the exact point of transition from the leader field change to the return stroke field change in the measured field waveforms are unknown, and hence some errors are involved in the determination of measured field peak amplitudes. Besides, the measured return stroke speeds used in calculating the model fields have absolute errors of 15-25% (see Table 3-3). For the same channel base current, larger speeds give larger values of field, at least for the first few microseconds, and smaller speed give comparatively smaller values of field. Therefore some of the errors in the calculated fields may be attributed to the uncertainty in the speed measurements. To illustrate with an example, consider stroke 8725_2 whose current is given in Figures 5-17a,b and whose speed measurement of 1.5×10^8 m/s has an absolute error of 25%. Then the lowest and highest speeds possible for this return stroke are 1.13×10^8 m/s and 1.88×10^8 m/s respectively. Figure 5-49 compares the fields calculated from the models for the minimum speed and the maximum speed with the fields calculated from the models with the nominal speed. The upper

traces indicated by letter H corresponds to the maximum speed, the lower traces indicated by the letter L corresponds to the minimum speed, the central trace corresponds to the nominal speed, and the solid line corresponds to the measured field. The fields calculated using the maximum and minimum speeds are approximately 20-25% larger or smaller than the fields calculated using the nominal speed. In Figure 5-49, the field peaks of all the models calculated from the minimum speed are lower than the measured field peaks whereas the field peaks calculated from the nominal speed are higher. Therefore it is possible to find a speed, within the range of speed measurement error, that would give a calculated field peak equal to the measured field peak for stroke 8725_1, a fact also true for a majority of strokes in the case of TL, MTL, and DU models and in some cases for the TCS model. However a good match between the model fields and the measured fields after the peak can not be obtained, in general, by a simple change of return stroke speed.

In the DU model it is possible to select the channel-charge discharge time constant, larger values giving smaller but generally narrower, initial field peak values (see Diendorfer and Uman, 1990). For 10 of the return strokes, discharge time constants ranging from 0.2 μs to 0.4 μs gave a better match between the calculated and measured field peaks than did the initially-chosen time constant of 0.1 μs. However, for two of the return stroke currents, 8726_2 and 8726_4, having slowly-rising ramp at the beginning, discharge time constants greater than 0.1 μs reduced the field peaks, but worsened the match after the peak between the calculated fields and the measured fields. A better match between the measured and calculated fields for all the return strokes can not be obtained for the DU model by a simple change to a new value of discharge time constant, although in most individual cases a time constant value can be found to give a better match between the calculated and measured fields. If time constants are customized to the individual return strokes, the DU model can be made to give the best match between the calculated and

measured fields. However, such an arbitrary exercise is probably not worth the effort without a better understanding of the physical relation between the particular choice of the time constant and the particular channel condition of the return stroke.

For strokes 8705_1, 8705_3, 8705_5, 8705_6, 8725_1, 8726_2, 8726_4, and 8732_1 (Figures 5-31, 5-32, 5-33, 5-34, 5-37, 5-42, 5-44, and 5-47 respectively) the measured fields exhibit a narrow initial spike of about 0.1 μs wide. Narrow spikes of about 0.1-0.3 μs are also exhibited by the TCS model fields in 10 cases (Figures 5-31, 5-32, 5-33, 5-34, 5-40, 5-42, 5-43, 5-44, 5-46, and 5-47) and by the DU model fields in 5 cases (Figures 5-31, 5-32, 5-42, 5-44, and 5-47). The narrow initial spikes are never exhibited by the TL and MTL models. Note that for all 7 return strokes that had narrow initial spikes in the measured fields, the TCS model also gave fields with narrow spikes, even though the spike amplitudes were 1.5 to 10 times larger than observed, and the DU model exhibited spikes in 5 cases, even though the amplitudes were 1.2 to 8 times larger than observed. As discussed in section 3.3, Willett et al. (1989) considered these narrow spikes to be due to bi-directional return stroke propagation from a junction point above the triggering structure where the downward leader and upward streamer meet. The initial field spikes were believed to be the doubling effect on the radiation field due to the two propagating current waveforms. As mentioned earlier, the TCS and DU models are also capable of producing similar narrow but large initial spikes. Since these models, nor any examined here, do not assume bi-directional return stroke propagation, the origin of the spikes in calculated waveforms has to be found in the current waveform itself. At a distance of 5 km the electric fields within a couple of microseconds of the start of the return strokes are mostly radiation field and hence determined mainly by the rate of change of current in the channel. A close inspection of channel base currents in Figures 5-2 to 5-29 reveals that in some current waveforms the maximum rate of change of current occurs close to the peak value of current (a current having

a more or less concave waveshape) and in some others the maximum rate-of-change of current occurs close to the beginning of the return stroke (a current having a more or less convex waveshape). The co-ordinates of the point on the current waveform where the maximum rate-of-change of current occurred were found using a computer program. The calculated derivatives suffer from spurious noise in the current records. To reduce the effect of noise, the maximum derivatives were found using straight line sections connecting two consecutive points, every third points, every fourth points, and every fifth points (10 ns, 20 ns, 30 ns, and 40 ns in length), and the calculated maximum current derivatives were compared with the directly measured maximum current derivatives (Table 3-1). It was found that the directly measured current derivative values and the current derivative values calculated from directly measured current values are closer when sections spanning 4 points were used. Table 5-3 gives the coordinates of the maximum rate-of-change of current (the origin of the coordinates is the same as that of the current waveforms in Figure 5-2 to 5-29) and the current value at the time of maximum derivative as a fraction of the peak current. Columns 2 and 3 of Table 5-3 give the measured peak current and the measured peak current derivative respectively of the 28 strokes listed in column 1. Column 4 gives the maximum current derivative calculated from the unaveraged measured currents. The derivatives were found by dividing the difference between the n^{th} and $(n-3)^{rd}$ points by the time span of 30 ns covered by those four points. The time, t_q, and current, i_q, at the mid-point of the span where the maximum current derivative occurred are given in column 6, and 8, respectively. Column 5 gives the 0-100% rise time, t_r, of the return stroke current fronts. In order to find the relative position of the point of the maximum derivative on the wavefront compared to the start time, t_o, of the wavefront (shown by arrows on Figures 5-2 to 5-29), the difference between t_q and t_o are normalized to the respective 0-100% rise time t_r, and the values of $(t_q-t_o)/t_r$ are listed in column 7. Column 9 gives the ratio of the current, i_q, at which maximum derivative is attained to the

respective peak current, i_p, of the return stroke. The amplitudes of the measured field spikes, obtained from the numerically integrated dE/dt, are given in column 10. The amplitudes are the difference between E_p and E_p', given in Table 3-1. Inspection of columns 7, 9, and 10 of Table 5-3 reveals a tendency in which the occurrence of field spikes (column 10) are associated with larger numbers in columns 7 and 9. That is, electric field spikes are associated with the position of occurrence of the maximum current derivatives on the channel-base current wavefront. If the maximum current derivative occurs at a later time and at a higher current on the wavefront, such return strokes are more likely to produce the narrow spikes in the observed field at about 5 km. This is illustrated in Figure 5-50 where the ratio of currents i_q/i_p (column 9) is plotted against the ratio t_q-t_o/t_r (column 7). The solid circles represent the 9 return strokes which produced narrow initial spikes in the electric fields, excluding two marginal cases, 8725_1 and 8725_4 (solid triangles), producing small field spikes of 1 V/m and 2 V/m, respectively. The hollow circles represent the remainder (17) of the return strokes. Note that the solid circles are clustered in the upper right portion of the plot.

For strokes 8726_2 and 8726_4 (Figures 5-42 and 5-44) the model fields from the TCS and DU models have larger (about 8 to 10 times) and broader (0.2-0.3 μs wide) initial narrow spikes than the field spikes on the measured waveforms. The TL and MTL model fields for these two strokes did not have any narrow spikes at all, but the rise times of the return stroke fields are comparable with the measured fields. Interestingly, the current waveforms of both return strokes 8726_2 and 8726_4 (Figure 5-42 and 5-44) have a slowly-rising ramp of about 4 μs and 2 μs at the beginning. A discussion of these current waveforms and their influence on calculated fields is given in the next section, section 5.2.

5.2 Discussion

The narrow initial peaks in the measured field waveforms were postulated by Willett et al. (1988) and Willett et al. (1989) to be due to the bi-directional return stroke development from the junction point between the upward connecting discharge and the downward leader occurring few tens of meters above ground. All 17 return stroke field waveforms, except one, measured in the 1985 experiment (Willett et al., 1988) had narrow initial spikes while only 11 of the 28 return stroke waveforms in the 1987 experiment (Willett et al., 1989) had narrow initial spikes. The mean amplitude of the spikes was about 18 V/m in the 1985 data (derived from Table 2 of Willett et al., 1988), and about 5 V/m in the 1989 data (derived from Table 1 of Willett et al., 1989). The difference in the spikes from these two years were postulated by Diendorfer and Uman (1990) to be due to the different physical configuration of the triggering sites; a striking rod height of 20 m in 1985 and 5 m in 1987. It appears that Le Vine et al. (1989) considered the narrow field spikes as part of a ringing of frequency 9 MHz, which is a persistent feature of the triggered lightning waveform and sometimes happen on the wavefront before the peak (see Figure 4 of Le Vine et al., 1989). Le Vine et al. (1989) did not observe any such ringing in natural lightning waveforms recorded by the same instruments. Leteinturier et al. (1990) compares the fields produced by a return stroke propagating up from ground and propagating in both directions from 15 m above ground. The bi-directional case, assuming no reflection at ground, produced a narrow spike while the upward propagation of the return stroke from ground did not.

As noted in section 3.3, the narrow electric field peaks were removed by Willett et al.(1989) while evaluating the Transmission Line model, for reasons which are not appropriate to the present study and may not be appropriate at all. The major motivation for invoking the

bi-directional return stroke theory to explain the narrow initial spikes was that such narrow spikes can not be explained by the simple Transmission Line model without a similar spike in the channel base current, which was never observed. However, removal of the narrow field peaks does not properly simulate the removal of the lower half of the bi-directional return stroke leaving a simulation of a pure upward TL model. The early return stroke development may well be bi-directional in natural as well as in triggered lightning. On the other hand, there are models which can give the narrow initial field peaks without invocating the bi-directional return stroke theory. The TCS model produces such narrow initial peaks, 0.1-0.3 μs wide, in 10 out of the 18 return strokes considered in this chapter, including 7 cases reported to have spikes in the measured fields by Willett et al. (1989). The DU model (τ = 0.1 μs) also gives narrow field peaks, 0.1-0.3 μs wide, in 5 return strokes, in all of which Willett et al. (1989) also reported narrow peaks in the measured fields. On the other hand, the amplitudes of the narrow peaks from the TCS and DU models are 1.2 to 10 times larger than the amplitudes of the corresponding peaks in the measured fields. However, the measured field peaks may well be larger prior to attenuation due to propagation and measuring system response. As expected, none of the calculated return stroke fields from the TL and the MTL models produce the narrow initial field spikes. In the last section it was shown that the channel base currents of the return strokes producing the narrow field spikes have a different characteristics than the current waveforms which did not produce the narrow field spikes. As evident from Table 5-3 and Figure 5-50, the current waveforms producing the narrow field spikes have their maximum derivatives closer to the peaks than the position of the maximum current derivatives in current waveforms not producing the field spikes. At present it is very difficult to speculate on the physical origin of current waveforms which has its maximum rate of rise near the peak. But what is clear is that these current waveforms are associated with the narrow field spikes observed by (but ignored by) Willett et al. (1989).

The origin of the slowly-varying ramps at the beginning of return stroke currents 8726_2 and 8726_4 is not known. The maximum current value at the end of the ramp is less than 5 kA, which is less than 20% of the peak current. Both these return strokes produced the narrow spikes in electric field records discussed in the preceding paragraph and also had maximum rate-of-rise of current closer to the peak of the current. It is not possible to determine the exact point of inception of the return stroke on the current waveform without time-resolved photographic records of the bottom of the channel correlated with the current waveforms to a fraction of a microsecond. Therefore the possibility that the slowly-rising ramp at the beginning of the current waveform is due to upward propagating positive streamers can not be ruled out.

Idone (1990) had inferred the mean length of the upward connecting discharge in triggered lightning subsequent strokes to be around 12 m (see section 2.2.3). In some strokes Idone (1992) had observed upward unconnected channels of length between 0.2 to 1.6 m in length. Idone (1992) has assumed that these unconnected channels were illuminated simultaneously with the return stroke. As a postscript, Idone (1992) mentions about a communication from A. Eybert-Berard of the French lightning research group stating that investigation of current waveforms of triggered subsequent strokes did not reveal any small currents attributable to connecting discharges just prior to the return stroke. Video images of upward streamers and the return stroke from the second stroke of flash 90-08 during the 1990 triggered lightning experiment conducted by Sandia at KSC are given by Fisher and Schnetzer (1991a). The return stroke current waveform for this stroke is given in Figure 5-51. Figure 5-51a shows the overall return stroke waveform and Figure 5-51b shows the front portion expanded. As noted in Figure 5-51b the position of the maximum rate-of-rise of current is near the peak, similar to those return stroke current waveforms associated with narrow initial spikes in electric field records. Moreover, in Figure 5-51a it can be seen that after the peak the current

falls off relatively rapidly. There are two related questions that can be asked. 1) Are the return strokes with maximum rate-of-rise of current near the peak always associated with strokes with upward discharges? If so, why? 2) Are the return strokes with maximum rate-of-rise of current near the beginning of the wavefront never associated with upward discharges? Correlated return stroke current waveforms with photographic records of the bottom portion of the channel are required to answer these questions. An immediate step in this direction would be to compare the return stroke current waveforms of the strokes for which Idone (1990) had observed upward discharges with those for which he has not observed upward discharges. This analysis might well provide new insights into the attachment process, that is, the transition phase from the leader to return stroke. Unfortunately, these data are not available to us at present.

Why do the TCS and DU models produce the pronounced field peaks for currents with the slow-ramp, while the TL and MTL models do not do so? At the beginning of the return stroke, the TL and the MTL model behave similarly, and the TCS and DU models behave similarly. As an example, consider the relationship between the current at height z' and the channel base current for the TL and the TCS models (see equations 2-13 and 2-14) before the current at the base has attained peak value . Since the current is monotonically increasing during the current front, the TCS model (or DU model) will give, compared to the TL model (or MTL model), larger current all along the channel for time t, as long as $t + z'/c$ is less than the time of the current peak. Figure 5-52 compares the current distribution along the channel for the TL and the DU models. The current distribution along the channel at 0.2, 0.4, and 0.8 μs are very similar for the TL and DU models for return stroke current 8715_10 (Figure 5-13a,b) but very dissimilar for return stroke current 8726_2 (Figure 5-22a,b). Return stroke current 8715_10 has a fast rise time to peak and return stroke current 8726_2 has a slowly-rising initial ramp. The larger magnitudes of the current and hence the larger derivatives along the whole bottom portion

of the channel for 8726_2, required by the TCS and DU models, produce the larger electric field peaks. But such large currents and derivatives at the bottom portion of the channel are not likely to be actually present since the measured fields are only about half that predicted by TCS and DU models. If the slowly-rising initial portion of the current waveform is not due to the return stroke, it is only logical to assume that the position corresponding to the beginning of the return stroke is the end of the ramp.

Up to this point, the return stroke speed has been assumed to be a constant for all the models. As mentioned in section 2.1.3 and 2.2.3, the return stroke speed is observed to decrease with increasing height over a distance of hundreds of meters, although neither the speed of the return stroke nor its variation at the bottom tens of meters of channel has been measured. It follows that variation of return stroke speed with height is a desirable feature to have in the models. In the next chapter the Diendorfer and Uman (1990) model is generalized and extended to include a variable return stroke speed with height.

Table 5-3. Position of maximum rate of change of current on the return stroke wavefront.

1	2	3	4	5	6	7	8	9	10
Stroke	i_p kA	$(di/dt)_p$ Measured kA/μs	$(di/dt)_p$ Calcula. (4pts) kA/μs	t_r 0-100% rise time μs	t_q, Time of $(di/dt)_p$ Calcula. μs	Ratio $(t_q-t_o)/t_r$	i_q, Current at $(di/dt)_p$ Calculat. kA	Ratio i_q/i_p	Field spike V/m
8705_1	8.2	97	87	0.44	1.00	0.73	6.10	0.74	15
8705_3	7.7	108	87	0.18	0.86	0.78	4.36	0.57	18
8705_5	10.3	141	116	0.21	0.99	0.38	6.54	0.63	9
8705_6	11.6	157	131	0.24	0.98	0.29	3.27	0.28	8
8715_2	7.4	76	111	0.46	1.22	0.04	1.66	0.22	0
8715_3	11.2	114	111	0.29	1.27	0.17	2.61	0.23	0
8715_4	10.1	103	95	0.33	1.30	0.27	5.23	0.52	0
8715_6	12.4	119	143	0.45	1.29	0.20	4.04	0.33	0
8715_7	19.9	216	238	0.50	1.46	0.16	5.94	0.30	0
8715_8	9.0	70	111	0.25	1.27	0.28	3.09	0.34	0
8715_9	33.	260	285	0.60	1.42	0.17	7.60	0.23	0
8715_10	15.6	108	111	0.48	1.30	0.17	5.46	0.35	0
8717_3	7.0	119	111	0.25	0.79	0.36	4.51	0.64	13
8717_5	9.1	162	174	0.17	0.79	0.29	4.51	0.50	18
8725_1	20.3	87	117	0.90	0.73	0.06	2.46	0.12	1
8725_2	16.7	110	117	0.60	0.63	0.02	1.05	0.06	0
8725_3	43.	254	304	0.62	0.79	0.15	9.48	0.22	0
8725_4	7.6	67	94	0.19	0.49	0.47	4.21	0.55	2
8725_5	11.7	107	140	0.18	0.51	0.28	4.21	0.36	0
8726_1	$\geq$38	187	187	0.96	0.52	0.08	4.91	0.14	0
8726_2	26.9	123	94	1.02	0.88	0.76	19.00	0.71	17
8726_3	16.4	140	164	0.48	0.46	0.21	5.27	0.32	0
8726_4	22.4	123	117	0.67	0.54	0.51	11.58	0.52	9
8726_5	24.8	153	187	0.70	0.43	0.07	4.91	0.20	0
8728_10	26.9	140	187	0.80	0.58	0.23	7.72	0.29	0
8728_11	16.1	97	187	0.34	0.35	0.26	6.32	0.39	0
8732_1	18.0	140	140	0.88	0.89	0.28	10.53	0.59	18
8732_2	16.8	113	117	0.74	0.73	0.07	3.16	0.19	0

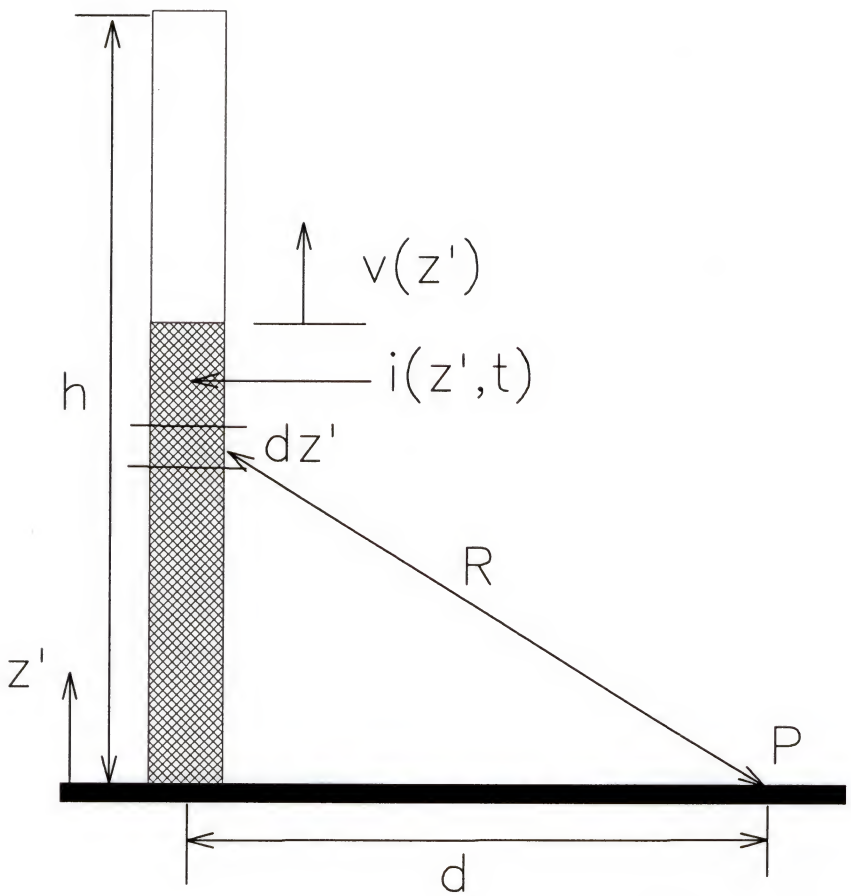

Figure 5-1. Geometrical parameters used in the models.

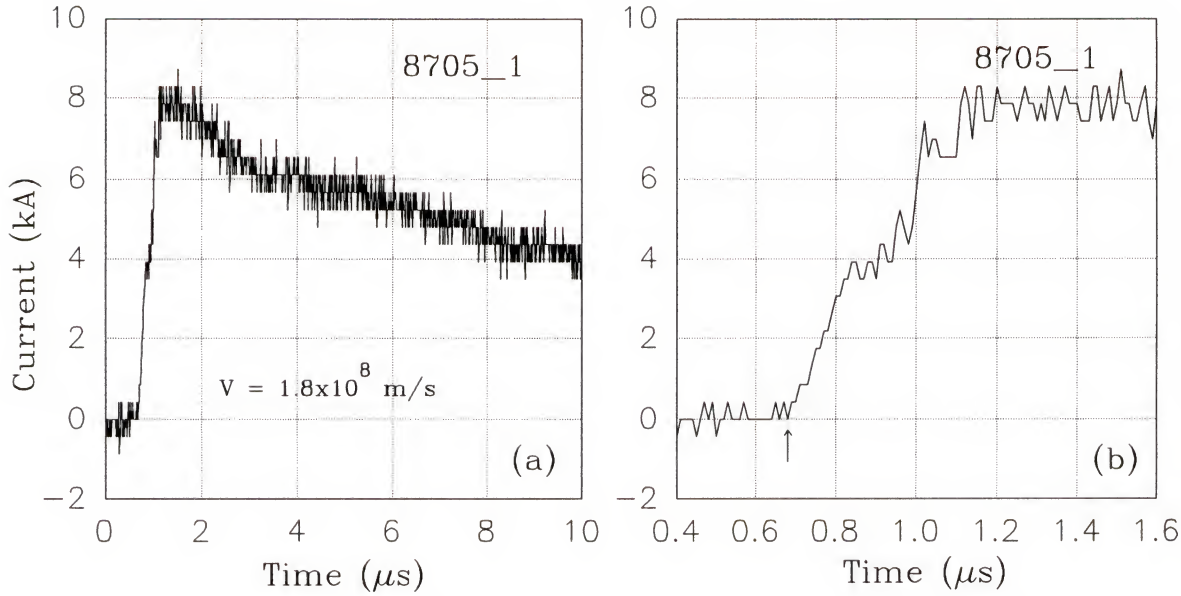

Figure 5-2. Current waveform for return stroke 8705_1 from triggered lightning at KSC, 1987. a) Total available waveform; b) The wavefront on an expanded scale.

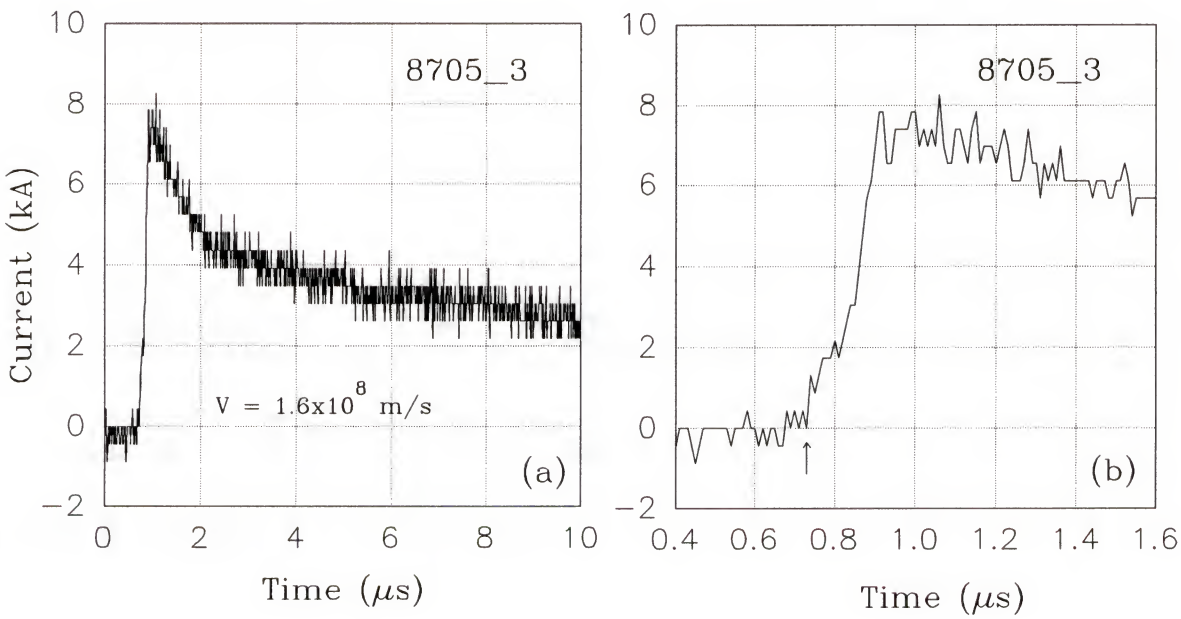

Figure 5-3. Current waveform for return stroke 8705_3. a) Total available waveform; b) The wavefront on an expanded scale.

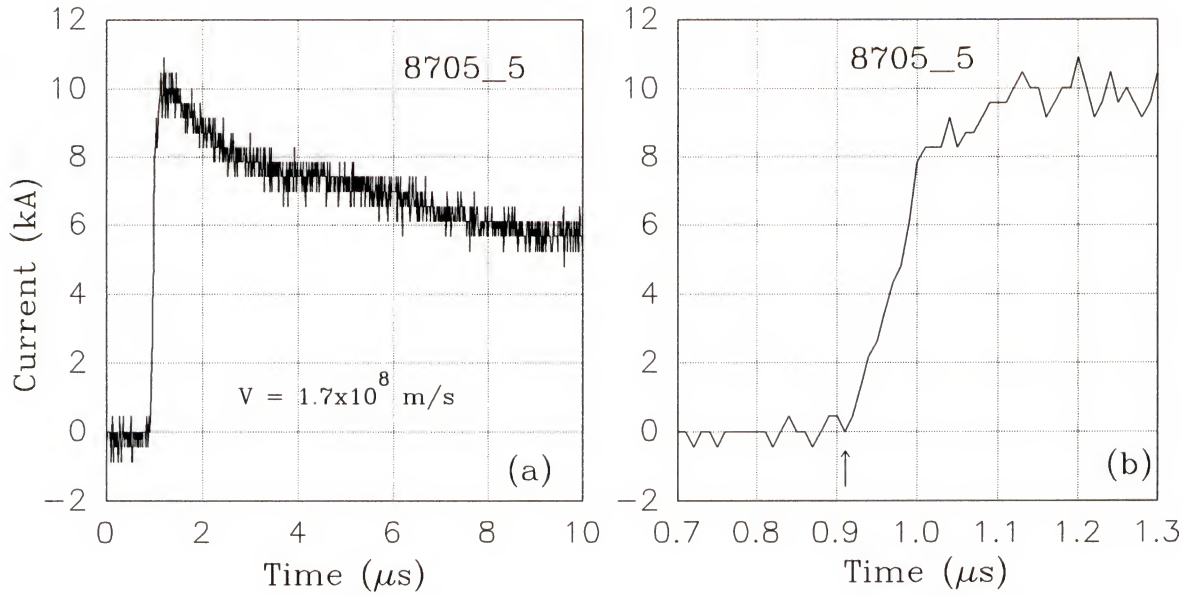

Figure 5-4. Current waveform for return stroke 8705_5. a) Total available waveform; b) The wavefront on an expanded scale.

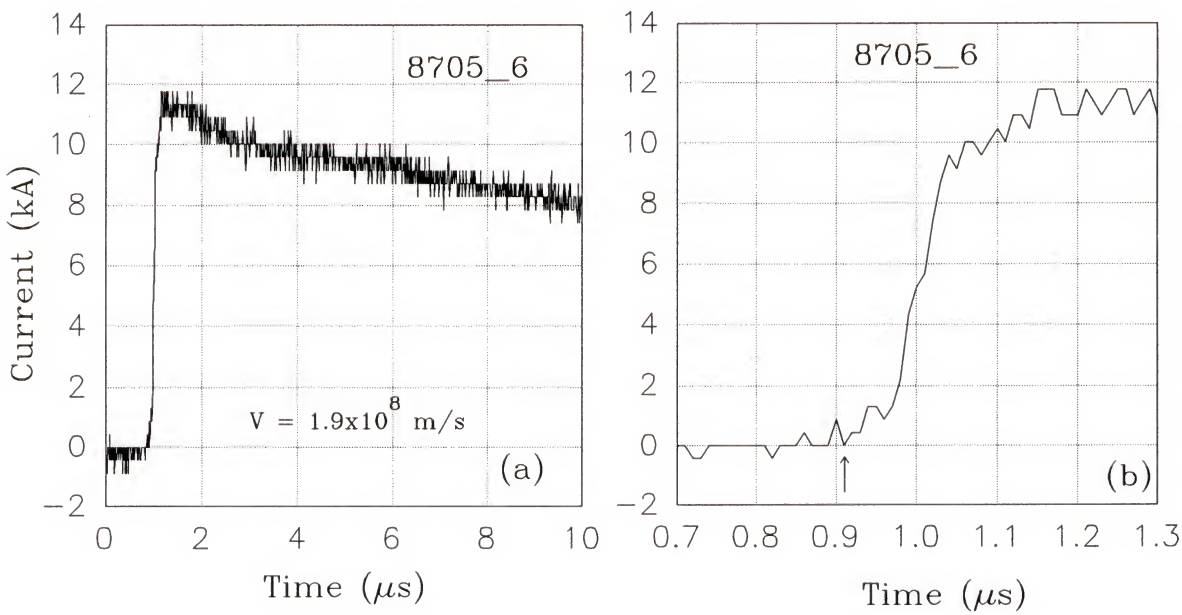

Figure 5-5. Current waveform for return stroke 8705_6. a) Total available waveform; b) The wavefront on an expanded scale.

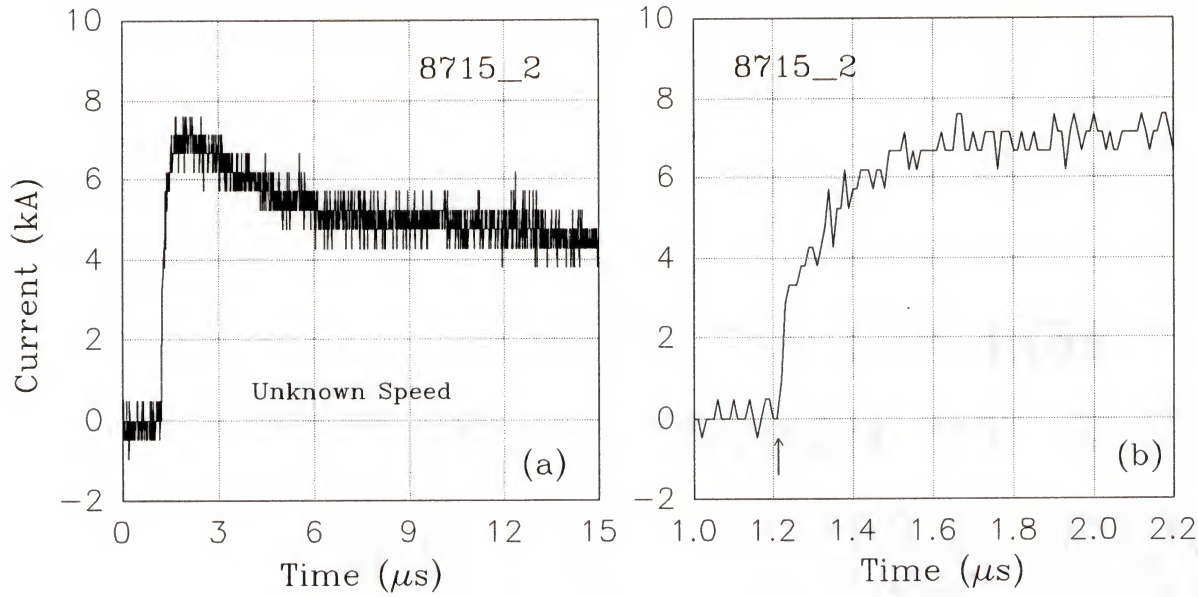

Figure 5-6. Current waveform for return stroke 8715_2. a) Total available waveform; b) The wavefront on an expanded scale.

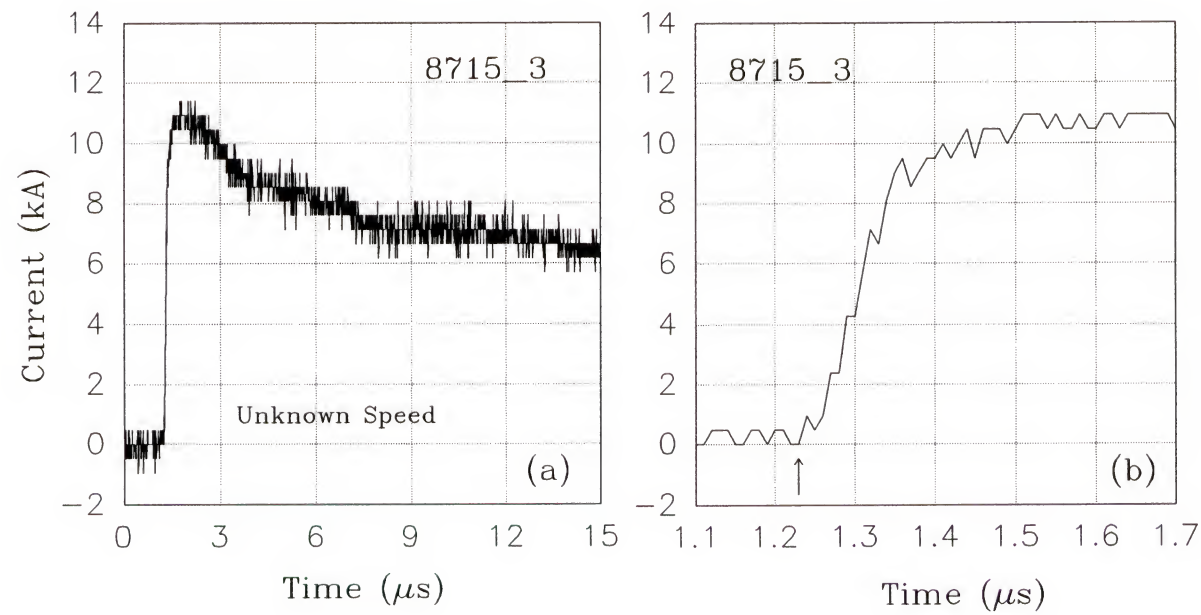

Figure 5-7. Current waveform for return stroke 8715_3. a) Total available waveform; b) The wavefront on an expanded scale.

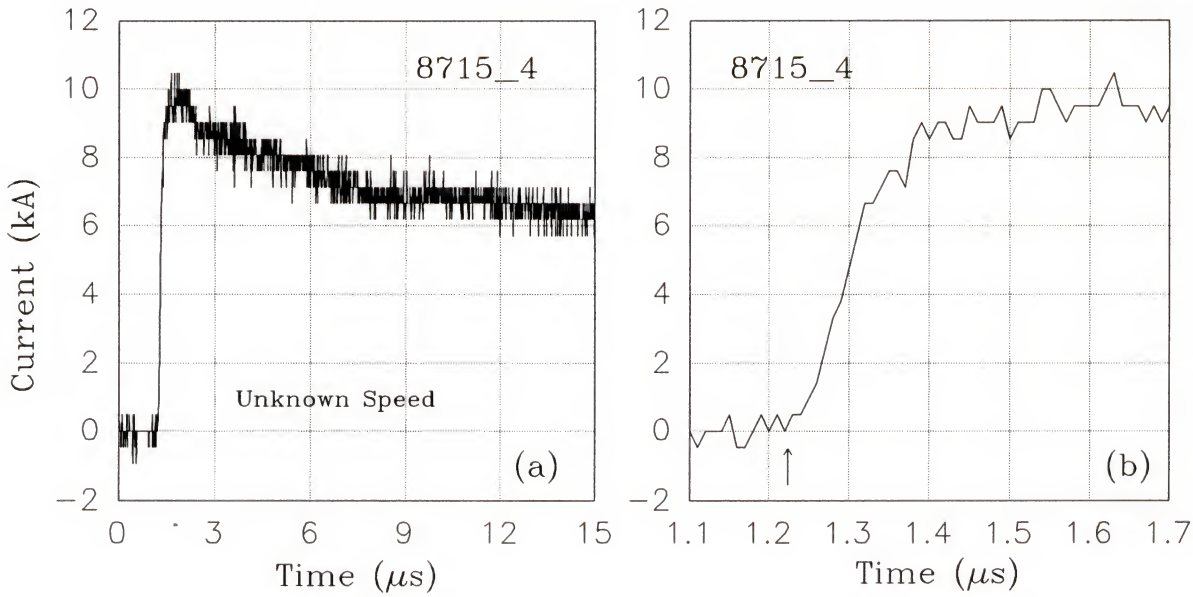

Figure 5-8. Current waveform for return stroke 8715_4. a) Total available waveform; b) The wavefront on an expanded scale.

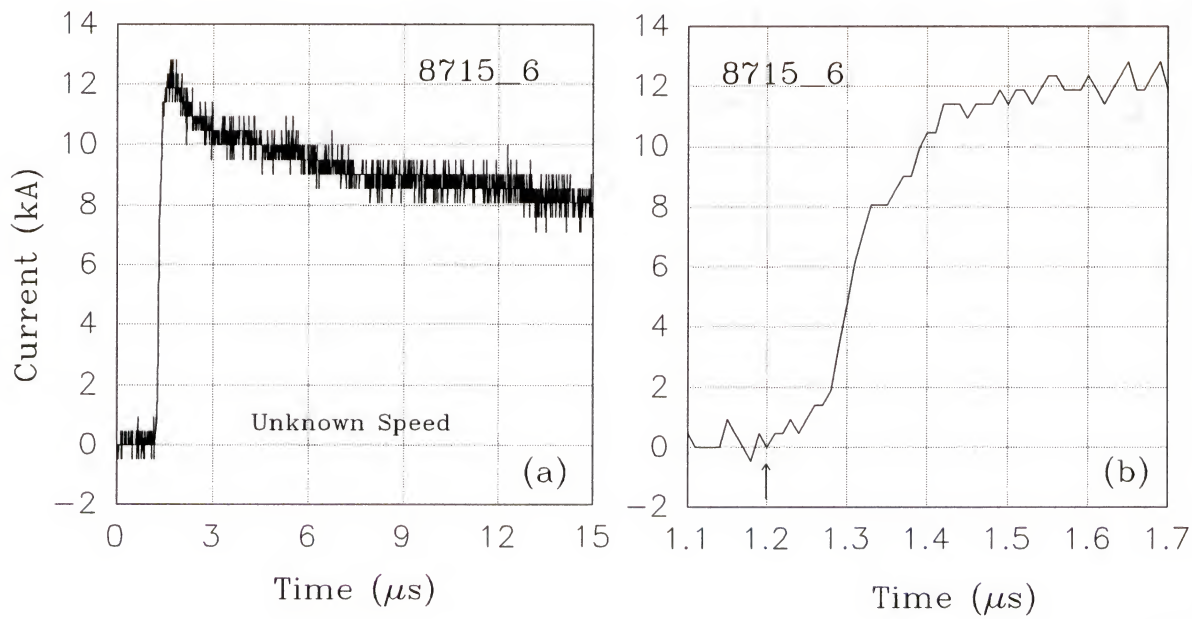

Figure 5-9. Current waveform for return stroke 8715_6. a) Total available waveform; b) The wavefront on an expanded scale.

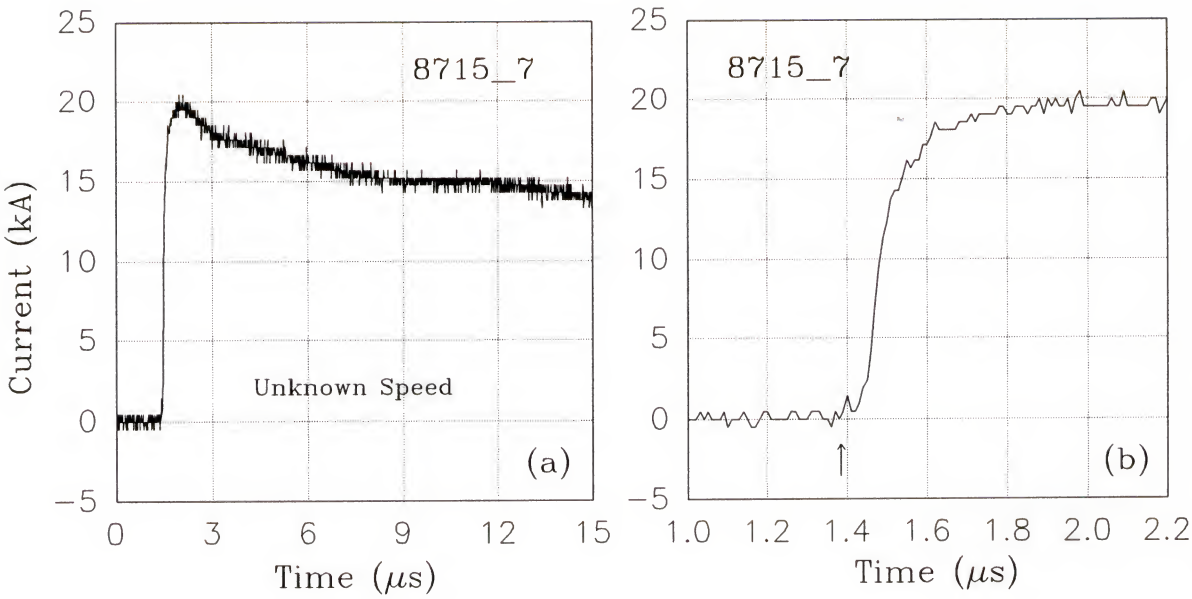

Figure 5-10. Current waveform for return stroke 8715_7. a) Total available waveform; b) The wavefront on an expanded scale.

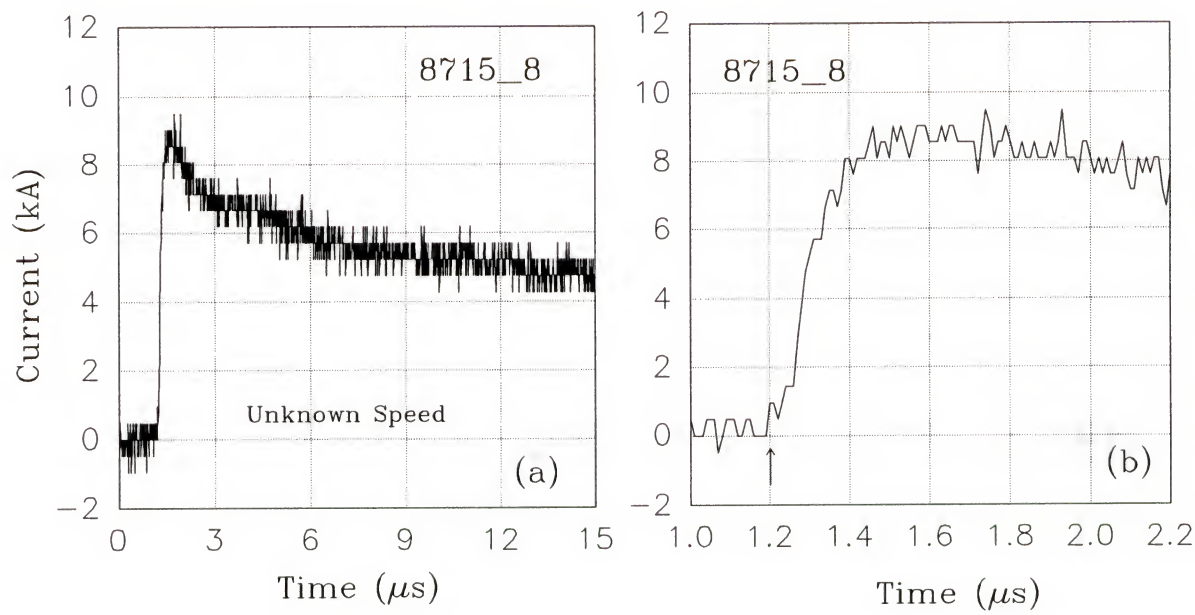

Figure 5-11. Current waveform for return stroke 8715_8. a) Total available waveform; b) The wavefront on an expanded scale.

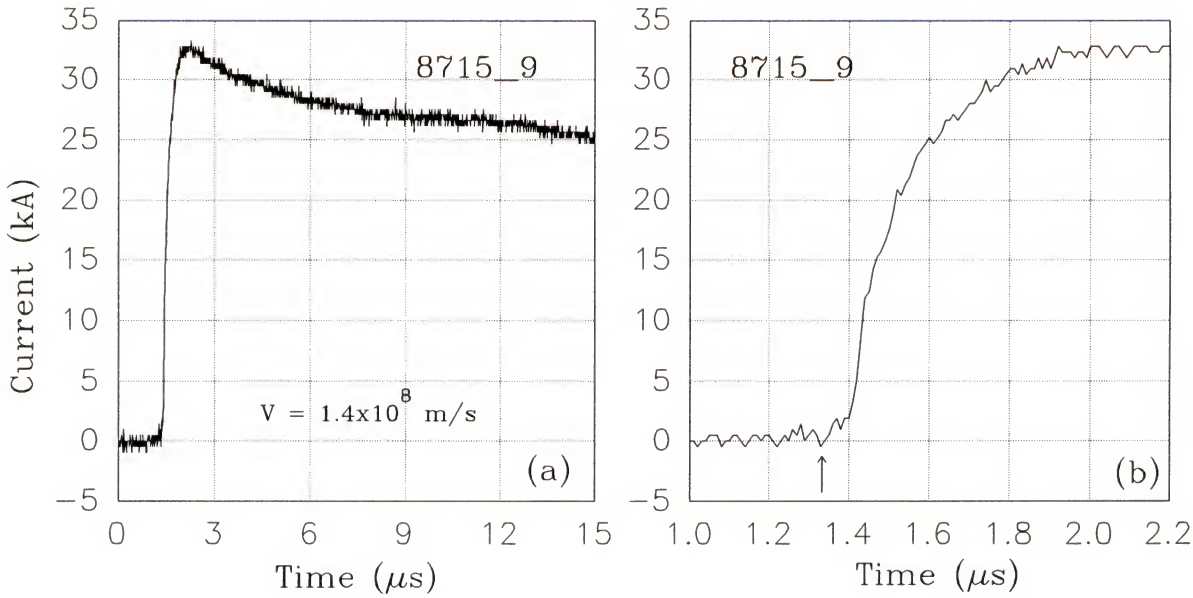

Figure 5-12. Current waveform for return stroke 8715_9. a) Total available waveform; b) The wavefront on an expanded scale.

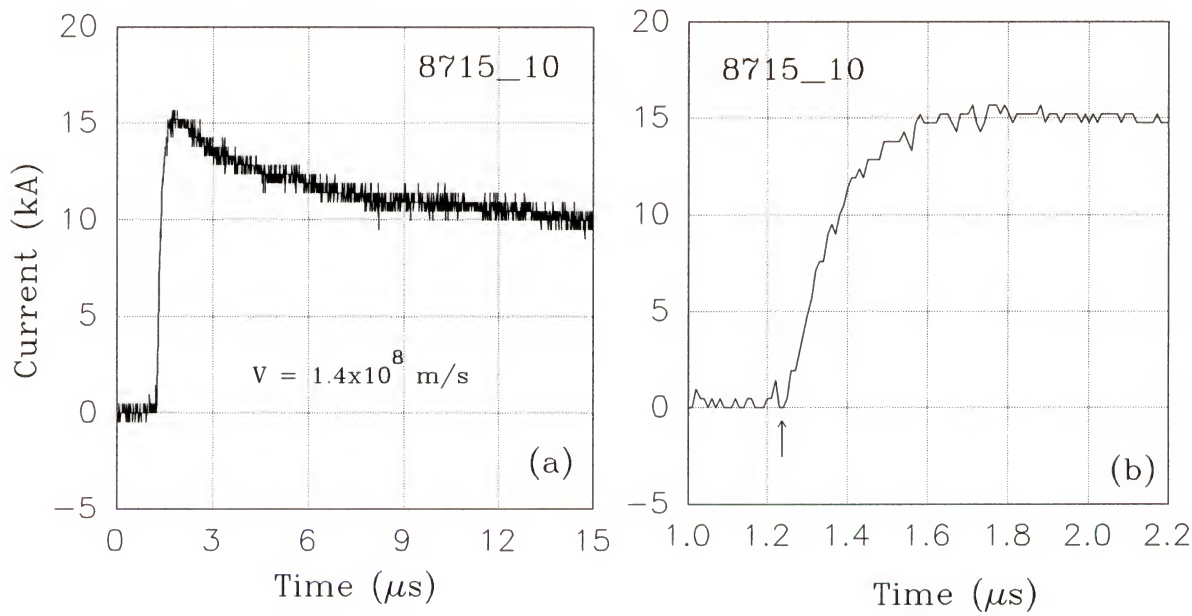

Figure 5-13. Current waveform for return stroke 8715_10. a) Total available waveform; b) The wavefront on an expanded scale.

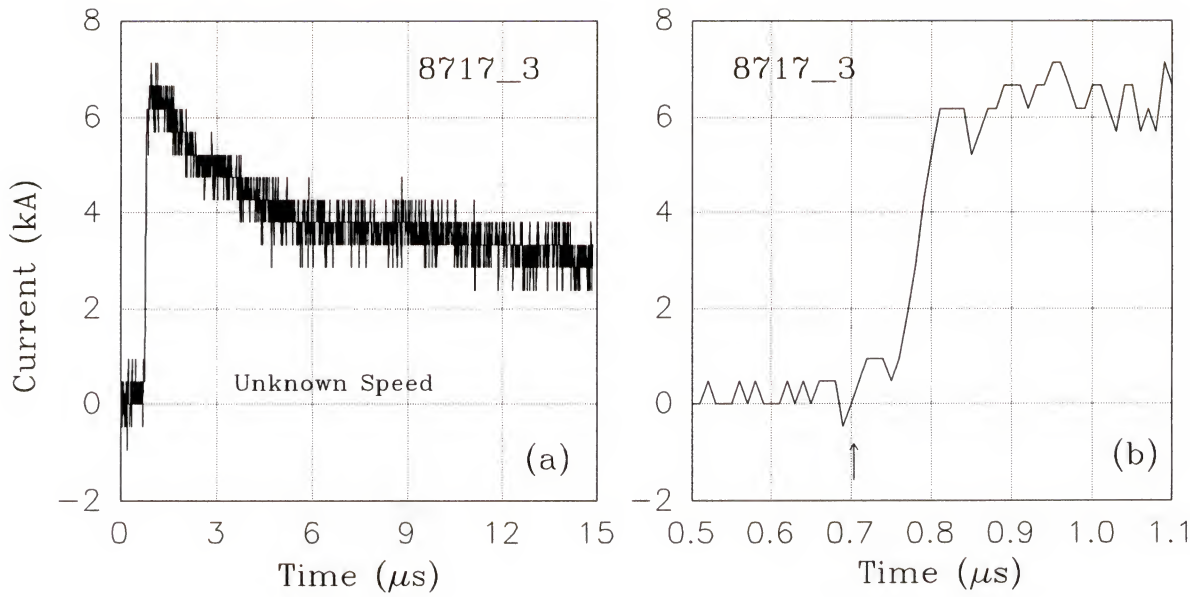

Figure 5-14. Current waveform for return stroke 8717_3. a) Total available waveform; b) The wavefront on an expanded scale.

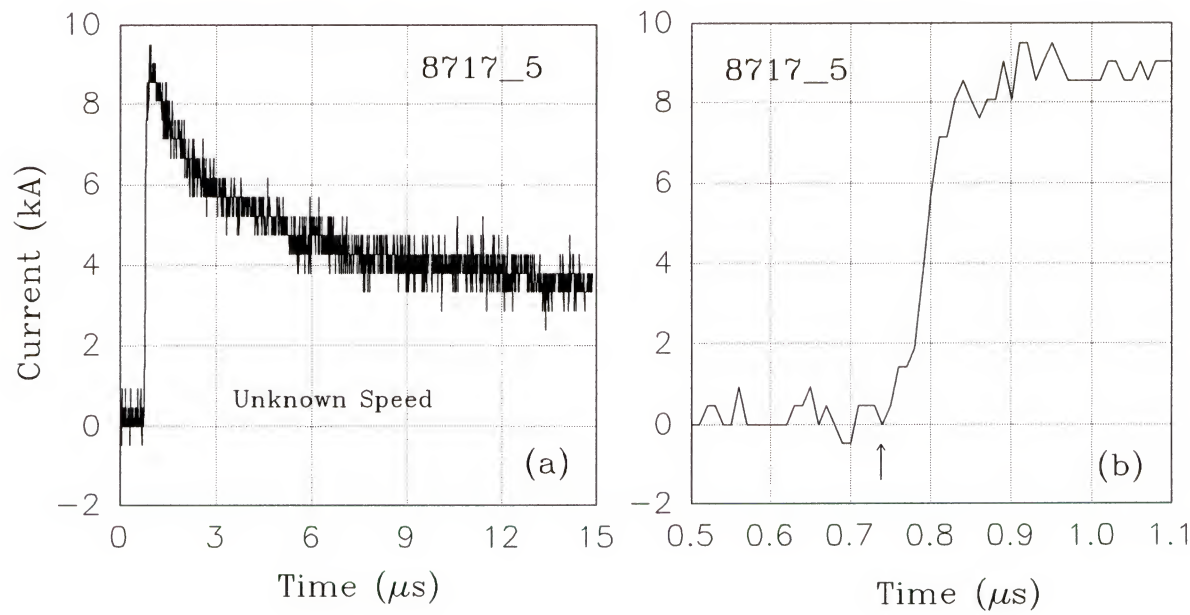

Figure 5-15. Current waveform for return stroke 8717_5. a) Total available waveform; b) The wavefront on an expanded scale.

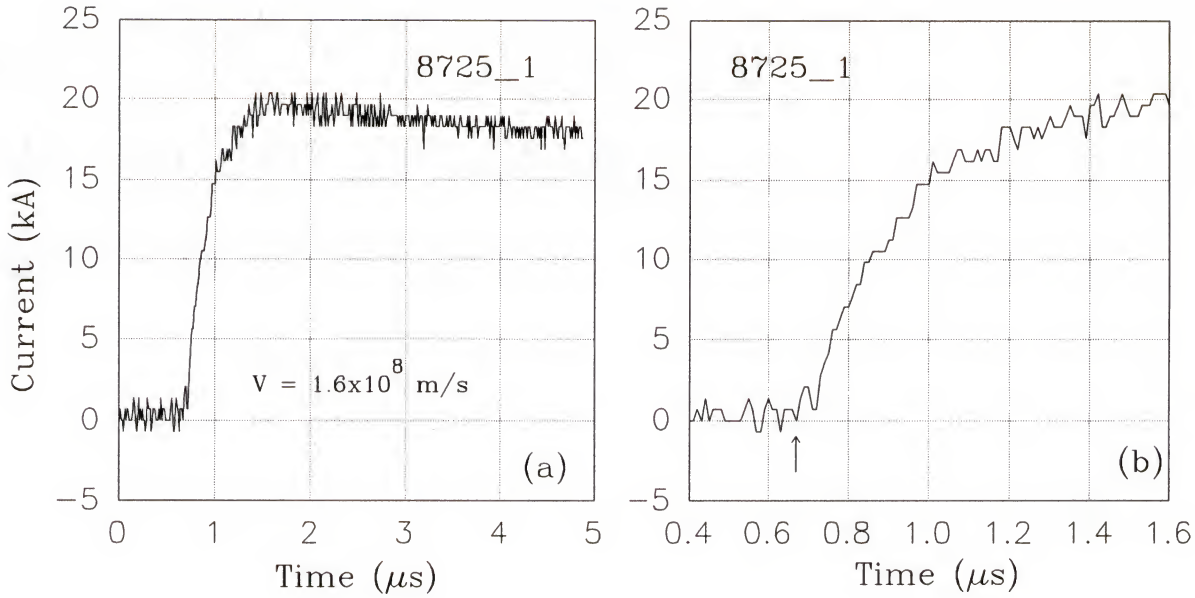

Figure 5-16. Current waveform for return stroke 8725_1. a) Total available waveform; b) The wavefront on an expanded scale.

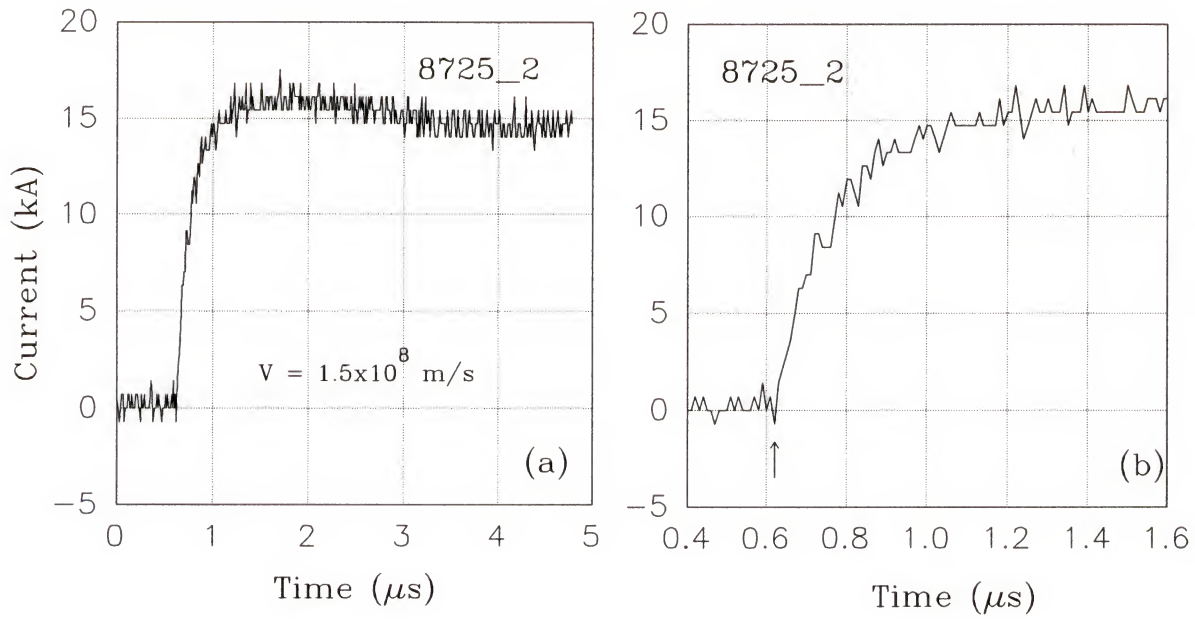

Figure 5-17. Current waveform for return stroke 8725_2. a) Total available waveform; b) The wavefront on an expanded scale.

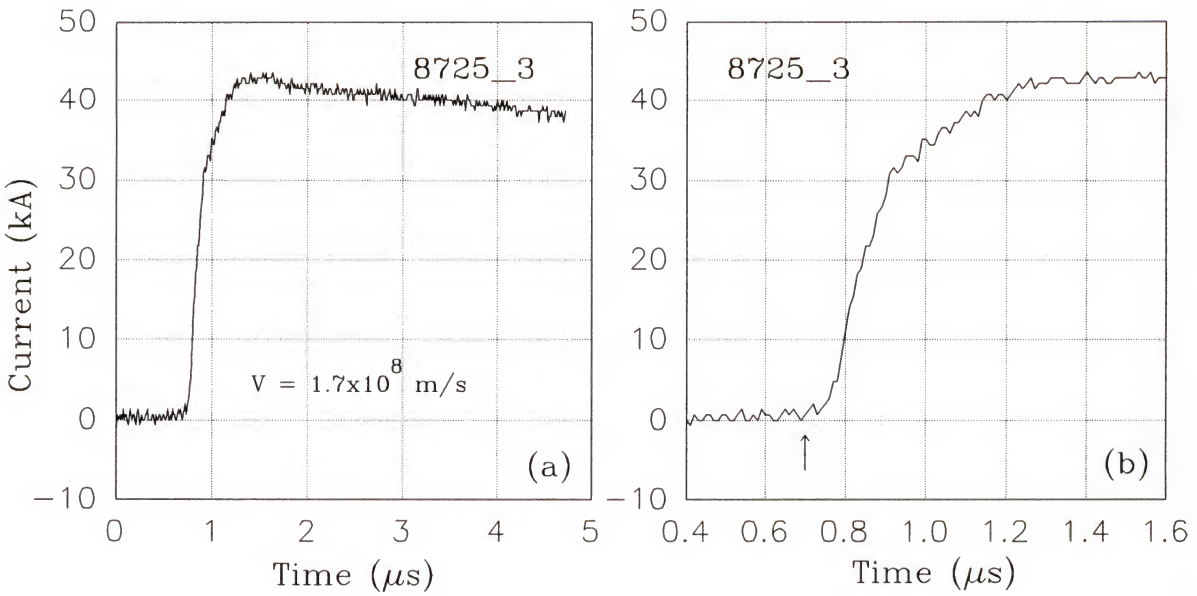

Figure 5-18. Current waveform for return stroke 8725_3. a) Total available waveform; b) The wavefront on an expanded scale.

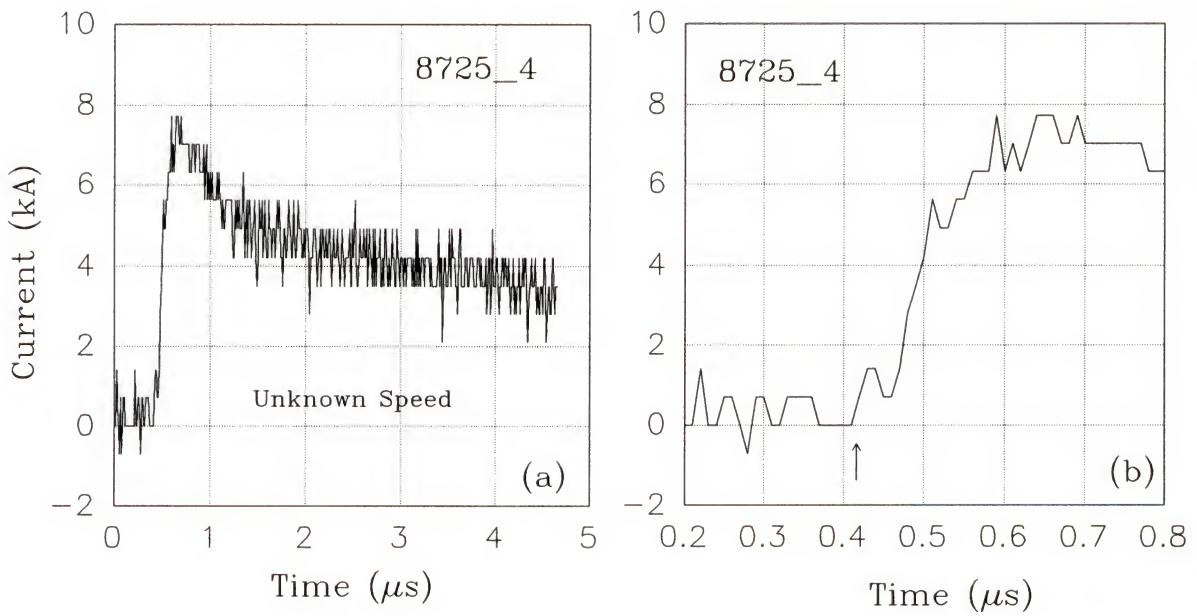

Figure 5-19. Current waveform for return stroke 8725_4. a) Total available waveform; b) The wavefront on an expanded scale.

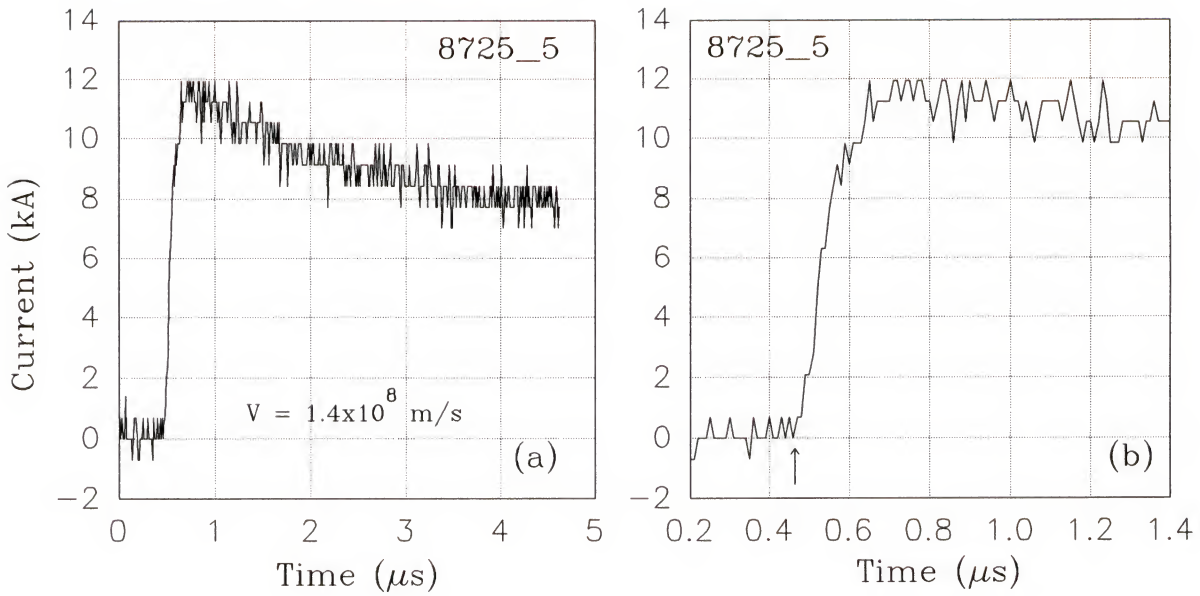

Figure 5-20. Current waveform for return stroke 8725_5. a) Total available waveform; b) The wavefront on an expanded scale.

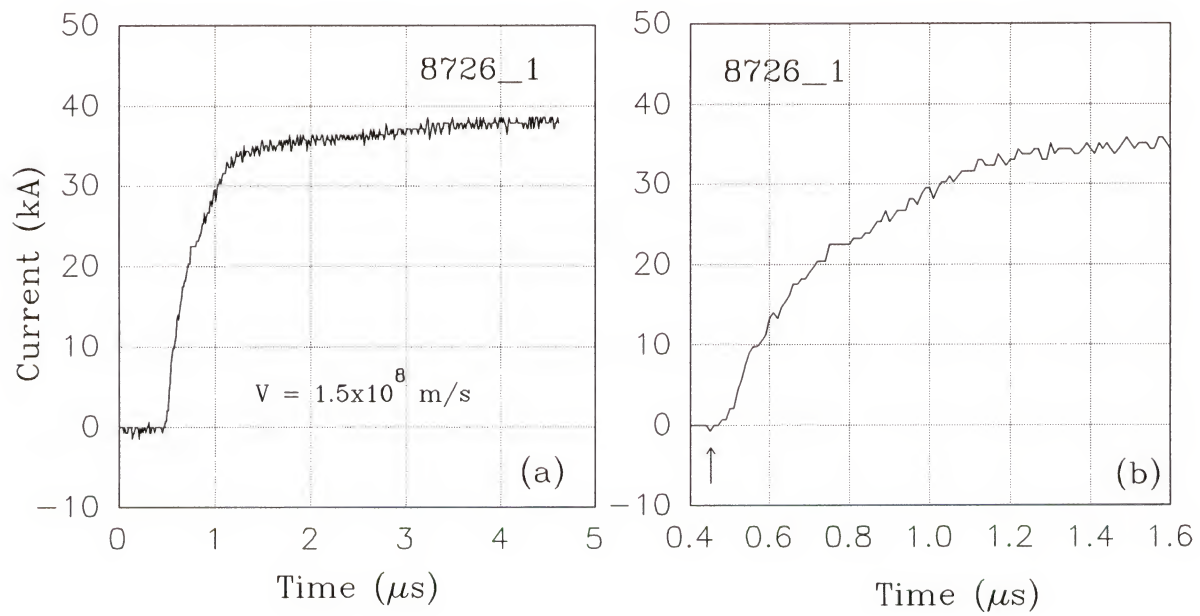

Figure 5-21. Current waveform for return stroke 8725_4. a) Total available waveform; b) The wavefront on an expanded scale.

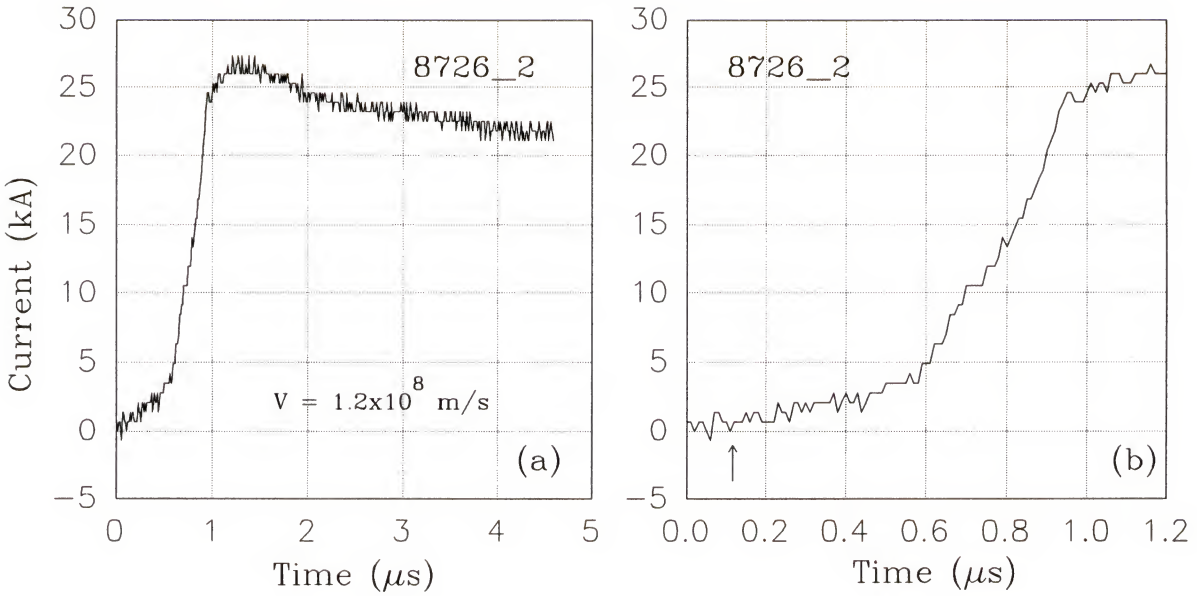

Figure 5-22. Current waveform for return stroke 8726_2. a) Total available waveform; b) The wavefront on an expanded scale.

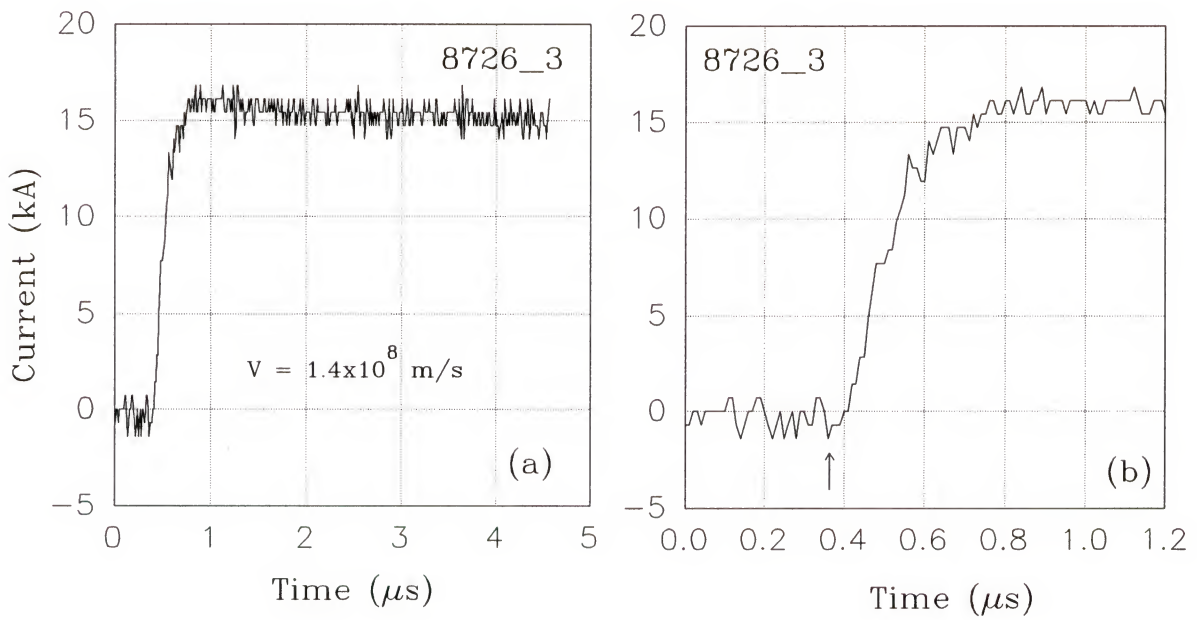

Figure 5-23. Current waveform for return stroke 8726_3. a) Total available waveform; b) The wavefront on an expanded scale.

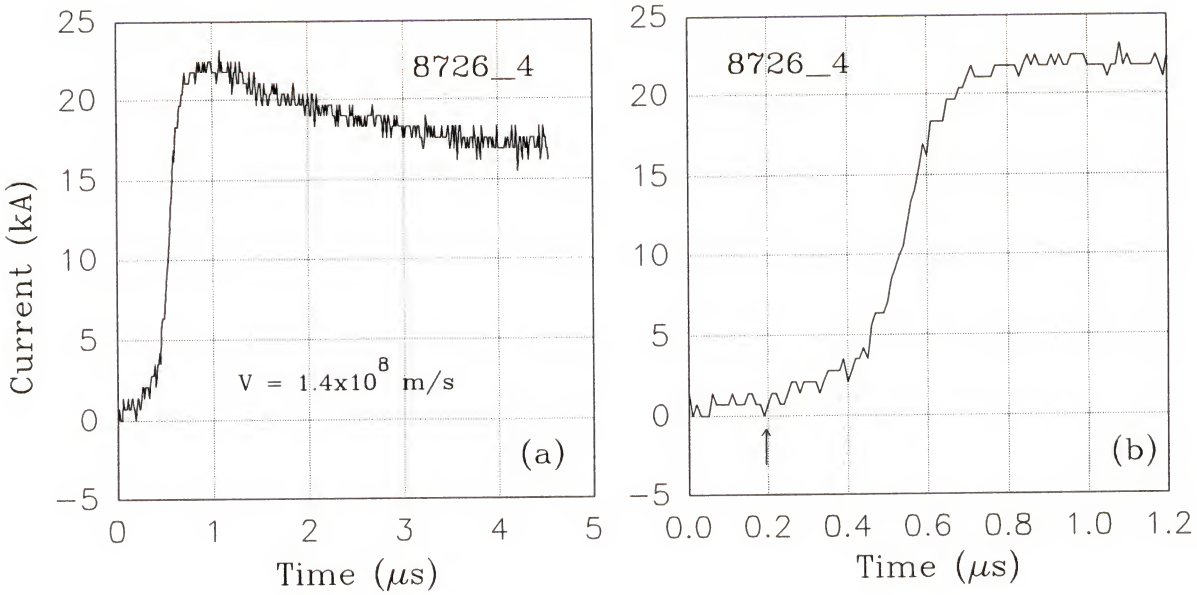

Figure 5-24. Current waveform for return stroke 8726_4. a) Total available waveform; b) The wavefront on an expanded scale.

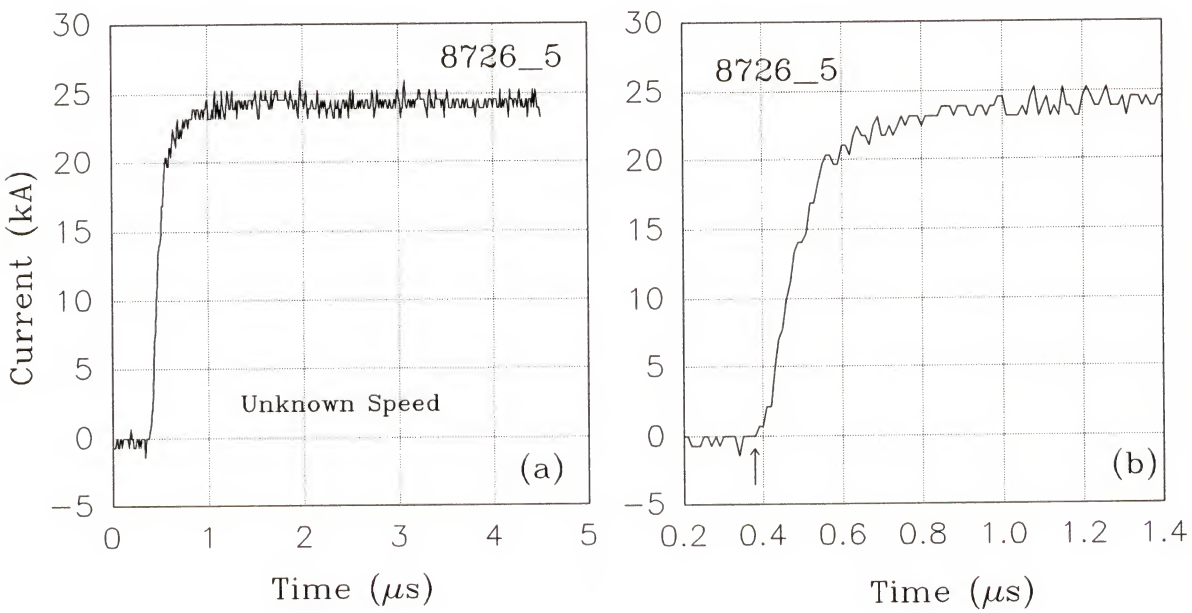

Figure 5-25. Current waveform for return stroke 8726_5. a) Total available waveform; b) The wavefront on an expanded scale.

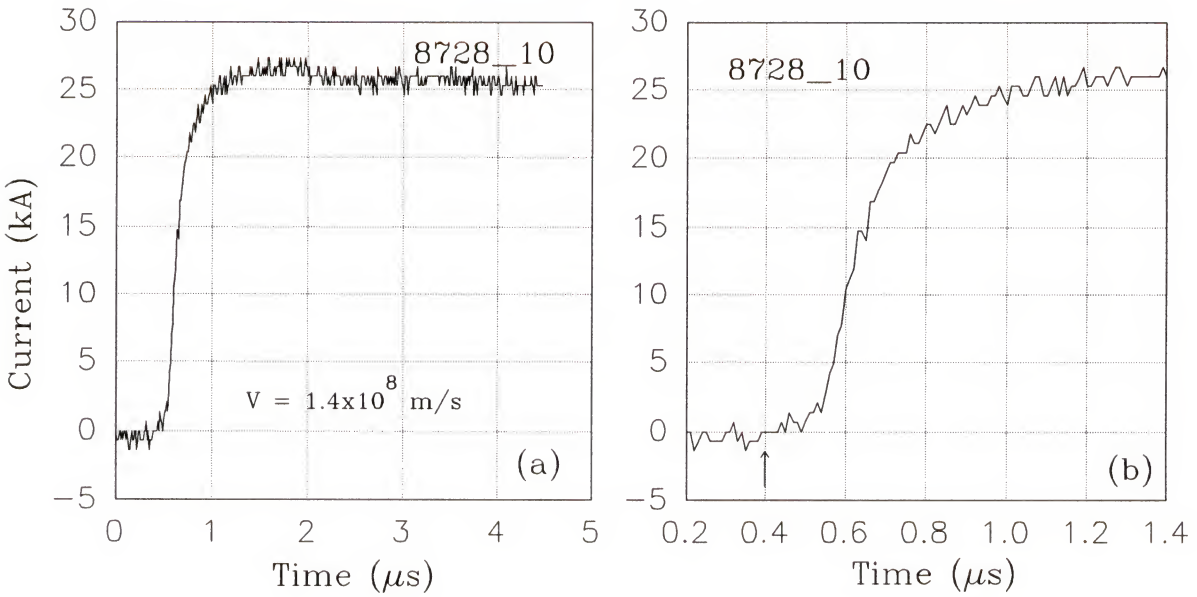

Figure 5-26. Current waveform for return stroke 8728_10. a) Total available waveform; b) The wavefront on an expanded scale.

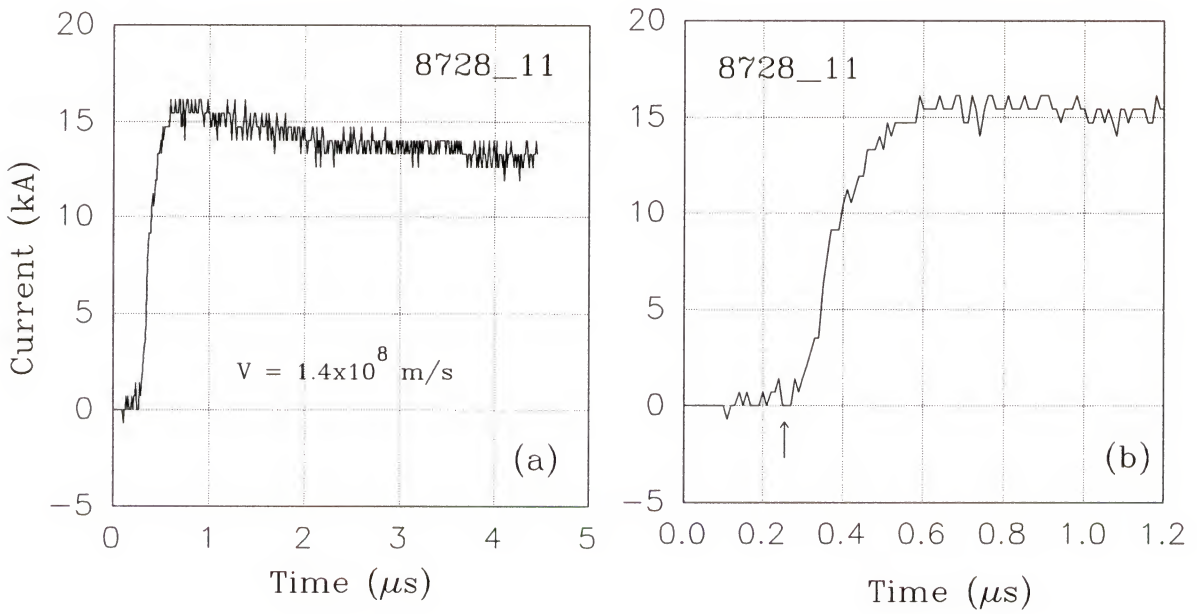

Figure 5-27. Current waveform for return stroke 8728_11. a) Total available waveform; b) The wavefront on an expanded scale.

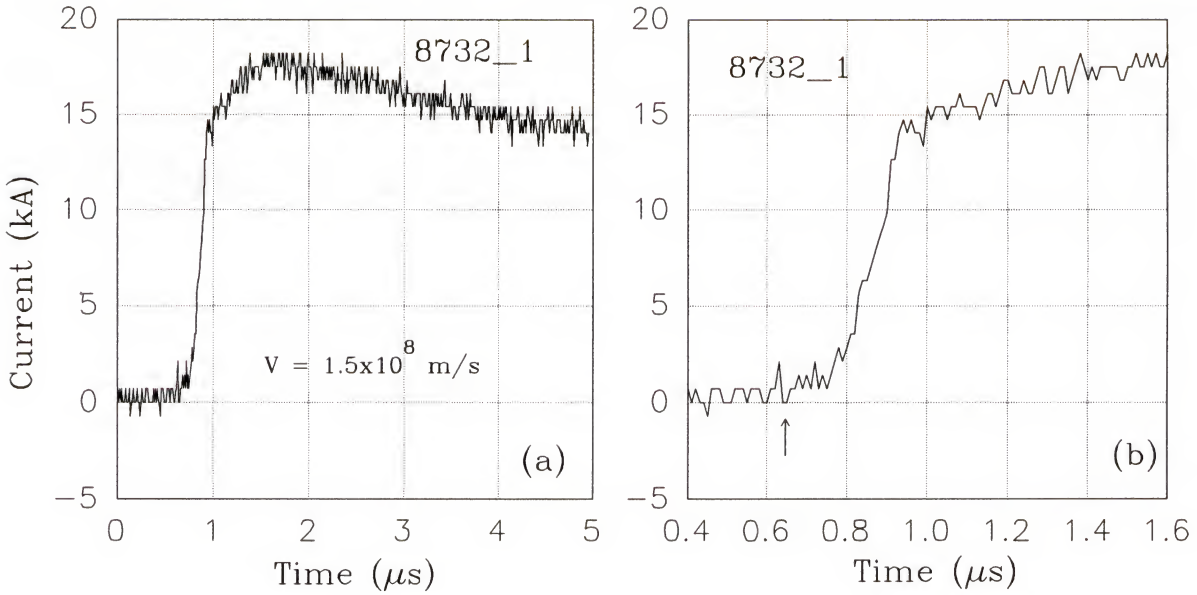

Figure 5-28. Current waveform for return stroke 8732_1. a) Total available waveform; b) The wavefront on an expanded scale.

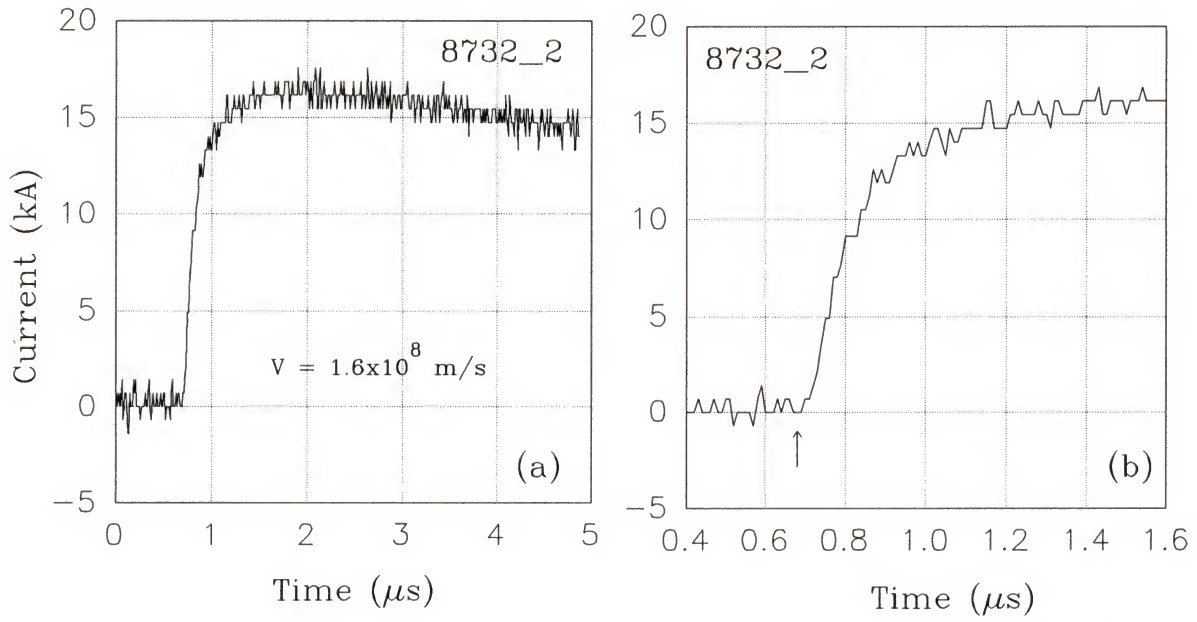

Figure 5-29. Current waveform for return stroke 8732_2. a) Total available waveform; b) The wavefront on an expanded scale.

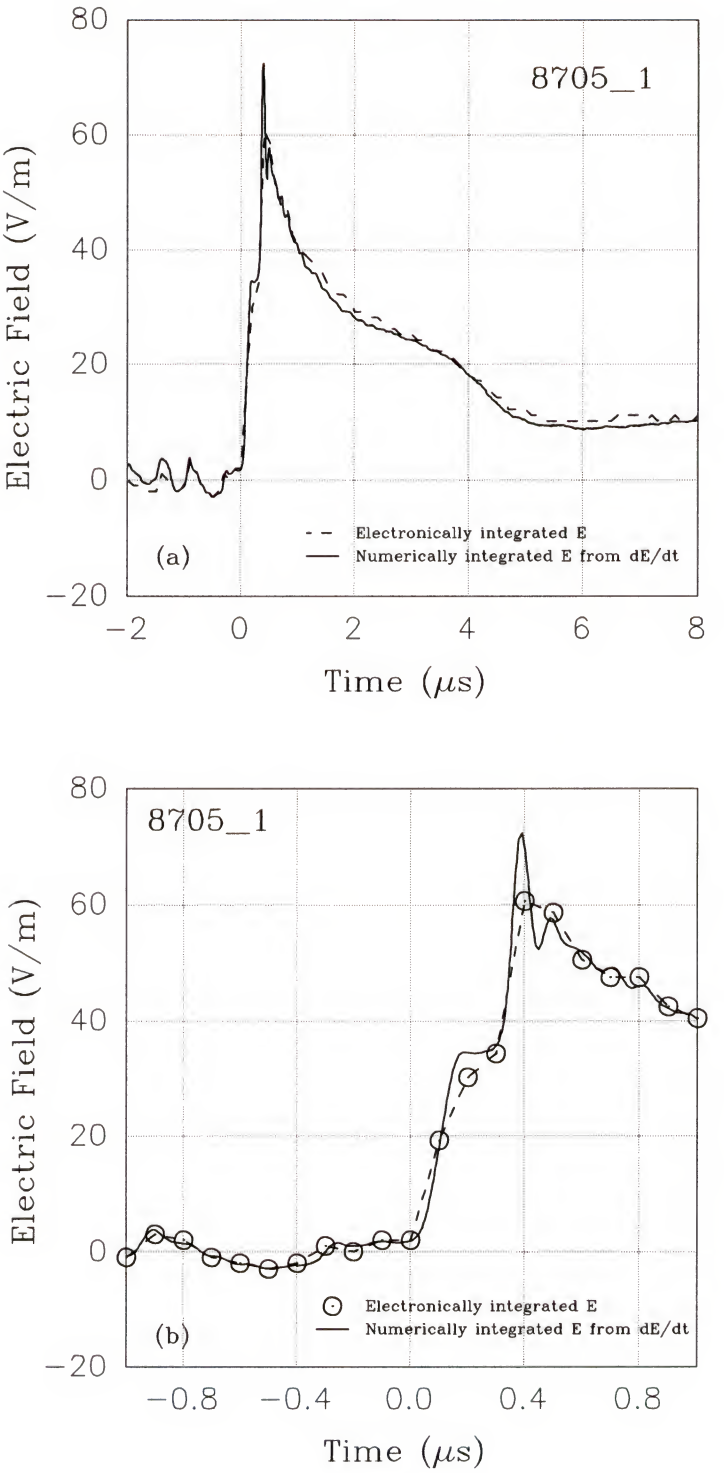

Figure 5-30. An example of comparison of electronically integrated and numerically integrated return stroke electric field waveforms. a) Overall waveform; b) The front portion on an expanded scale.

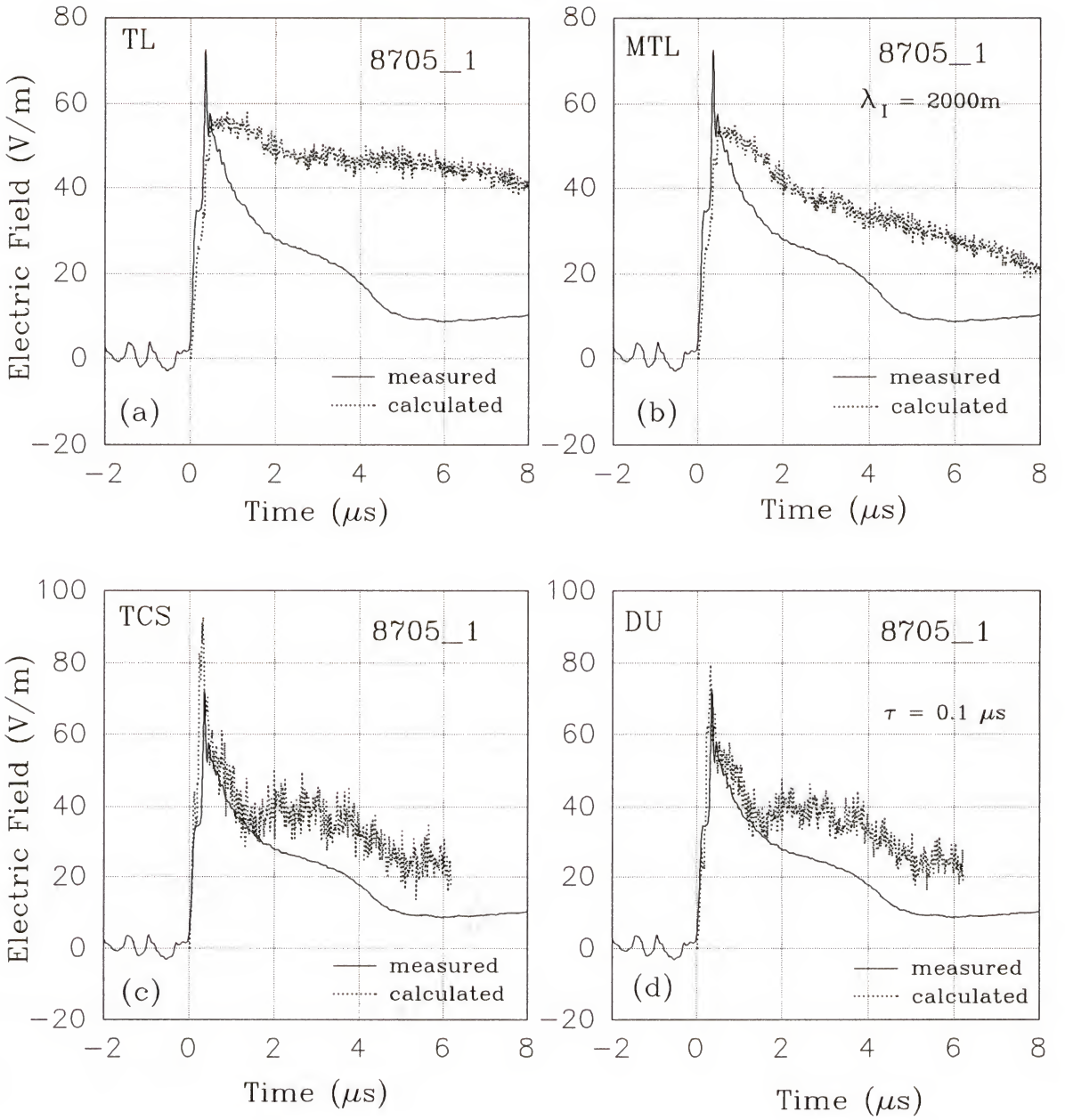

Figure 5-31. Comparison of calculated fields from the various models with the measured field at 5.16 km for the return stroke 8705_1. The measured current at the channel base and the measured return stroke speed are given in Figure 5-2. a) TL model; b) MTL model; c) TCS model; d) DU model.

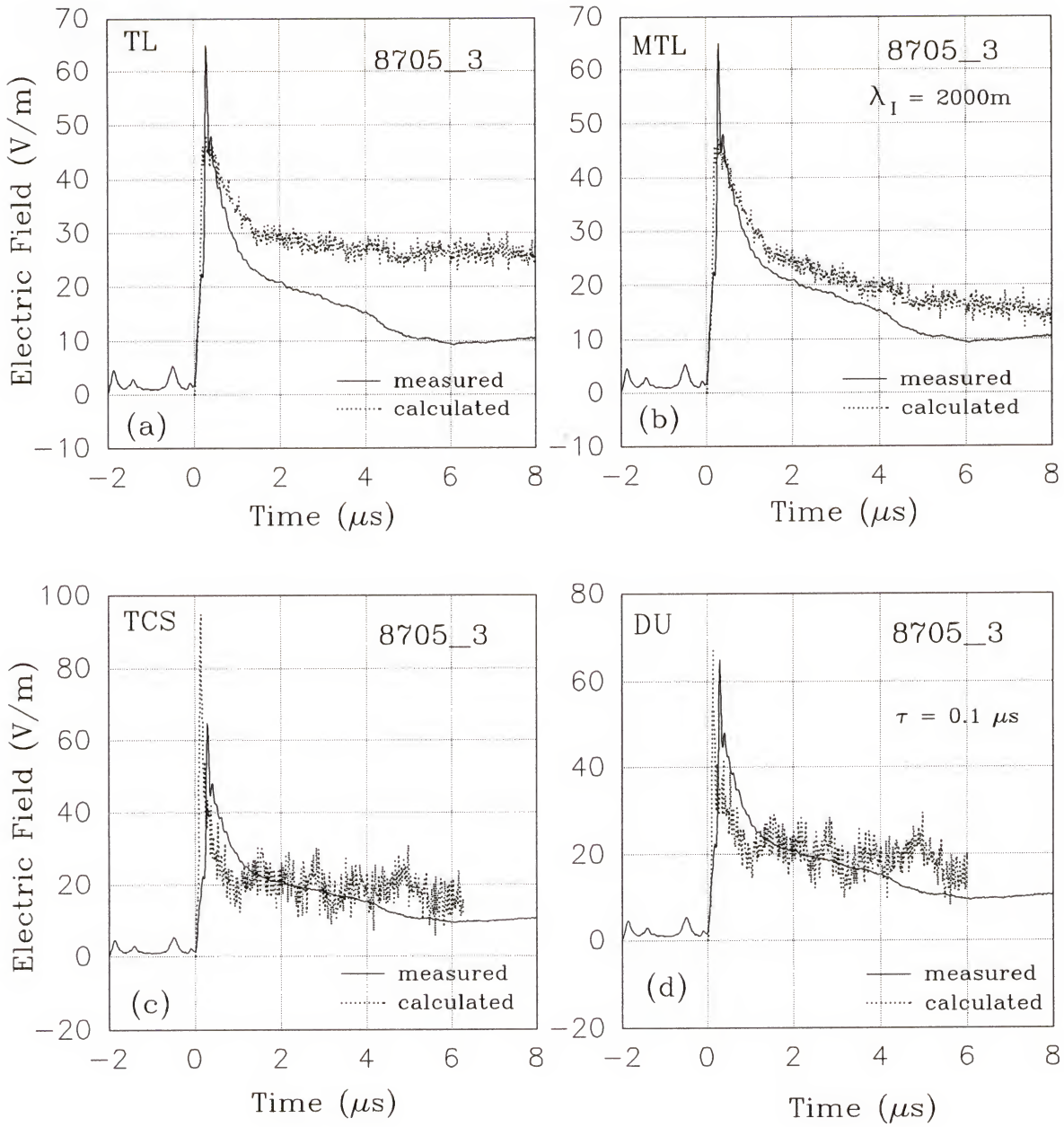

Figure 5-32. Comparison of calculated fields from the various models with the measured field at 5.16 km for the return stroke 8705_3. The measured current at the channel base and the measured return stroke speed are given in Figure 5-3. a) TL model; b) MTL model; c) TCS model; d) DU model.

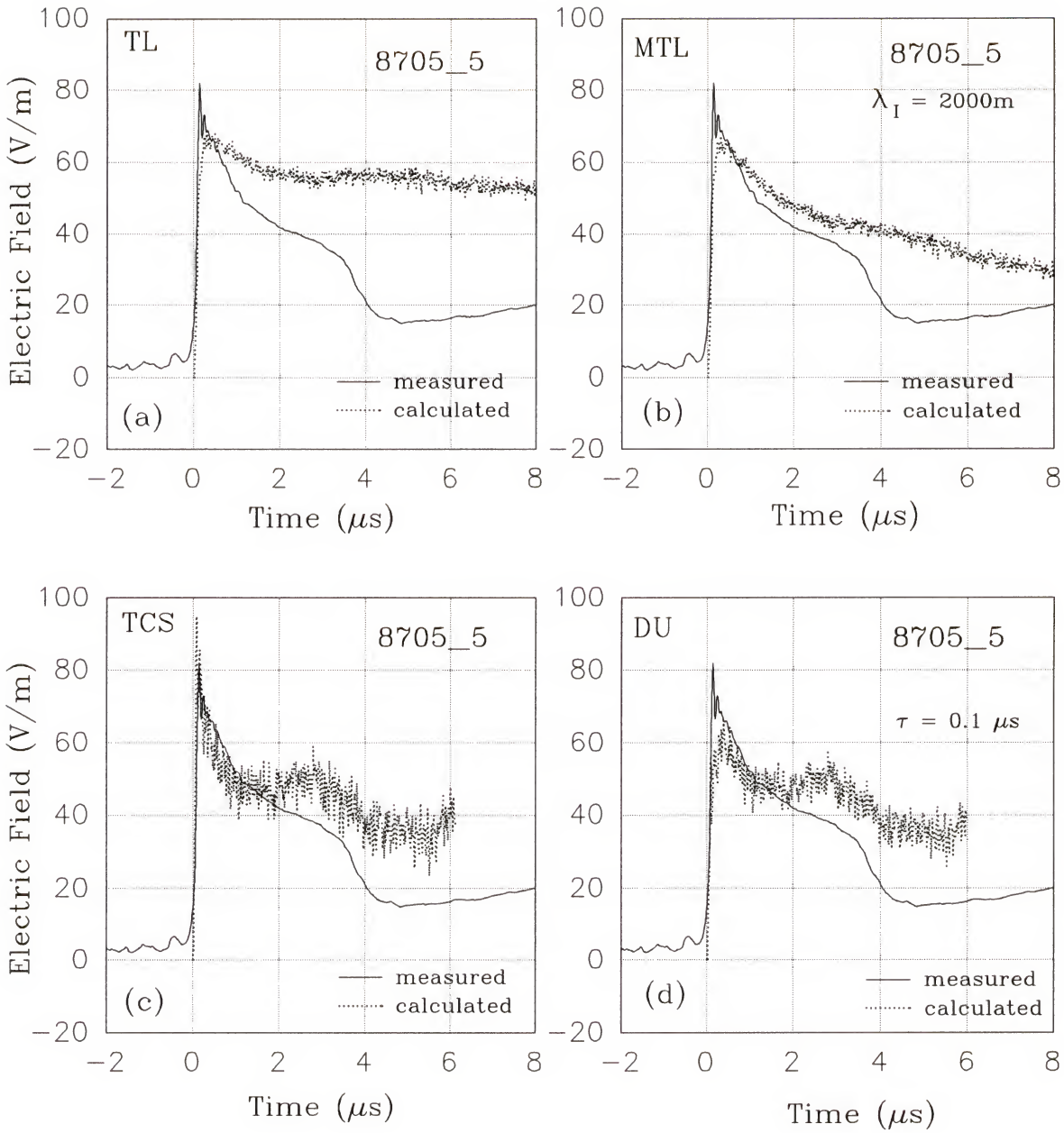

Figure 5-33. Comparison of calculated fields from the various models with the measured field at 5.16 km for the return stroke 8705_5. The measured current at the channel base and the measured return stroke speed are given in Figure 5-4. a) TL model; b) MTL model; c) TCS model; d) DU model.

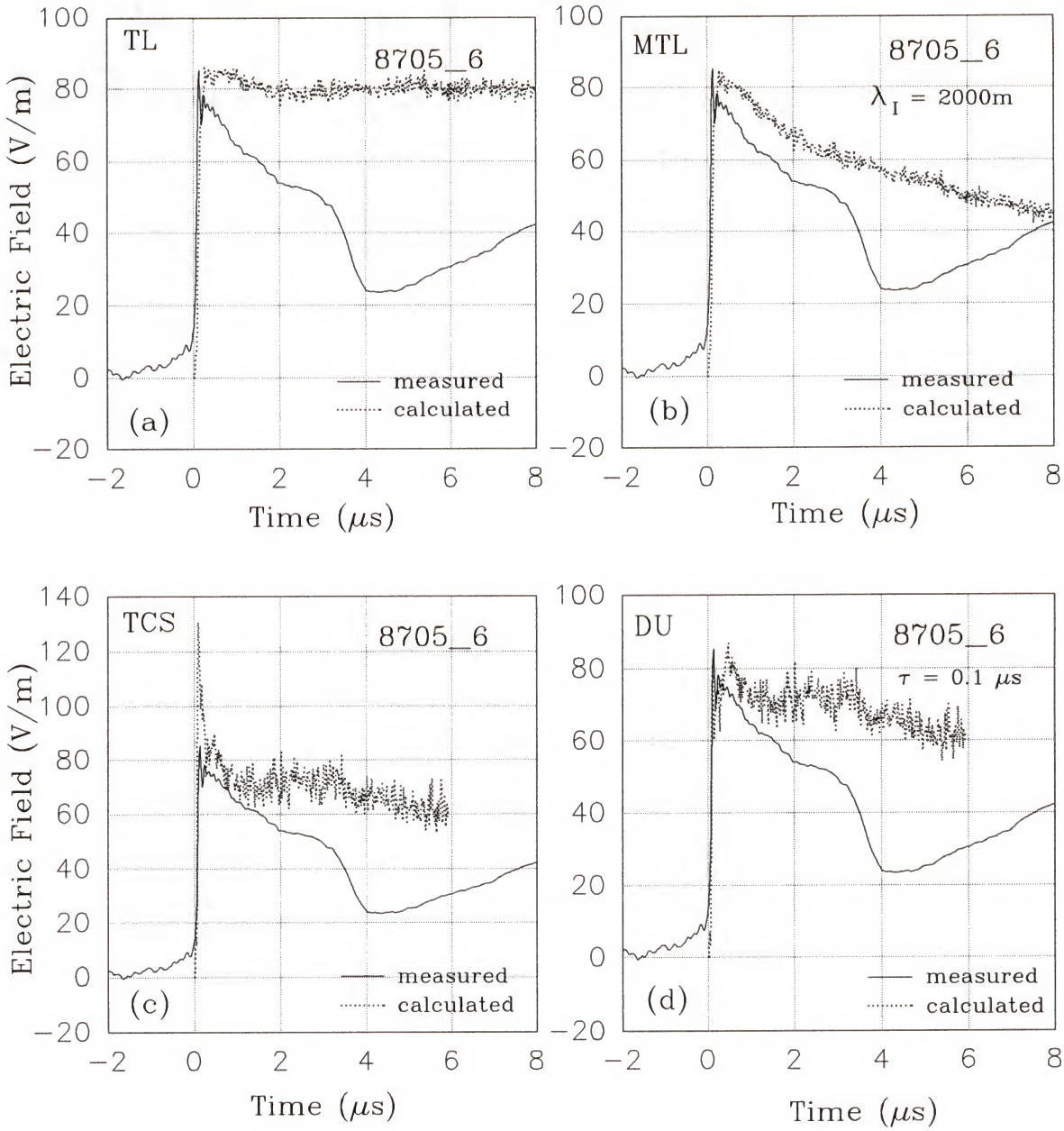

Figure 5-34. Comparison of calculated fields from the various models with the measured field at 5.16 km for the return stroke 8705_6. The measured current at the channel base and the measured return stroke speed are given in Figure 5-5. a) TL model; b) MTL model; c) TCS model; d) DU model.

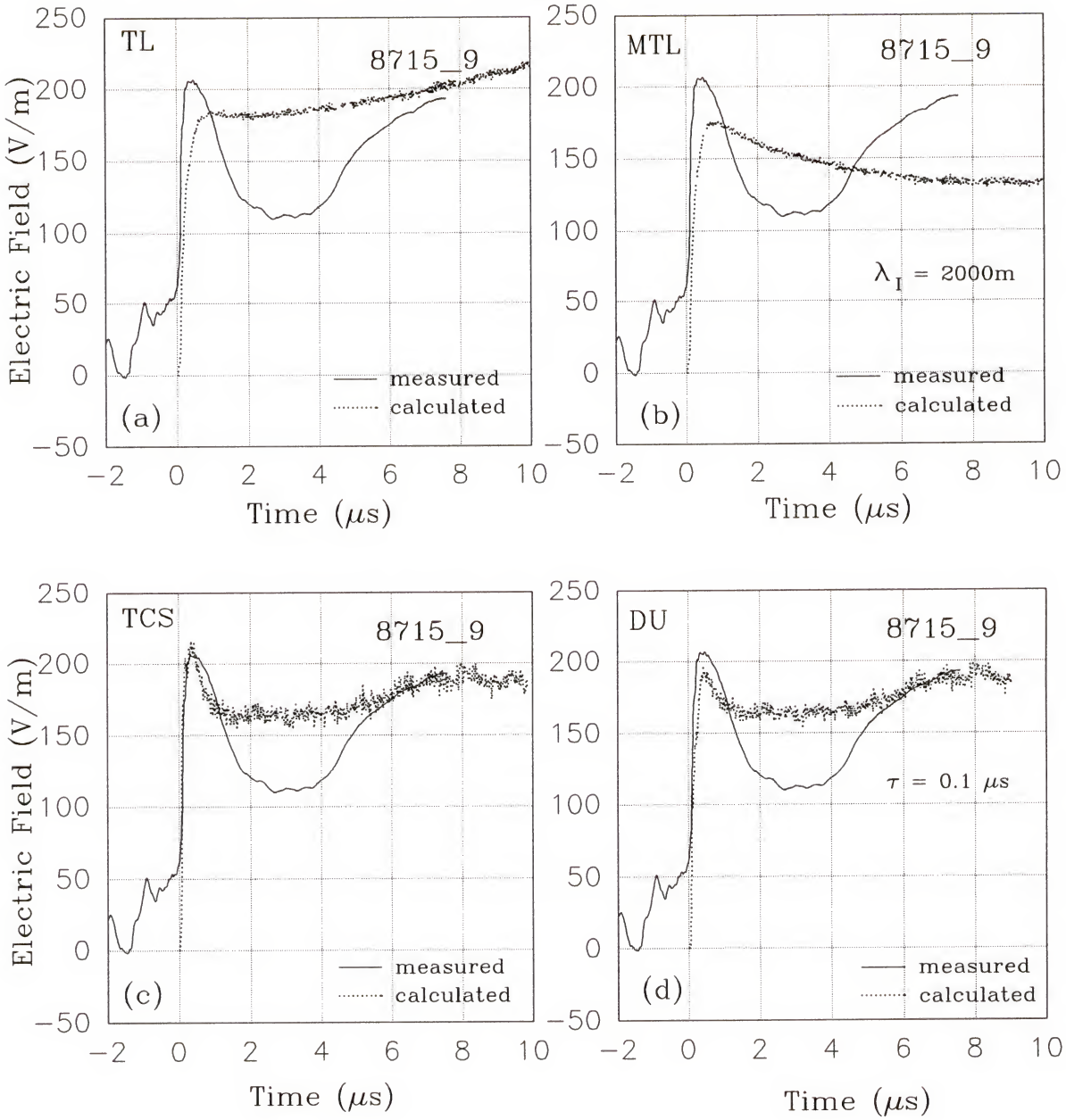

Figure 5-35. Comparison of calculated fields from the various models with the measured field at 5.16 km for the return stroke 8715_9. The measured current at the channel base and the measured return stroke speed are given in Figure 5-12. a) TL model; b) MTL model; c) TCS model; d) DU model.

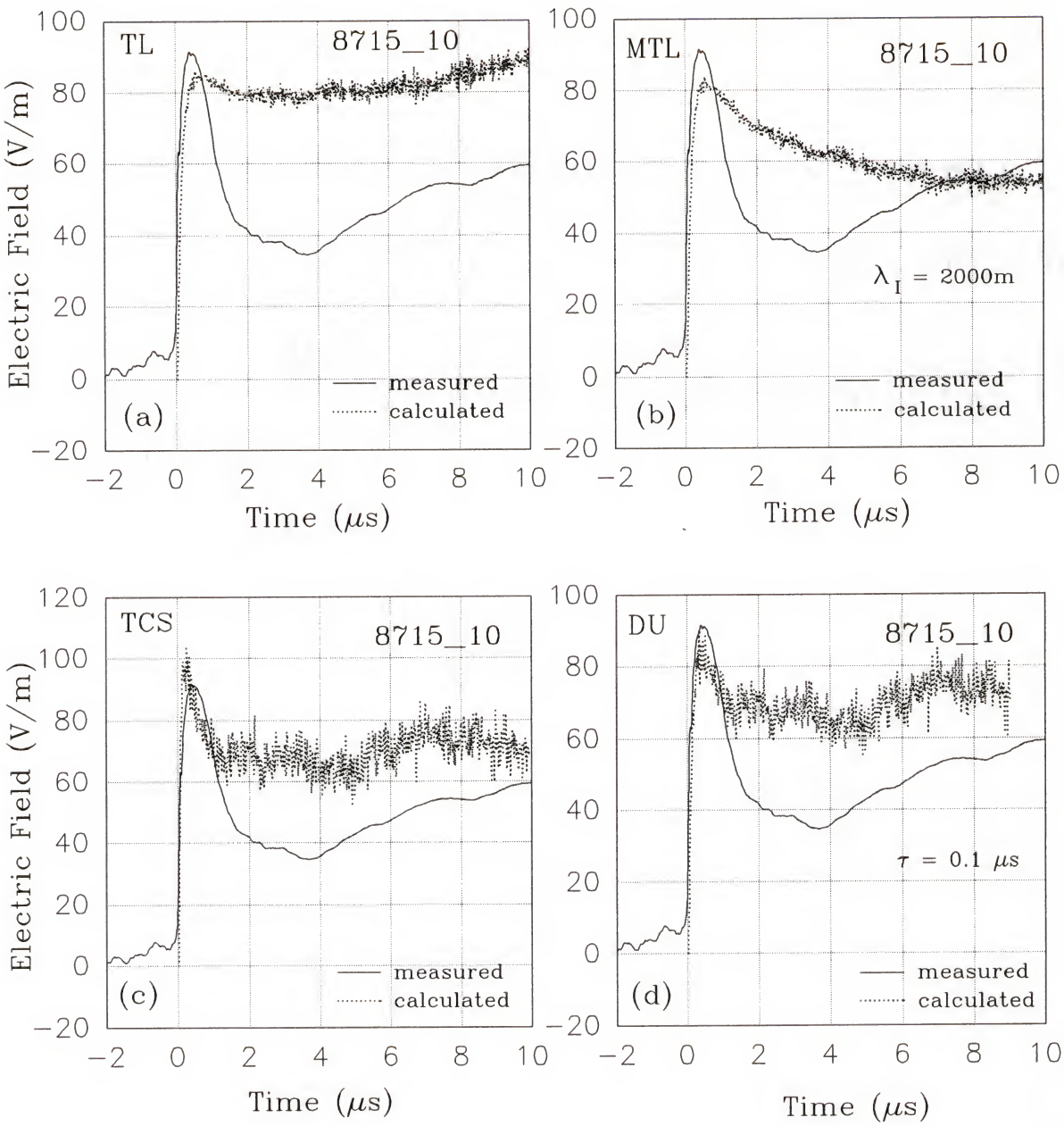

Figure 5-36. Comparison of calculated fields from the various models with the measured field at 5.16 km for the return stroke 8715_10. The measured current at the channel base and the measured return stroke speed are given in Figure 5-13. a) TL model; b) MTL model; c) TCS model; d) DU model.

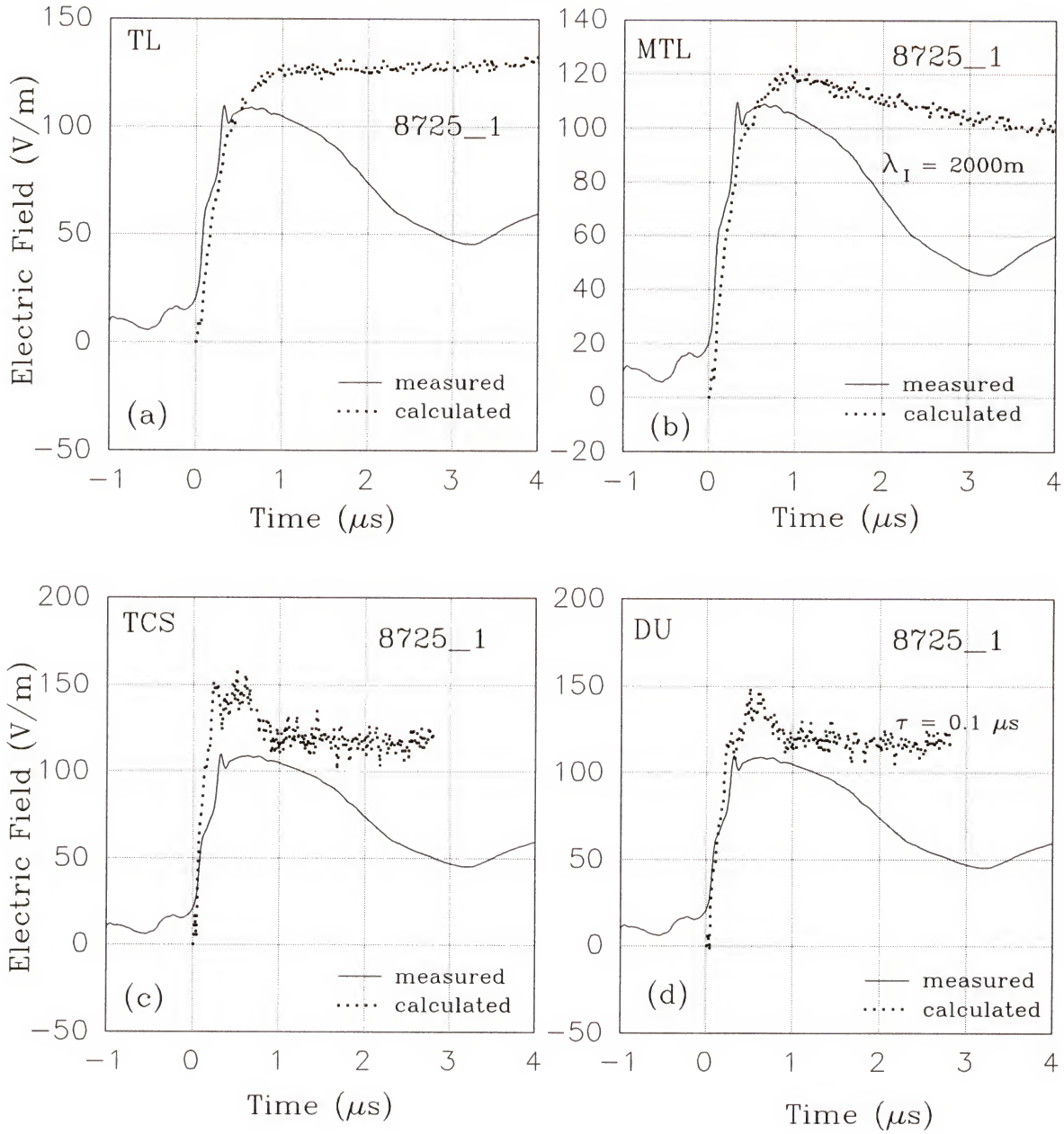

Figure 5-37. Comparison of calculated fields from the various models with the measured field at 5.16 km for the return stroke 8725_1. The measured current at the channel base and the measured return stroke speed are given in Figure 5-16. a) TL model; b) MTL model; c) TCS model; d) DU model.

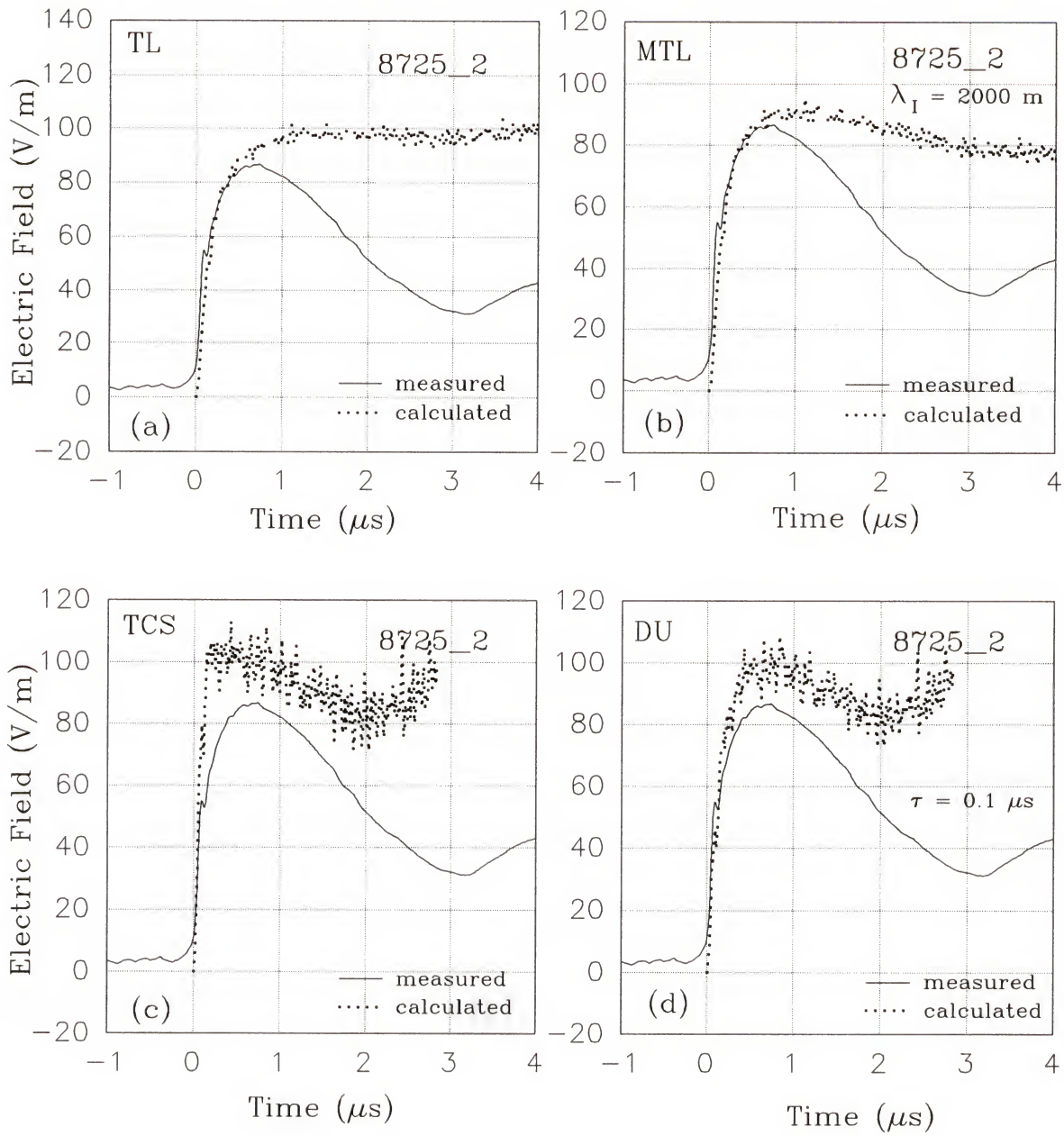

Figure 5-38. Comparison of calculated fields from the various models with the measured field at 5.16 km for the return stroke 8725_2. The measured current at the channel base and the measured return stroke speed are given in Figure 5-17. a) TL model; b) MTL model; c) TCS model; d) DU model.

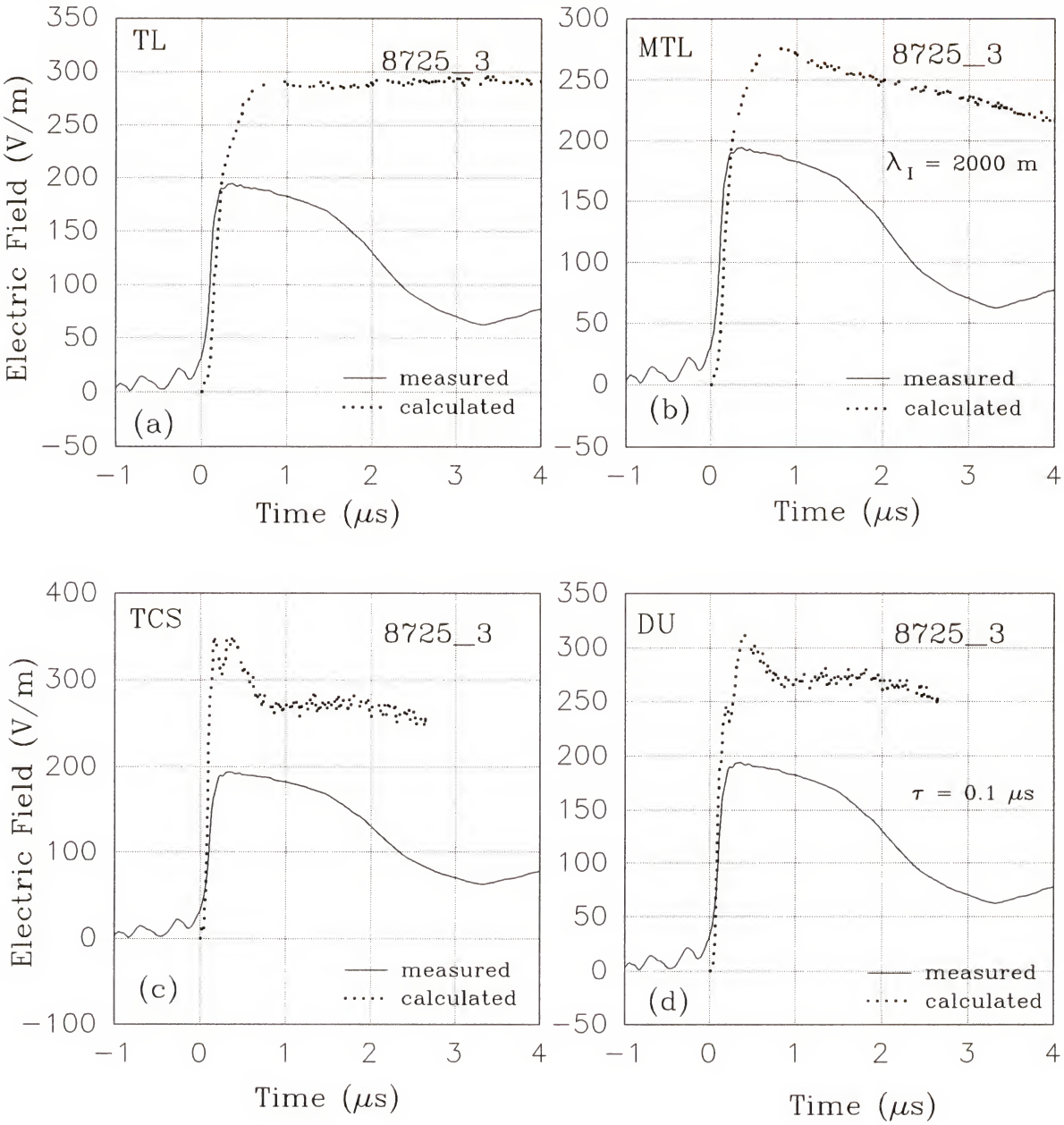

Figure 5-39. Comparison of calculated fields from the various models with the measured field at 5.16 km for the return stroke 8725_3. The measured current at the channel base and the measured return stroke speed are given in Figure 5-18. a) TL model; b) MTL model; c) TCS model; d) DU model.

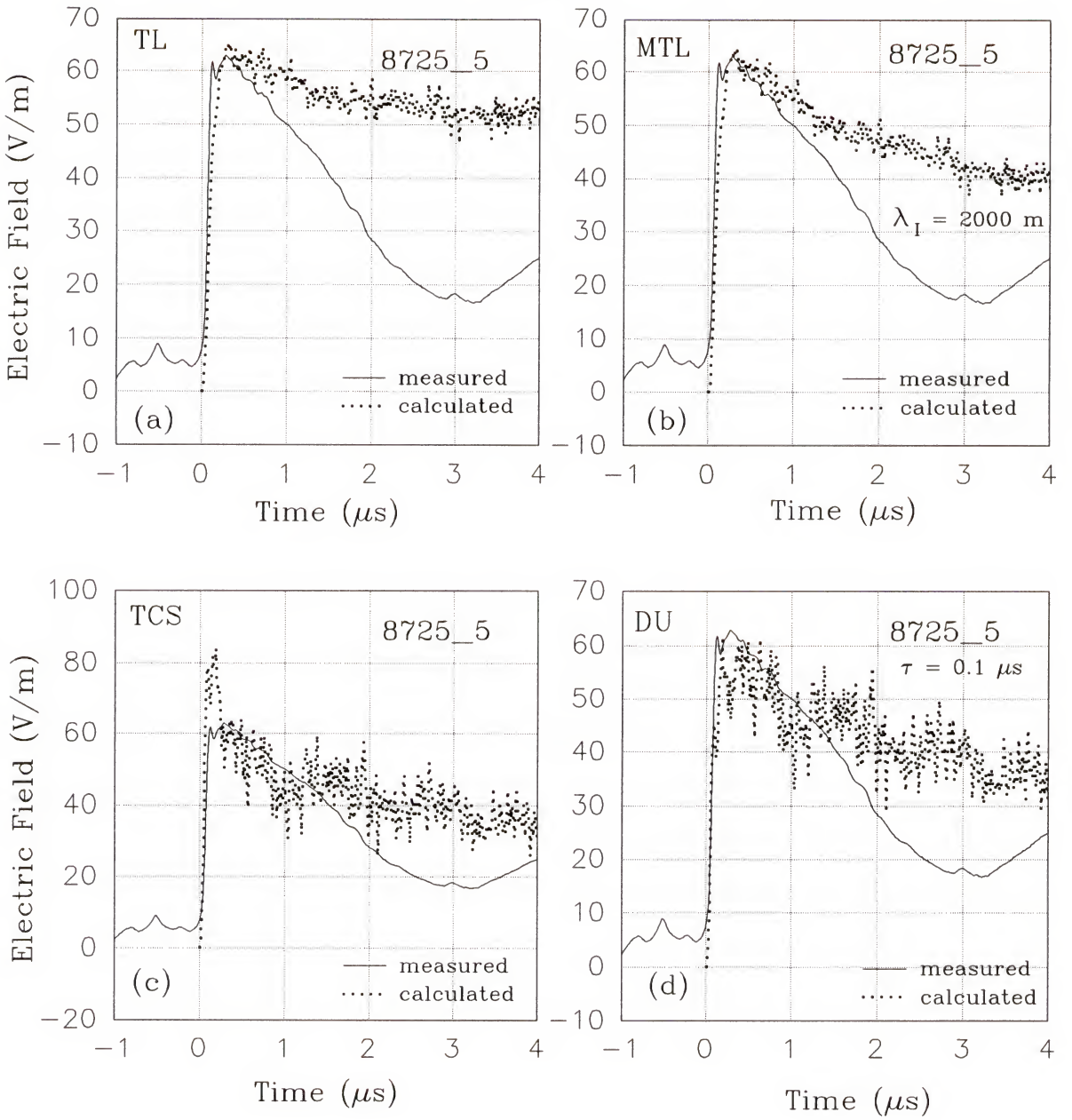

Figure 5-40. Comparison of calculated fields from the various models with the measured field at 5.16 km for the return stroke 8725_5. The measured current at the channel base and the measured return stroke speed are given in Figure 5-20. a) TL model; b) MTL model; c) TCS model; d) DU model.

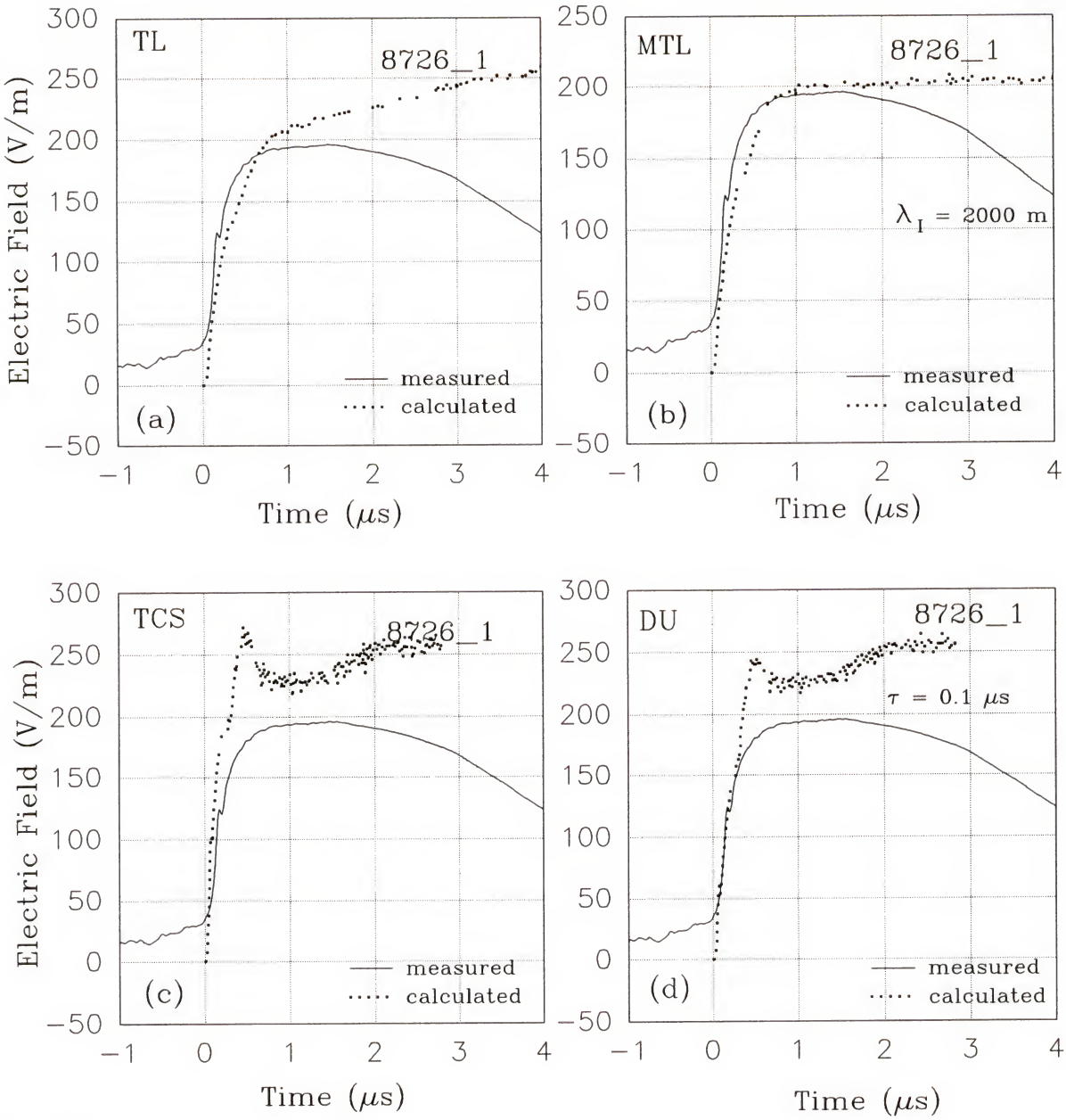

Figure 5-41. Comparison of calculated fields from the various models with the measured field at 5.16 km for the return stroke 8726_1. The measured current at the channel base and the measured return stroke speed are given in Figure 5-21. a) TL model; b) MTL model; c) TCS model; d) DU model.

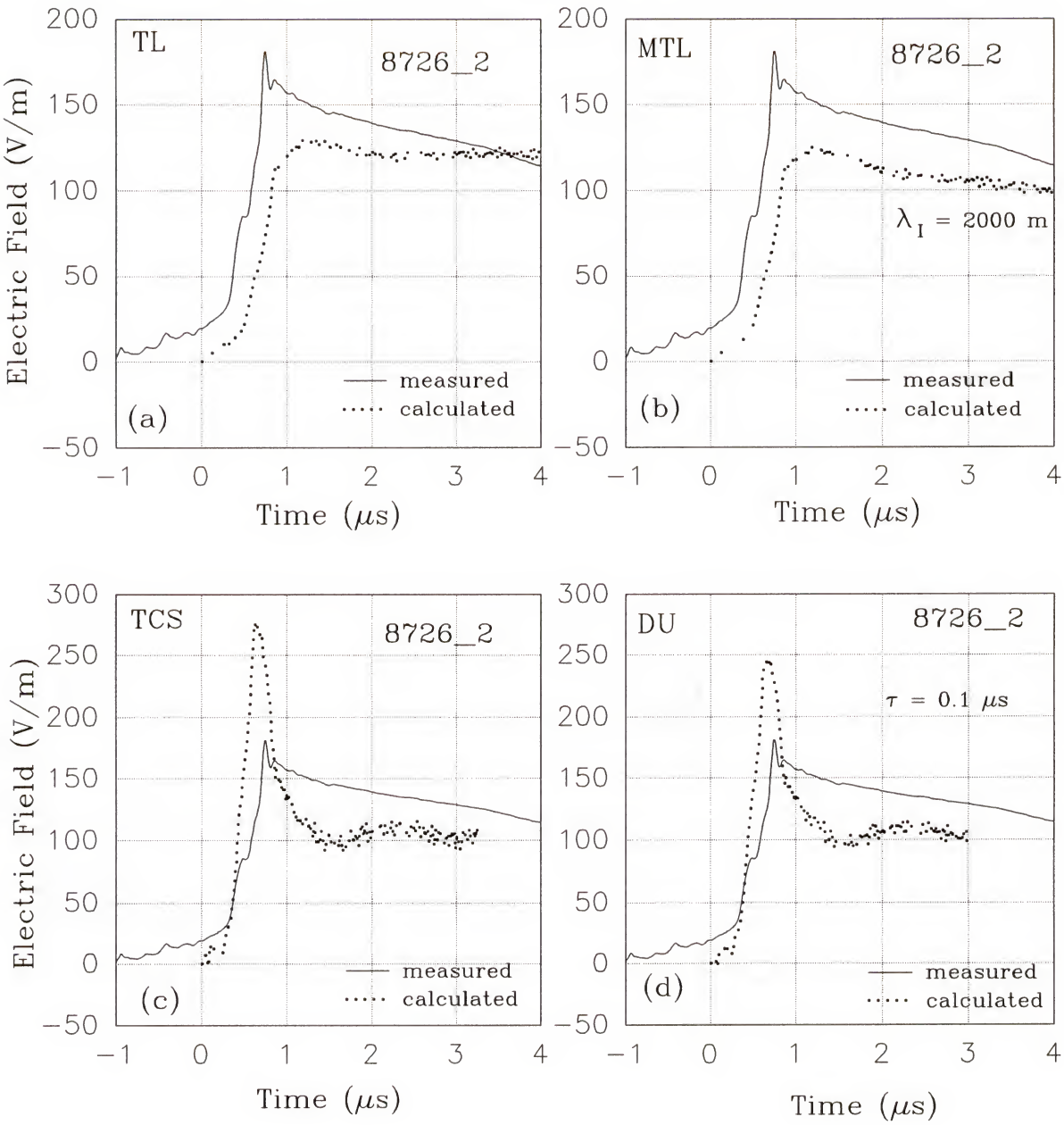

Figure 5-42. Comparison of calculated fields from the various models with the measured field at 5.16 km for the return stroke 8726_2. The measured current at the channel base and the measured return stroke speed are given in Figure 5-22. a) TL model; b) MTL model; c) TCS model; d) DU model.

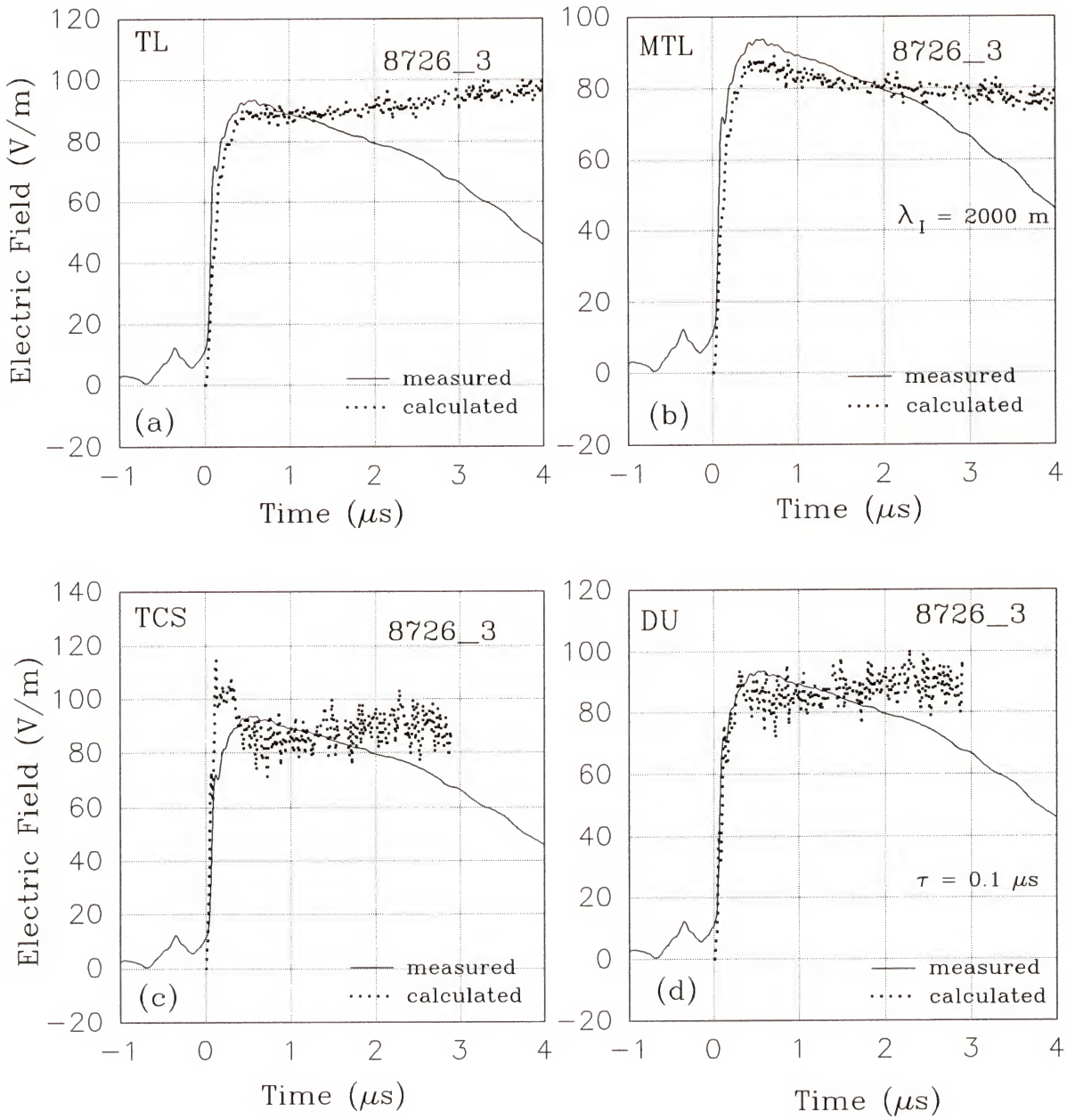

Figure 5-43. Comparison of calculated fields from the various models with the measured field at 5.16 km for the return stroke 8726_3. The measured current at the channel base and the measured return stroke speed are given in Figure 5-23. a) TL model; b) MTL model; c) TCS model; d) DU model.

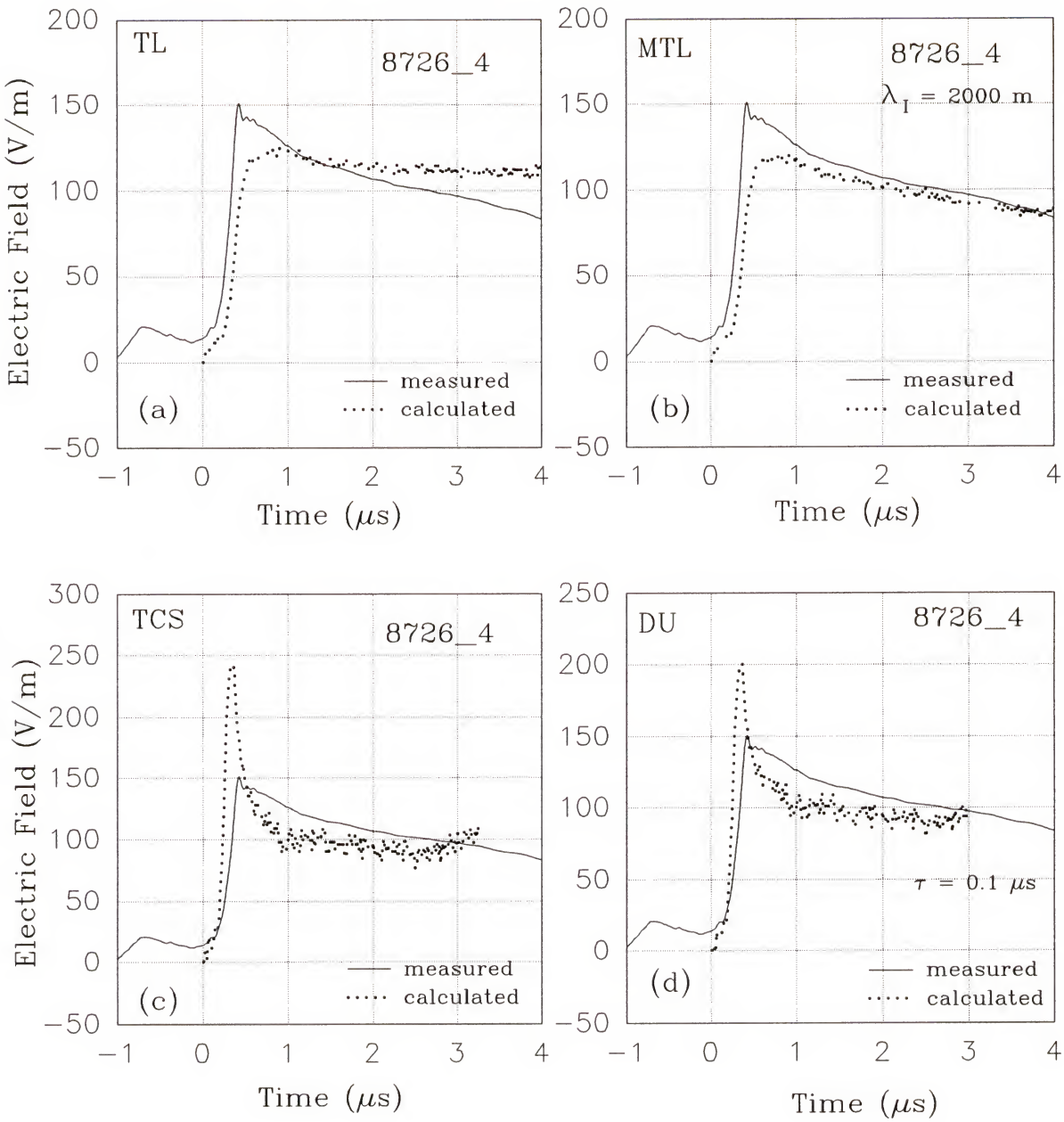

Figure 5-44. Comparison of calculated fields from the various models with the measured field at 5.16 km for the return stroke 8726_4. The measured current at the channel base and the measured return stroke speed are given in Figure 5-24. a) TL model; b) MTL model; c) TCS model; d) DU model.

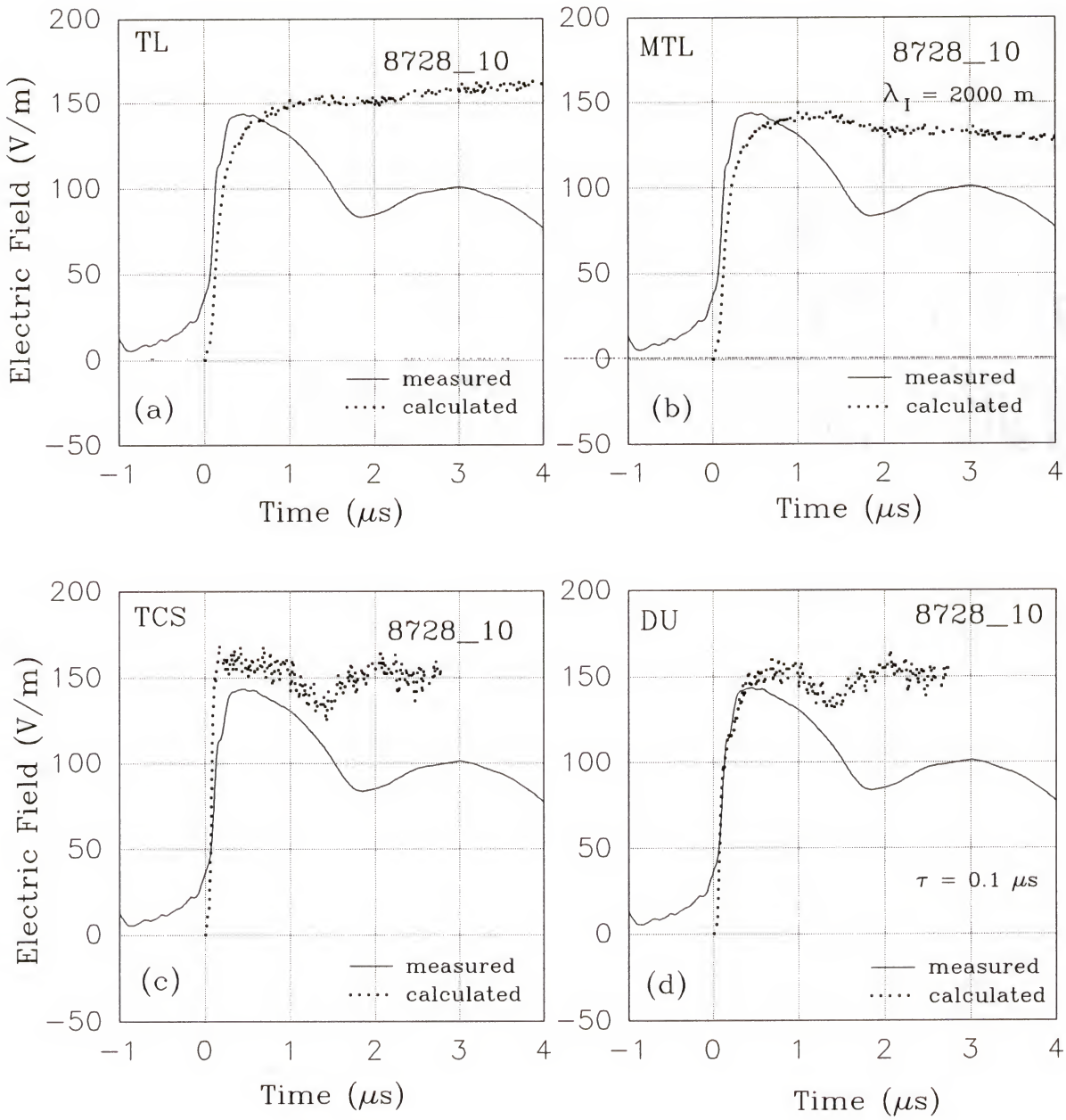

Figure 5-45. Comparison of calculated fields from the various models with the measured field at 5.16 km for the return stroke 8728_10. The measured current at the channel base and the measured return stroke speed are given in Figure 5-26. a) TL model; b) MTL model; c) TCS model; d) DU model.

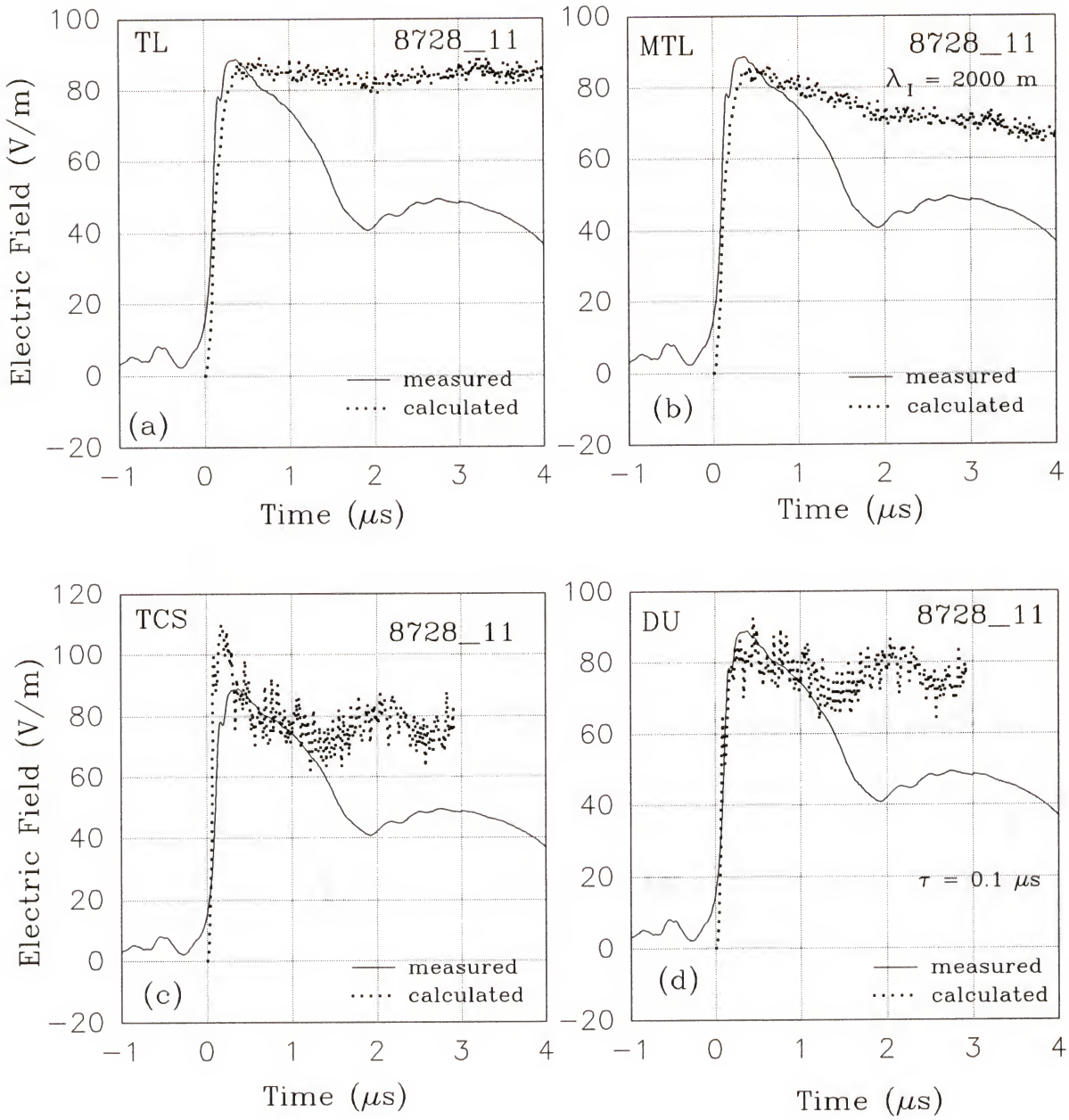

Figure 5-46. Comparison of calculated fields from the various models with the measured field at 5.16 km for the return stroke 8728_11. The measured current at the channel base and the measured return stroke speed are given in Figure 5-27. a) TL model; b) MTL model; c) TCS model; d) DU model.

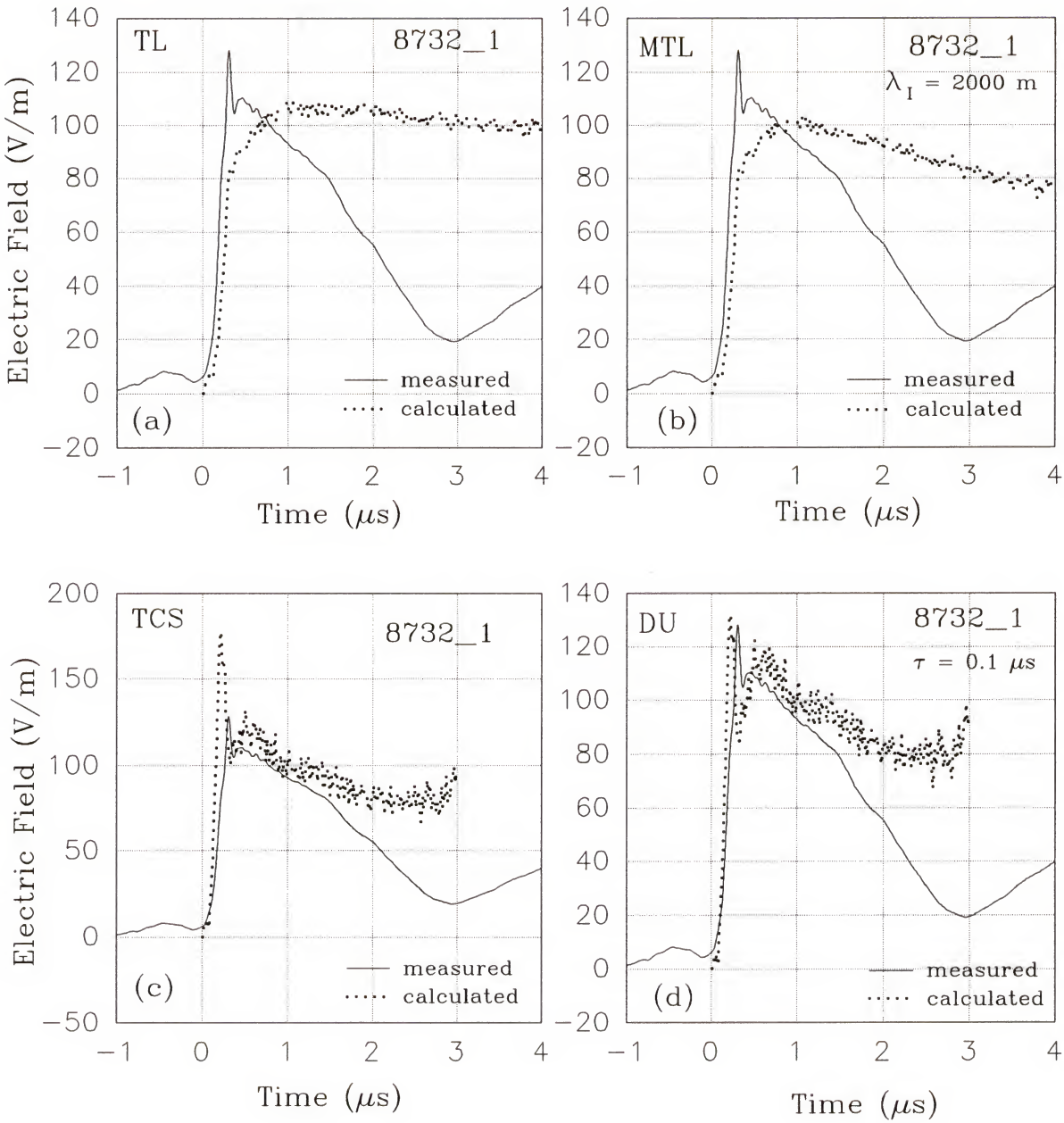

Figure 5-47. Comparison of calculated fields from the various models with the measured field at 5.16 km for the return stroke 8732_1. The measured current at the channel base and the measured return stroke speed are given in Figure 5-28. a) TL model; b) MTL model; c) TCS model; d) DU model.

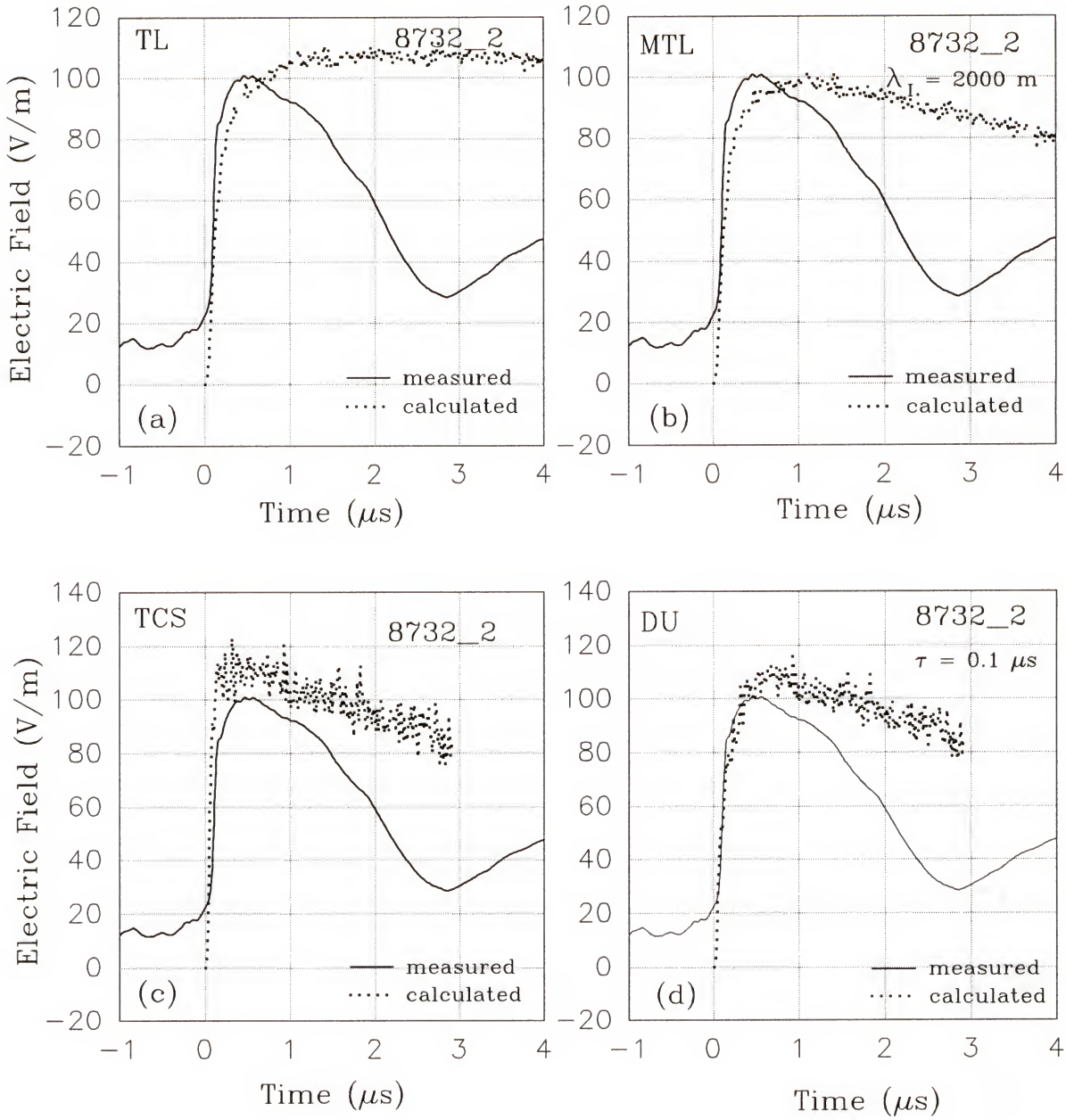

Figure 5-48. Comparison of calculated fields from the various models with the measured field at 5.16 km for the return stroke 8732_2. The measured current at the channel base and the measured return stroke speed are given in Figure 5-29. a) TL model; b) MTL model; c) TCS model; d) DU model.

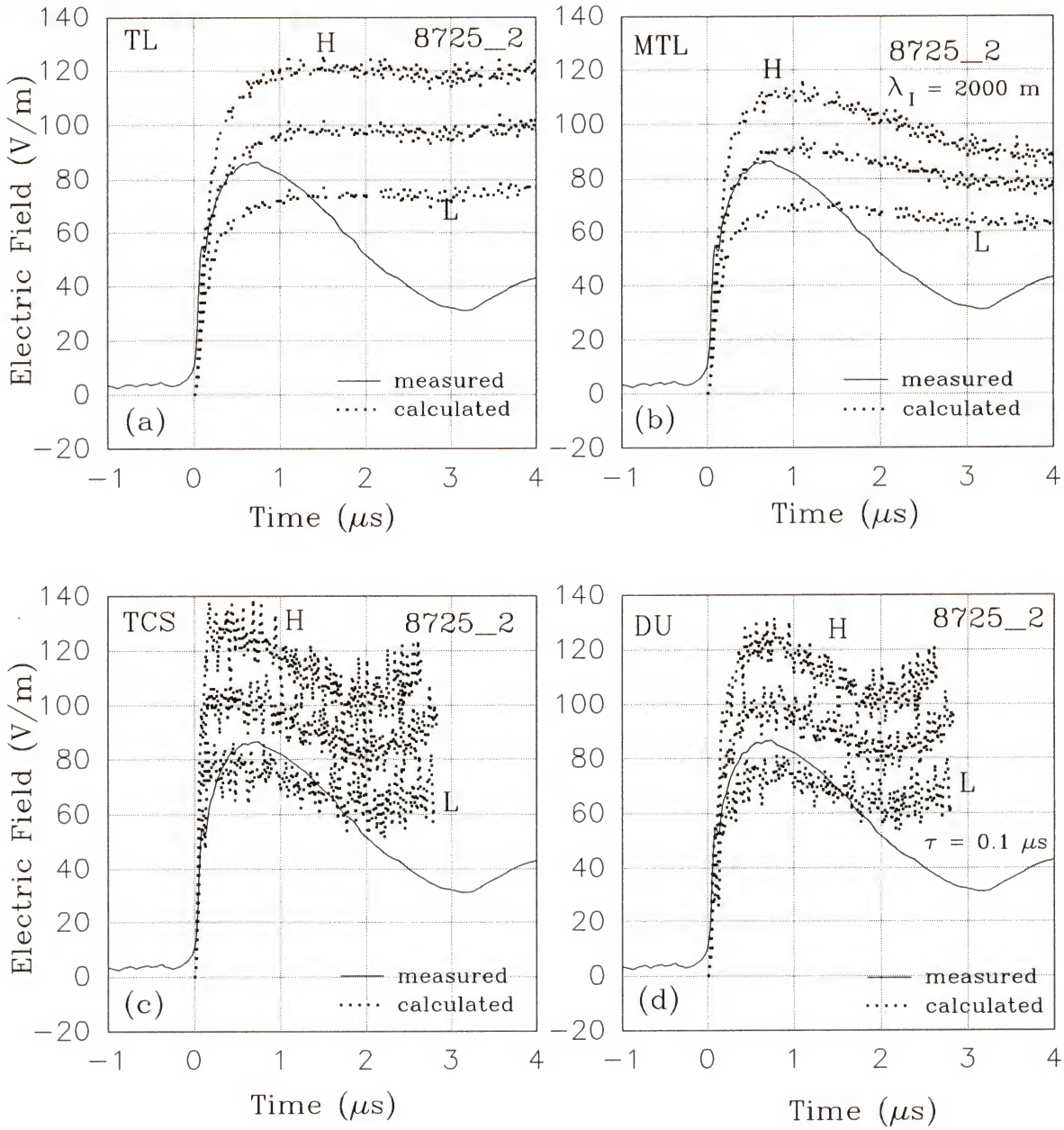

Figure 5-49. Example of the range of calculated electric field amplitudes possible due to 25% absolute error in return-stroke speed measurement for the return stroke 8725_2. a) TL model; b) MTL model; c) TCS model; d) DU model.

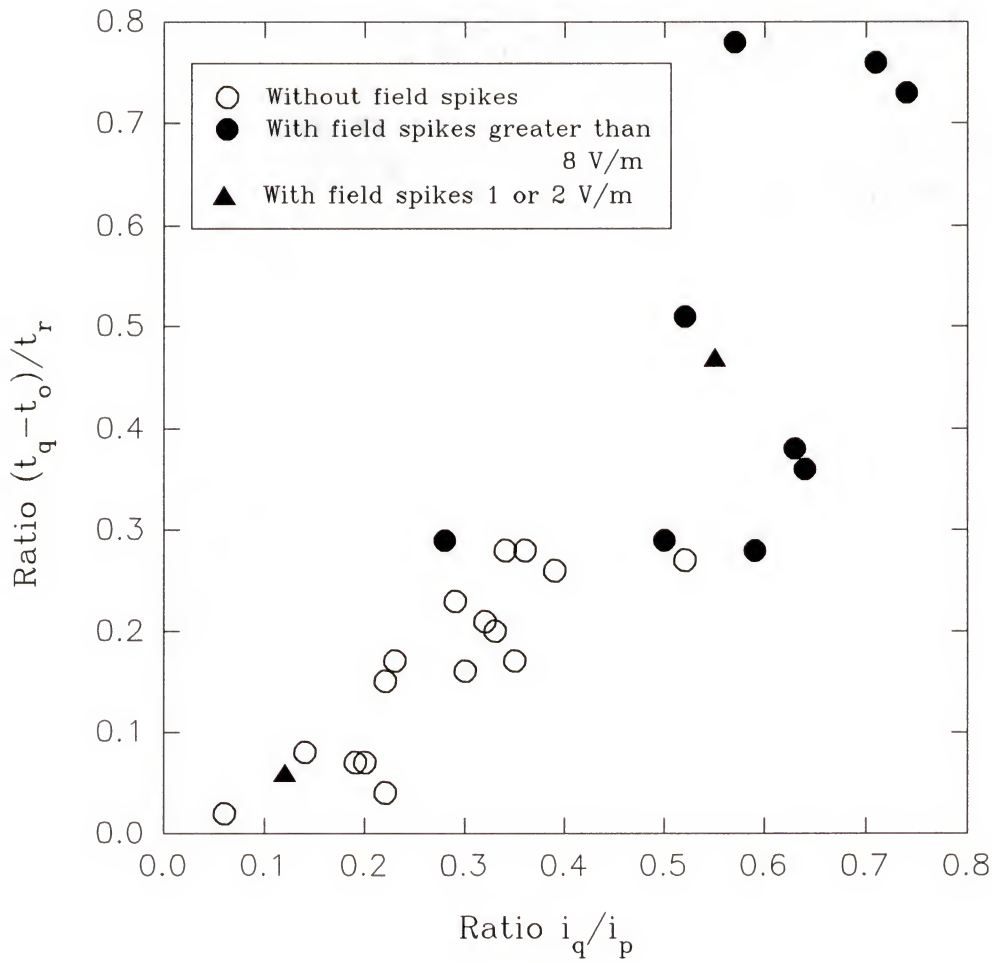

Figure 5-50. Scatter plot illustrating the tendency in which the measured return-stroke currents having a maximum di/dt occurring near the peak current is associated with remotely measured electric field having a very narrow spike at the field peak.

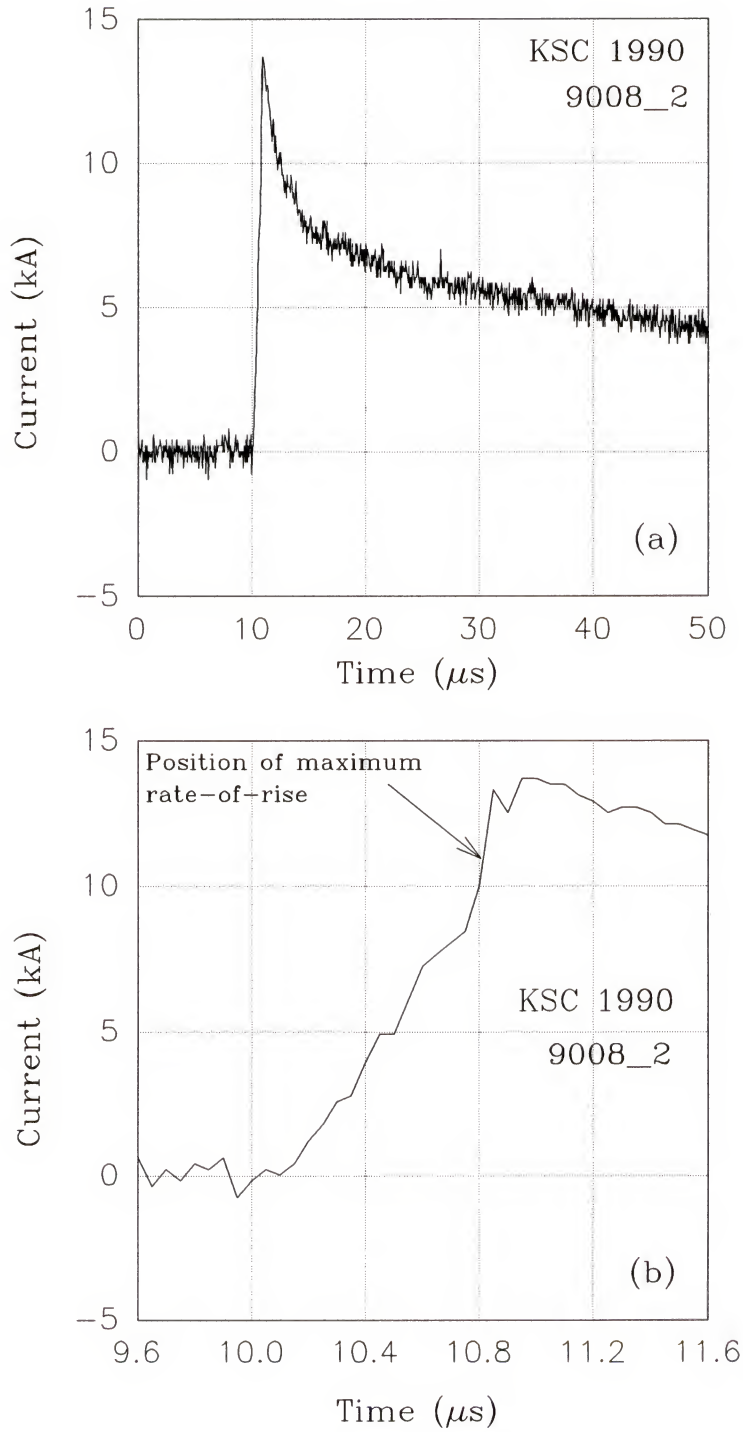

Figure 5-51. Return stroke channel-base current waveshape of a stroke which produced upward discharges as observed in video records. a) Overall current waveform; b) The front portion expanded showing the position of maximum rate-of-rise of current near the peak.

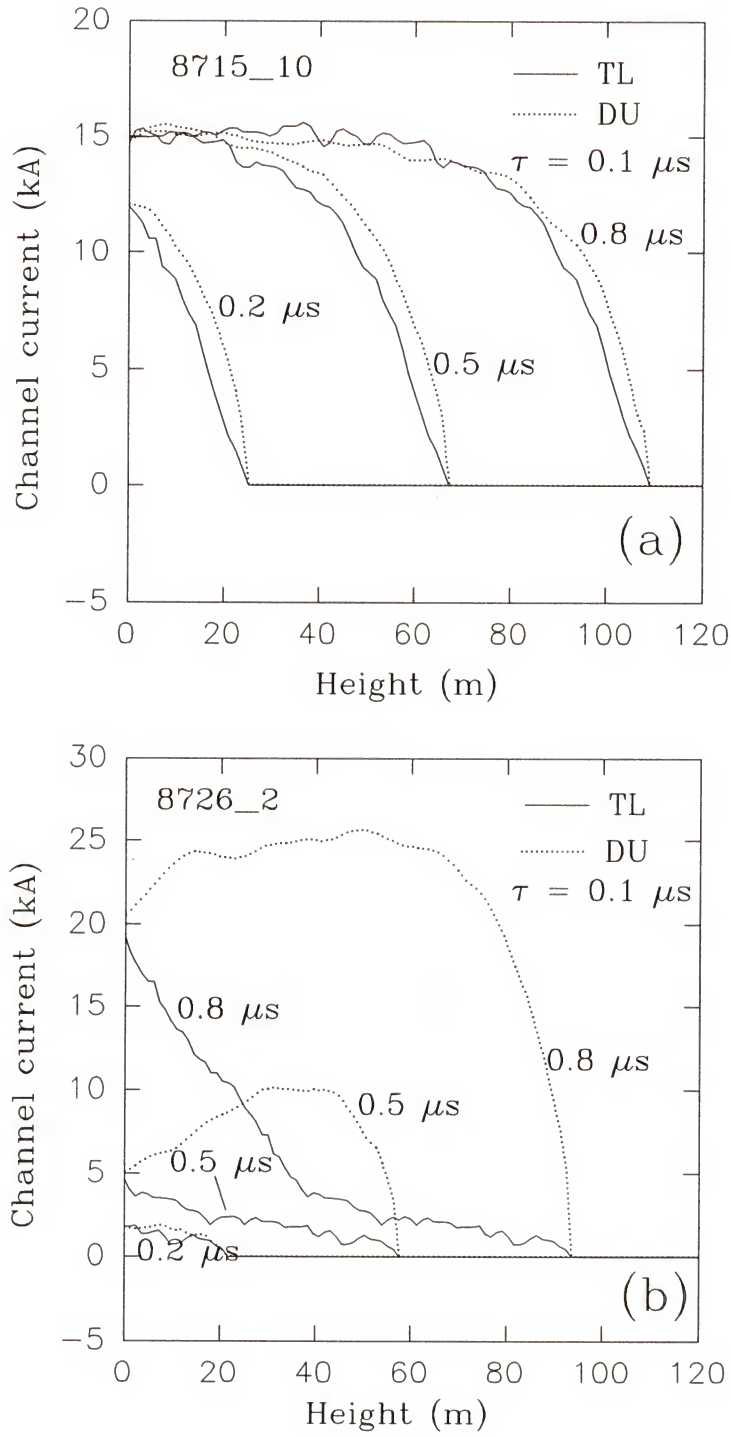

Figure 5-52. Comparison of channel current distribution at 0.2 μs, 0.5 μs, and 0.8 μs for TL and DU models. a) For return stroke 8715_10; b) For return stroke 8726_2.

CHAPTER 6
GENERALIZATION OF THE DIENDORFER-UMAN MODEL

In this chapter a more general and more straightforward mathematical derivation is presented for the DU model for finding the current and charge distribution along the lightning return stroke channel, given the channel base current and channel discharge time constant, than that originally presented by Diendorfer and Uman (1990). The new formulation has the additional advantage that the analytical results include both a variable upward return-stroke speed that is an arbitrary function of height and a variable downward speed, that is also an arbitrary function of height, for the discharge currents which are released by the return stroke wavefront. Both of these speeds are assumed constant in the original mathematical formulation of the DU model, the latter at the speed of light. The theory is first applied to the case of a variable return stroke speed and a two component current and two component channel discharge time constant, as used to model natural lightning by Diendorfer and Uman (1990), to illustrate the differences between the original Diendorfer-Uman model and the model with variable return stroke speed. After that, the Modified Diendorfer-Uman (MDU) model is applied to the calculation of triggered lightning electric fields at 5.16 km, for the measured currents and speeds used to compare the models in chapter 5.

6.1 Mathematical Analysis for Single Channel Discharge Time Constant

The return stroke channel is modeled as a straight vertical line above a perfectly conducting infinite plane. The geometry of the model is the same as that shown in Fig. 5-1. The leader has previously deposited charge along the channel. The return stroke is assumed to start at ground level, $z' = 0$, at time $t = 0$, as the leader tip makes contact with ground (any upward connecting leader and attachment process neglected) and thereafter propagates upward. The return-stroke front starts discharging the charge deposited at each cross section of the channel as it passes that section. The total current flowing past a given section of the channel at height z' is due only to the contribution of discharging currents above that section. Let $t_u(z')$ be the time at which the return stroke reaches the height $z = z'$. Let $t_d(z')$ be the time it takes for the discharge current at $z = z'$ to reach ground. Assume that the current injected at each cross section of the channel decays exponentially with a single time constant τ_D.

For a given point z' on the channel and time $t \geq t_u(z') + t_d(z')$, the current at the base of the channel consists of two parts: 1) the current from the part of the channel at and above $z=z'$, $i_A(z';t)$; and 2) the current from the part of the channel below $z=z'$, $i_B(z';t)$. That is,

$$i(0,t) = i_A(z';t) + i_B(z';t) \tag{6-1}$$

Note that the semicolon after z' in the arguments of i_A and i_B is meant to indicate that the function is not evaluated at z' but is as defined above. If a function is to be evaluated at z', a comma follows z' in the arguments of i. The current arriving at the base of the channel at time t from z' and above is the current which was flowing at z' at the time $(t-t_d(z'))$. Therefore

$$i_A(z';t) = i\left(z', t - t_d(z')\right) \tag{6-2}$$

and (6-1) becomes

$$i(0,t) = i\left(z',t-t_d(z')\right) + i_B(z';t) \tag{6-3}$$

At $t = t_u(z')$, the return stroke front has just reached z'. At $t = t_u(z') + t_d(z')$, the ground first "hears from" the complete "lower" channel $z < z'$. Equation (6-3) therefore becomes

$$i\left(0,t_u(z')+t_d(z')\right) = i\left(z',t_u(z')\right) + i_B\left(z';t_u(z')+t_d(z')\right) \tag{6-4}$$

Since the return stroke front has just reached z' at $t_u(z')$, $i(z', t_u(z')) = 0$ and equation (6-4) becomes

$$i\left(0,t_u(z')+t_d(z')\right) = i_B\left(z';t_u(z')+t_d(z')\right) \tag{6-5}$$

Since the current injected at each cross section of the channel decays with time constant τ_D once it is "turned on", it follows that $i_B(z';t)$ also decays with time constant τ_D for $t > t_u(z') + t_d(z')$. Therefore,

$$i_B(z';t) = i\left(0,t_u(z')+t_d(z')\right)e^{-\left(t-t_u(z')-t_d(z')\right)/\tau_D}, \quad t \geq t_u(z')+t_d(z') \tag{6-6}$$

Substituting (6-6) into (6-3), we obtain

$$i(0,t) = i\left(z',t-t_d(z')\right) + i\left(0,t_u(z')+t_d(z')\right)e^{-\left(t-t_u(z')-t_d(z')\right)/\tau_D}, \quad t \geq t_u(z')+t_d(z') \tag{6-7}$$

and rearranging the terms, we get

$$i\left(z',t-t_d(z')\right) = i(0,t) - i\left(0,t_u(z')+t_d(z')\right)e^{-\left(t-t_u(z')-t_d(z')\right)/\tau_D}, \quad t \geq t_u(z')+t_d(z') \tag{6-8}$$

Let $t^* = t - t_d(z')$. Then equation (6-8) becomes

$$i(z',t^*) = i\left(0,t^* + t_d(z')\right) - i\left(0,t_u(z') + t_d(z')\right)e^{-\left(t^* - t_u(z')\right)/\tau_D}, \quad t^* \geq t_u(z') \tag{6-9}$$

By changing the notation t^* to t in equation (6-9), we obtain the desired result relating current at ground to current in the channel above ground.

$$i(z',t) = i\left(0,t + t_d(z')\right) - i\left(0,t_u(z') + t_d(z')\right)e^{-\left(t - t_u(z')\right)/\tau_D}, \quad t \geq t_u(z') \tag{6-10}$$

If we consider the case of a constant return stroke speed v and constant discharge current speed c, the speed of light, then

$$\begin{aligned} t_u(z') &= z'/v \\ t_d(z') &= z'/c \end{aligned} \tag{6-11}$$

and equation (6-10) is reduced to equation (4) of Diendorfer and Uman (1990)

$$i(z',t) = i\left(0,t + \frac{z'}{c}\right) - i\left(0,\frac{z'}{v} + \frac{z'}{c}\right)e^{-\left(t - \frac{z'}{v}\right)/\tau_D}, t \geq \frac{z'}{v}. \tag{6-12}$$

If the return stroke speed, v(z′), is a function of height z′, then we can define an average return stroke speed, $V_{av}(z')$, such that

$$V_{av}(z') = \frac{z'}{t_u(z')} = \frac{z'}{\int_0^{z'} \frac{dz''}{v(z'')}} \tag{6-13}$$

If the speed of the discharge current down the channel, u(z′), is a function of z′, then we can define an average downward speed $U_{av}(z')$ as

$$U_{av}(z') = \frac{z'}{t_d(z')} = \frac{z'}{\int_0^{z'} \frac{dz''}{u(z'')}} \tag{6-14}$$

Substituting $t_u(z') = z'/V_{av}(z')$ and $t_d(z') = z'/U_{av}(z')$ in equation (6-10), we obtain

$$i(z',t) = i\left(0, t + \frac{z'}{U_{av}(z')}\right) - i\left(0, \frac{z'}{V_{av}(z')} + \frac{z'}{U_{av}(z')}\right) e^{-\left(t - \frac{z'}{V_{av}(z')}\right)/\tau_D}, \tag{6-15}$$

$$t \geq \frac{z'}{V_{av}(z')}$$

a completely generalized version of equation (6-12) giving the current at any height z′ in terms of the current at the ground. In the absence of experimental information on the discharge current speed down the channel, here it is assumed to be the constant c. Thus $U_{av}(z')$ in equation (6-15) is replaced by c as in equation (6-12) giving,

$$i(z',t) = i\left(0, t + \frac{z'}{c}\right) - i\left(0, \frac{z'}{V_{av}(z')} + \frac{z'}{c}\right) e^{-\left(t - \frac{z'}{V_{av}(z')}\right)/\tau_D}, \tag{6-16}$$

$$t \geq \frac{z'}{V_{av}(z')}$$

For time measured at the field point, P, shown in Figure 5-1, equation (6-16) becomes

$$i\left(z',t-\frac{R}{c}\right) = i\left(0,t+\frac{z'}{c}-\frac{R}{c}\right) - i\left(0,\frac{z'}{V_{av}(z')}+\frac{z'}{c}\right)e^{-\left(t-\frac{z'}{V_{av}(z')}-\frac{R}{c}\right)/\tau_D}, \qquad \textbf{(6-17)}$$

$$t \geq \frac{z'}{V_{av}(z')}+\frac{R}{c}$$

The charge per unit length associated with the exponential discharging of the channel can be expressed as

$$\rho_L(z',t) = \rho_L(z')e^{-\left(t-\frac{z'}{V_{av}(z')}\right)/\tau_D}, t \geq \frac{z'}{V_{av}(z')} \qquad \textbf{(6-18)}$$

From equation (6-16), (6-18), and the continuity equation relating charge and current, we get the distribution of the charge along the channel neutralized by the return stroke as

$$\rho_L(z') = -\frac{1}{\frac{dz'(t)}{dt}}\left[i\left(0,\frac{z'}{V_{av}(z')}+\frac{z'}{c}\right)+\tau_D\frac{di\left(0,\frac{z'}{V_{av}(z')}+\frac{z'}{c}\right)}{dt}\right] \qquad \textbf{(6-19)}$$

using the same approach as in Diendorfer and Uman (1990). Note that dz′(t)/dt in equation (6-18) is the speed of the return stroke front at z′ as seen by an observer at the base of the channel and can be obtained from the relation

$$t = \frac{z'}{V_{av}(z')}+\frac{z'}{c} \qquad \textbf{(6-20)}$$

6.2 Application

Examples of the application of the theory given above to the case of a variable return stroke speed are presented in this section, and the results are compared with the results obtained by Diendorfer and Uman (1990) in modeling natural lightning. Current-1 given by Diendorfer and Uman (1990) is assumed to be the current at the channel base. That current has a peak value of 14 kA and a 10 to 90 percent rise-time of about 0.2 μs and is similar to subsequent stroke currents observed both in natural lightning (Eriksson, 1978; Berger et al., 1975) and in triggered lightning (Leteinturier et al., 1990). The channel base current is shown in Figure 6-1, decomposed into two parts, one part which can be called the breakdown current, presumed to be due to the discharging of the core of the channel, and the other part, which can be called the corona current, presumed to be due to the discharging of the charged sheath around the channel core, although alternate physical interpretations have been given for the two current components, and the subdivision is to a considerable extent arbitrary (Diendorfer and Uman, 1990). Two different exponential channel-discharge time constants, for the core $\tau_{BD} = 0.6$ μs and for the corona $\tau_c = 5$ μs, are used corresponding to the breakdown current and corona current at ground, respectively, in Equation (6-17) to get the total current along the channel, the total charge distribution along the channel, and the fields remote from the channel, in the manner of Diendorfer and Uman (1990). The above values of time constants were used for the case of a constant model speed, so that the calculated field wave shapes would be consistent with the natural return stroke fields measured by Lin et al. (1979) (see Diendorfer and Uman, 1990).

In order to calculate return stroke fields using the DU model modified for variable speed, an appropriate function of speed with height must be selected. There are no detailed experimental

data in the literature describing exactly how the speed varies with height. Here, in an approximation following Bruce and Golde (1941), an exponential decrease with height given by

$$v(z') = v_0 \, e^{-(z'/\lambda_v)} \qquad \textbf{(6-21)}$$

is assumed, where v_0 is the speed at ground level and λ_v is the speed decay constant.

For a maximum return stroke speed of 1.3×10^8 m/s at ground level decreasing with height with $\lambda_v = 2000$ m, the charge and current distribution on the channel calculated from equation (6-19) and (6-16), respectively, are compared with the charge and current distribution for a constant return stroke speed of 1.3×10^8 m/sec (λ_v = infinity) in Figures 6-2 and 6-3, respectively. Close to the ground the charge and current are essentially the same for the variable speed and the constant speed cases, as is evident from Figures 6-2 and 6-3, respectively. It follows that the initial peak electric fields and peak field derivatives for the variable speed return stroke must also remain the same as for the constant speed case, as we shall see. At higher points on the channel, differences in the distributions are evident. In fact, the distribution of current at a given height for a decreasing speed is different in magnitude even if the shift in time associated with the decreasing speed is accounted for. Since the speed at $z' = 0$ is assumed to be the same for both the constant speed and the decreasing speed cases, average speed $V_{av}(z')$ is necessarily less than constant speed V at all heights above ground. The first terms of equations (6-12) and (6-16) are independent of speed, while the second terms are functions of speed. If a uniform current at the base of the channel is assumed, the second term of equation (6-16) is greater than the second term of equation (6-12), making the current with a decreasing return stroke speed smaller than the constant speed case for the same starting speed at ground. For an increasing channel base current with time, the current at a given height for the case of decreasing speed is also smaller than the corresponding current for the constant speed case, by the same

argument. If the channel base current is decreasing with time, which is the case much of the time for lightning channel base currents, the current at a given height for the decreasing speed may be greater, smaller, or equal the constant speed case, the exact relationship being determined by the choice of the return stroke speed and the channel base current waveshape, as is evident from equations (6-12) and (6-16).

From equation (2-3), it can be seen that the electric fields are determined by the current, time derivative of the current, and the time integral of the current (charge neutralized) along the channel. Similarly from equation (2-4), it can be seen that the magnetic fields are determined by the current and the time derivative of the current along the channel. Both fields are also influenced by the distance of each radiating element on the channel from the field measuring point, ratio of the height of the element to the distance of the field point from the channel base, and the total height of the channel that contributes to the field at a given time. The current, time derivative of the current, and the time integral of the current are expressed in terms of the current at the channel base and hence will vary according to the assumed channel base current. The maximum height of the channel that contribute to the field at the measuring point is determined by the speed of the return stroke and the distance to the measuring point from the channel. Moreover in the model, the current and the derivative and integral of the current at a given height are indirectly a function of the average speed as explained in the previous paragraph. Thus, the effect that a variable speed has on the field is not immediately apparent and can depend on many factors such as the waveshape of the channel base current, the distance to the measuring point, and the maximum height of the channel contributing to the field at a given time. Nevertheless as a typical example, the effect of an exponentially decreasing speed on the calculated fields for the specific channel base current given in Figure 6-2 is discussed.

The calculated electric fields on a 5 μs time scale and the field derivatives on a 1 μs time scale at a distance of 100 km from the channel are shown in Figure 6-4a and 6-4b, respectively, for an initial speed of 1.3 x 10^8 m/s and several values of λ_v including λ_v = infinity, that is, a constant speed. For the first few microseconds the field wave shapes for decay constants λ_v = 1000 m, 2000 m, and 3000 m do not differ significantly from the constant speed case. For times greater than a few microseconds the far fields are smaller and reverse polarity earlier, as illustrated in Figure 6-5. For λ_v = 2000 m, the zero crossing of the fields at a distance of 100 km is at about 40 μs, about 15 μs earlier than for a constant speed.

Figures 6-6 and 6-7 show the fields produced at 1 km distance for decreasing return stroke speeds with ground level value of 1.3 x 10^8 m/s and for a constant return stroke speed of 1.3 x 10^8 m/s. Figure 6-6a shows that at about 5 μs the electric fields associated with a constant return stroke speed have higher values whereas at about 20 μs they have lower values than for the decreasing speed case. Nevertheless, the peak fields are almost the same in all cases. Later in time, for the case of the decreasing return stroke speed the total near fields become larger than the constant speed case, as can be seen from Figure 6-6b. Figures 6-7a and 6-7b show that the magnetic fields produced by a decreasing return stroke speed with height are always less than the field produced by the constant speed.

6.3 Comparison With Other Models for Triggered Lightning

The simultaneously measured currents, return stroke speeds and electric fields for triggered lightning used to compare the TL, MTL, TCS, and DU models in chapter 5 are now used in this section to compare the fields produced by the Modified Diendorfer Uman (MDU) model developed in section 6.2. A single current component with a discharge time constant of

0.1 μs is adopted, the same as that for the DU model in chapter 5. The return stroke speed at ground level is assumed to be the measured speed, and it is allowed to decrease with height exponentially (equation 6-21) with a speed decay factor λ_v = 2000 m. Electric fields at 5.16 km are calculated for all 18 current waveshapes for which there are speed measurements and are compared with measured fields in Figures 6-8 to 6-12. Comparing the calculated return stroke fields for the MDU model given in Figures 6-8 to 6-12 with the corresponding return stroke model fields from the DU model given in Figures 5-31 to 5-48, we can see that the peak of the calculated fields are not reduced appreciably by the decreasing return stroke speed, as expected, but with increasing time the difference in the electric fields from the DU and the MDU model increase. Overall the match between the MDU model fields and the measured fields is better than the DU model. In Table 6-1 the calculated return stroke peak field amplitudes from the MDU model are compared with the measured peak field amplitudes in the same way as was done with other models in Table 5-1. Column 2 and 3 of Table 6-1 give, respectively, the measured field peak amplitude and calculated field peak amplitude from MDU model. The absolute error in the calculated field peak amplitude, normalized to the respective measured field peak amplitude is given in column 4. Table 6-2 gives the statistics on the error of the calculated field peaks from the MDU model. The normalized absolute error range from 0.02 to 0.60 with a mean of 0.21 (standard deviation = 0.19). These values concerning the initial field peaks are a small improvement from the corresponding values for the DU model (see Table 5-2). However, after the peak, the MDU model fields are a better match to the measured fields than the DU model fields (see Figures 5-31 to 5-48 and 6-8 to 6-12).

Table 6-1. Comparison of calculated field peak amplitudes from the MDU model with the measured field peak amplitudes.

1	2	3	4
Stroke	Measured Peak Field, E_m V/m	Calculated Peak fields, E_c, V/m	Ratio, $(E_c-E_m)/E_m$
8705_1	72	79	+0.10
8705_3	64	66	+0.03
8705_5	78	62	-0.21
8705_6	78	80	+0.03
8715_9	157	190	+0.21
8715_10	88	86	-0.02
8725_1	98	140	+0.43
8725_2	82	95	+0.16
8725_3	190	304	+0.60
8725_5	58	55	-0.05
8726_1	165	240	+0.45
8726_2	160	242	+0.51
8726_3	88	85	-0.03
8726_4	140	195	+0.39
8728_10	125	148	+0.18
8728_11	88	83	-0.06
8732_1	122	130	+0.07
8732_2	82	105	+0.28

Table 6-2. Summary of statistics on the error of the modal peak fields given in Table 6-1.

	Error	Absolute error
	MDU	MDU
Mean	+0.17	0.21
Standard deviation	0.23	0.19
Minimum	-0.21	0.02
Maximum	0.60	0.60

In the previous chapter the initial slow-rising ramp of the current waveforms of the return strokes 8726_2 and 8726_4 were speculated to be due to the upward propagating streamers. If

the slowly-rising portion of the current waveform is due to the return stroke process, rather than due to the streamers, or if the streamers can be considered part of the return stroke process, intuitively it would appear that the return stroke could be modelled as starting from ground with a low speed value and increase its speed for some height until it reaches its maximum, thereafter decreasing. The MDU model can avoid the large initial peak at the beginning of the field waveform by adopting such a speed variation. In fact, a similar mechanism for return stroke initiation has been proposed by Gorin (1985). The return stroke starts from ground level with a speed v_0, comparable to the streamer speed, increases speed exponentially until it reaches a maximum value within tens of meters and within a time of the order of the risetime, and then decreases exponentially with a decay factor of 2000 m as before. Figure 6-13 shows the field for return stroke 8726_2 from the MDU model if the return stroke starts from ground with a speed, $v_0 = 3.5 \times 10^7$ m/s and increases exponentially to the measured return stroke speed, $v_b = 1.2 \times 10^8$ m/s within a distance $z_b = 55$ m. The field peak is reduced from about 242 V/m in Figure 6-10d to about 150 V/m in Figure 6-13, a value comparable to the measured field peak. There is a better match in the overall waveshape of the calculated and measured field in Figure 6-13 than there is in Figure 6-10d.

6.4 Summary and Discussion

In this chapter the mathematical theory for a return stroke model which allows an upward return stroke speed that is an arbitrary function of height and a downward discharge current speed that is an arbitrary function of height is developed. This is a generalization of the Diendorfer-Uman model which allows only constant speeds for the return stroke currents and the discharge currents. The theory is applied to a case of exponentially decaying upward return-stroke speed

with height and a constant (at the speed of light) downward discharge current speed with height. It was shown that with respect to the constant speed case, for the typical return stroke properties assumed, the decreasing speed affects primarily the zero-crossing time of the far fields and the electrostatic field change at very close distances: the zero crossing time is reduced of the order of 10 μs and the electrostatic values after about 50 μs is increased of the order of 50 percent. Different results may well be obtained for different assumed channel-base currents.

Using the measured currents and return stroke speeds of Willett et al. (1989), the Modified Diendorfer-Uman (MDU) model was used to find the fields at 5.16 km from the triggered lightning and these fields were compared with the measured fields. There was a closer match between the measured and calculated fields for the MDU model compared to the match between the measured and calculated fields of the DU model. The slowly-varying ramp at the beginning of two of the measured current waveforms were hypothesized to be associated with initially low return stroke starting speeds (some or part being due perhaps to upward streamers) that increase rapidly to reach the maximum value within a few tens of meters and slowly decrease thereafter. For one return stroke with a slowly-rising initial ramp in its current waveform, it was shown that the fast acceleration of return stroke speed from a low value reduces the initial field peak value obtained without such an acceleration by about 60%. The reduced field peak is comparable to the measured field peak.

The two channel discharge constants used in section 6.2 and in Diendorfer and Uman (1990) have not been varied as a function of height in either the original DU model or the modification presented here. The use of two discharge time constants, each corresponding to one component of the total current assumed at the channel base, a fast time constant for the initial fast portion of the channel base current which physically represents the discharge of channel charge relatively near the earth and a slower time constant for the tail of the channel-base current

associated with the charge from relatively higher regions of the channel, effectively produces an overall time constant which increases with height. In principle, the discharge of the leader channel should be able to be modeled by a single time constant that varies with height, a new theoretical approach which is given in the next chapter.

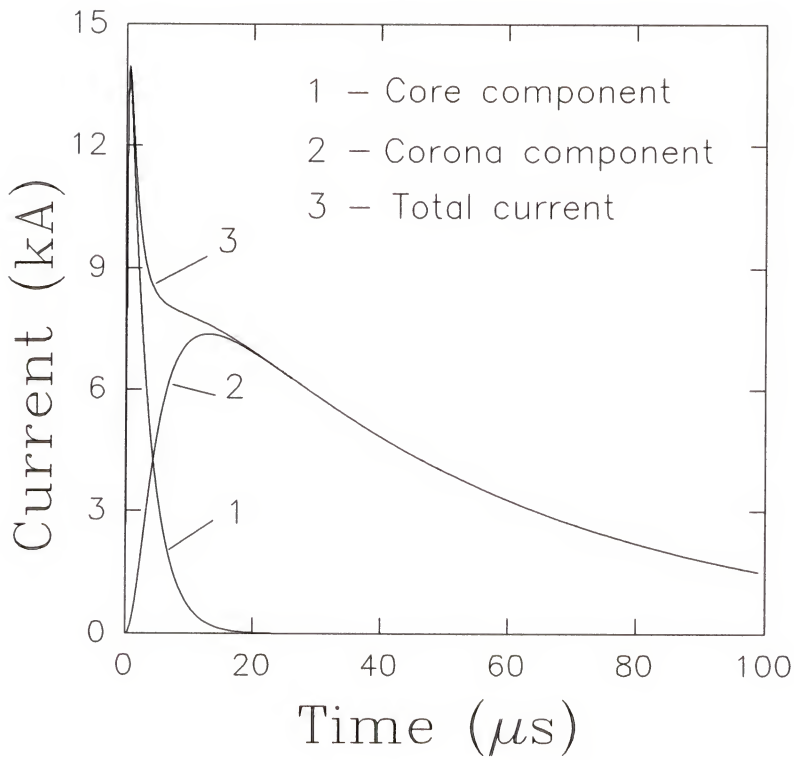

Figure 6-1. Channel base current and its division into two components assumed for the calculation of the fields in Diendorfer and Uman (1990) and in Figures 6-2 to 6-7.

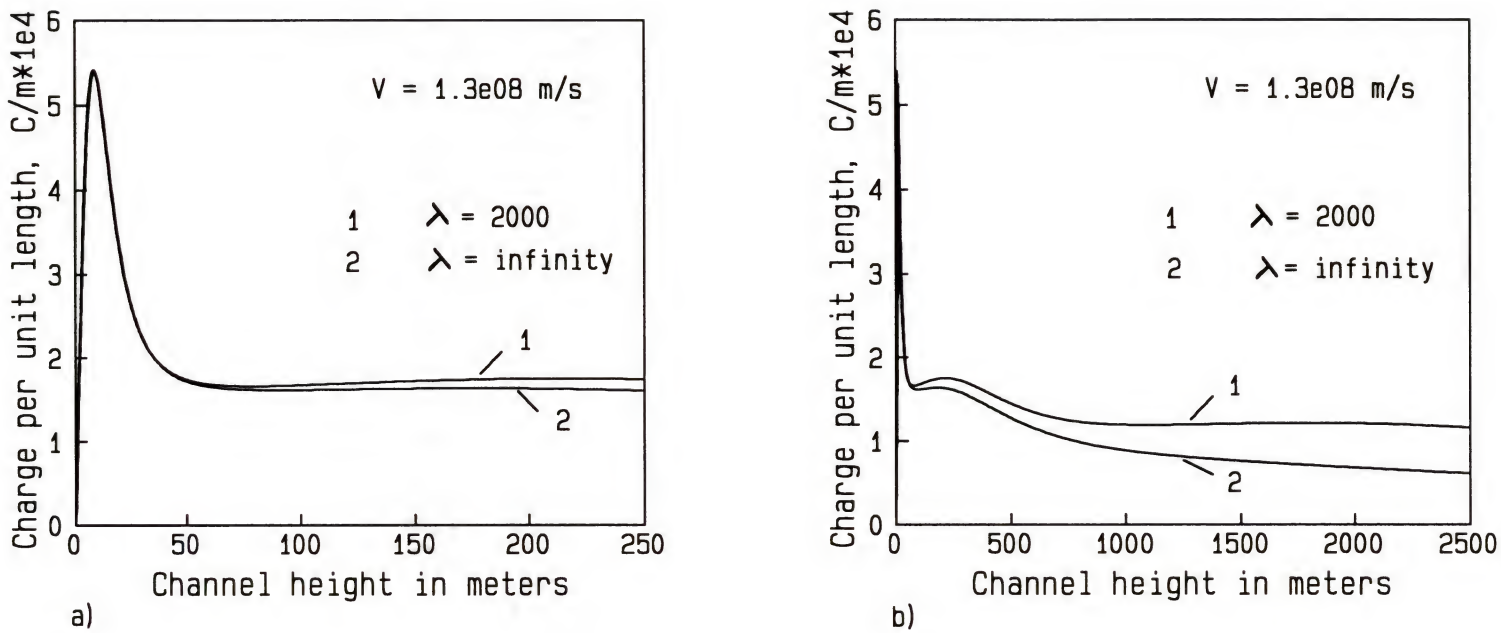

Figure 6-2. Comparison of the channel charge distribution for an initial return stroke speed of 1.3 x 10^8 m/s exponentially decaying with height with decay constant λ = 2000 m and the charge distribution for a constant return stroke speed of 1.3 x 10^8 m/s, both cases producing the same total channel base current, shown in Figure 6-1. a) Up to a height of 250 m; b) Up to a height of 2500 m.

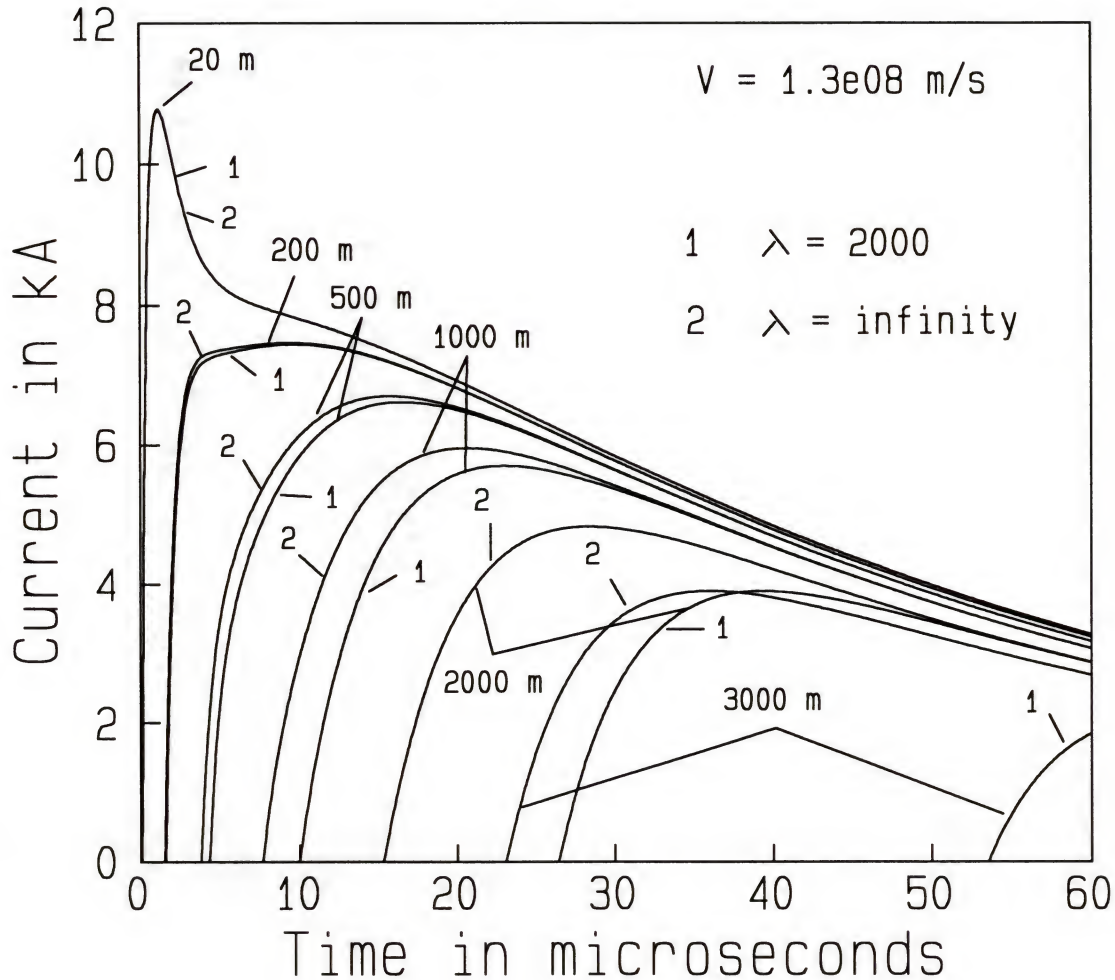

Figure 6-3. Comparison of the current distribution along the channel as a function of time for an initial return stroke speed of 1.3×10^8 m/s exponentially decaying with height with a decay constant $\lambda = 2000$ and the current distribution for a constant return stroke speed of 1.3×10^8 m/s, both cases producing the same total channel base current, shown in Figure 6-1.

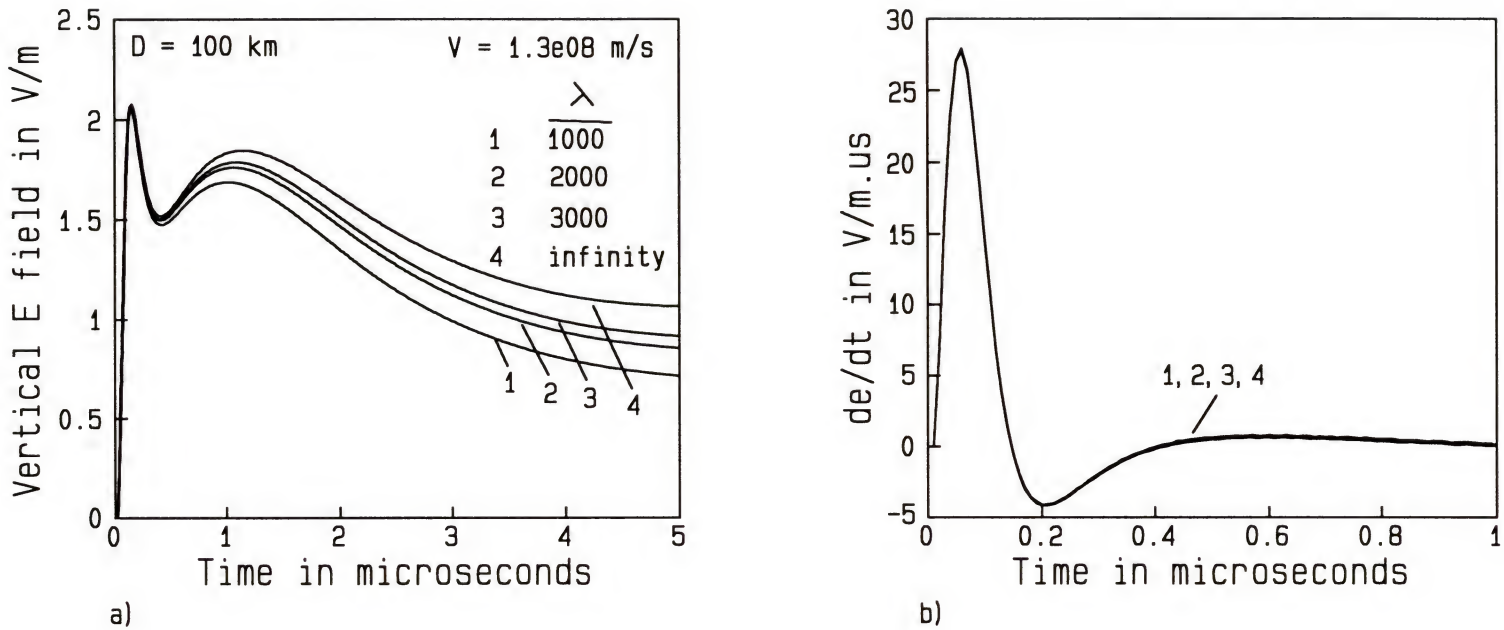

Figure 6-4. Comparison of the early part of the far electric fields for an initial return stroke speed of 1.3 x 10^8 m/s with exponential decay constant λ = 1000 m, 2000 m, 3000 m and infinity. a) Comparison of initial field peaks; b) Comparison of initial field derivatives.

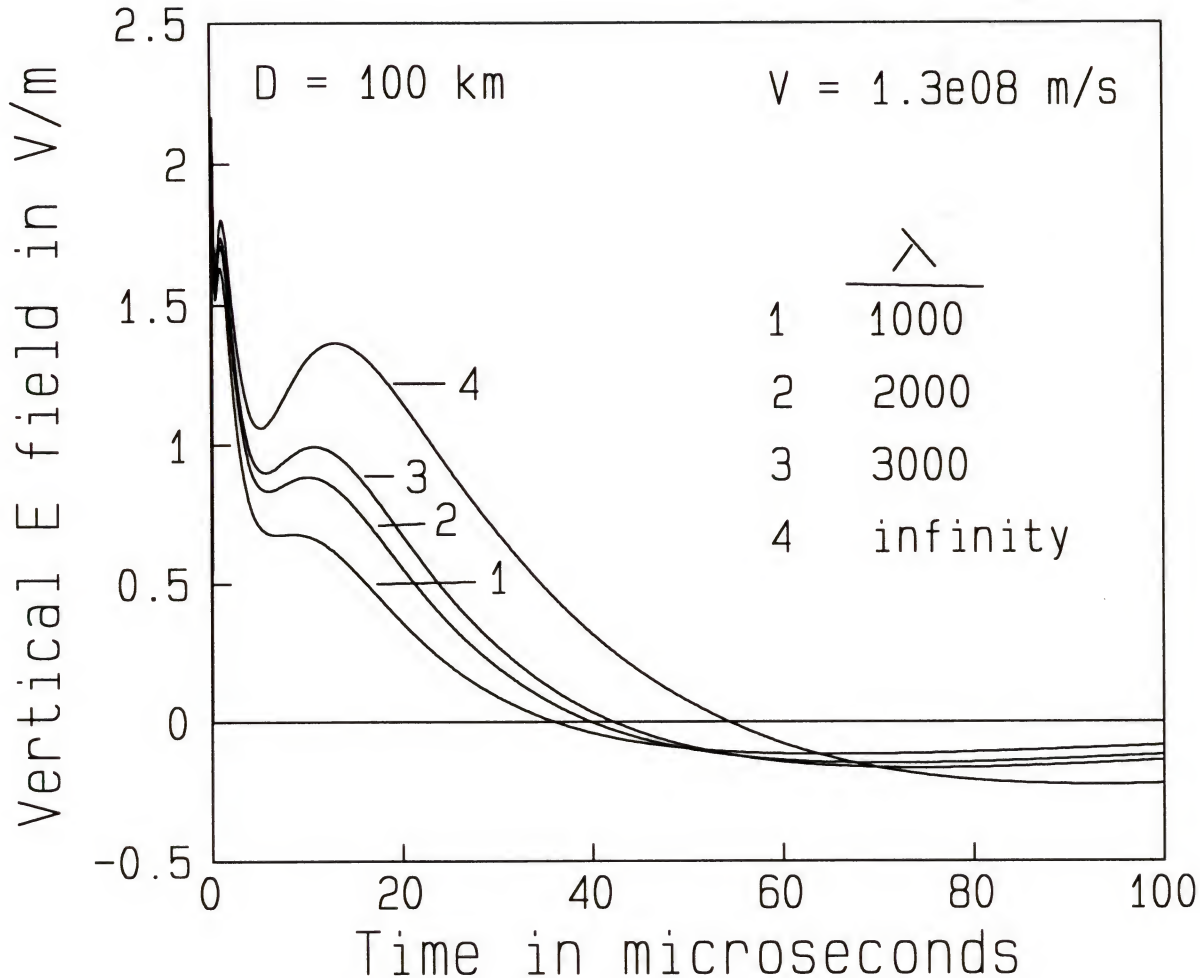

Figure 6-5. Comparison of the zero crossing and other features of the far fields for an initial return stroke speed of 1.3 x 10^8 m/s with exponential decay factors λ = 1000 m, 2000 m, 3000 m, and infinity.

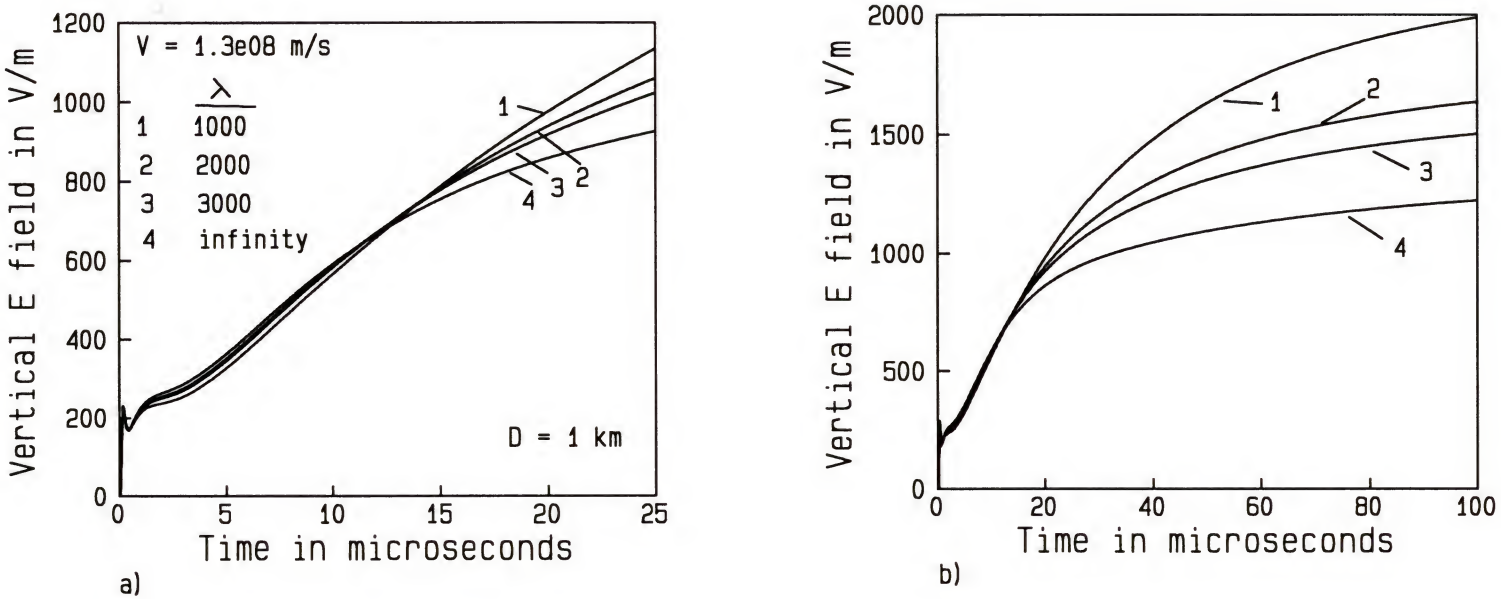

Figure 6-6. Comparison of the near electric fields for an initial return stroke speed of 1.3 x 10^8 m/s with exponential decay factors λ = 1000 m, 2000 m, 3000 m, and infinity. a) Fields for the first 25 μs; b) Fields for 100 μs.

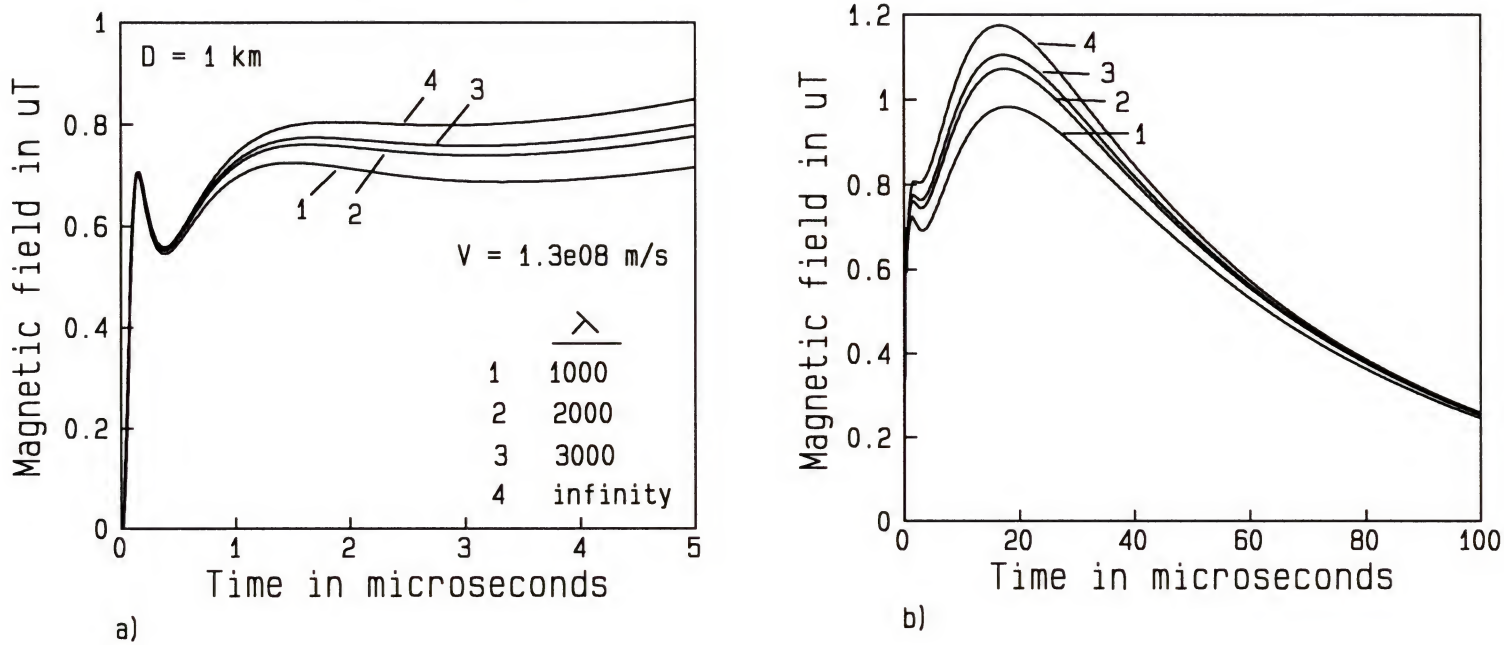

Figure 6-7. Comparison of the near magnetic fields for an initial return stroke speed of 1.3 x 10^8 m/s with exponential decay factors λ = 1000 m, 2000 m, 3000 m, and infinity. a) Fields for the first 25 μs; b) Fields for 100 μs.

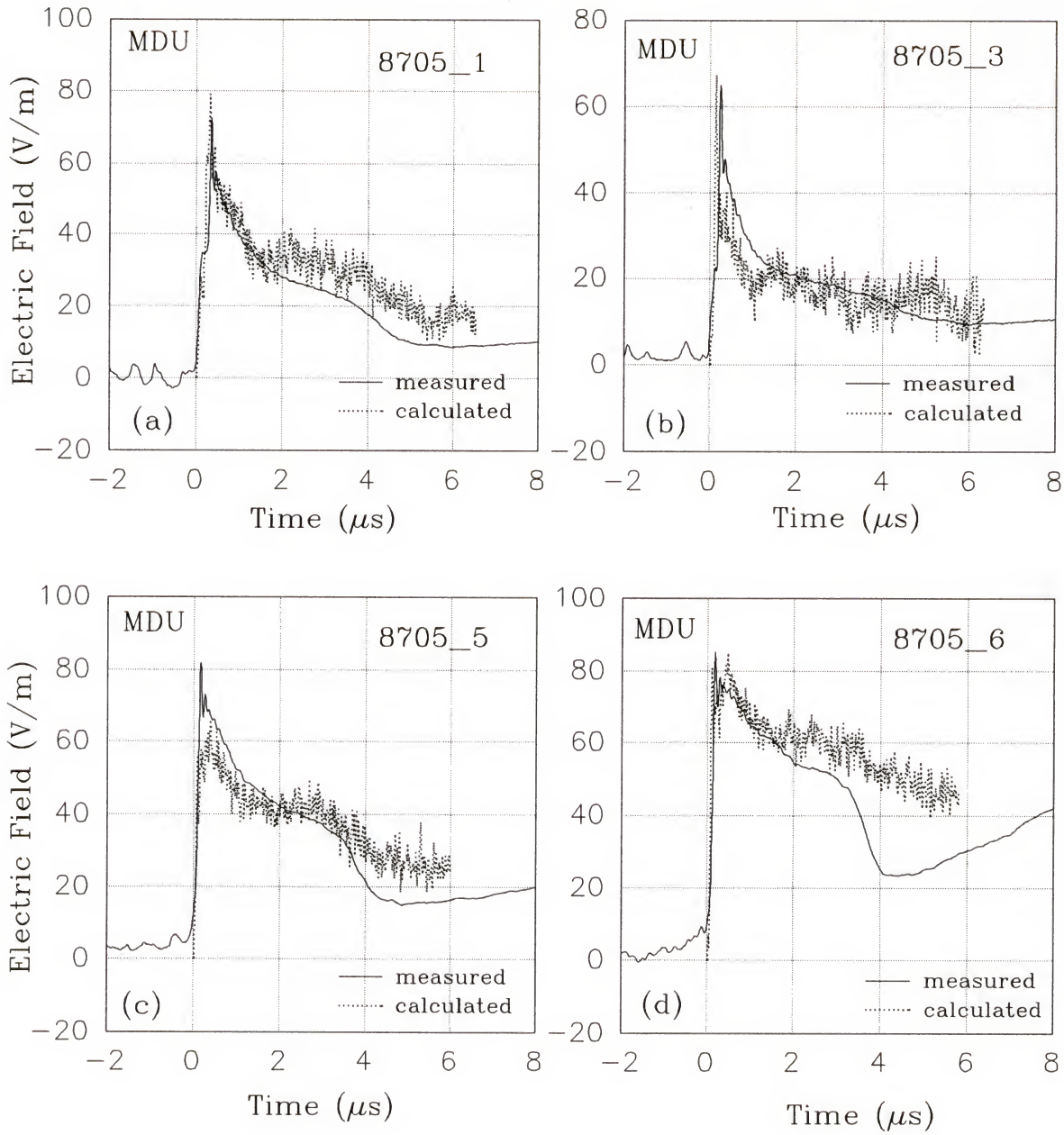

Figure 6-8. Comparison of calculated field from the MDU model with the measured field at 5.16 km. a) Return stroke 8705_1; b) Return stroke 8705_3; c) Return stroke 8705_5; d) Return stroke 8705_6.

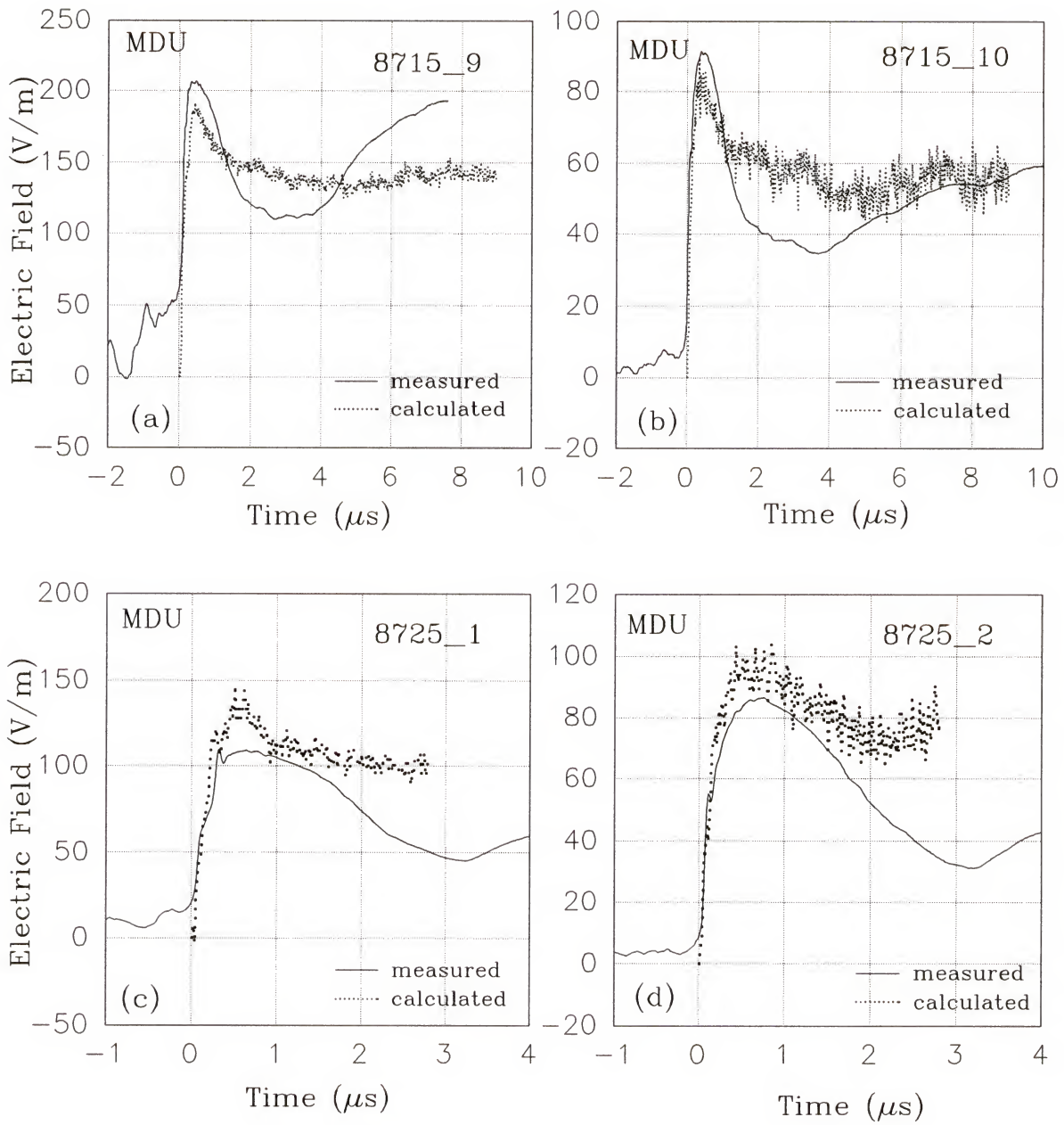

Figure 6-9. Comparison of calculated field from the MDU model with the measured field at 5.16 km. a) Return stroke 8715_9; b) Return stroke 8715_10; c) Return stroke 8725_1; d) Return stroke 8725_2.

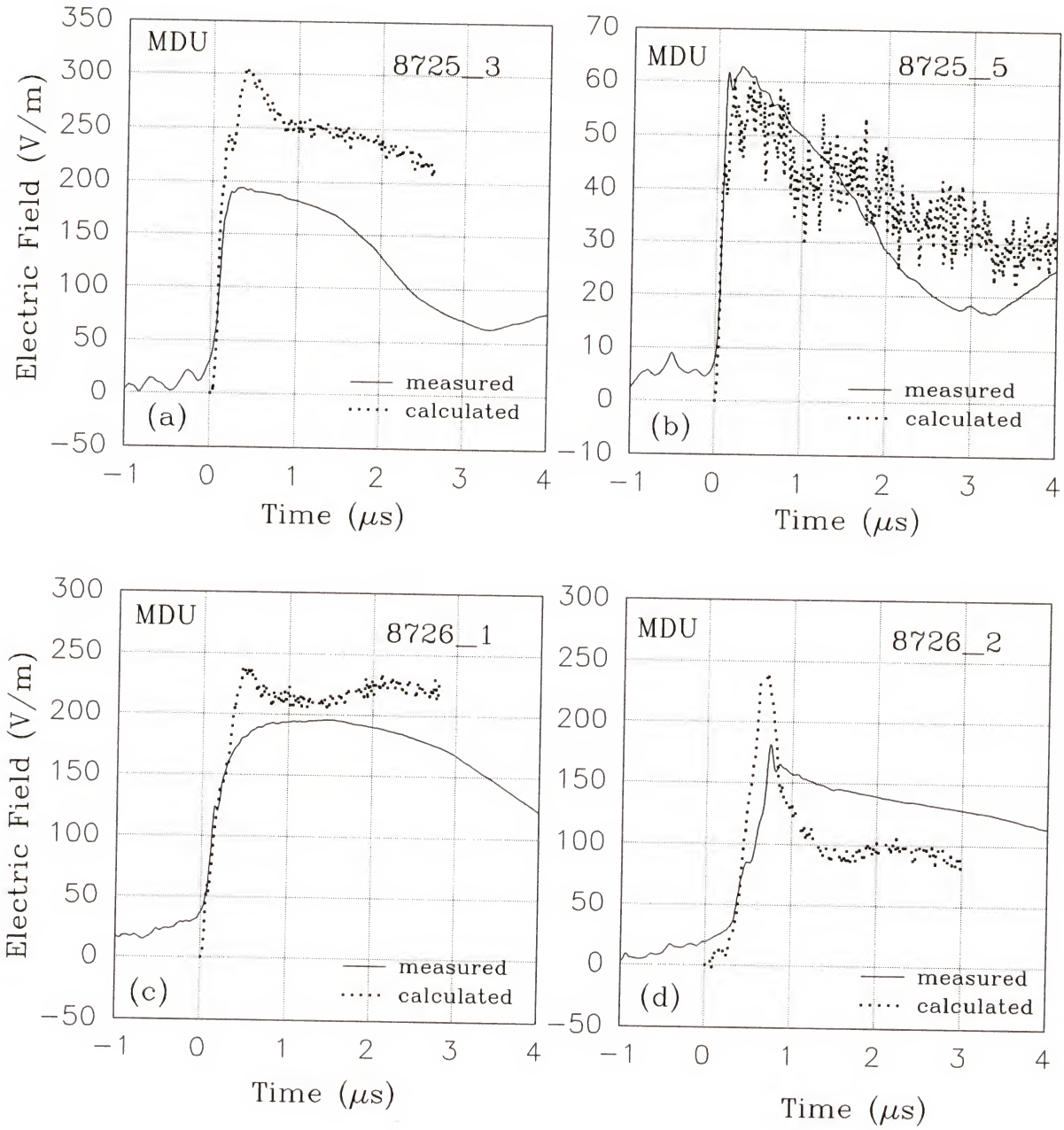

Figure 6-10. Comparison of calculated field from the MDU model with the measured field at 5.16 km. a) Return stroke 8725_3; b) Return stroke 8725_5; c) Return stroke 8726_1; d) Return stroke 8726_2.

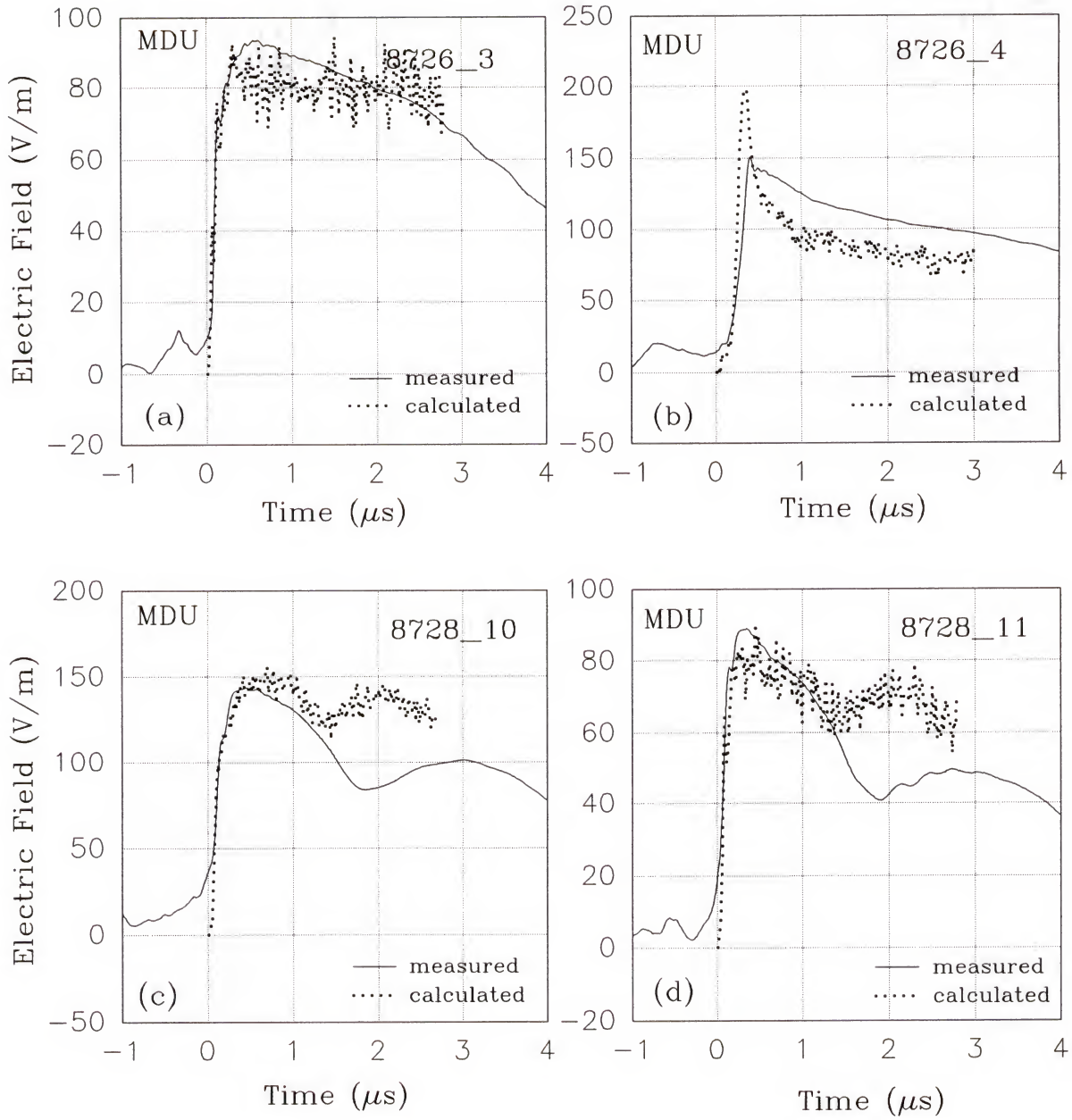

Figure 6-11. Comparison of calculated field from the MDU model with the measured field at 5.16 km. a) Return stroke 8726_3; b) Return stroke 8726_4; c) Return stroke 8728_10; d) Return stroke 8728_11.

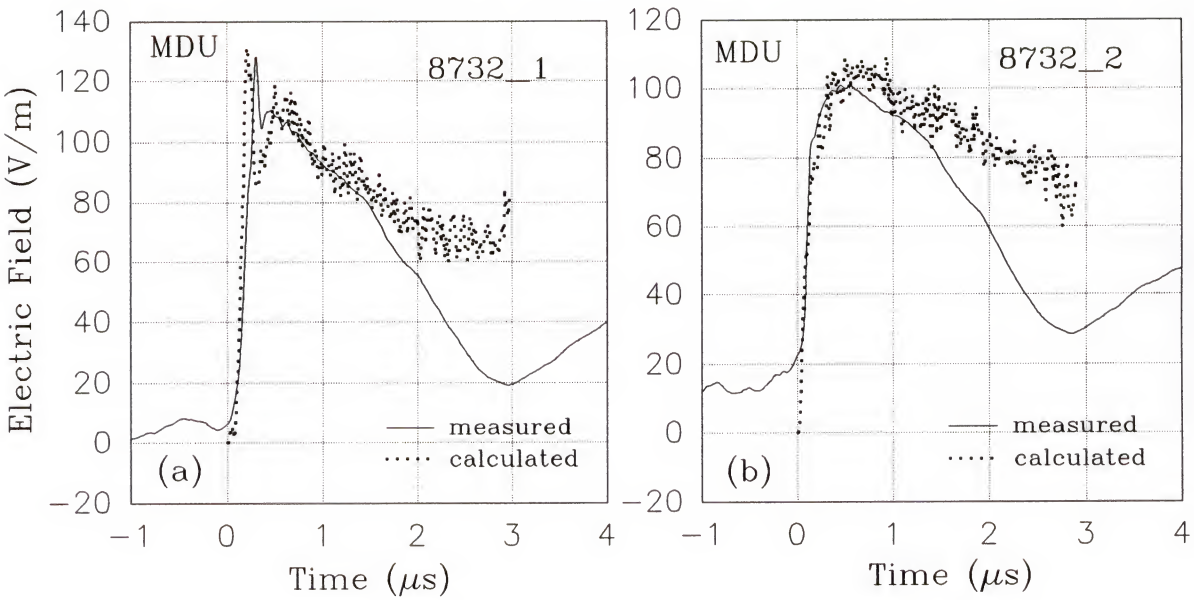

Figure 6-12. Comparison of calculated field from the MDU model with the measured field at 5.16 km. a) Return stroke 8732_1; b) Return stroke 8732_2.

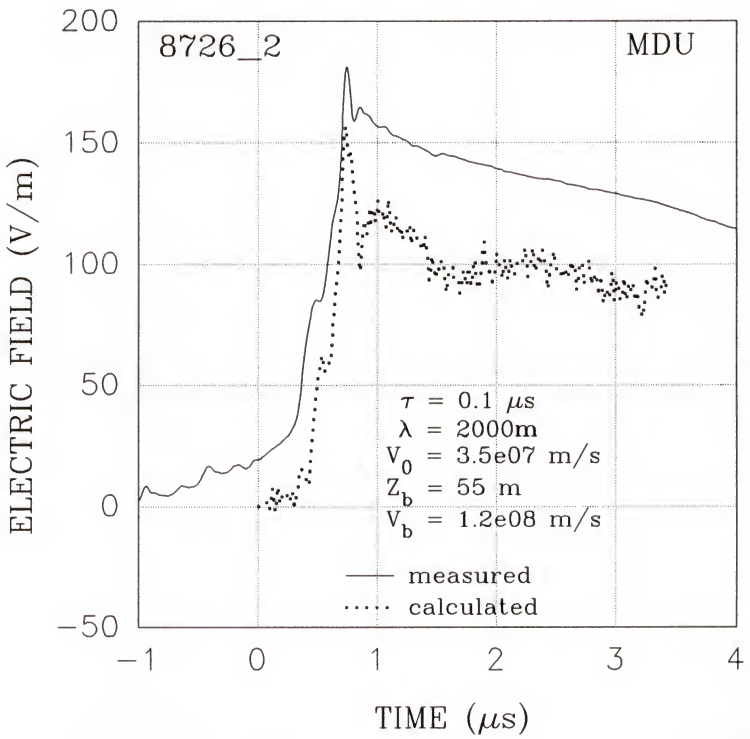

Figure 6-13. Comparison of calculated field from the MDU model with the measured field at 5.16 km for return stroke 8726_2. The return stroke is assumed to start from ground with a speed v_0 and increase the speed exponentially to reach the measured speed v_b at a height z_b, and thereafter decrease the speed exponentially with a decay factor λ.

CHAPTER 7
A NEW CHANNEL DISCHARGE MODEL WITH HEIGHT-VARIABLE TIME CONSTANT

One drawback of the two component current version of the DU and the MDU models discussed in chapters 5 and 6 is that they require an arbitrary division of channel-base current into two components. The single current component DU and MDU models used in Chapters 5 and 6 are strictly applicable only for the first few microseconds. Moreover, as mentioned in the previous chapter, it is more physically reasonable to expect a gradual variation of channel discharge rate with height rather than constant discharge rates represented by two fixed time constants. In the model proposed in this chapter the return stroke propagates with a speed which can be any arbitrary function of height, discharging the charge stored on the leader channel exponentially with a time constant that can be any arbitrary function of height. An exponential discharge is assumed because in nature discharging of the stored charges generally obeys an exponential law. While the theory developed in this chapter is for an exponential discharge function, the method is valid for any other specified discharge function. The discharge current propagates down the channel with a speed that can be any arbitrary function of height comprising, at the bottom, the channel base current. The mathematical theory of such a model is developed in section 7.1 followed by examples of the application of the model in section 7.2.

7.1 Mathematical Analysis

Consider the return stroke channel to be composed of a large number of small segments, each of equal length $\Delta z'$. When the return stroke front reaches each segment, the charge stored in it is assumed to begin discharging exponentially. Let $\rho_L(n)$ be the charge density per unit length at segment n, $t_u(n)$ be the time taken by the return stroke front to reach the n^{th} segment, $t_d(n)$ be the time taken by the discharge current at the n^{th} segment to reach ground, and τ_n be the discharge time constant for the charge at the n^{th} segment. Let v(n) be the speed of the return stroke at channel segment n, and u(n) be the speed of the downward current at channel segment n. The current assumed at the channel base is $i(z'=0,t)$.

The current injected at the n^{th} segment due to the discharging of the charge in that segment is given by

$$i_n(t) = \frac{\rho_L(n)\Delta z'}{\tau_n} e^{\frac{-(t-t_u(n))}{\tau_n}}, \quad t \geq t_u(n) \tag{7-1}$$

and this current reaches ground after a time $t_d(n)$. Therefore, the contribution to the channel base current of the current injected at the n^{th} segment is given by

$$i_n(0,t) = \frac{\rho_L(n)\Delta z'}{\tau_n} e^{\frac{-(t-t_u(n)-t_d(n))}{\tau_n}}, \quad t \geq t_u(n) + t_d(n) \tag{7-2}$$

The current at ground level at time t due to the discharging of the charges on the channel is given by

$$i(0,t) = \sum_{n=1}^{N} i_n(0,t) \tag{7-3}$$

where N is the maximum number of segments that the ground can "hear from" at time t and is given by the solution of

$$\begin{aligned} t &= t_u(N) + t_d(N) \\ &= \frac{N\Delta z'}{V_{av}(N)} + \frac{N\Delta z'}{U_{av}(N)} \end{aligned} \tag{7-4}$$

Note that $V_{av}(n)$ is the effective average speed of the return stroke within the channel starting from ground (segment 1) and arriving at segment n, and is defined by

$$\begin{aligned} V_{av}(n) &= \frac{n\Delta z'}{t_u(n)} \\ &= \frac{n}{\sum_{m=1}^{n} \frac{1}{v(m)}} \end{aligned} \tag{7-5}$$

and $U_{av}(n)$ is the average speed of the total discharge current while travelling the channel between segment n and ground, and is defined by

$$\begin{aligned} U_{av}(n) &= \frac{n\Delta z'}{t_d(n)} \\ &= \frac{n}{\sum_{m=1}^{n} \frac{1}{u(m)}} \end{aligned} \tag{7-6}$$

Substituting equation (7-2) in equation (7-3), we get

$$i(0,t) = \sum_{n=1}^{N} \frac{\rho_L(n)\Delta z'}{\tau_n} e^{\frac{-(t-t_u(n)-t_d(n))}{\tau_n}}, \qquad t \geq t_u(n) + t_d(n) \tag{7-7}$$

Consider the time t_n, defined by

$$t_n = t_u(n) + t_d(n) = \frac{n\Delta z'}{V_{av}(n)} + \frac{n\Delta z'}{U_{av}(n)}, \quad n = 1,....N \tag{7-8}$$

The current at the base of the channel at time t_1 is obtained by substituting the value n=1 in equation (7-8) and by substituting equation (7-8) in equation (7-7) with n=1. That is,

$$i(0,t_1) = \frac{\rho_L(1)\Delta z'}{\tau_1} \quad \textit{and hence,} \qquad \rho_L(1) = \frac{\tau_1 i(0,t_1)}{\Delta z'} \tag{7-9}$$

Following a similar procedure as above, the current at the base of the channel at time t_2 is given by

$$i(0,t_2) = \frac{\rho_L(1)\Delta z'}{\tau_1} e^{-\frac{(t_2 - t_1)}{\tau_1}} + \frac{\rho_L(2)\Delta z'}{\tau_2} \tag{7-10}$$

In equation (7-10), $\rho_L(1)$ is given by equation (7-9) and $\rho_L(2)$ is the only unknown which is given by,

$$\rho_L(2) = \left[i(0,t_2) - \frac{\rho_L(1)\Delta z'}{\tau_1} e^{-\frac{(t_2-t_1)}{\tau_1}} \right] \frac{\tau_2}{\Delta z'} \tag{7-11}$$

To generalize the procedure, for an arbitrary time, t_n, ($n \leq N$) we get,

$$i(0,t_n) = \frac{\rho_L(1)\Delta z'}{\tau_1} e^{-\frac{(t_n - t_1)}{\tau_1}} + \frac{\rho_L(2)\Delta z'}{\tau_2} e^{-\frac{(t_n - t_2)}{\tau_2}} + \ldots + \frac{\rho_L(n-1)\Delta z'}{\tau_{n-1}} e^{-\frac{(t_n - t_{n-1})}{\tau_{n-1}}} + \frac{\rho_L(n)\Delta z'}{\tau_n} \qquad (7\text{-}12)$$

$$= \sum_{m=1}^{n} \frac{\rho_L(m)\Delta z'}{\tau_m} e^{-\frac{(t_n - t_m)}{\tau_m}}$$

Note that equation (7-12) is similar to equation (A6) of Diendorfer and Uman (1990) if the time constant is a constant and the summation is replaced by integration. The complete charge distribution along the channel, $\rho_L(n)$, where $n \leq N$ can be determined by rearranging equation (7-12).

$$\rho_L(n) = \left[i(0,t_n) - \sum_{m=1}^{n-1} \frac{\rho_L(m)\Delta z'}{\tau_m} e^{-\frac{(t_n - t_m)}{\tau_m}} \right] \frac{\tau_n}{\Delta z'} \qquad (7\text{-}13)$$

where $\rho_L(n)$ must determined sequentially as illustrated in equations (7-9) and (7-11).

Consider a channel segment k, below the return stroke front, corresponding to a height z′. Then the total current at z′ is the sum of the contributions of currents from all the segments above z′, including the segment k. That is,

$$i(z',t) = \sum_{m=k}^{K} \frac{\rho_L(m)\Delta z'}{\tau_m} e^{\frac{-(t - t_u(m) - t_d(m) + t_d(k))}{\tau_m}}, \qquad (7\text{-}14)$$

$$t \geq t_u(m) + t_d(m) - t_d(k)$$

where $t_d(m)$-$t_d(k)$ is the time required for the discharge current injected at segment m to reach segment k, and K is the segment number corresponding to the maximum height from which segment k can "hear" at time t. K is found from the solution of the equation

$$t = \frac{K\Delta z'}{V_{av}(K)} + \frac{K\Delta z'}{U_{av}(K)} - \frac{k\Delta z'}{U_{av}(k)} \qquad \textbf{(7-15)}$$

$$= t_u(K) + t_d(K) - t_d(k)$$

Equation (7-14) gives the current distribution along the channel, which is similar to equation (A8) of Diendorfer and Uman (1990).

An alternate expression for i(z′,t) can be found by expressing i(0,t) as the sum of the contribution of currents from segment k and above, and the contribution from currents below segment k. That is,

$$i(0,t) = i(z',t-t_d(k)) + \sum_{n=1}^{k} \frac{\rho_L(n)\Delta z'}{\tau_n} e^{\frac{-(t-t_u(n)-t_d(n))}{\tau_n}} \qquad \textbf{(7-16)}$$

Rearranging the terms of equation (7-16) and making the substitution $t-t_d(k) = t^*$, we get,

$$i(z',t^*) = i(0,t^*+t_d(k)) - \sum_{n=1}^{k} \frac{\rho_L(n)\Delta z'}{\tau_n} e^{\frac{-(t^*-t_u(n)-t_d(n)+t_d(k))}{\tau_n}} \qquad \textbf{(7-17)}$$

Changing the notation t^* to t in equation (7-17), we get the current distribution along the channel

$$i(z',t) = i(0,t+t_d(k)) - \sum_{n=1}^{k} \frac{\rho_L(n)\Delta z'}{\tau_n} e^{\frac{-(t-t_u(n)-t_d(n)+t_d(k))}{\tau_n}} \qquad \textbf{(7-18)}$$

where the segment k corresponds to the channel height z′.

Taking the time derivative of equation (7-18), we get

$$\frac{\partial\, i(z',t)}{dt} = \frac{\partial\, i(0,t+t_d(k))}{dt} + \Delta z' \sum_{n=1}^{k} \frac{\rho_L(n)}{\tau_n^2} e^{\frac{-(t-t_u(n)-t_d(n)+t_d(k))}{\tau_n}} \qquad \textbf{(7-19)}$$

Time integration of equation (7-18) gives

$$\int_{t_u(k)}^{t} i(z',t)dt' = \int_{t_u(k)+t_d(k)}^{t+t_d(k)} i(0,t+t_d(k))dt' + \Delta z' \sum_{n=1}^{k} \rho_L(n)\left(e^{-\frac{(t-t_u(n)-t_d(n)+t_d(k))}{\tau_n}} - e^{-\frac{(t_u(k)+t_d(k)-t_u(n)-t_d(n))}{\tau_m}}\right) \quad \textbf{(7-20)}$$

where the segment k again corresponds to the channel height z′. Once the temporal and spatial variation of current, its derivative, and time integral are determined (equations 7-18, 7-19, and 7-20), the electric and magnetic fields can be calculated using equations (5-3) and (5-4).

7.2 Application

In the Variable Channel Time Constant (VCTC) model developed in the previous section, the upward return stroke speed, v(z′), the total downward discharge current speed, u(z′), and the discharge time constant, τ(z′) can be chosen independently. In the model of Diendorfer and Uman (1990), the return stroke speed is assumed to be a constant, equal to 1.3×10^8 m/s, the discharge current speed is assumed to be a constant c, the speed of light, and the core and corona discharge time constants are assumed to be 0.6 μs and 5.0 μs respectively for natural lightning return strokes. The application of the VCTC model can be demonstrated by calculating the time constant profile along the channel associated with a single current at the channel base that effectively replaces the two time constants and the associated two current components of the DU model. Given the charge distribution along the channel obtained from the DU model (see Figure 6-2) for the current at the base given in Figure 6-1, the equivalent time constant profile along the channel can be calculated from equation (7-13) iteratively. The time constant profile is shown in Figure 7-1. Figure 7-1a shows the time constant profile for the bottom 250 m of the channel

and Figure 7-1b shows the time constant profile for the bottom 2500 m. Near the ground the time constant is about 0.6 μs, the value assumed for break-down time constant in the DU model. The time constant increases rapidly, reaching a value slightly over 5 μs, the value assumed for corona time constant in DU model, at about 700 m and remains more or less constant above that point. Recall that the inputs to the model were only the total charge distribution given in Figure 6-2 (curve 2) and reproduced in Figure 7-2, the total current at ground level given in Figure 6-1 (curve 3) and the return stroke speed 1.3e08 m/s. Figure 7-2 also shows the breakup of the total charge into core and corona components corresponding to the time constants 0.6 μs and 5.0 μs, respectively, in the DU model. From Figure 7-2a it can be seen that the time constant of 0.6 μs near the ground level obtained from the new model is consistent with the dominance of the fast discharge of the core region of the channel near the ground in the DU model. In the DU model, with increasing height along the channel progressively larger portion of channel charge at a given height is discharged slowly with a time constant of 5 μs and only smaller portion of the charge is discharged faster with a time constant of 0.6 μs (see Figure 7-2). The rapidly increasing time constant with height of the new model is consistent with this picture. At about 700 m the discharge time constant of the channel in the new model is about 5 μs and remains the same above that height, which is consistent with the almost complete dominance of the slow discharge with time constant of 5 μs at comparable heights in the DU model (see Figure 7-2b).

For a given channel charge distribution with height and the specified return stroke speed, the new model gives the discharge rates (time constants) required along the channel to have the specified current at ground. Conversely, for a specified time constant profile with height and the return stroke speed, the new model can determine the charge distribution along the channel and hence the channel currents required to produce the specified current at the channel base.

As a demonstration of the new model, the channel currents as a function of time at heights 20 m, 200 m, 500 m, and 1000 m are calculated using equation (7-14) and are shown in Figure 7-3 (solid line). For comparison, the current given in Figure 6-3, for constant speed, is also shown (dotted line) in Figure 7-3. Both set of curves are very similar, though not identical. Once the current distribution along the channel in space and time is computed, the calculation of fields using equations (2-3) and (2-4) is straightforward. Like the case of TL, MTL, TCS, DU, and MDU models in chapter 5 and 6, the electric fields at 5.16 km can be compared with the measured fields for the new model. However, a time constant profile has to be arbitrarily assumed since none is known. In view of the fact that there is no information in the literature about the variation of discharge rate with height and the fact that measured fields and currents are only available for a few microseconds, it is not be a fruitful exercise to calculate the fields from the VCTC model and compare it with the measured fields for all the 18 return strokes as was done in chapter 5 and 6. However, as an example, the VCTC model field is calculated for return stroke 8715_10 assuming a discharge time constant of 0.1 μs at ground level increasing linearly with height at a rate of 1.0 μs per km (Figure 7-4). As in the case of the MDU model in chapter 6, the return stroke speed of 1.4×10^8 m/s is assumed to decrease exponentially with height with a decay factor of 2000 m. There is a good match between the calculated and measured fields in Figure 7-4.

It may be possible to design an experiment that could give estimates for the discharge time constants at different heights for triggered lightning return stroke channels. Simultaneous measurements of channel-base current, upward return-stroke speed, and the remote electric and magnetic fields can be measured using well established techniques (e.g., Willett et al., 1988,1989; Lin et al., 1979). If we assume the downward discharge current speeds to be the speed of light, equation (7-18) and (7-19) give the current $i(z',t)$, and the current derivative

di(z',t)/dt at height z' (corresponding segment k) in terms of the unknown time constants τ_1, τ_2, .. , τ_k. Note that ρ(n) is also a function of the unknown time constants τ_n, n = 1, .. , k (see equations 7-9 to 7-13). The measured channel-base current and the field can be divided into number of equal time intervals, dt, and correspondingly the channel is also divided into same number of segments such that the time taken by the return stroke wavefront to cover one segment is dt. Consider the time dt at which the return stroke has covered the first segment only. From the measured magnetic field, channel-base current, and the return stroke speed the discharge time constant τ_1 can be uniquely determined (equations 7-18, 7-19, 7-9, and 2-4). Note that here magnetic field measurements are preferable over the electric fields because magnetic fields do not have the current integral term and hence are less complicated in calculations. This value of τ_1 can be used to find τ_2 in the next time step when the return stroke covers the next segment. In this manner the discharge time constant at each segment can be determined from the calculated discharge time constants from all the segments below it, measured channel-base current, measured field, and measured return stroke speed. Of course a basic assumption involved is that the VCTM model is correct and given the appropriate time constants it can predict the field that exactly matches the measured field. In practice single station field measurement will probably not be sufficient because errors in the time constant determination of lower segments introduce error in the calculated time constants of segments above it. Having multiple stations at different distances simultaneously measuring the fields will yield improved estimates for the time constants.

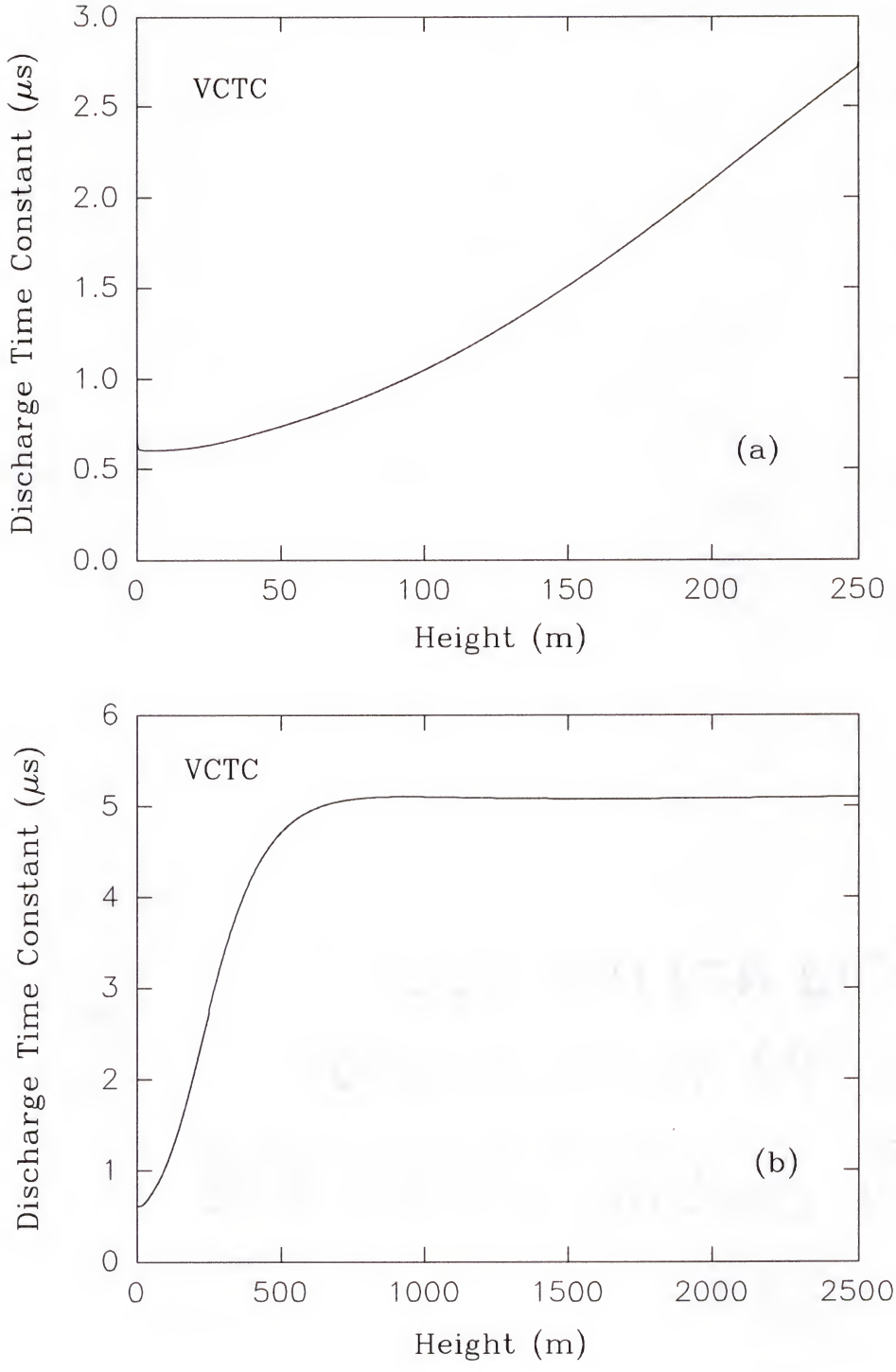

Figure 7-1. Channel discharge time constant as a function of height for the VCTC model for the charge distribution given in Figure 6-2 (curve 2) and channel base current given in Figure 6-1 (curve 3). a) For a height of 250 m; b) For a height of 2500 m.

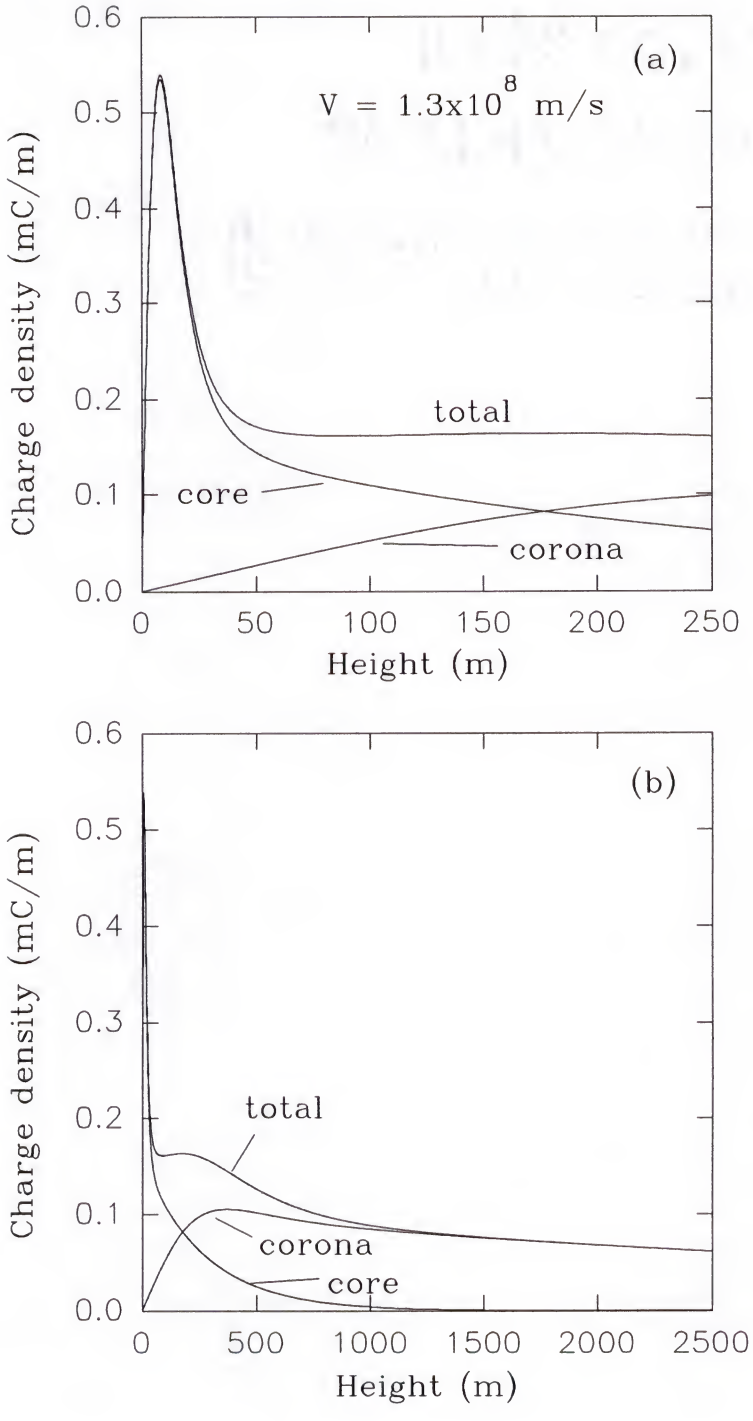

Figure 7-2. Charge distribution along the channel for the DU model (Figure 8 of Diendorfer and Uman, 1990) for two time constants 0.1 μs and 5 μs, and the associated channel-base currents shown in Figure 6-1. a) The bottom 250 m; b) The bottom 2500 m.

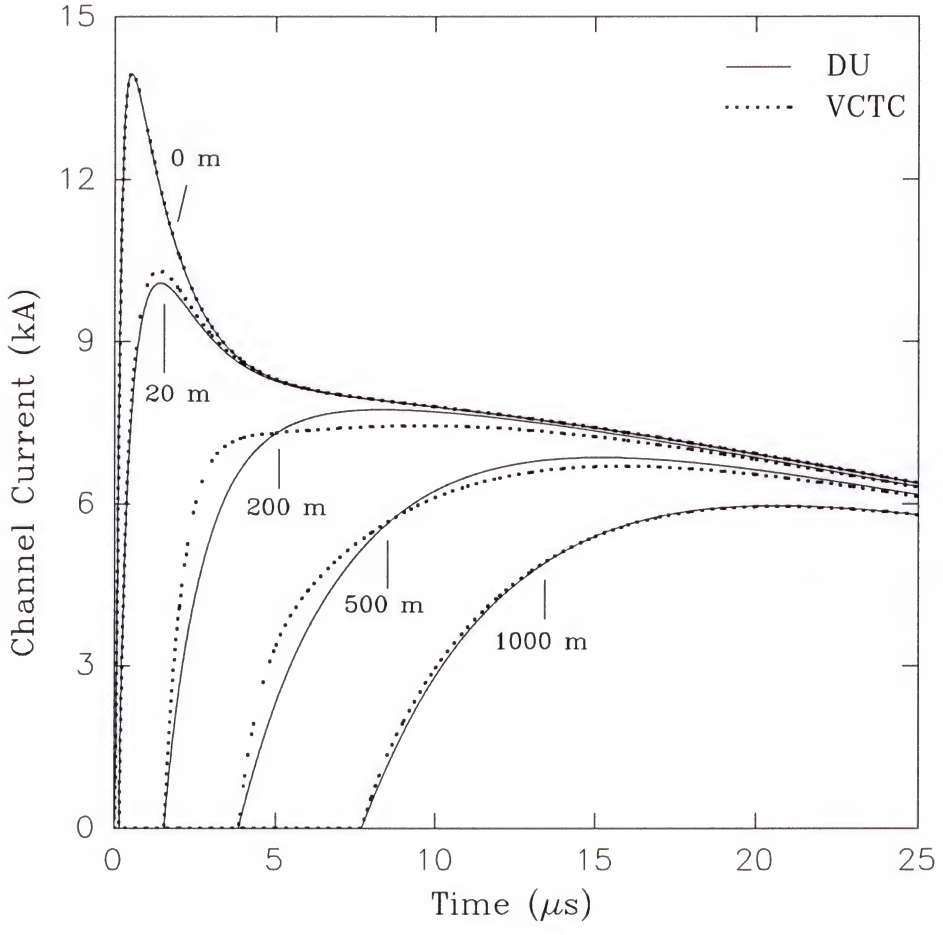

Figure 7-3. Comparison of current distribution along the channel as a function of time for the assumed return stroke speed of 1.3×10^8 m/s for the DU and VCTC models.

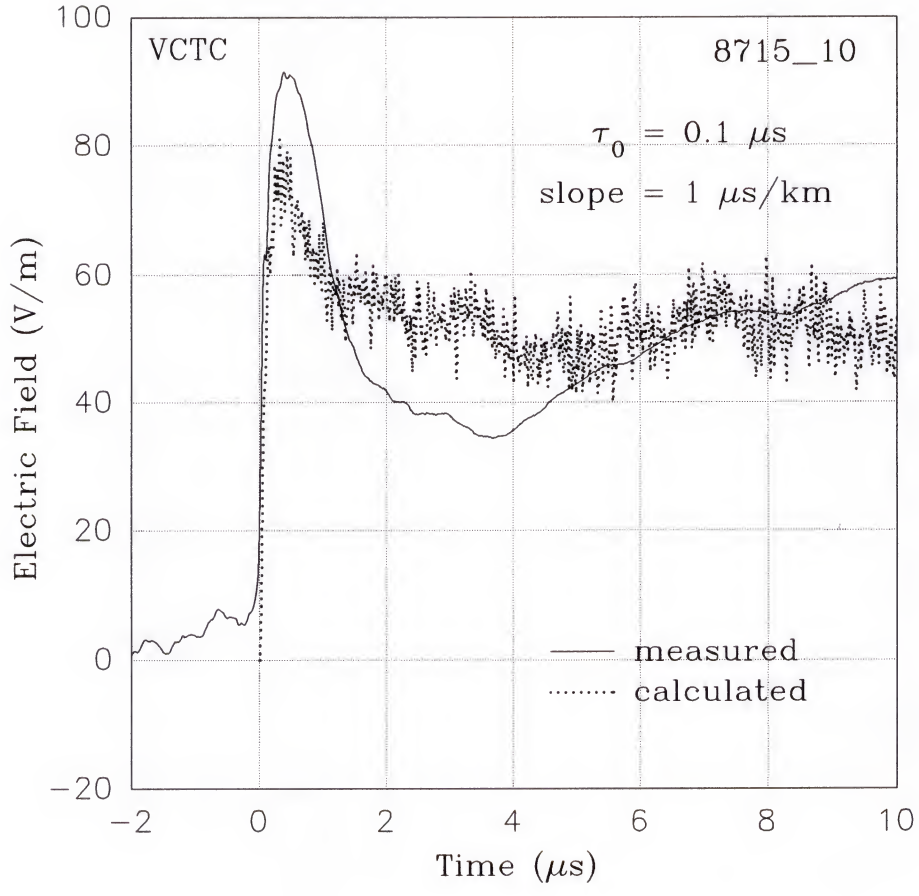

Figure 7-4. Comparison of calculated field from the VCTC model at 5.16 km for return stroke 8715_10. The measured current at the channel base and the measured return stroke speed are given in Figure 5-13. The discharge time constant is assumed to be 0.1 μs at ground and increases linearly with height with a slope 1 μs/km. The return stroke speed is assumed to decrease exponentially with a decay factor of 2000 m.

CHAPTER 8
MODELING OF CONTINUING CURRENTS AND M COMPONENTS

As reviewed in section 2.5, point charge electrostatic models have been used by Brook et al. (1962) and Krehbiel et al. (1979) to calculate the charge lowered from cloud to ground by the continuing current from measured electric field changes at ground. To date there is no published literature on the mathematical modeling of M components. The different views on M components, often conflicting, are reviewed in section 2.1.3 and 2.1.4. In section 4.2 some properties of the continuing currents and M components from the Sandia triggered lightning data are presented. In this chapter a model for the continuing current and the M component is presented. As an illustration of the model, a measured current record of triggered lightning continuing current and M components analyzed in section 4.2 is used to calculate the electric fields at ground level, and the calculated field waveshapes are compared with the field waveshapes from continuing currents and M components from natural lightning available in the literature.

8.1 Theory

During the continuing current phase of the flash, tens of amperes or more of current (e.g., Brook et al., 1962; Section 4.2 of this dissertation) flow in the channel previously created by the leader and the return stroke. Under this condition the channel is highly conducting and may be modeled as a transmission line. Jordan (1990) observed in streak camera records that

the relative peak light intensity and the rise time of the light waveform did not change measurably with height for M components whereas, for return strokes, the relative light intensity decreased and the rise time of the waveform increased with height. This observation of Jordan (1990) suggests that the cloud-to-ground channel is more conductive during the continuing current phase than during the return stroke phase, and therefore the channel can be modeled, to a first approximation, as a lossless transmission line carrying a slowly-varying current superimposed on which current pulses due to M processes travel. A current pulse travelling along a transmission line is expected to suffer reflection from impedance discontinuities at the ends or branch points. The presence of reflection can not be detected from the channel-base current waveform because only an enhancement of amplitude is expected. The published electric field waveforms of M components (e.g., Thottappillil et al., 1990; Rakov et al., 1992) do not have any features suggestive of reflection. It may that the ground do not act as a short circuit for the downward current pulse and hence the reflected pulse is very small in amplitude. It is assumed here that any reflection that may be present is not significant and can be ignored. From simultaneous eight-station measurements and using a point charge model (see section 2.5) Krehbiel et al. (1979) inferred that the continuing current charge volumes are extended in space horizontally inside the cloud rather than being like the discrete stroke charge volumes. Therefore the model being proposed for continuing current incorporates a straight inclined section of the channel in continuation of a straight vertical channel above a perfectly conducting ground. For simplicity, the channel is assumed to be branchless. Rakov et al. (1992) present data showing that in majority of cases the microsecond scale electric field pulses, indicative of the breakdown process associated with the M component, occur at the very beginning of the hook-shaped M component electric field changes. If the hooks are produced by the movement of charges (currents) along the channel, then the observation of Rakov et al. (1992) suggest that M current pulses travel

towards the ground from the cloud rather than from ground towards cloud. Jordan (1990) also inferred from streak camera records that the M component pulses travel from cloud to ground. There is the possibility that the M component charge sources are spatially separated from the continuing current charge sources. For simplicity it is assumed in the model that the continuing current charge source and the M component charge source are located in the same region of the cloud. In that case the continuing current and the M component can be modeled together as a composite current waveshape travelling towards the ground along a lossless transmission line, without making any distinction between the continuing current part and the M component part.

Figure 8-1 shows the geometry of the model. The x, y, and z coordinates are as indicated. The point at which the channel makes contact with ground is assumed to be the origin. In Figure 8-1, the coordinates of the extreme end, S_0', of the inclined channel section, the coordinates of the top of the vertical channel section, and the coordinates of the field measuring (observer) point are given as (x_0',y_0',z_0'), (0,0,h'), and (d,0,0) respectively. (x',y',z') is the coordinate of any arbitrary point, S', on the channel. The current at any arbitrary point, S', for a current waveform travelling from S_0' towards the ground at an arbitrary speed, v(s'), can be expressed in terms of the current at S_0' by the relation

$$i(S',t) = i\left(S_0',t-\frac{S'-S_0'}{V_{av}(s')}\right) \qquad \textbf{(8-1)}$$

where S_0'-S' denote the distance between S_0' and S' along the channel and $V_{av}(s')$ is the effective speed given by

$$V_{av(s')} = \frac{S_0'-S'}{\int_{S_0'}^{S'} \frac{ds''}{V(s'')}} \qquad \textbf{(8-2)}$$

8.2 Application

First, the model is demonstrated for the case in which the continuing current and M component currents start from the top, h′, of the vertical channel section without any horizontal extension and travel down towards ground at a constant speed, v. In all the calculations presented in this chapter the speed is assumed to be a constant. The current at time, t, at any point (0,0,z′) on the channel can be expressed in terms of the assumed current fed into the top of the channel by the relation

$$i(z',t) = i(h',t-\frac{h'-z'}{v}) \qquad \textbf{(8-3)}$$

Once the spatial and temporal distribution of the current in the channel is determined, the fields at ground can be calculated using equations (2-3) and (2-4), with the modification that the integration is performed over the limits z′ = h′ to z′ = 0. A measured continuing current at the base of the channel from the Sandia data set analyzed in section 4.2 and shown in Figure 8-2 is assumed at the top of the channel. In Figure 8-2 the M-current pulses are marked as M_1 through M_6. Note that in a transmission line model without any reflections from the ends, the current as a function of time at any point on the line is unchanged, but only delayed in time.

Figure 8-3 shows the calculated fields at 1 km distance assuming the current shown in Figure 8-2 at the top of the channel and a constant downward speed of $1x10^7$ m/s. In Figures 8-3 to 8-8 the top of the channel is assumed to be at a height of 7.5 km without any horizontal extension. The current is assumed to start propagating down and the field simulation is started only after a time (h′/v + d/c) in order to eliminate the introduction of initial transients. The static, induction, and radiation components are shown separately. Since the induction and radiation components are relatively very small, the total field is essentially the same as the static

field component. The hook-shaped field changes during the slow continuing current field change in Figure 8-3 are labeled as M_1 through M_6 and correspond to the M-current pulses in Figure 8-2. The calculated field waveshapes shown in Figure 8-3 are generally similar to the waveshapes of the continuing current stage of the field records of natural cloud-to-ground lightning presented by Rakov et al. (1992).

In Figure 8-4 the electric field components at a distance of 5 km and a downward speed of $1x10^8$ m/s are given for the assumed channel top current given in Figure 8-2. From Figure 8-4 it is seen that the electric field at 5 km for speed $1x10^8$ m/s is completely dominated by the static field component. Therefore the contribution of the induction and radiation components to the total field can be neglected at distances less than or equal to 5 km and speeds less than or equal to $1x10^8$ m/s. Note that in Figure 8-4 the hook-shaped field changes has disappeared which will be discussed later in this chapter. The static component of the field is the sum of the field change due to the charge on the channel and the field change of opposite sign due to depletion of charge of equal amount at the top end of the channel. Calculation of the fields due to the charge on the channel and the depletion of charge in the cloud separately can give an intuitive understanding of the reasons for the field waveshapes. From the continuity equation relating the charge density and current density at any point on the channel, we find

$$\frac{di(s',t)}{ds'} = -\frac{\partial \rho(s',t)}{\partial t} \qquad \textbf{(8-4)}$$

where $\rho(s',t)$ is the charge density on the channel. Integrating both sides of equation (8-4) and substituting for $i(s',t)$ from equation (8-3), we get

$$\int_0^t \frac{\partial i(s_0', t - \frac{s_0' - s'}{v})}{\partial s'} dt = \rho(s', t) \tag{8-5}$$

But,

$$\frac{\partial i(s_0', t - \frac{s_0' - s'}{v})}{\partial s'} = \frac{1}{v} \frac{\partial i(s_0', t - \frac{s_0' - s'}{v})}{\partial t} \tag{8-6}$$

Substituting equation (8-6) in equation (8-4), we get

$$\rho(s', t) = -\frac{i(s', t)}{v} \tag{8-7}$$

The fields at ground from each small segment of the channel due to the charge density given by equation (8-7) is calculated using Coulomb's Law. The appropriate travel time of the electromagnetic waves from each section of the channel to the field point is taken into account in the calculations. The charge depletion in the cloud, at any given time, due to the drainage of current is given by the time integral of the current at that time. Here also the travel time of the electromagnetic waves from the cloud to the field point is properly taken into account. The field due to the change of charge in the cloud is calculated using Coulomb's Law. Figure 8-5 shows the fields due to the downward travel of the current shown in Figure 8-2 with a constant speed of 1×10^7 m/s from a height of 7500 m, the same case as in Figure 8-3. The fields due to the charges in the channel and the cloud are shown separately. From the figure it can be seen that the movement of the charge along the channel is responsible for producing the hook-shaped field changes of the M components observed in natural lightning.

The electrostatic fields at 1000 m are shown in Figure 8-6 for a downward speed of 1×10^6 m/s, which is 10 times less than the speed in Figure 8-5. The contribution of the field change

due to the charges on the channel has increased and the contribution due to the cloud has decreased (from Figure 8-5 and Figure 8-6). The hook-shaped field changes are more pronounced and have larger duration (time interval from the beginning to the end of a hook) in Figure 8-6, for the lower speed, than in Figure 8-5, for the higher speed.

The electrostatic fields at 1000 m for a downward speed of $1x10^8$ m/s are shown in Figure 8-7. The hooks have almost disappeared and the total field is dominated by the contribution from the charge depletion in the cloud. Some of the larger M component field changes in the total field resembles the step-like field changes of K changes in natural lightning (e.g., Thottappillil et al., 1990; Rakov et al., 1992).

In Figure 8-8 and 8-9 the calculated electrostatic fields at 5000 m from the channel for downward speeds of $1x10^7$ m/s and $1x10^6$ m/s, respectively, are shown. The hook-shaped field changes have mostly disappeared, and the larger M component field changes are more step-like.

Thus far the channel has been assumed to have only a vertical section. Figure 8-10 to 8-11 present fields calculated by adding another straight section to the top of the vertical channel section at various inclinations and lengths. The geometry of the channel, the coordinates, and the speeds are indicated on the figures. In Figure 8-10 the fields are calculated at 1000 m for a channel geometry having a vertical section and an inclined straight section for a speed of $1x10^7$ m/s. For this geometry and the field point indicated, the currents are always moving towards the observer and pronounced hook-shaped field changes are produced. In Figure 8-11 the fields are calculated at 5000 m and the horizontal section extends to 10000 m in the same direction as the observer. The larger M components now produce hooks, while in Figure 8-8, a case identical to that presented in Figure 8-11 except for no horizontal section, there were no hook-shaped field changes.

8.3 Discussion

It was assumed in all the field calculations presented above that the continuing currents and M current pulses travel from cloud to ground. Malan and Collens (1937) reported that two out of nine M components that they observed photographically with a streak camera progressed from ground to the cloud, as discussed in section 2.1.3. In Figure 8-12 the fields at 1000 m are presented for a case in which the continuing currents and M current pulses are propagated up from the ground. The channel was assumed to be vertical with a maximum height of 7500 m and the upward speed was assumed to be 1×10^7 m/s. The hook-shaped field changes have now an initial polarity that is the same as the polarity of the continuing current field change, which is opposite to the waveshape polarity of M components in natural lightning presented by Malan and Schonland (1947), Thottappillil et al. (1990), and Rakov et al. (1992). Therefore it seems unlikely that the continuing currents and M current pulses can travel upward and at the same time produce the characteristic hook-shaped field changes observed close to the channel. Unfortunately, Malan and Collens (1937) do not present the electric field records associated with the two M components that they observed to travel upward.

From the analysis presented in the previous section, it appears that very fast M components, with a speed of about one third the speed of light, do not necessarily produce hook-shaped field changes even for an observer as close as 1 km to the channel and hence may not be identified in electric field change records. At those speeds the smaller M current pulses do not produce identifiable field changes and the larger M current pulses produce field changes that are step-like. At about 5 km from the channel, even for lower speeds (1/10 to 1/100 the speed of light), hooks are not produced for vertical channel geometry. But hook-shaped field changes can be produced at about 5 km if the channel has an in-cloud horizontal section in the same plane and

direction as the observer. Note that Thottappillil et al. (1990) observed hook-shaped field changes as far away as 12 km (ground strike point). With an increase in speed, the duration and amplitude of the hook-shaped field changes decrease. This phenomena is illustrated in Figure 8-13 where the calculated hook-shaped field change from an M-current pulse, propagated down the channel at different speeds, are presented. Figure 8-13a shows the M-current pulse waveshape, which is pulse M_5 of Figure 8-2 with an amplitude of about 600 A and a duration of about 5 ms. In figure 8-13b the hook-shaped electric field change calculated at 1 km for a downward speed of $2x10^6$ m/s has an amplitude of about 2000 V/m, about 4 times larger than the amplitude (about 500 V/m) of the hook-field change produced by a speed 5 times larger ($1x10^7$ m/s). The duration of the hook is about 6 ms for a speed of $2x10^6$ m/s, which is about twice the duration of the hook for a speed of $1x10^7$ m/s (about 3 ms). The field produced if the propagation speed is one-third the speed of light ($1x10^8$ m/s) is more step-like than hook shaped. The significant reduction in the M-component field shape amplitude and duration with increasing speed can partly explain the observed difference in the M component durations measured in field records (GM = 0.9 ms, see Thottappillil et al., 1990) and in current records (GM = 2.0 ms, see section 4.2 of this dissertation). From simultaneous current and field change records of M components it is possible to estimate the speed of the M-component current pulse by comparing the durations observed in the current and field records, assuming the model proposed or a future better model.

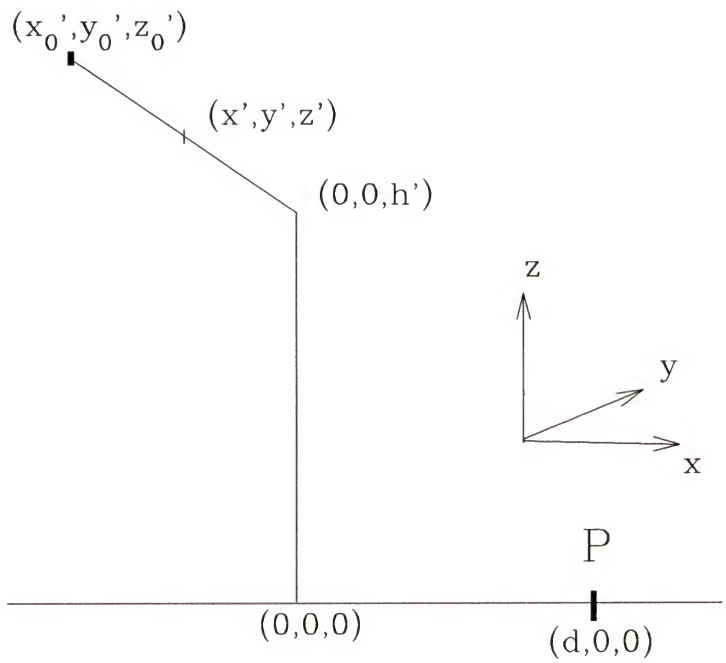

Figure 8-1. Geometry used to calculate the electric fields from the continuing current and M components.

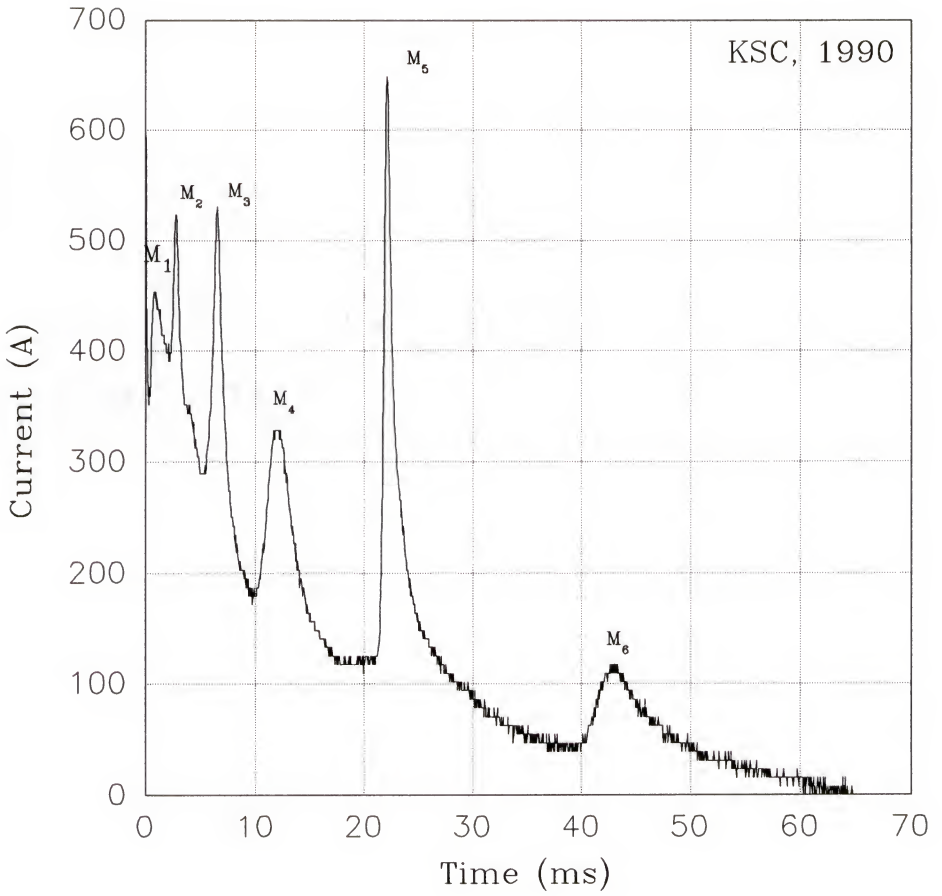

Figure 8-2. Measured continuing current waveshape from triggered lightning used for calculating the electric fields given in Figure 6-3 to 6-11.

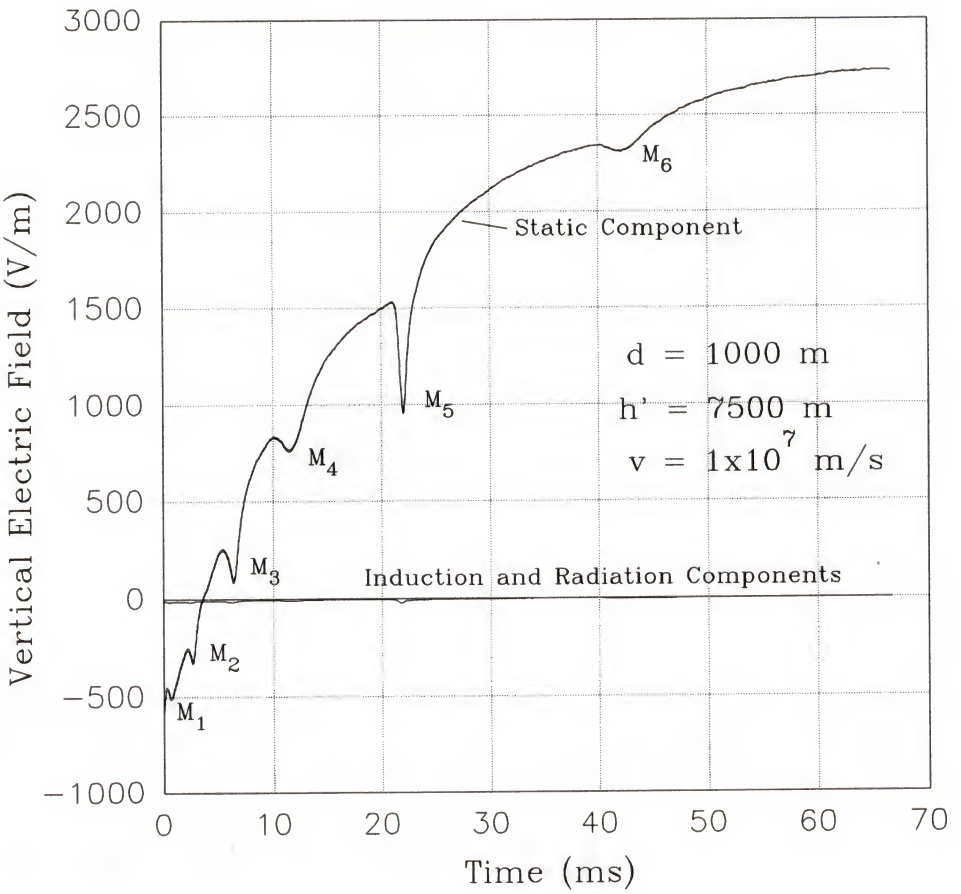

Figure 8-3. Calculated electric fields at 1000 m from the channel with the current waveshape in Figure 8-2 propagating down the vertical channel with a speed of 1×10^7 m/s. Current source is assumed at a height of 7500 m.

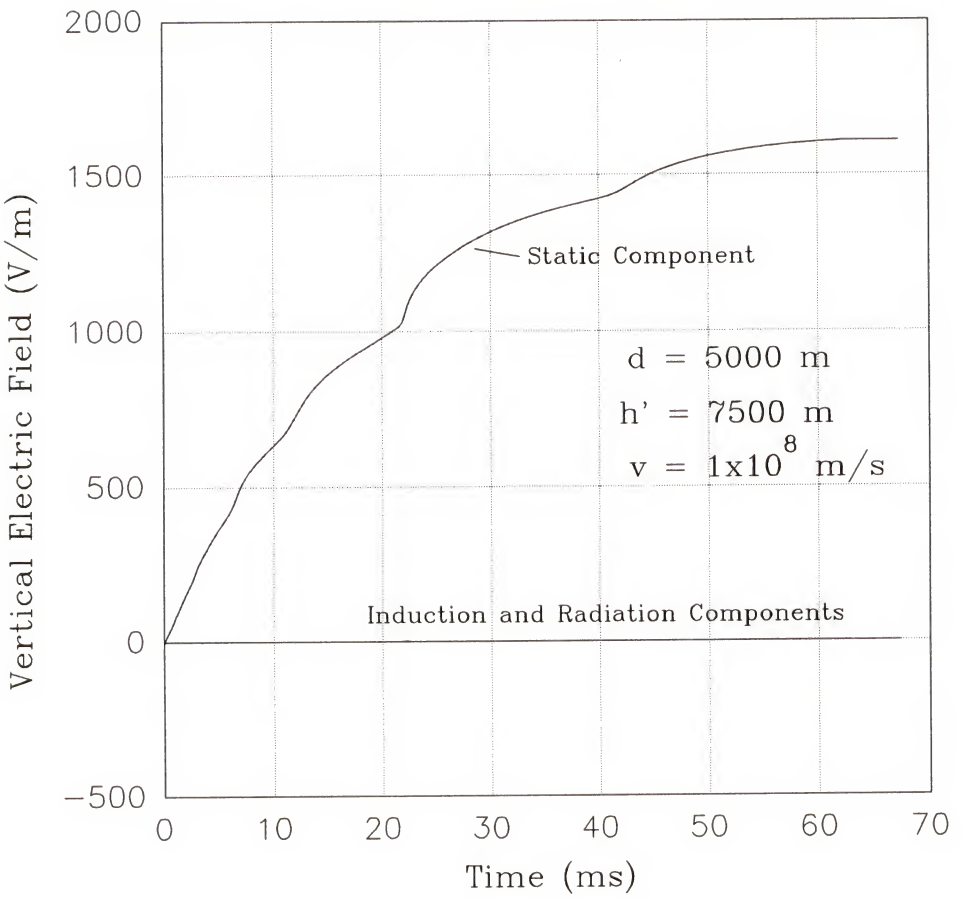

Figure 8-4. Calculated electric fields at 5000 m from the channel with current waveshape in Figure 8-2 propagating down the vertical channel with a speed of $1x10^8$ m/s. Current source is assumed at a height of 7500 m.

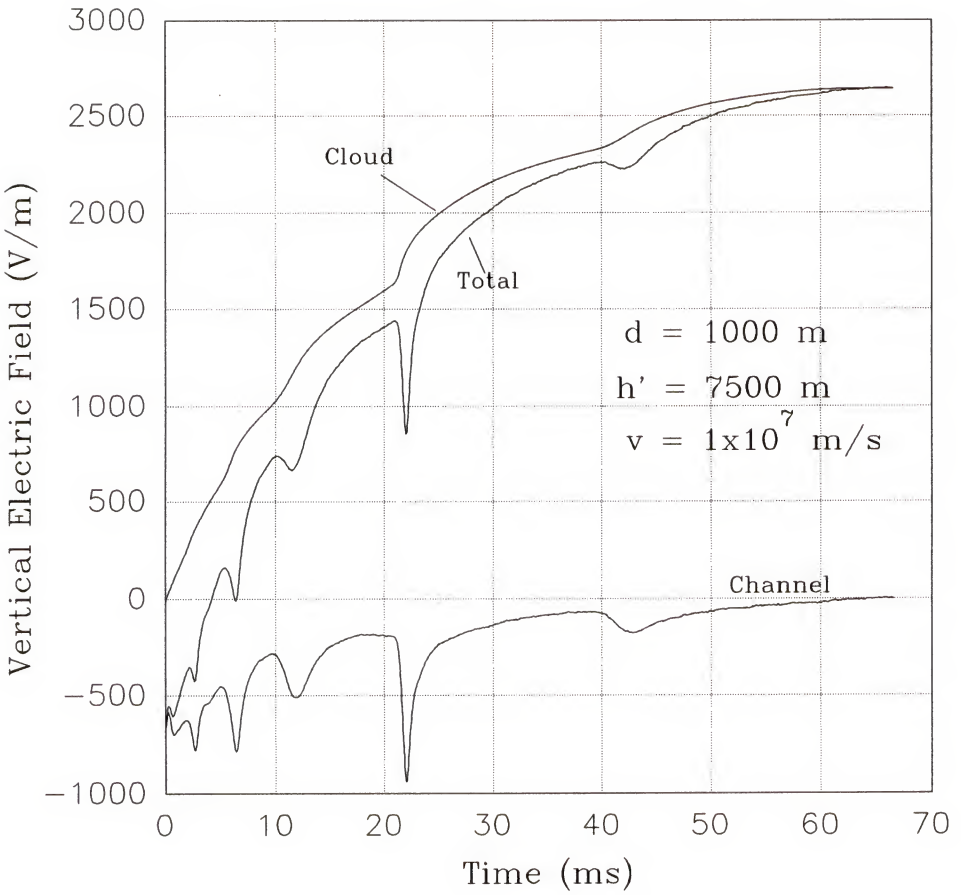

Figure 8-5. A case identical to that described in Figure 8-3. But only the static component of the field is calculated. The contribution to the field due to the charges on the channel and the due to charge depletion at the top of the channel in the cloud are shown separately.

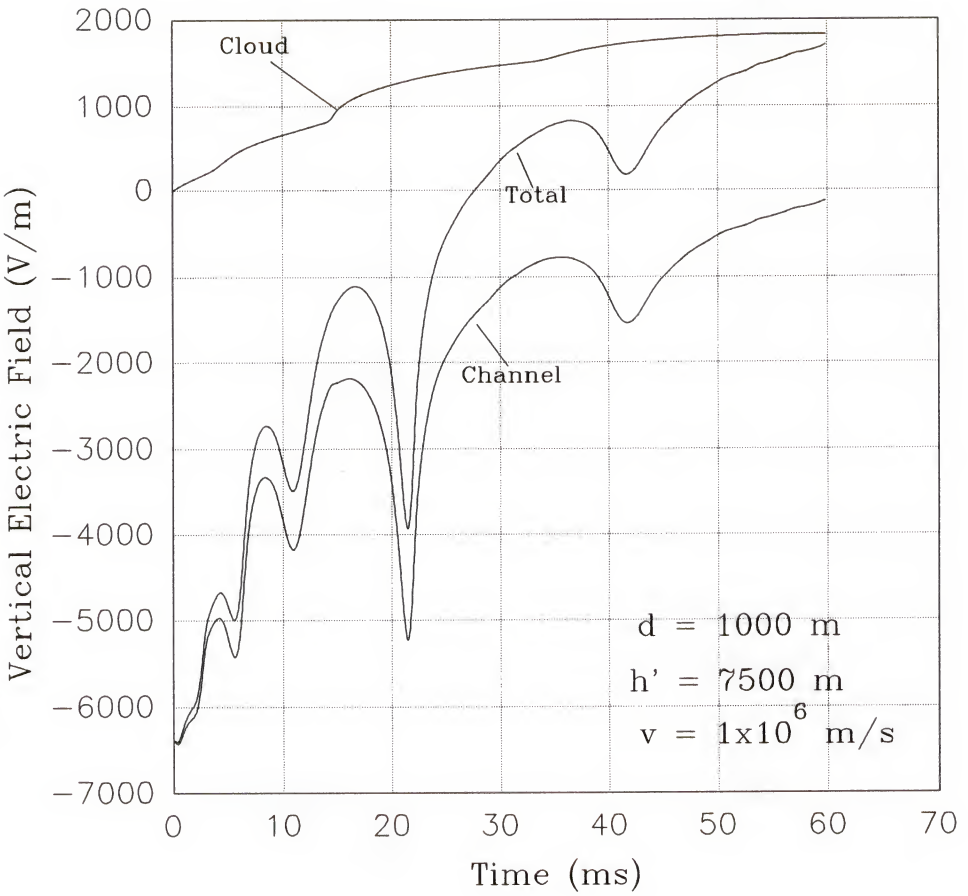

Figure 8-6. Calculated electrostatic fields at 1000 m from the channel with the current waveshape in Figure 8-2 propagating down the vertical channel with a speed of 1×10^6 m/s. Current source is assumed at a height of 7500 m.

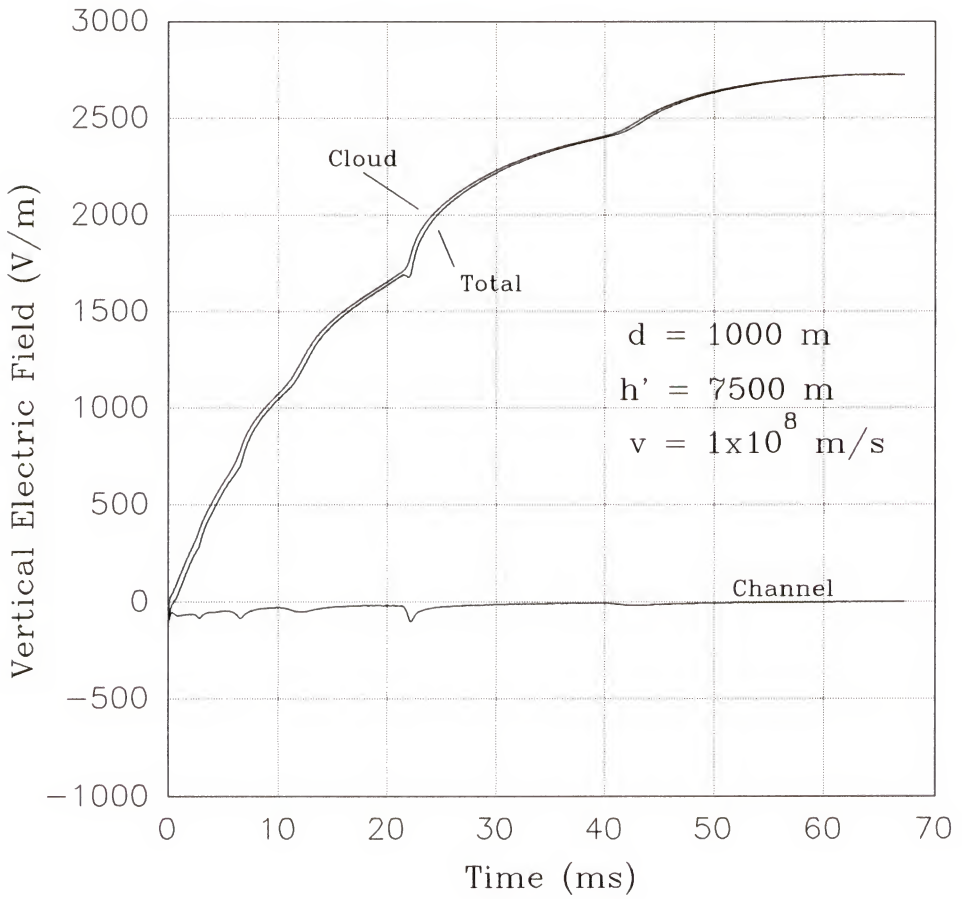

Figure 8-7. Calculated electrostatic fields at 1000 m from the channel with the current waveshape in Figure 8-2 propagating down the vertical channel with a speed of $1x10^8$ m/s. Current source is assumed at a height of 7500 m.

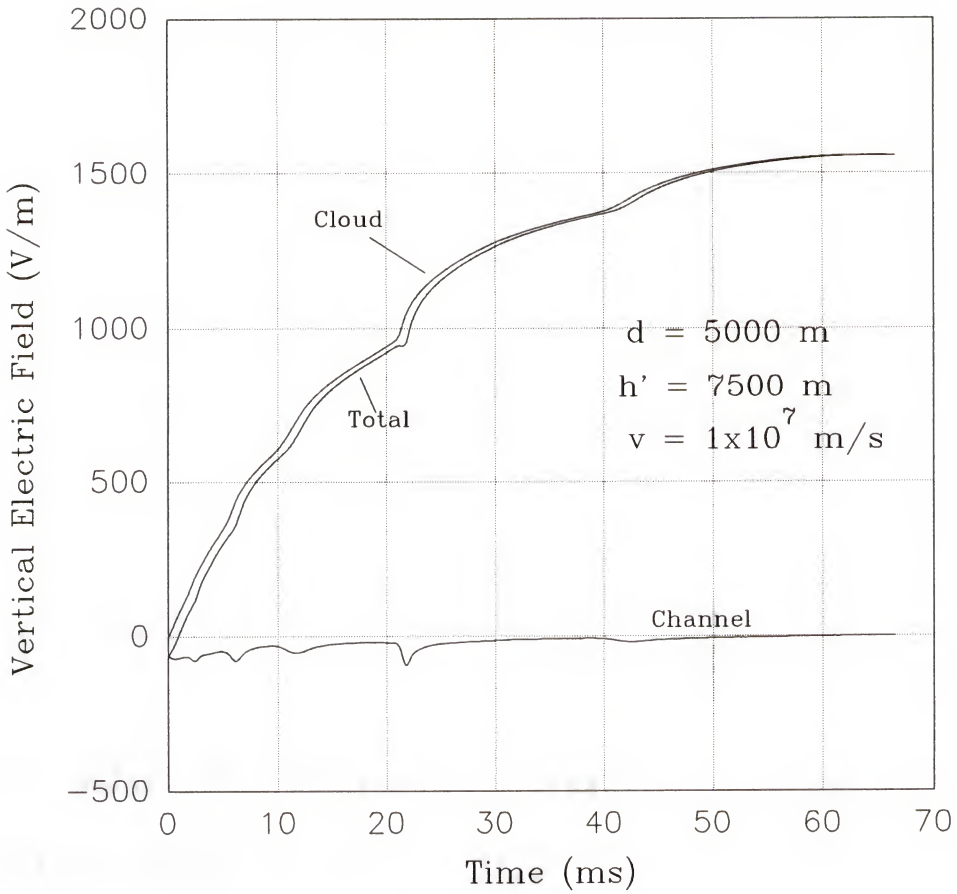

Figure 8-8. Calculated electrostatic fields at 5000 m from the channel with the current waveshape in Figure 8-2 propagating down the vertical channel with a speed of 1×10^7 m/s. Current source is assumed at a height of 7500 m.

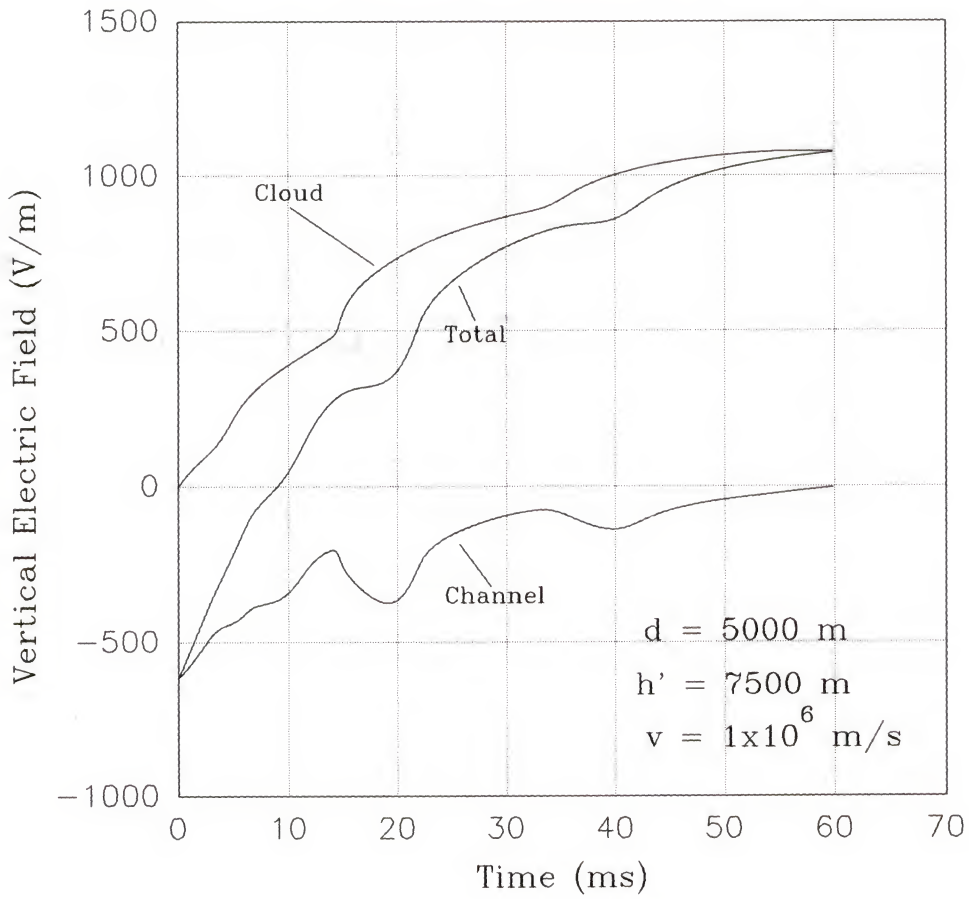

Figure 8-9. Calculated electrostatic fields at 5000 m from the channel with the current waveshape in Figure 8-2 propagating down the vertical channel with a speed of $1x10^6$ m/s. Current source is assumed at a height of 7500 m.

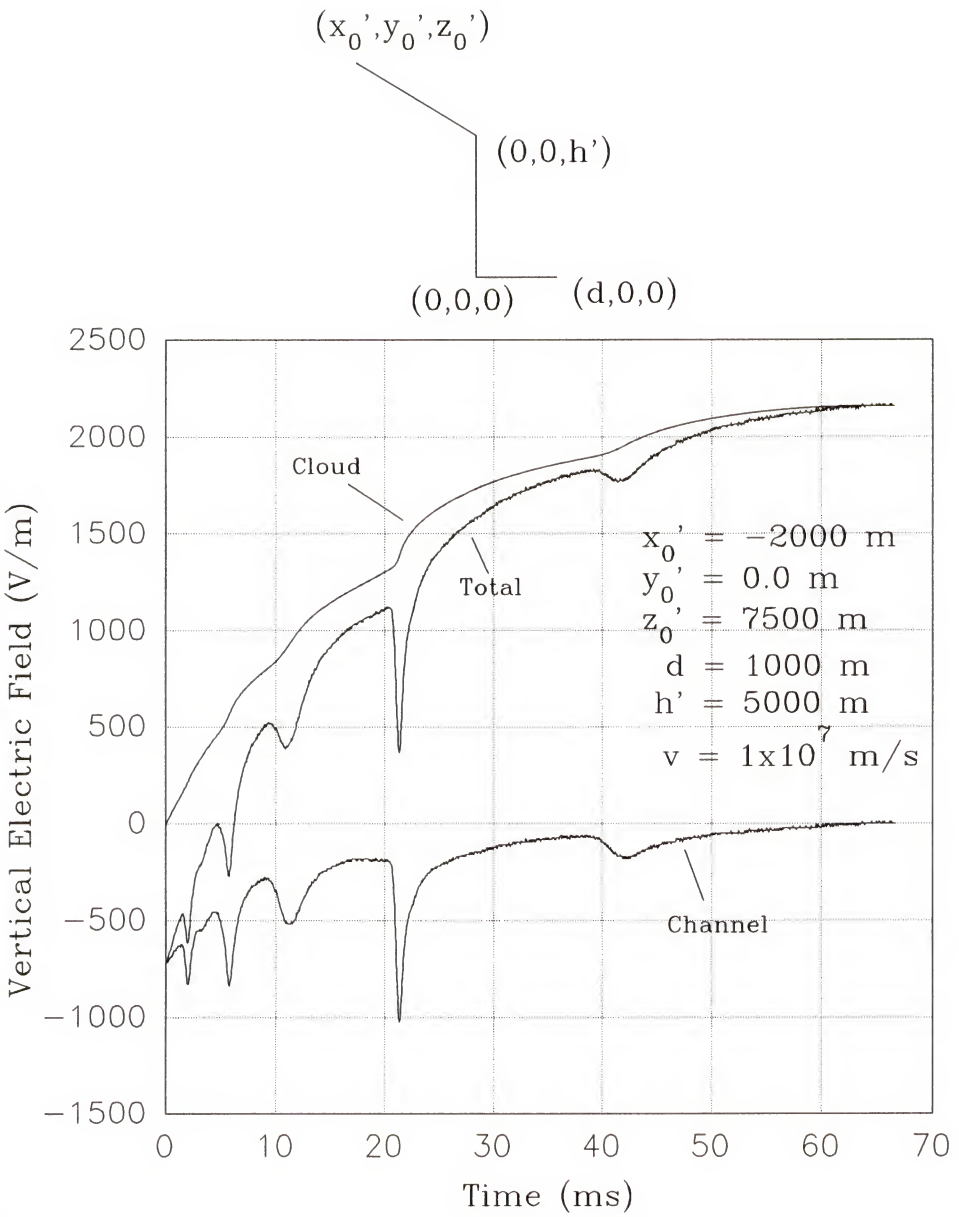

Figure 8-10. Calculated electrostatic fields at 1000 m with the current waveshape in Figure 8-2 propagating towards the ground with a speed of $1x10^7$ m/s. The geometry of the problem is shown on the figure.

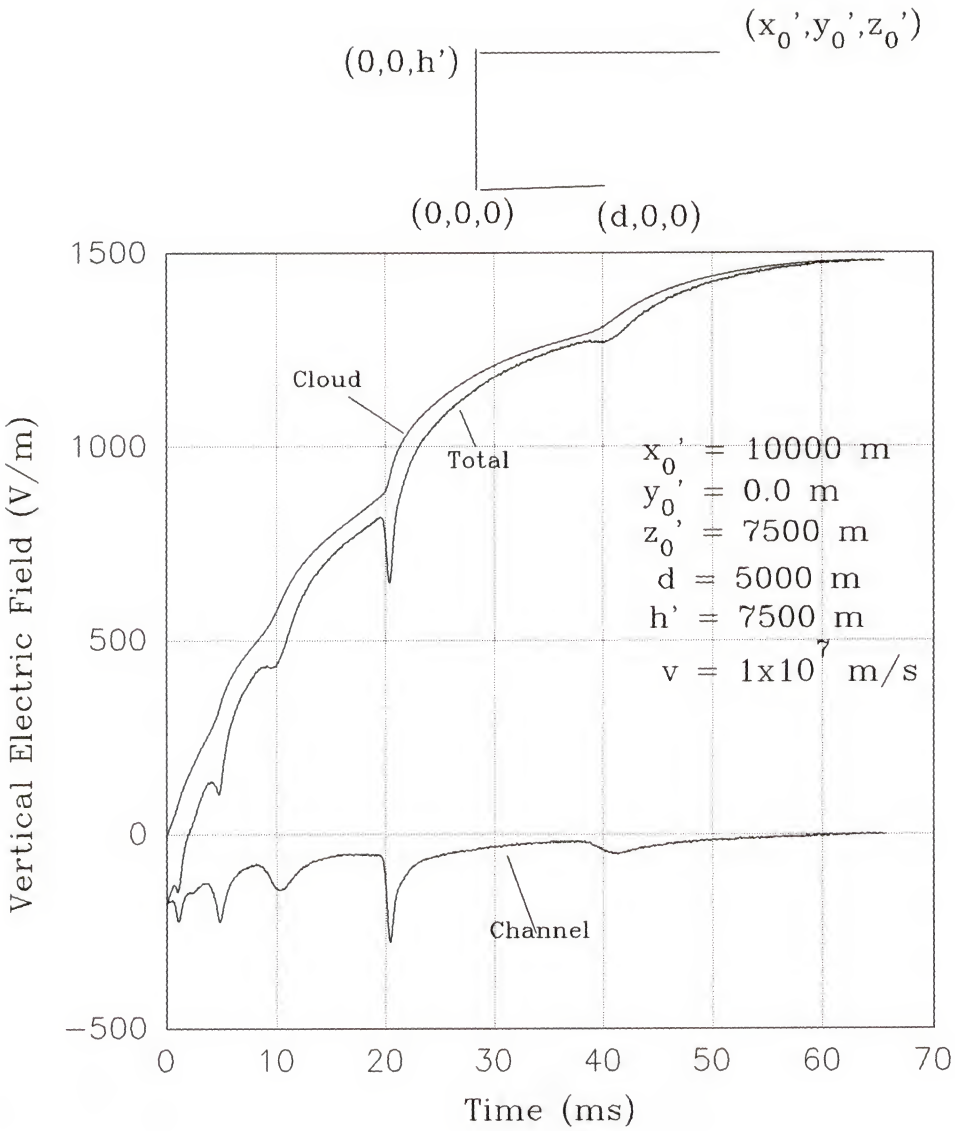

Figure 8-11. Calculated electrostatic fields at 10000 m with the current waveshape in Figure 8-2 propagating towards the ground with a speed of 1×10^7 m/s. The geometry of the problem is shown on the figure.

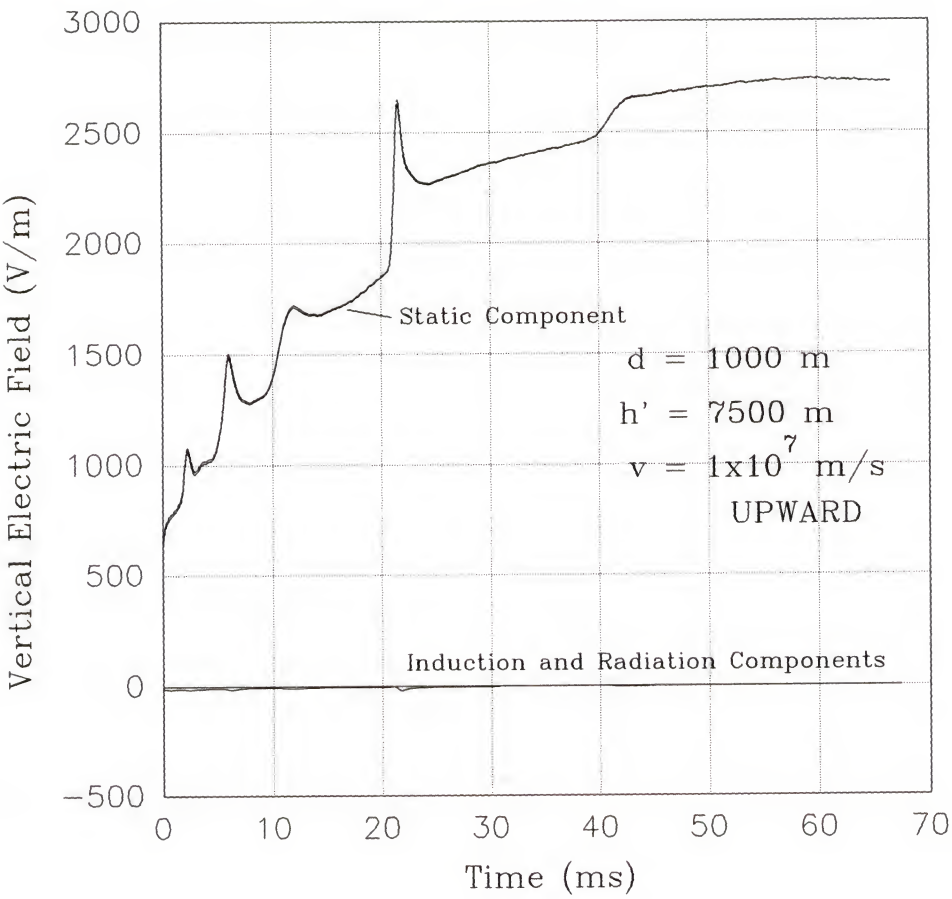

Figure 8-12. Calculated electrostatic fields at 1000 m from the channel with the current waveshape in Figure 8-2 propagating up the vertical channel from ground with a speed of $1x10^7$ m/s. Current source is assumed at a height of 7500 m. Note that the direction of the M-component field change relative to the continuing current field change is opposite to what is observed in natural lightning flashes.

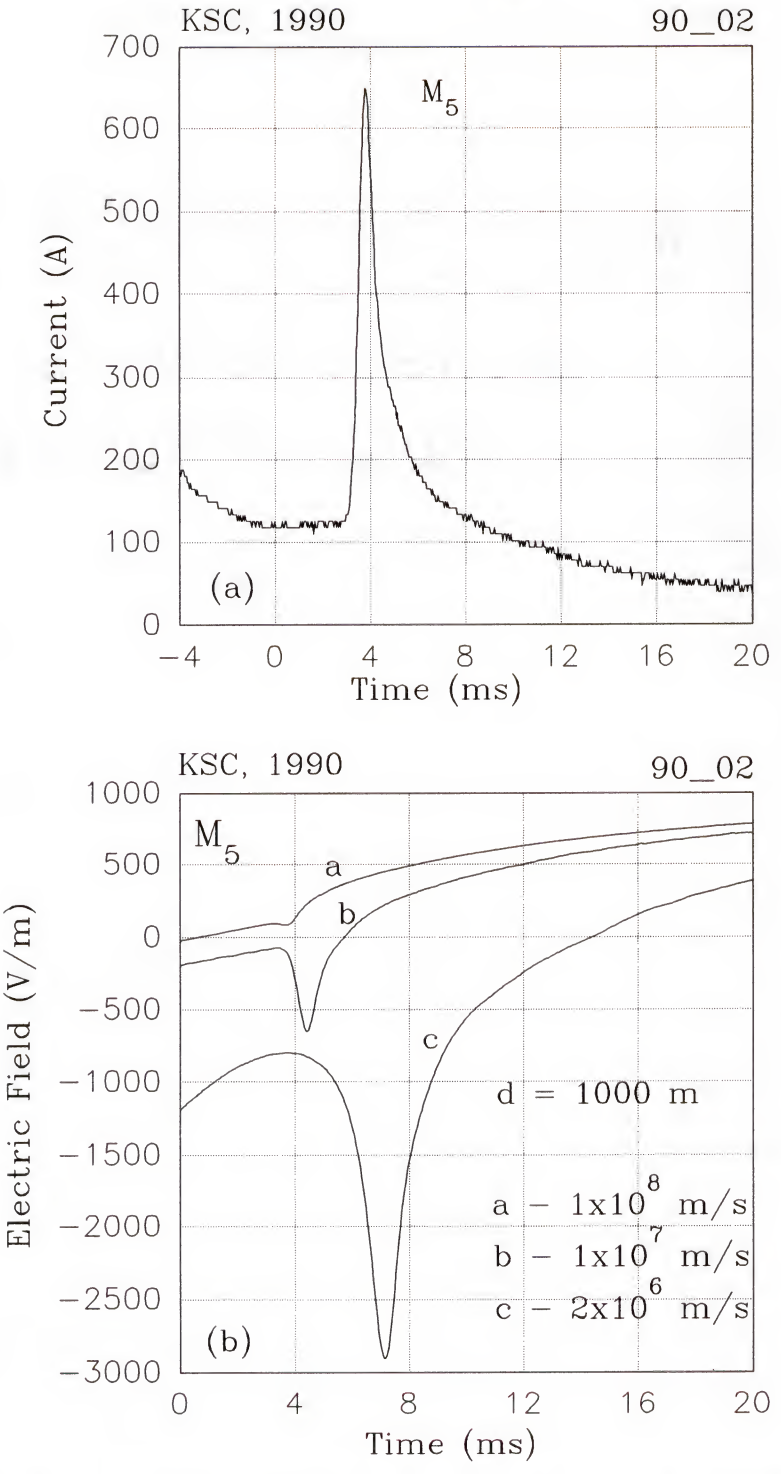

Figure 8-13. Calculated field waveshapes at 1000 m from a M-component current pulse propagating down a vertical channel at various speeds. Current source is assumed at a height of 7500 m. a) Measured M-current pulse waveshape assumed at the top of the channel; b) Increase in the amplitude and duration of the electric field waveshapes with decreasing downward propagation speeds.

CHAPTER 9
SUMMARY AND CONCLUSIONS

Properties of natural and triggered cloud-to-ground lightning flashes have been determined from electric field, current, and optical records. Natural lightning data from correlated electric field and a network of TV camera records were used to investigate the subsequent strokes in a flash that had larger field peaks than the first stroke and to find the distance between the ground terminations within a flash. Thirty-three percent of the 46 multiple-stroke flashes had at least one subsequent stroke whose initial electric field peak was greater than that of the first return stroke, and hence possibly the largest current peak in the flash. Subsequent strokes with larger field peaks that followed the same channel as the first stroke were initiated by relatively fast leaders as inferred from the leader durations. The multiple channel terminations on ground within a flash were separated by 0.3 to 7.3 km with a geometric mean separation distance of 1.7 km.

The triggered lightning data obtained by Sandia National Laboratories at Kennedy Space Center, Florida in 1990, and at Ft. McClellan, Alabama in 1991, were used to investigate the parameters of the return strokes and other flash parameters. Statistics on the return stroke and flash characteristics such as return-stroke peak current, 10-90% current rise time, interstroke interval, stroke current duration, and zero-current interval preceding the return stroke were presented. The geometric mean (GM) of the return stroke peak current was 11 kA and the GM of the 10-90% rise time of the current wavefront was 0.37 μs. Before every return stroke there was a period where the channel was cutoff at the bottom, inferred from the current records where the current amplitudes went below the minimum measurable amplitude of about 4 A. This

observation appears to be supportive of the conclusion of Uman and Voshall (1968) who from theoretical considerations argued that no dark currents of the order of 10 A, as postulated by Brook et al. (1962), are necessary to maintain the channel conditions such that the succeeding strokes follow the same path to the ground. At the same time, the possibility of current flowing in the upper portions of the channel, while being cut off from the bottom, can not be ruled out from the experimental observations presented here. The GM of the interstroke interval, stroke duration, and the zero-current interval were 47 ms, 11 ms, and 29 ms, respectively.

Some of the largest current pulses during continuing currents in triggered lightning were identified in streak-camera records as due to the optical M components. Statistics on the properties of the M current pulses such as duration, 10-90% rise time, and inter-pulse interval are also presented from the analysis of the triggered lightning data. The rise times of the M current pulses (GM = 0.44 ms) are 2 to 3 orders of magnitude larger than the return stroke rise times (GM = 0.37 μs). The duration of the M current pulses (GM = 2.0 ms) in triggered lightning is about twice the duration of M changes (GM = 0.9 ms) in electric field records for natural lightning presented by Thottappillil et al. (1990). A mathematical model for continuing current and M components is presented to investigate the field waveshapes produced by the M components. From the model it is inferred that M currents travel from cloud to ground, rather than from ground to cloud by comparing the experimentally observed waveshapes of continuing current and M-component field changes in natural lightning with the field change waveshape obtained from mathematical modeling for triggered lightning. At a distance of 1 km from the channel the duration of the hook-shaped M field change is increased about two times and the amplitude is increased about 4 times if the speed of propagation is decreased from 1×10^7 m/s to 2×10^6 m/s. For propagation speeds one third the speed of light (1×10^8 m/s) the M-component field waveshape is more step-like rather than hook-shaped at a distance of 1 km. From this

theoretical consideration it appears that the speed of the M-current pulse is typically an order of magnitude less than the speed of subsequent return strokes in natural (Orville et al., 1978) and triggered (Idone et al., 1984) lightning. Step-like M-component field changes were observed even for lower speeds of the order of 1×10^7 m/s at a larger distance of 5 km. It may be possible to estimate the speed of the M-component pulses from simultaneous current and electric field records by comparing the time duration of the events.

Existing return-stroke current models that allow the use of measured channel-base current and speed as inputs are compared and evaluated using simultaneously measured channel-base current, return-stroke speed, and electric field at 5 km from triggered lightning. The models thus compared are the Transmission Line (TL) model, the Modified Transmission Line (MTL) model, the Travelling Current Source (TCS) model, and the Diendorfer-Uman (DU) model. The fields calculated from the models are found to be sensitive to the channel-base current waveshape. The return strokes producing very narrow spikes (about 0.1 μs wide) in the measured electric fields at 5 km also have maximum rate-of-rise of the current closer to the peak of the wavefront of the measured channel-base current, when compared to the return strokes not producing such narrow spikes in the measured fields. For one return stroke which had a current waveform with a slow wavefront and fast rate-of-rise near the peak, upward discharges from the striking object were observed in the video records. It is necessary to study many return stroke current waveforms which have correlated optical records of the bottom portion of the channel to see if there is any relationship between the upward discharges and the current waveforms with maximum rate-of-rise occurring near the peak. The calculated fields from the TL and MTL models using measured currents and speeds never produced any narrow spikes whereas the calculated fields from the TCS and DU ($\tau = 0.1$ μs) models produced narrow spikes at the initial field peaks in many cases even though the amplitude of the field spikes produced by the models were typically 2 to 4 times

larger. The mean difference in the measured initial field peak and the calculated initial peak from the TL, MTL, and the DU (τ = 0.1 μs) models were about 20%, which is a very good match considering the 15% to 25% absolute error involved in the measured return stroke speeds used in the calculations. For the TCS model the mean difference in the calculated and measured fields was higher at about 40%. None of the models were able to predict the field waveshapes after the peak in a consistent manner.

The DU model is generalized to include a variable upward return stroke speed and a variable downward discharge-current speed using a simpler mathematical approach than was originally used by Diendorfer and Uman (1990). The theory is applied to a case of exponentially decaying upward return stroke speed, and it was found that, for the typical channel base current and discharge time constants assumed, the decreasing speed primarily affects the zero-crossing time of the far fields and the electrostatic field changes at very close distances, when compared to the constant speed case. The Modified Diendorfer-Uman (MDU) model was compared with the other models and evaluated using the same set of simultaneous measurements. The field peaks calculated from the DU and MDU models are nearly the same, but after the peak the MDU model fields are closer than the DU model fields to the measured fields. In the MDU model field calculation for one return stroke having a slowly rising ramp at the beginning of the current waveform, the return stroke was allowed to start at a low speed, rapidly increasing in the first few tens of meters, in effect simulating an upward streamer (or attachment process), and thereafter slowly decreasing, simulating the normal return stroke phase. In this way a very good match between the calculated and the measured field peak is obtained, suggesting perhaps that the slow current ramps at the beginning of some of the waveforms might be due to upward streamers. Certainly correlated current records and photographic observation of the bottom portion of the channel are required to verify this. The return stroke current models compared

in this dissertation predict different current distributions along the channel. If the nature of relationship between light intensity and current were better understood, it may be possible to estimate the current along the return stroke channel with sufficient accuracy from the remote measurement of the light intensity profile of the channel to distinguish between different models.

A new return stroke model is developed which is similar to the MDU model but allows a varying channel-charge discharge time constant with height. The Variable Channel Time Constant (VCTC) model eliminates the division of the channel into an inner core or break-down region and an outer corona region, as well as eliminating the associated division of channel base current into two current components. The model is used to calculate the discharge time constant profile along the channel associated with a single current at the channel base that effectively replaces the two current components and the associated two time constants of the DU model. At the present stage there is not enough experimental information to estimate the discharge rates at different channel heights. It may be possible to estimate the discharge time constants at various heights from simultaneous measurement of channel-base current, return stroke speed and fields at multiple stations. These measurements can also be used for a more reliable estimation of the return stroke channel parameters used in MTL, DU, and MDU models and a more thorough comparison of the return stroke models. Information on channel geometry should also be included in the models. A detailed experimental investigation of the bottom portion of the lightning channel is required in order to learn the origins of the variety of waveshapes observed for the current wavefront and their relationships to the wavefront of the remotely measured electric fields.

APPENDICES

APPENDIX A
LIST OF JOURNAL AND CONFERENCE PAPERS DEVELOPED AS PART OF THIS Ph.D. DISSERTATION WORK

Fisher, R. J., G. H. Schnetzer, R. Thottappillil, V. A. Rakov, and M. A. Uman, Return stroke and M component current pulses in triggered lightning (Abstract), Transactions of the American Geophysical Union, 72, p. 88, 1991.

Fisher, R. J., G. H. Schnetzer, R. Thottappillil, V. A. Rakov, M. A. Uman, D. M. Jordan, and S. Sumi, Properties of triggered lightning flashes in Florida and Alabama, Proceedings of the 9th International Conference on Atmospheric Electricity, Leningrad, USSR, June 15-19, 1992.

Rakov, V. A., R. Thottappillil, and M. A. Uman, Electric field pulses in K and M changes of lightning ground flashes, J. Geophys. Res., 97, 9935-9950, 1992.

Rakov, V. A., R. Thottappillil, and M. A. Uman, On the empirical formula of Willett et al. (1989) relating lightning return stroke peak current and peak electric field, J. Geophys. Res., 97, 11527-11533, 1992.

Rakov, V. A., R. Thottappillil, and M. A. Uman, First vs. Subsequent stroke intensity and multiple channel terminations in cloud-to-ground lightning, 21st International Conference on Lightning Protection (ICLP), Berlin, Germany, Sept. 22-25, 1992 (accepted).

Rakov, V. A., M. A. Uman, and R. Thottappillil, Review of lightning properties determined from electric field and TV observations, Proceedings of the 9th International Conference on Atmospheric Electricity, Leningrad, USSR, June 15-19, 1992.

Thottappillil, R., V. A. Rakov, M. A. Uman, W. H. Beasley, M. J. Master, and D. V. Shelukhin, Lightning subsequent stroke electric field peak greater than the first stroke peak and multiple ground terminations, J. Geophys. Res., 97, 7503-7509, 1992.

Thottappillil, R., D. K. Mclain, M. A. Uman, and G. Diendorfer, Extension of Diendorfer-Uman lightning return stroke model to the case of a variable upward return stroke speed and a variable downward discharge current speed, J. Geophys. Res., 96, 17143-17150, 1991.

Thottappillil, R., M. A. Uman, and G. Diendorfer, Influence of channel base current and varying return stroke speed on the calculated fields of three important return stroke models, Proceedings of the International Aerospace and Ground Conference on Lightning and Static Electricity, Cocoa Beach, Florida, April 16-19, 1991.

Uman, M. A., R. Thottappillil, Lightning return stroke models, Proceedings of the 9th International Conference on Atmospheric Electricity, Leningrad, USSR, June 15-19, 1992.

APPENDIX B
COMPUTER PROGRAM LISTINGS

Fortran program listing to find the remote electric fields at ground from the return stroke

```
      PROGRAM EVMODWIL

c     Calculation of vertical electric fields for BG, TL, TCS, MTL, DU, and MDU models.

c     Rajeev Thottappillil, Nov 1991

c     Constant r.s. speed for BG, TL, TCS, MTL, and DU models.
c     Variable r.s. speed for MDU model; V(z) = Vb*EXP(-z/lambda)

      PARAMETER (MZ=1501)

      CHARACTER*12 bgf, tlf, tcsf, mtlf, duf, mduf, rdf
      REAL eq(mz), ei(mz), er(mz), ev(mz), edik(mz), time(mz)
      REAL deq(mz), dei(mz), der(mz), dev(mz), dedik(mz)
      REAL*8 st(mz), sti(mz), dst(mz)
      REAL*8 rlam,dt,c,vk,dz,dtt,ddt1,ddt3,taubd,stk,vb,vb2,c2,eps
      REAL*8 pi,rbyc,vb2c2,c2r2,vb2r2,vbc2vb2,vbvb2c2,r2byc2,c2byvb
      REAL*8 tt,t2,h1k,h2k,hpk,h2,rk,rk2,rk3,rk4,rk5,t3,t1,ezq,ezi
      REAL*8 ezr,stkb,stikb,stkb1,stkb3,dstkb1,fak,z21,h4,hk,tmhk
      REAL*8 rkbyc,hbyc,stikb1,stikb3,rrl,a1,b1,r,r2,dzmax,h3k,vpk,h
      REAL*8 stik,dstk,stik1,stik3,h2r2
      REAL*8 vav, fh, dfh, eh, phpk, pex, vv, dlam

      INTEGER nmax
      c = 299792458.D0
      c2 = c*c
      eps = 8.85D-12
      pi = 3.141592653589793238D0
      PRINT*, 'Distance D from the channel where the field is to be found (m):'
      READ*, r
      r2 = r*r
      PRINT*, 'Return stroke speed (m/s):'
      READ*, vb
      vb2 = vb*vb
      PRINT*,'Whichmodel?(1-BG,2-TL,3-TCS,4-MTL,5-DU,6-MDU,7-MTLRakov-Dulzon):'
      READ*, model

c     Input channel base current
      CALL current(nmax, dt, st, dst)

c     Current in A; Time in s ; didt in A/s
```

```
      PRINT*,'dt =',dt
      PRINT*, 'nmax=',nmax
      DO n = 1, nmax
         time(n) = (n-1)*dt*1.D06
      END DO

c     Find time integral of the current
      sti(1) = 0.D0
      Do n = 2, nmax
         sti(n) = sti(n-1) + 0.5D0*(st(n) + st(n-1))*dt
      END DO

      PRINT*, 'Factor to increase the dipole length (1...1.2):'
      READ*, fak
      IF (fak .EQ. 0.) fak = 1.05D0
      PRINT*, 'Current decay factor for MTL model (m):'
      READ*, rlam
      PRINT*,'Breakdown time constant for DU and MDU models (us):'
      READ*, taubd
      taubd = taubd*1D-06
      PRINT*,'Decay constant with height for r.s speed for MDU model (m):'
      READ*, dlam
      rbyc = r/c
      vb2c2 = vb2*c2
      c2r2 = c2*r2
      vb2r2 = vb2*r2
      vbc2vb2 = vb/(c2-vb2)
      vbvb2c2 = vb/(1.D0-vb2/c2)
      r2byc2 = r2/c2
      dlamvb = dlam/vb
      vk = vb*c/(vb+c)
      dzmax = MIN(r/50.D0,1.D0)
      c2byvb = c2/vb
      h4 = 0.5D0/(pi*eps)*r2/c2
      nstart = INT(r/(c*dt) + 0.5D0)
      z21 = -0.5D0/(pi*eps)

      DO n = nstart, nstart+nmax-1
         l = n - nstart + 1
         IF (mod(l,50) .EQ. 0) PRINT*, l
         tt = n*dt
         t2 = tt*tt

c        hpk is the effective height of the channel at a given time seen by the observer at the field
c         measuring point.
         IF (model .NE. 6) THEN
           h1k = DSQRT(vb2c2*t2 + c2r2 - vb2r2)
           h2k = c2*tt-h1k
```

```
          hpk = vbc2vb2*h2k
          edik(l) = 0.0
          IF (model .EQ. 1 .OR. model .EQ. 3) THEN
            h3k = 1.D0 - vb2*tt/h1k
            vpk = vbvb2c2*h3k
            IF (model .EQ. 1) THEN
              tmhk = hpk/vb
            ELSE IF (model .EQ. 3) THEN
              tmhk = hpk/vk
            END IF
            ntmhk = INT(tmhk/dt)
            IF (ntmhk .GT. 0 .AND. ntmhk .LE. nmax) THEN
              dtt = tmhk-ntmhk*dt
              stk = st(ntmhk) + dtt*(st(ntmhk+1)-st(ntmhk))/dt
              edik(l) = h4*vpk/((r2 + hpk*hpk)**1.5)*stk
            ELSE
              edik(l) = 0.0
            END IF
          END IF

c     Finding hpk using Newton-Raphson iteration for MDU model.
          ELSE IF(model .EQ. 6) THEN
            hpk = phpk
101         pex = DEXP(hpk/dlam)
            eh = pex - 1D0
            fh = c2*t2 + dlamvb*c2*eh*(dlamvb*eh-2*tt)-hpk*hpk-r2
            dfh = 2*c2byvb*pex*(dlamvb*eh-tt)-2*hpk
            phpk = hpk
            hpk = hpk - fh/dfh
            IF (ABS(hpk-phpk) .GT. 0.001) GO TO 101
          END IF

          IF (hpk .GT. 0.0) THEN
          ev(l) = 0.0
          eq(l) = 0.0
          ei(l) = 0.0
          er(l) = 0.0

          dz = 0.237D0
          ifin = 0
          h = 0.1185D0

c     Calculating the fields from each segment of the channel.
          DO KX = 1,100000
            hk = dz*z21
            h2 = h*h
            rk = DSQRT(r2 + h2)
            rk2 = rk*rk
```

```
rk3 = rk2*rk
rk4 = rk3*rk
rk5 = rk4*rk
rkbyc = rk/c
hbyc = h/c
IF (model .EQ. 1 .OR. model .EQ. 3) THEN
  IF (model .EQ. 1) THEN
    t1 = tt - rkbyc
    t3 = h/vb
  ELSE IF(model .EQ. 3) THEN
    t1 = tt - rkbyc + hbyc
    t3 = h/vk
  END IF
  n1 = INT(t1/dt)
  n3 = INT(t3/dt)
  ddt1 = t1 - n1*dt
  ddt3 = t3-n3*dt
  stik = 0.D0
  IF (n1 .GT. 0 .AND. n1 .LE. nmax .AND. n3 .GT .0) THEN
    stk = st(n1) + ddt1*(st(n1+1)-st(n1))/dt
    dstk = dst(n1) + ddt1*(dst(n1+1)-dst(n1))/dt
    stik1 = sti(n1) + ddt1*(sti(n1+1)-sti(n1))/dt
    stik3 = sti(n3) + ddt3*(sti(n3+1)-sti(n3))/dt
    stik = stik1 - stik3
    ezr = -r2byc2/rk3*dstk
    h2r2 = h2 + h2 - r2
    ezi = h2r2/(c*rk4)*stk
    ezq = h2r2/rk5*stik
  ELSE
    ezr = 0.D0
    ezi = 0.D0
    ezq = 0.D0
  END IF
ELSEIF(model .EQ. 2 .OR. model .EQ. 4 .OR. model .EQ. 7) THEN
  t1 = tt - rkbyc - h/vb
  n1 = INT(t1/dt)
  IF (n1 .GT. 0) THEN
    ddt1 = t1 - n1*dt
    stik = sti(n1) + ddt1*(sti(n1+1)-sti(n1))/dt
    stk = st(n1) + ddt1*(st(n1+1)-st(n1))/dt
    dstk = dst(n1) + ddt1*(dst(n1+1)-dst(n1))/dt
    IF (model .EQ. 4) THEN
       rrl = DEXP(-h/rlam)
       stik = stik*rrl
       stk = stk*rrl
       dstk = dstk*rrl
    ELSE IF (model .EQ. 7) THEN
       rrl = 1.D0 - h/7500.D0
```

```
        stik = stik*rrl
        stk = stk*rrl
        dstk = dstk*rrl
      END IF
      ezr = -r2byc2/rk3*dstk
      h2r2 = h2 + h2 - r2
      ezi = h2r2/(c*rk4)*stk
      ezq = h2r2/rk5*stik
    ELSE
      ezr = 0.D0
      ezi = 0.D0
      ezq = 0.D0
    END IF
  ELSE IF (model .EQ. 5 .OR. model .EQ. 6) THEN
    t1 = tt - rkbyc + hbyc
    n1 = INT(t1/dt)
    IF (model .EQ. 5) THEN
      t2 = tt - rkbyc - h/vb
      t3 = h/vk
    ELSE IF(model .EQ. 6) THEN
      vv = vav(h, vb, dlam)
      t2 = tt - rk/c - h/vv
      t3 = h/vv + h/c
    END IF
    n1 = INT(t1/dt)
    n3 = INT(t3/dt)
    ddt1 = t1 - n1*dt
    ddt3 = t3-n3*dt
    kflag = 0
    IF (n1 .GT. 0 .AND. n3 .GT .0 .AND. t2 .GT. 0.0) THEN
      kflag = 1
    END IF
    IF (kflag .EQ. 1 .AND. n1 .LE. nmax) THEN
      stkb1 = st(n1) + ddt1*(st(n1+1)-st(n1))/dt
      stkb3 = st(n3) + ddt3*(st(n3+1)-st(n3))/dt
      b1 = DEXP(-t2/taubd)
      stkb = stkb1 - stkb3*b1
      dstkb1 = dst(n1) + ddt1*(dst(n1+1)-dst(n1))/dt
      dstkb = dstkb1 + stkb3*b1/taubd

      IF (n1 .GT. n3) THEN
        a1 = b1 - 1.D0
        stikb1 = sti(n1) + ddt1*(sti(n1+1)-sti(n1))/dt
        stikb3 = sti(n3) + ddt3*(sti(n3+1)-sti(n3))/dt
        stikb = stikb1 - stikb3 + taubd*stkb3*a1
      ELSE
        stikb = 0.D0
      END IF
```

```
            ezr = -r2byc2/rk3*dstkb
            h2r2 = h2 + h2 - r2
            ezi = h2r2/(c*rk4)*stkb
            ezq = h2r2/rk5*stikb
           ELSE
            ezr = 0.D0
            ezi = 0.D0
            ezq = 0.D0
           END IF
          END IF
          eq(l) = eq(l) + hk*ezq
          ei(l) = ei(l) + hk*ezi
          er(l) = er(l) + hk*ezr

          IF (ifin .EQ. 1) GO TO 100
           h = h + 0.5D0*dz
           IF (h+dz .LT. hpk) THEN
            dz = fak*dz
            IF (dz .GT. dzmax) dz=dzmax
            h = h + 0.5D0*dz
           ELSE
            dz = hpk - h
            h = h + 0.5D0*dz
            ifin = 1
           END IF
         END DO
100      ev(l) = eq(l) + ei(l) + er(l) + edik(l)
         END IF
      END DO

      IF (model .EQ. 1) THEN
         PRINT*, 'Output file for BG model:'
         READ (*,'(A)') bgf
         OPEN (12, FILE=bgf, STATUS='UNKNOWN')
         DO j = 1, nmax
          WRITE (12,*) ev(j)
         END DO
         CLOSE (12)
      ELSE IF (model .EQ. 2) THEN
         PRINT*, 'Output file for TL model:'
         READ (*,'(A)') tlf
         OPEN (12, FILE=tlf, STATUS='UNKNOWN')
         DO j = 1, nmax
          WRITE (12,*) ev(j)
         END DO
         CLOSE (12)
      ELSE IF (model .EQ. 3) THEN
         PRINT*, 'Output file for TCS model:'
```

```
   READ (*,'(A)') tcsf
   OPEN (12, FILE=tcsf, STATUS='UNKNOWN')
   DO j = 1, nmax
    WRITE (12,*) ev(j)
   END DO
   CLOSE (12)
ELSE IF (model .EQ. 4) THEN
   PRINT*, 'Output file for MTL model:'
   READ (*,'(A)') mtlf
   OPEN (12, FILE=mtlf, STATUS='UNKNOWN')
   DO j = 1, nmax
    WRITE (12,*) ev(j)
   END DO
   CLOSE (12)
ELSE IF (model .EQ. 5) THEN
   PRINT*, 'Output file for DU model:'
   READ (*,'(A)') duf
   OPEN (12, FILE=duf, STATUS='UNKNOWN')
   DO j = 1, nmax
    WRITE (12,*) ev(j)
   END DO
   CLOSE (12)
ELSE IF (model .EQ. 6) THEN
   PRINT*, 'Output file for MDU model:'
   READ (*,'(A)') mduf
   OPEN (12, FILE=mduf, STATUS='UNKNOWN')
   DO j = 1, nmax
    WRITE (12,*) ev(j)
   END DO
   CLOSE (12)
ELSE IF (model .EQ. 7) THEN
   PRINT*, 'Output file for RD (MTL) model:'
   READ (*,'(A)') rdf
   OPEN (12, FILE=rdf, STATUS='UNKNOWN')
   DO j = 1, nmax
    WRITE (12,*) ev(j)
   END DO
   CLOSE (12)
END IF

STOP
END


SUBROUTINE current(nmax, dt, st, dst)

PARAMETER(mz=1501)
```

```
      REAL*8 st(mz),dst(mz)
      REAL*8 dt,sum
      INTEGER nmax
      CHARACTER*13 infile

c     Current in A; Time in s

      PRINT*, 'Time interval between points (us):'
      READ*, dt
      dt = dt*1D-06
      PRINT*, 'Input file for base current (kA):'
      READ(*,'(A)') infile
      OPEN (11, FILE=infile, STATUS='OLD')
      DO n = 1, mz
          READ (11,*,END=10) st(n)
      END DO
10    nmax = n - 1
      CLOSE(11)
      DO n = 1, nmax
       st(n) = st(n)*1000.D0
      END DO

      DO n = 2, nmax-1
         sum = 0.D0
         DO i = n-1, n + 1
           sum = sum + st(i)
         END DO
         st(n) = sum/3.D0
      END DO
      DO n = 2, nmax
       dst(n) = (st(n)-st(n-1))/dt
      END DO

      RETURN
      END

c     Calculation of average return stroke speed.
      REAL*8 FUNCTION VAV(HH,VB,DLAM)
      REAL*8 HH,DLAM,VB
      VAV = VB * HH /(DLAM*(EXP(HH/DLAM)-1.0))

      RETURN
      END
```

Fortran program listing to calculate the discharge time constants and current distribution as a function of height for the VCTC model

```
      PROGRAM DUTAU_CH

c     RAJEEV THOTTAPPILLIL, October 1991

c     Return stroke model with arbitrary variation of discharge
c     time constant with height.

c     Specifying the channel-base current, and charge along the channel and finding the time
c     constant varying with height.

c     INPUT: Charge distribution, and Channel-base current
c     Channel is divided into equal segments, dz.

      PARAMETER(mz=2501)

      REAL*8 t(2*mz),rho(mz),tau(mz),z(mz),st(2*mz),stbd(2*mz),
     1     stc(2*mz),dstbd(2*mz), dstc(2*mz), stp(mz), h(4)
      EQUIVALENCE (stbd(1),tau(1))
      EQUIVALENCE (stc(1),z(1))
      EQUIVALENCE (dstbd(1),stp(1))

      REAL*8 sum, c, vb, dz, tt, tt2, ttc, ttc2, tauc1, tauc2, sst,
     1       ft, vk, tau1, x1, x2, y1, y2, st1, st2, charge, const,
     2       tau2, bdtau, cotau
      CHARACTER*12 outfile

      PRINT*, 'Return stroke speed (m/s):'
      READ*, vb
      c = 3.D08
      PRINT*, 'Incremental channel length (m):'
      READ*, dz

      PRINT*, 'Maximum channel height (m):'
      READ*, zmax
      nmax = INT(zmax/dz)
      st1 = 13000.0
      st2 = 7000.0
      tau1 = 0.15D-06
      tauc1 = 5.0D-06
      tau2 = 3.0D-06
      tauc2 = 50.0D-06
      con = 0.73D0
      conc = 0.64D0
      ft = dz*(1D0/vb + 1D0/c)
```

```
      vk = 1D0/(1D0/vb + 1D0/c)
      PRINT*, 'Break down time constant of DU model (us):'
      READ*, bdtau
      bdtau = bdtau*1D-06
      PRINT*, 'Corona time constant of DU model (us):'
      READ*, cotau
      cotau = cotau*1D-06

c     Generating the channel base current used in Diendorfer and Uman (1990)
      DO n = 1, 2*nmax
         t(n) = n*ft
         tt = t(n)/tau1
         tt2 = tt*tt
         ttc = t(n)/tauc1
         ttc2 = ttc*ttc
         y1 = DEXP(-t(n)/tau2)
         y2 = DEXP(-t(n)/tauc2)
         x1 = tt2 + 1D0
         x2 = ttc2 + 1D0
         stbd(n) = st1*tt2*y1/(con*x1)
         stc(n) = st2*ttc2*y2/(conc*x2)
         st(n) = stbd(n) + stc(n)
         dstbd(n) = (st1*y1/con)*(2*tt/(tau1*x1*x1) - tt2/(tau2*x1))
         dstc(n) = (st2*y2/conc)*(2*ttc/(tauc1*x2*x2) - ttc2/(tauc2*x2))
      END DO

c     Generating the charge distribution
      DO n = 1, nmax
          rho(n) = (stbd(n) + bdtau*dstbd(n) + stc(n) + cotau*dstc(n))/vk
      END DO


      PRINT*, 'Output file name for base current and channel charge:'
      READ (*,'(A)') outfile
      OPEN(12, FILE=outfile, STATUS='UNKNOWN')

      DO n = 1, nmax
         WRITE(12,*) t(n)*1e06, st(n)*0.001, rho(n)*1000
      END DO

c     Finding the time constant distribution
      tau(1) = rho(1)*dz/st(1)
      z(1) = dz
      DO n = 2, nmax
         z(n) = n*dz
         sst = 0.5*(st(n) + st(n-1))
         sum = 0D0
         DO m = 1, n-1
```

```
          sum = sum + (rho(m)*DEXP(-(t(n)-t(m))/tau(m)))/tau(m)
        END DO
        tau(n) = rho(n)*dz/(sst-sum*dz)
      IF (MOD(n,50) .EQ. 0) THEN
         PRINT*,n,tau(n)
      END IF
    END DO
    PRINT*, 'Output file name for time constant variation:'
    READ (*,'(A)') outfile
    OPEN(12, FILE=outfile, STATUS='UNKNOWN')

    DO n = 1, nmax
       WRITE(12,*) z(n), tau(n)*1e06
    END DO

c   Verification by recalculating the current at ground from the charge and time constant

    DO n = 1, nmax
       sum = 0D0
       DO m = 1, n
         sum = sum + rho(m)*DEXP(-(t(n)-t(m))/tau(m))/tau(m)
       END DO
       stp(n) = sum*dz
     IF (MOD(n,50) .EQ. 0) THEN
        PRINT*,n,stp(n)
     END IF
    END DO

c   Current distribution with height
    outfile = 'current0'
    OPEN (13, FILE=outfile, STATUS='UNKNOWN')
    DO n = 1, nmax
       WRITE(13,*) t(n)*1e06,stp(n)*0.001
    END DO
    CLOSE(13)
    DO n = 1, nmax
       stp(n) = 0.0
    END DO

    PRINT*, 'Height where current is required (4 Numbers., m)'
    READ*,(h(j), j = 1,4)

    DO j = 1,4
       j1 = INT(h(j)/dz)
       nz = INT(h(j)/(vb*ft))
       DO n = nz, nmax
          tt = t(n)+h(j)/c
          nt = INT(tt/ft+0.5)
```

```
        sum = 0D0
        DO m = 1, j1
          sum = sum + rho(m)*DEXP(-(tt-t(m))/tau(m))/tau(m)
        END DO
        IF (nt .GT. 0) THEN
          stp(n) = st(nt) - sum*dz
        END IF
        IF (MOD(n,50) .EQ. 0) THEN
          PRINT*,n,stp(n)
        END IF
      END DO
      PRINT*,'File name for channel current',j
      READ(*,'(A)') outfile
      OPEN (13, FILE=outfile, STATUS='UNKNOWN')
      DO n = 1, nmax
        WRITE(13,*) stp(n)*0.001
      END DO
      CLOSE(13)
      DO n = 1, nmax
        stp(n) = 0.0
      END DO
    END DO


    STOP
    END
```

Fortran program listing for finding the electric fields at ground from continuing currents and M components from a vertical channel section

```
      PROGRAM EVMCOMP

c     Rajeev Thottappillil, Feb. 1992

c     Program to find the fields from c.c and M components (TL model) assuming a vertical
c     channel. The currents are assumed to propagate down. Static, induction and radiation field
c     components are calculated.

      PARAMETER (MZ=2001)

      CHARACTER*12 tlf, ans
      REAL eq(mz), ei(mz), er(mz), ev(mz), time(mz)
      REAL*8 st(mz), sti(mz), dst(mz)
      REAL*8 hmax,dt,c,dz,vk,ddt1,stk,vb,vb2,c2,eps
      REAL*8 pi,rbyc,vb2c2,c2r2,vb2r2,vbc2vb2,vbvb2c2,r2byc2,c2byvb
      REAL*8 tt,t2,h2,rk,rk2,rk3,rk4,rk5,t1,ezq,ezi
      REAL*8 ezr,z21,h4,hk
      REAL*8 rkbyc,r,r2,dzmax,h
      REAL*8 stik,dstk,hh2r2

      INTEGER nmax
      c = 299792458.D0
      c2 = c*c
      eps = 8.85D-12
      pi = 3.141592653589793238D0
      PRINT*, 'Distance D to the field point (m):'
      READ*, r
      r2 = r*r
      PRINT*,'Height of charge center (m):'
      READ*, hmax
      hmax2 = hmax*hmax
      PRINT*, 'Speed of downward c.c or M current (m/s):'
      READ*, vb
      vb2 = vb*vb
      CALL current(nmax, dt, st, dst)
c     Current in A; Time in s ; didt in A/s

      PRINT*,'dt =',dt
      PRINT*, 'nmax=',nmax
      DO n = 1, nmax
         time(n) = (n-1)*dt*1.D06
      END DO
      sti(1) = 0.D0
      Do n = 2, nmax
```

```
   sti(n) = sti(n-1) + 0.5D0*(st(n) + st(n-1))*dt
END DO
PRINT*, 'Dipole length (m):'
READ*, dz
PRINT*, 'Do you want current distri. along the channel?(y/n):'
READ(*,'(A)') ans

IF (ans .EQ. 'y' .OR. ans .EQ. 'Y') THEN
    CALL channel (nmax,st,time,dt,hmax,vb,dz)
END IF
PRINT*, 'TL model: i(z,t) = i(H,t-(hmax-z)/v)'
rbyc = r/c
vb2c2 = vb2*c2
c2r2 = c2*r2
vb2r2 = vb2*r2
vbc2vb2 = vb/(c2-vb2)
vbvb2c2 = vb/(1.D0-vb2/c2)
r2byc2 = r2/c2
c4 = c2*c2
vk = vb*c/(vb+c)
dzmax = MIN(r/50.D0,1.D0)
c2byvb = c2/vb
h4 = 0.5D0/(pi*eps)*r2/c2
nstart = INT((hmax/vb + r/c)/dt)
z21 = -0.5D0/(pi*eps)
DO n = nstart, nstart+nmax-1
   l = n - nstart + 1
   IF (mod(l,50) .EQ. 0) PRINT*, l
   tt = n*dt
   t2 = tt*tt
     ev(l) = 0.0
     eq(l) = 0.0
     ei(l) = 0.0
     er(l) = 0.0

     ifin = 0
     h = dz/2D0

     DO KX = 1,100000
      hk = dz*z21
      h2 = h*h
      hh = hmax - h
      hh2 = hh*hh
      rk = DSQRT(r2 + hh2)
      rk2 = rk*rk
      rk3 = rk2*rk
      rk4 = rk3*rk
      rk5 = rk4*rk
```

```
          rkbyc = rk/c
           t1 = tt - rkbyc - h/vb
           n1 = INT(t1/dt)
           IF (n1 .GT. 0) THEN
             ddt1 = t1 - n1*dt
             stik = sti(n1) + ddt1*(sti(n1+1)-sti(n1))/dt
             stk = st(n1) + ddt1*(st(n1+1)-st(n1))/dt
             dstk = dst(n1) + ddt1*(dst(n1+1)-dst(n1))/dt
             ezr = -r2byc2/rk3*dstk
             hh2r2 = hh2 + hh2 - r2
             ezi = hh2r2/(c*rk4)*stk
             ezq = hh2r2/rk5*stik
           ELSE
             ezr = 0.D0
             ezi = 0.D0
             ezq = 0.D0
           END IF
          eq(l) = eq(l) + hk*ezq
          ei(l) = ei(l) + hk*ezi
          er(l) = er(l) + hk*ezr

          IF (ifin .EQ. 1) GO TO 100
           h = h + 0.5D0*dz
           IF (h+dz .LT. hmax) THEN
             h = h + 0.5D0*dz
           ELSE
             dz = hmax - h
             h = h + 0.5D0*dz
             ifin = 1
           END IF
         END DO
100      ev(l) = eq(l) + ei(l) + er(l)
       END DO

         PRINT*, 'Output file for TL model:'
         READ (*,'(A)') tlf
         OPEN (12, FILE=tlf, STATUS='UNKNOWN')
         DO j = 1, nmax
           WRITE (12,*) ev(j), eq(j), ei(j), er(j)
         END DO
         CLOSE (12)

       STOP
       END


       SUBROUTINE current(nmax, dt, st, dst)
```

```
      PARAMETER(mz=2001)

      REAL*8 st(mz),dst(mz)
      REAL*8 dt, dummy
      INTEGER nmax
      CHARACTER*13 infile

c     Current in A; Time in s

      PRINT*, 'Time interval between points (us):'
      READ*, dt
      dt = dt*1D-06
      PRINT*, 'Input file for base current (A):'
      READ(*,'(A)') infile
      OPEN (11, FILE=infile, STATUS='OLD')
      DO n = 1, mz
          READ (11,*,END=10) dummy, st(n)
      END DO
10    nmax = n - 1
      CLOSE(11)

      DO n = 2, nmax
       dst(n) = (st(n)-st(n-1))/dt
      END DO

      RETURN
      END


      SUBROUTINE channel (nmax,st,time,dt,hmax,vb,dz)

      PARAMETER (mz=2001)

      REAL eqt1(mz),eqt2(mz),eqt3(mz),eqh1(mz),eqh2(mz),eqh3(mz)
      REAL*8 st(mz),dt,hmax,vb,dz
      REAL t(3),hc(3),tt,th,height(mz),time(mz)
      CHARACTER*12 tlf

      PRINT*, 'Time at which current distribution as a function of height
     1 is to be found (ms)  [three numbers]:'
      READ*, (t(n),n=1,3)
      DO n = 1,3
         t(n) = t(n)*1e-03
      END DO
      PRINT*,'Height at which current distribution as a function of time
     1 is to be found (km)  [three numbers]:'
      READ*, (hc(n),n=1,3)
      DO n = 1, 3
```

```
      hc(n) = hc(n)*1000
    END DO
    DO j = 1, nmax
      eqt1(j) = 0.0
      eqt2(j) = 0.0
      eqt3(j) = 0.0
      eqh1(j) = 0.0
      eqh2(j) = 0.0
      eqh3(j) = 0.0
    END DO
    jmax = INT(hmax/dz+0.5)
    DO n = 2, jmax
      height(n) = (n-1)*dz
    END DO
    print*,'jmax=',jmax
    DO n = 1, nmax
      time(n) = time(n)*1e-06
    END DO

    DO n = 1, 3
      IF (n .EQ. 1) THEN
c       j1 = INT((hmax-hc(1))/(vb*dt))
        DO j = 1, nmax
          tt = (time(j)-(hmax-hc(1))/vb)/dt
          nt = INT(tt)
          IF (nt. GT. 0) THEN
            eqt1(j) = st(nt)
          END IF
        END DO
      ELSE IF(n .EQ. 2) THEN
c       j1 = INT((hmax-hc(2))/(vb*dt))
        DO j = 1, nmax
          tt = (time(j)-(hmax-hc(2))/vb)/dt
          nt = INT(tt)
          IF (nt. GT. 0) THEN
            eqt2(j) = st(nt)
          END IF
        END DO
      ELSE IF(n .EQ. 3) THEN
c       j1 = INT((hmax-hc(3))/(vb*dt))
        DO j = 1, nmax
          tt = (time(j)-(hmax-hc(3))/vb)/dt
          nt = INT(tt)
          IF (nt .GT. 0) THEN
            eqt3(j) = st(nt)
          END IF
        END DO
      END IF
```

```
END DO
PRINT*, 'Output file 1 for TL (time as base):'
READ (*,'(A)') tlf
OPEN (13, FILE=tlf, STATUS='UNKNOWN')
DO j = 1, nmax
   WRITE (13,*) time(j)*1000.0,eqt1(j), eqt2(j), eqt3(j)
END DO
CLOSE (13)

DO n = 1, 3
   IF (n .EQ. 1) THEN
     DO j = 1, jmax
       th = t(1) - (hmax-height(j))/vb
       nh = INT(th/dt)
       IF (nh .NE. 0) THEN
         eqh1(j) = st(nh)
       END IF
     END DO
   ELSE IF(n .EQ. 2) THEN
     DO j = 1, jmax
       th = t(2) - (hmax-height(j))/vb
       nh = INT(th/dt)
       IF (nh .NE. 0) THEN
         eqh2(j) = st(nh)
       END IF
     END DO
   ELSE IF(n .EQ. 3) THEN
     DO j = 1, jmax
       th = t(3) - (hmax-height(j))/vb
       nh = INT(th/dt)
       IF (nh .NE. 0) THEN
         eqh3(j) = st(nh)
       END IF
     END DO
   END IF
END DO
PRINT*, 'Output file 2 for TL (height as base):'
READ (*,'(A)') tlf
OPEN (13, FILE=tlf, STATUS='UNKNOWN')
DO j = 1, jmax
   WRITE (13,*) height(j),eqh1(j),eqh2(j),eqh3(j)
END DO
CLOSE (13)

RETURN
END
```

Fortran program listing for finding the electric fields at ground from continuing currents and M components from a channel having an inclined section at the top of a vertical section

```
      PROGRAM EVMHORIZ

c     Rajeev Thottappillil, Feb. 1992

c     Inclined section at the top of a vertical channel section.  Only static fields calculated.

      PARAMETER (MZ=2001)

      CHARACTER*12 tlf
      REAL ei(mz), ev(mz), time(mz), ec(mz)
      REAL*8 st(mz), sti(mz), dst(mz)
      REAL*8 hmax,dt,c,vk,ddt1,stk,vb,vb2,c2,eps
      REAL*8 pi,rbyc,vb2c2,c2r2,vb2r2,vbc2vb2,vbvb2c2,r2byc2,c2byvb
      REAL*8 tt,rk,rk3,t1,ezi,z21,hk,delay,range3,rk2
      REAL*8 rkbyc,r,r2,dzmax,x0,y0,z0,delx,dely,delz,s,range,ds
      INTEGER nmax,nd,n1,nzmax,nsmax,s2

      c = 299792458.D0
      c2 = c*c
      eps = 8.85D-12
      pi = 3.141592653589793238D0
      PRINT*, 'Distance D to the field point (m):'
      READ*, r
      r2 = r*r
      PRINT*,'Max. height of vertical channel section (m):'
      READ*, hmax
      hmax2 = hmax*hmax
      PRINT*,'x, y, z coordinates of charge center (m):'
      READ*, x0,y0,z0
      PRINT*, 'Speed of downward c.c or M current (m/s):'
      READ*, vb
      vb2 = vb*vb
      CALL current(nmax, dt, st, dst)
c     Current in A; Time in s ; didt in A/s

      PRINT*,'dt =',dt
      PRINT*, 'nmax=',nmax
      DO n = 1, nmax
         time(n) = (n-1)*dt*1.D06
      END DO
      sti(1) = 0.D0
      Do n = 2, nmax
         sti(n) = sti(n-1) + 0.5D0*(st(n) + st(n-1))*dt
      END DO
```

```
      PRINT*, 'Dipole length (1...1.2):'
      READ*, ds
      nzmax = INT(hmax/ds)
      hlen = DSQRT((z0-hmax)**2+x0**2+y0**2)
      nsmax = INT(hlen/ds)
      IF (nsmax .NE. 0) THEN
         delx = x0/nsmax
         dely = y0/nsmax
         delz = (z0-hmax)/nsmax
      END IF
      rbyc = r/c
      vb2c2 = vb2*c2
      c2r2 = c2*r2
      vb2r2 = vb2*r2
      vbc2vb2 = vb/(c2-vb2)
      vbvb2c2 = vb/(1.D0-vb2/c2)
      r2byc2 = r2/c2
      c4 = c2*c2
      vk = vb*c/(vb+c)
      dzmax = MIN(r/50.D0,1.D0)
      c2byvb = c2/vb
      range = DSQRT((x0-r)**2+y0**2+z0**2)
      range3 = range**3
      delay = range/c
      PRINT*, 'nstart:'
      READ*, nstart
      z21 = 0.5D0/(pi*eps)
      DO n = nstart, nstart+nmax-1
         l = n - nstart + 1
         IF (mod(l,50) .EQ. 0) PRINT*, l
         tt = n*dt
         ev(l) = 0.0
         ei(l) = 0.0
         ec(l) = 0.0
         s = ds/2D0
         nd = INT((tt - delay)/dt)
         ec(l) = z21*(sti(nd)-sti(nstart))*z0/range3
         hk = ds*z21
         DO KX = 1,nsmax+nzmax
c          s2 = s*s
           IF (kx .LE. nsmax) THEN
              x = x0 - kx*delx
              y = y0 - kx*dely
              z = z0 - kx*delz
           ELSE
              x = 0D0
              y = 0D0
              z = hmax - ds*(kx-nsmax)
```

```
          END IF
          rk = DSQRT((x-r)*(x-r)+y*y+z*z)
          rk2 = rk*rk
          rk3 = rk2*rk
          rkbyc = rk/c
          t1 = tt - rkbyc - s/vb
          n1 = INT(t1/dt)
          IF (n1 .GT. 0) THEN
             ddt1 = t1 - n1*dt
             stk = st(n1) + ddt1*(st(n1+1)-st(n1))/dt
             ezi = stk*z/(vb*rk3)
           ELSE
             ezi = 0.D0
           END IF
           ei(l) = ei(l) + ezi
         END DO
100      ei(l) = -hk*ei(l)
         ev(l) = ei(l) + ec(l)
         s = s + ds
      END DO

      PRINT*, 'Output file for TL model:'
      READ (*,'(A)') tlf
      OPEN (12, FILE=tlf, STATUS='UNKNOWN')
      DO j = 1, nmax
          WRITE (12,*) ev(j),ei(j),ec(j)
      END DO
      CLOSE (12)

      STOP
      END


      SUBROUTINE current(nmax, dt, st, dst)

      PARAMETER(mz=2001)

      REAL*8 st(mz),dst(mz)
      REAL*8 dt, dummy
      INTEGER nmax
      CHARACTER*13 infile

c     Current in A; Time in s

      PRINT*, 'Time interval between points (us):'
      READ*, dt
      dt = dt*1D-06
      PRINT*, 'Input file for base current (kA):'
```

```
      READ(*,'(A)') infile
      OPEN (11, FILE=infile, STATUS='OLD')
      DO n = 1, mz
           READ (11,*,END=10) dummy, st(n)
      END DO
10    nmax = n - 1
      CLOSE(11)
      DO n = 1, nmax
       st(n) = st(n)
      END DO

      DO n = 2, nmax
       dst(n) = (st(n)-st(n-1))/dt
      END DO

      RETURN
      END
```

REFERENCES

Anderson J. G., Lightning performance of transmission lines, in Transmission Line Reference Book - 345 kV and above, 2nd ed., pp 545-597, Electric Power Research Institute, Palo Alto, Calif., 1982.

Anderson, R. B., and A. J. Eriksson, Lightning parameters for engineering application, Electra, 69, 65-105, 1980.

Beasley, W.H., M.A. Uman, and P.L. Rustan, Electric fields preceding cloud -to-ground flashes, J. Geophys. Res., 87, 4883-4902, 1982.

Berger, K., Novel observations on lightning discharges, results and research on Mount San Salvatore, J. Franklin Inst., 283, 478-525, 1967.

Berger, K., R. B. Anderson, and H. Kroninger, Parameters of lightning flashes, Electra, 41, 23-37, 1975.

Brook M., G. Armstrong, R.P.H. Winder, B. Vonnegut, and C. B. Moore, Artificial initiation of lightning discharges, J. Geophys. Res., 66, 3967-3969, 1961.

Brook, M., N. Kitagawa, and E.J. Workman, Quantitative study of strokes and continuing currents in lightning discharges to ground, J. Geophys. Res., 67, 649-659, 1962.

Bruce C. E. R., and R. H. Golde, The lightning discharge, J. Inst. Electr. Eng., 88, 487-520, 1941.

Cooray, V., A return stroke model, International Conference on Lightning and Static Electricity, University of Bath, England, 1989.

Cooray, V., and S. Lundquist, On the characteristics of some radiation fields from lightning and their possible origin in positive ground flashes, J. Geophys. Res., 87, 11203-11214, 1982.

Cooray, V., and S. Lundquist, Effects of propagation on the rise times and the initial peaks of radiation fields from return strokes, Radio Sci., 18, 409-415, 1983.

Cooray, V., and S. Lundquist, Characteristics of radiation fields from lightning in Sri Lanka in the tropics, J. Geophys. Res., 90, 6099-6109, 1985.

Cooray, V., and R. E. Orville, The effects of variation of current amplitude, current risetime, and return stroke velocity along the return stroke channel on the electromagnetic fields generated by return strokes, J. Geophys. Res., 95, 18617-18630, 1990.

Dessler, J., Infrasonic thunder, J. Geophys. Res., 78, 1889-1896, 1973.

Diendorfer, G., and M. A. Uman, An improved return stroke model with specified channel-base current, J. Geophys. Res., 95, 13,621-13,644, 1990.

Dulzon A. A., and V. A. Rakov, Estimation of errors in lightning peak current measurements by frame aerials (in Russian), Izvestiya VUZov SSSR, ser. Energetika, 11, 101-104, 1980.

Eriksson, A. J., Lightning and tall structures, Trans. South Afr. IEE, 69, pt 8, 238-252, 1978.

Few, A. A., Power spectrum of thunder, J. Geophys. Res., 74, 6926-6934, 1969.

Few, A. A., Acoustic radiations from lightning, Handbook of Atmospherics, Vol. II, CRC Press, Boca Raton, Florida, 1981.

Fieux, R. P., C. Gary, and P. Hubert, Artificially triggered lightning above land, Nature (London), 275, 212-214, 1975.

Fisher, R. J., and G. H. Schnetzer, 1990 Sandia rocket-triggered lightning field tests at Kennedy Space Center, Florida, Sandia Report SAND90-2926, March 1991a.

Fisher, R. J., and G. H. Schnetzer, Damage to metallic samples produced by measured lightning currents, Proc. 1991 International Aerospace and Ground Conference on Lightning and Static Electricity, Cocoa Beach, Florida, April 16-19, 1991b.

Fowler, R. G., Nonlinear electron acoustic waves, Part II, Adv. Electronics Electron Physics, Vol. 41, Academic Press, New York, 1976.

Fowler, R. G., Lightning, Appl. At. Collision Phys., 5, 31-67, 1982.

Ganesh, C., M. A. Uman, W. H. Beasley, and D. M. Jordan, Correlated optical and electric field signals produced by lightning return strokes, J. Geophys. Res., 89, 4905-4909, 1984.

Garbagnati, E., E. Giudice, G. B. Lo Piparo, and U. Magagnoli, Relieve delle caratteristiche dei fulmini in Italia. Risultati ottenuti negli anni 1970-1973, Electtrotecnica, LXII, 237-249, 1975.

Garbagnati, E., and G. B. Lo Piparo, Parameter von blitzstromen., Elektrotech. Z. etz-a, 103, 61-65, 1982.

Gorin, B.N., Mathematical modeling of lightning return stroke (in Russian), Elektrichestvo, No. 4, 10-16, 1985.

Guo C., and E. P. Krider, The optical and radiation field signatures produced by lightning return strokes, J. Geophys. Res., 87, 8913-8922, 1982.

Heidler, F., Traveling current source model for LEMP calculation, Proc. 6th symp. Electromagn. Compat. paper 29F2, (Zurich, Switzerland), 157-162, 1985.

Hill, R. D., Channel heating in return stroke lightning, J. Geophys. Res., 76, 637-645, 1971.

Hill, R. D., Comments on "Quantitative analysis of a lightning return stroke for diameter and luminocity changes as a function of space and time" by R. E. Orville, J. H. Heldson, Jr., and W. H. Evans, J. Geophys. Res., 80, 1188, 1975.

Hubert, P. and G. Mouget, Return stroke velocity measurements in two triggered lightning flashes, J. Geophys. Res., 86, 5253-5261, 1981.

Hubert, P., P. Laroche, A. Eybert-Berard, and L. Barret, Triggered lightning in New Mexico, J. Geophys. Res., 89, 2511-2521, 1984.

Idone, V. P., Length bounds for connecting discharges in triggered lightning subsequent strokes, J. Geophys. Res., 95, 20409-20416, 1990.

Idone, V. P., and R. E. Orville, Lightning return stroke velocities in the Thunderstorm Research International Program (TRIP), J. Geophys. Res., 87, 4903-4915, 1982.

Idone, V. P., and R. E. Orville, Correlated peak relative light intensity and peak current in triggered lightning subsequent return strokes, J. Geophys. Res., 90, 6159-6164, 1985.

Idone, V.P., R.E. Orville, P. Hubert, L. Barret, and A. Eybert-Berard, Correlated observations of three triggered lightning flashes, J. Geophys. Res., 89, 1385-1394, 1984.

Jordan, D. M., Relative light intensity and electric field intensity of cloud-to-ground lightning, Ph.D. Dissertation, University of Florida, 1990.

Jordan, D. M., V. P. Idone, V. A. Rakov, M. A. Uman, W. H. Beasley, and H. Jurenka, Observed dart leader speed in natural and triggered lightning, J. Geophys. Res., 97, 9951-9957, 1992.

Jordan, D. M., and M. A. Uman, Variation in light intensity with height and time from subsequent lightning return strokes, J. Geophys. Res., 88, 6555-6562, 1983.

Kitagawa, N., M. Brook, and E. J. Workman, Continuing currents in cloud to ground lightning discharges, J. Geophys. Res., 67, 637-647, 1962.

Kito, Y., K. Horii, Y. Higashiyama, and K. Nakamura, Optical aspects of winter lightning discharge triggered by rocket-wire technique in Hokuriku district of Japan, J. Geophys. Res., 90, 6147-6157, 1985.

Klingbeil, R., D. A. Tidman, and R. F. Fernsler, Ionizing gas breakdown waves in strong electric fields, Phys. Fluids, 15, 1969-1973, 1972.

Krehbiel P. R., M. Brook, and R. A. McCrory, An analysis of the charge structure of lightning discharges to ground, J. Geophys. Res., 84, 2432-2456, 1979.

Leteinturier, C., J. H. Hamelin, and A. Eybert-Berard, Submicrosecond Characteristics of Lightning Return-stroke currents, IEEE Transactions on Electromagnetic Compatibility, 33, 351-357, 1991.

Leteinturier, C., C. Weidman, J. Hamelin, Current and electric field derivatives in triggered lightning return strokes, J. Geophys. Res., 95, 811-828, 1990.

Leteinturier, C., J. Hamelin, L. Nicot, C. Weidman, J. Willett, E. P. Krider, Lightning current-derivative and electric field-derivative correlation-measurements and models, Proceedings Int. Conf. Atmospheric Electricity, Uppsala, 503-508, 1988.

Le Vine, D. M., J. C. Willett, and J. C. Bailey, Comparison of fast electric field changes from subsequent return strokes of natural and triggered lightning, J. Geophys. Res., 94, 13259-13265, 1989.

Lin, Y. T., M. A. Uman, and R. B. Standler, Lightning return stroke models, J. Geophys. Res., 85, 1571-1583, 1980.

Lin, Y. T., M. A. Uman, J. A. Tiller, R. D. Brantley, W. H. Beasley, E. P. Krider, and C. D. Weidman, Characterization of lightning return stroke electric and magnetic fields from simultaneous two station measurements, J. Geophys. Res., 84, 6307-6314, 1979.

Little, P. F., Transmission line representation of a lightning return stroke, J. Phys. D: Appl. Phys., 11, 1893-1910, 1978.

Little, P. F., The effect of altitude on lightning hazards to aircrafts, Proceedings of the 15th European Conference on Lightning Protection, Vol. 2, Institute of High Voltage Research, Uppsala University, Sweden, 1979.

Mach, D. M., and W. D. Rust, Photoelectric return-stroke velocity and peak current estimates in natural and triggered lightning, J. Geophys. Res., 94, 13,237-13,247, 1989.

Malan, D. J., Les descharges orageuses intermittentes et continu de la colonne de charge negative, Ann. Geophys., 10, 271-281, 1954.

Malan, D. J., H. Collens, Progressive lightning III-The fine structure of return lightning strokes, Proc. R. Soc. London Ser. A, 162, 175-203, 1937.

Malan, D. J., and B. F. J. Schonland, Progressive lightning, Pt 7, Directly correlated photographic and electrical studies of lightning from near thunderstorms, Proc. R. Soc. London Ser. A, 191, 485-503, 1947.

Malan, D. J., and B. F. J. Schonland, The electrical processes in the intervals between the stroke of a lightning discharge, Proc. R. Soc. London Ser. A, 206, 145-163, 1951.

Master, M. J., Lightning induced voltages on power lines: Theory and experiment, Ph.D. dissertation, University of Florida, Gainesville, Florida, 1982.

Master, M. J., M. A. Uman, Y. T. Lin, and R. B. Standler, Calculations of lightning return-stroke electric and magnetic fields above ground, J. Geophys. Res., 86, 127-132, 1981.

Master, M.J., M.A. Uman, W.H. Beasley, and M. Darvenzia, Lightning induced voltages on power lines:experiment, IEEE Trans. PAS, PAS-103, 2519-2529, 1984.

Military Standard, Lightning Qualification Test Techniques for Aerospace Vehicles and Hardware, MIL-STD-1757A, July 20, 1983.

Namasivayam, S., S. Lundquist, and V. Scuka, Some characteristics of electromagnetic transient waveforms from lightning in Sweden, Proc. 20th Int. Conf. on Lightning Protection, Paper 6.5, Interlaken, 1990.

Newman, M. M., J. R. Stahmann, J. D. Robb, E. A. Lewis, S. G. Martin, and S. V. Zinn, Triggered lightning strokes at very close range, J. Geophys. Res., 72, 4761-4764, 1967.

Nucci, C. A., C. Mazzetti, F. Rachidi, and M. Ianoz, On lightning return stroke models for LEMP calculations, Proc. 19th Int. Conf. on Lightning Protection, Graz, Austria, 1988.

Nucci, C. A., G. Diendorfer, M. A. Uman, F. Rachidi, M. Ianoz, and C. Mazzetti, Lightning return stroke current models with specified channel-base current: a review and comparison, J. Geophys. Res., 95, 20395-20408, 1990.

Ogawa, T., and M. Brook, The mechanism of the intracloud lightning discharge, J. Geophys. Res., 69, 5141-5150, 1964.

Orville, R. E., A high speed time-resolved spectroscopic study of the lightning return stroke: Part I. A quantitative analysis, J. Atmos. Sci., 25, 827-838, 1968a.

Orville, R. E., A high speed time-resolved spectroscopic study of the lightning return stroke: Part II. A quantitative analysis, J. Atmos. Sci., 25, 839-851, 1968b.

Orville, R. E., A high speed time-resolved spectroscopic study of the lightning return stroke: Part III. A time-dependent model, J. Atmos. Sci., 25, 852-856, 1968c.

Orville, R. E., J. H. Helsdon, and W. H. Evans, Quantitative analysis of a lightning return stroke for diameter and luminosity changes as a function of space and time, J. Geophys. Res., 79, 4059-4067, 1974.

Orville, R. E., G. G. Lala, and V. P. Idone, Daylight time resolved photographs of lightning, Science, 201, 59-61, 1978.

Papet-LeVine, J., Electromagnetic radiation and physical structure of lightning discharges, Ark. Geophys., 3, 391-400, 1961.

Paxton, A. H., R. L. Gardner, and L. Baker, Lightning return stroke, A numerical calculation of the optical radiation, Phys. Fluids., 29, 2736-2741, 1986.

Plooster, M. N., Numerical simulation of spark discharges in air, Phys. Fluids, 14, 2124-2133, 1971

Price, G. H., and E. T. Pierce, The modeling of channel current in the lightning return stroke, Radio Sci., 12, 381-388, 1977.

Rachidi, F., and C. A. Nucci, On the Master, Uman, Lin, Standler and the modified transmission line lightning return stroke current models, submitted for publication (1990).

Rakov, V.A., and A.A. Dulzon, Calculated electromagnetic fields of lightning return strokes (in Russian), Tekhnicheskaya Elektrodinamika, No. 1, 87-89, 1987.

Rakov, V.A., and M.A. Uman, Some properties of negative cloud-to-ground lightning vs. stroke order, J. Geophys. Res., 95, 5447-5453, 1990a.

Rakov, V.A., and M.A. Uman, Long continuing current in negative ground flashes, J. Geophys. Res., 95, 5455-5470, 1990b.

Rakov, V.A., and M.A. Uman, Waveforms of first and subsequent leaders in negative lightning flashes, J. Geophys. Res., 95, 16561-16577, 1990c.

Rakov, V.A., and A.A. Dulzon, A modified transmission line model for lightning return stroke field calculations, Proc. 9th Int. Symp. on Electromagnetic Compatibility, Zurich, Switzerland, March 12-14, 1991, 229-235, 1991.

Rakov, V.A., M.A. Uman, D.M. Jordan, and C.A. Priori III, Ratio of leader to return-stroke electric field change for first and subsequent lightning strokes, J. Geophys. Res., 95, 16,579-16,587, 1990.

Rakov, V. A., R. Thottappillil, and M. A. Uman, On the empirical formula of Willett et al. (1989) relating lightning return stroke peak current and peak electric field, J. Geophys. Res., 97, 11527-11533, 1992.

Rakov, V. A., R. Thottappillil, and M. A. Uman, Electric field pulses in K and M changes of lightning ground flashes, J. Geophys. Res., 97, 9935-9950, 1992.

Rakov, V. A., M. A. Uman, and R. Thottappillil, Review of lightning properties determined from electric field and TV observations, Proceedings of the 9th International Conference on Atmospheric Electricity, Leningrad, USSR, June 15-19, 1992.

Schnetzer, G. H., and R. J. Fisher, The Sandia transportable triggered lightning instrumentation facility (SATTLIF), Proc. 1991 International Aerospace and Ground Conference on Lightning and Static Electricity, Cocoa Beach, Florida, April 16-19, 1991.

Schonland, B. F. J., Progressive Lightning, Pt 4, The discharge mechanisms, Proc. R. Soc. London Ser. A, 164, 132-150, 1938.

Schonland, B. F.J., The lightning discharge, Handb. Phys., 22, 576-628, 1956.

Schonland, B. F. J., D. J. Malan, and H. Collens, Progressive Lightning, Proc. R. Soc. London Ser. A, Pt. 2, 152, 595-625, 1935.

Shindo, T. and M.A. Uman, Continuing current in negative cloud-to-ground lightning, J. Geophys. Res., 94, 5189-5198, 1989.

Sommerfeld, A., Ueber die Ausbreitung der Wellen in der Drahtlosen Telegraphie, Annalen der Physics (4), 28, 665, 1909.

Straw, D. F., Non-linear modeling of lightning return strokes, Proceedings of the Federal Aviation Administration/Florida Institute of Technology Workshop on Grounding and Lightning Technology, Melbourne, Florida, March 6-8, pp. 9-15, 1979.

Thomson, E. M., The dependence of lightning return stroke characteristics on latitude, J. Geophys. Res., 85, 1050-1056, 1980.

Thomson, E.M., M.A. Galib, M.A. Uman, W.H. Beasley, and M.J. Master, Some features of stroke occurrence in Florida lightning flashes, J. Geophys. Res., 89, 4910-4916, 1984.

Thomson E. M., P. J. Medelius, M. Rubinstein, M. A. Uman, J. Johnson, and J. W. Stone, Horizontal Electric Fields from Lightning Return Strokes, J. Geophys. Res., 93, 2429-2441, 1988.

Thomson, E.M., M.A. Uman, and W.H. Beasley, Speed and current for lightning stepped leaders near ground as determined from electric field records, J. Geophys. Res., 90, 8136-8142, 1985.

Thottappillil, R., V. A. Rakov, and M.A. Uman, K and M changes in close lightning ground flashes in Florida, J. Geophys. Res., 95, 18,631-18,640, 1990.

Thottappillil, R., M. A. Uman, and G. Diendorfer, Influence of channel base current and varying return stroke speed on the calculated fields of three important return stroke models, Proceedings of the International Aerospace Ground Conference on Lightning and Static Electricity, Florida, April 16-19, 1991.

Uman, M. A., Lightning return stroke electric and magnetic fields, J. Geophys. Res., 90, 6121-6130, 1985.

Uman, M. A., 1987. The Lightning Discharge, Academic Press, London.

Uman, M. A., and D. K. McLain, Magnetic field of the lightning return-stroke, J. Geophys Res., 74, 6899-6910, 1969.

Uman, M. A., and R. E. Voshall, Time interval between lightning strokes and the initiation of dart leaders, J. Geophys. Res., 73, 497-506, 1968.

Uman, M. A., D. K. McLain, and E. P. Krider, The electromagnetic radiation from a finite antenna, Am. J. Phys., 43, 33-38, 1975.

Wagner, C. F., Determination of the wavefront of lightning stroke currents from field measurements, AIEE Trans., 79 (Pt. 3), 581-589, 1960.

Weidman, C. D., and E. P. Krider, The radiation field waveforms produced by intracloud lightning discharge processes, J. Geophys Res., 83, 6239-6247, 1978.

Willett, J. C., J. C. Bailey, V. P. Idone, R. E. Orville, A. Eybert-Berard, and L. Barret, Submicrosecond intercomparison of radiation fields and currents in triggered lightning return strokes based on the transmission-line model, J. Geophys. Res, 94, 275-13,286, 1989.

Willett, J. C., V. P. Idone, R. E. Orville, C. Leteinturier, A. Eybert-Berard, L. Barret, and E. P. Krider, An experimental test of the transmission-line model of electromagnetic radiation from triggered lightning return strokes, J. Geophys. Res., 93, 3,867-3878, 1988.

BIOGRAPHICAL SKETCH

Rajeev Thottappillil was born in Kerala, India in 1958. He received a bachelor's degree in electrical engineering in 1981 from the University of Calicut after which he worked in industry in various capacities. In 1987 he qualified in the Graduate Aptitude Test in Engineering examination and joined Anna University, Madras, for the masters's program in power systems. Later in Fall 1988 he transferred to the Electrical Engineering Department of the University of Florida in Gainesville. In August 1989 he received the M.S. degree in electrical engineering from the University of Florida. In August 1992 he received the Ph.D. in electrical engineering from the University of Florida. Dr. Thottappillil's research interests are in the areas of lightning, electromagnetics, and power systems.

I certify that I have read this study and that in my opinion it conforms to acceptable standards of scholarly presentation and is fully adequate, in scope and quality, as a dissertation for the degree of Doctor of Philosophy.

Martin A. Uman, Chairman
Professor of Electrical Engineering

I certify that I have read this study and that in my opinion it conforms to acceptable standards of scholarly presentation and is fully adequate, in scope and quality, as a dissertation for the degree of Doctor of Philosophy.

Ewen M. Thomson
Associate Professor of Electrical Engineering

I certify that I have read this study and that in my opinion it conforms to acceptable standards of scholarly presentation and is fully adequate, in scope and quality, as a dissertation for the degree of Doctor of Philosophy.

Dennis P. Carroll
Professor of Electrical Engineering

I certify that I have read this study and that in my opinion it conforms to acceptable standards of scholarly presentation and is fully adequate, in scope and quality, as a dissertation for the degree of Doctor of Philosophy.

Alex Domijan
Associate Professor of Electrical Engineering

I certify that I have read this study and that in my opinion it conforms to acceptable standards of scholarly presentation and is fully adequate, in scope and quality, as a dissertation for the degree of Doctor of Philosophy.

Humberto Campins
Associate Professor of Astronomy

I certify that I have read this study and that in my opinion it conforms to acceptable standards of scholarly presentation and is fully adequate, in scope and quality, as a dissertation for the degree of Doctor of Philosophy.

Vladimir A. Rakov
Associate Professor of Electrical Engineering

I certify that I have read this study and that in my opinion it conforms to acceptable standards of scholarly presentation and is fully adequate, in scope and quality, as a dissertation for the degree of Doctor of Philosophy.

Douglas M. Jordan
Assistant Professor of Electrical Engineering

This dissertation was submitted to the Graduate Faculty of the College of Engineering and to the Graduate School and was accepted as partial fulfillment of the requirements for the degree of Doctor of Philosophy.

August, 1992

Winfred M. Phillips
Dean, College of Engineering

Madelyn M. Lockhart
Dean, Graduate School